Ionic effects on subunit interactions in a cold-active alkaline phosphatase from the marine bacterium *Vibrio splendidus*.

Jens Guðmundur Hjörleifsson

Faculty of Physical Sciences

School of Engineering and Natural Sciences

Ionic effects on subunit interactions in a cold-active alkaline phosphatase from the marine bacterium *Vibrio splendidus*.

Jens Guðmundur Hjörleifsson

180 ECTS thesis submitted in partial fulfillment of a
Philosophiae Doctor degree in Biochemistry

Advisor
Bjarni Ásgeirsson

PhD Committee
Bjarni Ásgeirsson
Magnús Már Kristjánsson
Elena Papaleo

Opponents
Tony Collins
Stjepan Orhanovic

Faculty of Physical Sciences
School of Engineering and Natural Sciences
University of Iceland
Reykjavik, February 2018

Ionic effects on subunit interactions in a cold-active alkaline phosphatase from the marine bacterium *Vibrio splendidus*.
Subunit and ionic interactions of a cold-active enzyme.
180 ECTS thesis submitted in partial fulfillment of a Philosophiae Doctor degree in biochemistry.

Faculty of Physical Sciences
School of Engineering and Natural Sciences
University of Iceland
Dunhaga 5
107 Reykjavík

Phone: +354 525 4000

Bibliographic information:
Jens Guðmundur Hjörleifsson, 2018, *Ionic effects on subunit interactions in a cold-active alkaline phosphatase from the marine bacterium Vibrio splendidus*, Ph.D. thesis, University of Iceland, 218 pages.

ISBN 978-9935-9320-6-8
Printing: Háskólaprent hf.
Reykjavík, May 2018

Abstract

Protein quaternary structures are fundament for life. Proteins have evolved towards large assemblies of subunits needed for the execution of complex chemistry, for building structural components or for compartmentalization. Most oligomeric enzymes exist as homodimers, having two subunits with identical active sites. It is largely unknown why enzymes have evolved in so many cases towards the homodimer structure (and larger oligomeric structures). Alkaline phosphatase (AP) is an excellent model enzyme for the large family of homodimeric hydrolases. Its activity is dependent on dimerization and correct metal occupancy of the three metal ions in the active site. The reason why the enzyme does not function in the monomeric form is still unknown. The focus of this Ph.D. work was on the AP ortholog from *Vibrio splendidus* (VAP), a cold-adapted marine bacterium. This enzyme is thermally unstable above room-temperature, but also one of the most active variants of its kind at low temperatures. These characteristics are very dependent on the solution conditions. Stability is only maintained at high ionic strength and pH. Here, the focus was on studying the importance of the dimeric structural state for the function, in particular the role of the metal ions for catalysis. The results suggested that the enzyme inactivates irreversibly to a dimeric intermediate state. This dimeric intermediate state was shown to be more dynamic than the native state, defined as measurable changes in the range of conformations of the ensemble of enzyme molecules, yet fully metalated. Furthermore, the enzyme lost its putative half-of-sites reactivity which is dependent on subunit interactions and communication between active sites. The effect of ionic strength on the activity and stability was studied and found to be positive for both features. It is proposed that a deprotonation step causes a conformational change in VAP, based on pH specific effects on physical parameters. Furthermore, the large interface loop, which characterizes VAP, was shown to be mostly important for stability but also needed for local structural rigidity close to the catalytically active residues. This thesis promotes the idea that the role of the homodimeric state is to provide a conformational energy for both stabilization and catalysis of the enzyme, through the interface, not available in the monomeric state.

Útdráttur

Fjórða stigs bygging próteina er grunnur alls lífs á jörðinni eins og við þekkjum það. Prótein hafa þróast í átt að stórum komplexum til að hvata flókin efnahvörf, til margvíslegra byggingahlutverka, eða hólfunar. Flest ensím eru virk sem einþátta tvíliður með tvær eins hvarfstöðvar. Hvers vegna svo mörg ensím finnast sem einþátta tvíliður er ekki vel rannsakað. Alkalískur fosfatasi (AP) er módel ensím fyrir hýdrólasa sem eru einþátta tvíliður. Virkni AP er háð tvíliðumyndun og málmjónum í hvarfstöð. Hvers vegna hvarfstöðvarnar hafa ekki hvarfgetu í einliðuforminu er ekki vitað. Rannsóknarefni þessarar doktorsritgerðar var AP úr *Vibrio splendidus* (VAP) kaldsjávarbakteríu. VAP er eitt hitaóstöðugasta ensím sem þekkist en einnig eitt það virkasta við lág hitastig miðað við sambærileg ensím. Áhersla var lögð á að skýra hlutverk tvíliðumyndunar hjá VAP og áhrif jóna á hvötun og stöðugleika, en einnig að útskýra hvers vegna AP hafa ekki virkar einliður. Þessir þættir eru mjög háðir lausnaaðstæðum. Niðurstöður bentu til þess að við afvirkjun ensímsins verði óafturkræf myndbreyting sem leiðir til óvirkrar tvíliðu. Óvirka tvíliðan var lausbundnari, innihélt allar þrjár málmjónirnar í hvarfstöð en hafði mögulega misst eiginleikann til þess að hvata með svokölluðum “half-of-sites” hvarfgangi. Áhrif jónastyrks voru mikil á virkni og stöðugleika og voru áhrifin háð pH, þar sem afprótónering óþekkts sýruhóp veldur myndbreytingu. Að auki var kannað hlutverk löngu yfirborðlykkjunnar sem einkennir VAP frá flestum AP. Meginhlutverk lykkjunna er að stuðla að stöðugleika hvarfstöðvar en einnig í að halda ákveðinni stífni í lykkjum nálægt virkum hliðarkeðjum. Niðurstaða vinnu þessarar ritgerðar bendir til þess að meginhlutverk tvíliðunnar sé það tillegg byggingarfríorku sem verður til á snertiflötum einliðanna sem stuðlar bæði að stöðugleika og hvötun, sem ekki eru til staðar í einliðunum.

If your experiment needs statistics,
you ought to have done a better experiment.
Ernest Rutherford

List of publications

Paper I

Hjorleifsson, J. G., and Asgeirsson, B. (2016) Cold-active alkaline phosphatase is irreversibly transformed into an inactive dimer by low urea concentrations, *Biochim Biophys Acta 1864*, 755-765.

Paper II

Hjorleifsson, J. G., and Asgeirsson, B. (2017) pH-Dependent binding of chloride to a marine alkaline phosphatase affects the catalysis, active site stability, and dimer equilibrium, *Biochemistry 56*, 5075-5089.

Paper III

Hjorleifsson, J. G., and Asgeirsson, B. (2018) Cold-active alkaline phosphatase undergoes a subtle structural change at the dimer interface upon inactivation. Manuscript submitted to *Biochemistry* (2018).

Paper IV

Papaleo E., Magnúsdóttir M., Hjörleifsson J. G., Invernizzi G., Ásgeirsson B. (2015) Modulation of activity and stability of a dimeric cold-adapted enzyme acting on a disordered region at the monomer-monomer interface. Manuscript submitted to *JBC* (2015).

Preface

This is the first Ph.D. thesis dedicated to the enzyme alkaline phosphatase from *Vibrio splendidus* (VAP). Therefore, the introduction of this thesis can be thought of as a review of the ongoing research on VAP for the last two decades. In fact, each sub-chapter of the introduction was written in the style of "mini-review", where some of the topics are: Alkaline phosphatases, effect of solutes on enzymatic properties, cold-adaptation of enzymes, enzyme promiscuous activity, and the role of enzyme quaternary structure.

VAP is truly an amazing enzyme. It is fascinating that research on a single enzyme is still delivering new and original ideas about enzymatic functions many decades since a book was written about it (McComb, 1979). The reason for VAP success as a model enzyme is that it harbors many structural aspects that other enzymes are lacking. First, VAP is a metalloenzyme, having three metals where both the two zinc ions and the magnesium ion are crucial for its native function. Secondly, VAP is a homodimer with two active sites, where the benefit of dimerization for such enzymes is still largely unknown. Thirdly, VAP harbors promiscuous activity (as other APs), sulphatase activity and possibly protease activity. Finally, VAP is a cold-active enzyme, opening the opportunity to study the effect of cold-adaptation on all the aforementioned features.

What has been lacking during previous VAP research, is to properly define the mechanism for inactivation and the effect of ions on its activity. In fact, VAP is one of the most unstable cold-active enzymes towards heat at low ionic strength, losing activity in few hours at room temperature, while at 0.5 M NaCl (pH 8.0) the enzyme is stable for weeks at 40°C. The stability of the dimer has also been disputed, and the role of dimerization in catalysis was also mostly unknown. These aspects are elucidated here. I hope that the data presented in this thesis will serve as a wholesome "manual" on how the enzyme is inactivated at low ionic strength, how ions activate the enzyme at a defined pH range, and how environmental conditions influence the stability of the homodimer.

Table of contents

Figures

Tables

Abbreviations

AP, alkaline phosphatase; **VAP**, *Vibrio* splendidus alkaline phosphatase; **PAGE**, polyacrylamide gel electrophoresis; **SEC**, size- exclusion chromatography; **ECAP**, *E. coli* alkaline phosphatase; **PLAP**, placental alkaline phosphatase; **GCAP**, germ cell alkaline phosphatase; **pNPP**, para-nitro phenyl phosphate; **HaAP**, *Halomonas sp*. alkaline phosphatase; **NMR**, nuclear magnetic resonance; **TNAP**, tissue non-specific alkaline phosphatase; **GPI**, glycosylphosphatidylinositol; **PPi**, pyrophosphate; **CHO**, Chinese hamster ovary; **IgG**, immunoglobulin G; **CDK**, chronic kidney disease; **LPS**, lipopolysaccharide; IAP, intestinal AP; ELISA, enzyme-linked immunosorbent assay; **TAP**, Antarctic bacterium TAB5 alkaline phosphatase; **SAP**, shrimp alkaline phosphatase; **SCAP**, *Shewenella sp*. alkaline phosphatase; **PON**, serum paraoxonase; **PMH**, phosphonate monoester hydrolase; **AS**, aryl sulphatase; **NPP**, nucleotide pyrophosphatdiesterase; **pNPS**, para-nitro phenyl sulphate; **MDNPP**, methyl 2,4-dinitrophenyl phosphate; **PTP**, protein tyrosine phosphatase; **MS**, mass spectrometry; **HPLC**, high pressure liquid chromatography; **CLASP**, catalytic active site prediction; **MWC**, Monod-Wyman-Changeux model; **KNF**, Koshland-Némethy-Filmer model; **HT**, Hilser and Thomson model; **HOSB**, half-of-sites binding; **HOSR**, half-of-sites reactivity; **AOSB**, all-of-sites binding; **PNP**, purine nucleoside phosphorylase; **MMRT**, macromolecular rate theory; **IPMDH**, isopropyl malate dehydrogenase; **MD**, molecular dynamics; **HABA**, 2-[4 -hydroxy-benzeneazo] benzoic acid; **FRET**, Förster resonance energy transfer; **TRIQ/TyrIQ**, tryptophan and tyrosine induced quenching;

Acknowledgements

Above all, I want to gratefully thank my supervisor Bjarni Ásgeirsson for a faithful guidance during my years as his Ph.D. student. He has truly been my mentor both in the lab and in the lecture hall as an educator. Today, there are not many professors that still get their hands dirty in the lab, ordering lab consumables and fixing equipment. He is a proof that the professor job is not simply an office job. The respect that he shows his students is admirable, and I want to personally thank him for sharing countless conversations over a cup of coffee about science or everyday small talk. I will be his last Ph.D. student before retirement and I can say with gratitude that he will be greatly missed by his students and staff at the Science Institute of Iceland.

I wish to thank the doctoral committee, Prof. Magnús Már Kristjánsson and Assoc. Prof. Elena Papelo for their contribution and inspirations to improve the work of this thesis.

I want to especially thank Ronny Helland for his excellent guidance in protein crystallography. I very much value the time you have giving me in Tromsø and I hope our continuing collaboration will be long and prosperous.

Prof. Magnús Már Kristjánsson, thank you for great discussions and for being my company at conference trips. I always enjoy dropping by your office, my so called academic pit stop towards the coffee machine.

Kristinn Ragnar Óskarsson (Kiddi), I want to thank you for personally taking care of my experiments while I was away, most likely taking care of my children (even if it meant you were just pushing one button). I also value our friendship and our common passion for beer, wine and steak.

Kristófer Arnar Eiríksson (Krilli), you are doing great and you will nail this master thesis, if you give it time. Thank you for the discussions about VAP reaction mechanism and enzyme promiscuity, keeping me on my toes towards these matters.

Turning to the years in Stockholm University during my master's studies, I would like to thank my previous supervisor Ülo Langel for accepting me to his group as a master student. I hope you will enjoy some more Santana during your retirement (I still have the blue-ray you gave me). I also want to thank Einar Hallberg for his guidance and to teach me all I know about cloning. And Jonas, thank you for all the times in the lab and I hope our continuing friendship will be long and fruitful.

I want to thank the Icelandic Centre for Research (RANNÍS) for its financial support during this thesis.

To the staff and students of the Science Institute of Iceland (Raunó), I want to express my deep gratitude.

I want to thank my family for all the support over the years, my mother Ólöf and my father Hjörleifur. I would have loved to spend more time at home, but you know how it is when we live on two separate islands. I also want to express my gratitude to my parents in law, Haddý and Diddi for their tremendous support in raising my three daughters during these hectic years of my Ph.D work. Without you it would have been much more difficult.
To my brother Þói, I want to personally thank for his support. You are always very good to my girls and I appreciate that. Also, thank you for the trips to your home in Switzerland. They were very important for some relaxation and to forget about things for a while (drinking beer is relaxing).

And finally, the existence of my children, Snædís, Sara Dís and Heiðbjört makes the significance of this degree much more than it can be. You will likely not remember the years when your father was away a lot due to his studies, but I hope you will appreciate it when you are older. Daddy promises to be more home now (you have it on paper here!).
Íris, my love, I am sure that without you I would not have finished this thesis. You are my rock, and I cannot think of a better person to share this milestone with. We will make something great together in the future!

1 Introduction

1.1 Alkaline phosphatase

Alkaline phosphatases (APs) are among the most studied enzymes in nature. Many reviews and at least two books on the matter have been published (McComb, Bowers, Posen, 1977 and Millán, 2006. Here, a brief introduction is given to comment on the role of AP and to give a fundamental basis for the work of this thesis.

1.1.1 AP structure

According to the Structural Classification of Proteins data base (SCOP) alkaline phosphatase lineage is of the *phoA* genotype and is further catalogued as follows: 1) *Class:* Alpha-Beta proteins (α/β); 2) *Fold:* Alkaline phosphatase-like (3 layers of α/β/α; mixed beta-sheet of 8 strands in the sequence order 43516728 and strand 7 is antiparallel to the rest); 3) *Superfamily:* Alkaline phosphatase-like; 4) *Family:* Alkaline phosphatase (the common fold is decorated with several large insertions). All APs are functional as homodimers, where the individual monomers are inactive.

The active site

The active site has three metal binding sites, where two Zn^{2+} ions occupy the M1 and M2 sites and Mg^{2+} the M3 site (Figure 1.1). The active site residues within the region of the phosphate binding site (or sulphate when binding as an inhibitor) are very conserved. A nucleophilic Ser interacts with the substrate (S65 for VAP or S102 for *E. coli* AP [ECAP]) forming a covalent bond. An Arg residue (R129 in VAP or R166 for ECAP) directly binds the substrate forming an ionic bond with two non-bridging oxygen atoms of the phosphoryl group. Additional Asp and His residues coordinate Zn^{2+} in sites M1 and M2, and those are conserved in all compared sequences. The only two sequence variances in the active site are seen near the M3 site where H116 in VAP has Asp in ECAP, but His in eukaryotes, and W274 in VAP is replaced by Lys in ECAP and His in eukaryotes. There are in addition few isolated examples of Co^{2+} activation of APs, e.g. for *Thermotoga maritima* AP [1] and *B. subtilis* AP [2]. Furthermore, replacements of native metals in ECAP have been frequently described, where Co^{2+} [3, 4], and other metals such as Cd^{2+}, Mn^{2+} and Ni^{2+} have

been titrated into the apoenzyme, sometimes for NMR studies. Most of the metal-substituted variants had little or no activity. Wang et al. [5] proposed that D153 and K328 present in ECAP controlled the metal specificity, where the Co^{2+} substituted wild type and D153H had close to no activity. The K328W variant showed 80% less k_{cat} with Co^{2+} compared to the Zn-Mg occupied enzyme, while the Co^{2+} substituted variant D153H/K328W showed 4-fold higher k_{cat} than the Zn-Mg enzyme. The latter variant is identical to VAP in these positions. In all cases, K_M was higher for the Co^{2+} substituted enzymes. Crystal structure of Co^{2+} substituted wild type and D153H/K328W indicated differences in metal coordination, where the phosphate bound less tightly, resulting in the increase in activity. This indicated that phosphate release is the slowest step in the reaction mechanism, since the D153H/K328 showed increased k_{cat}.

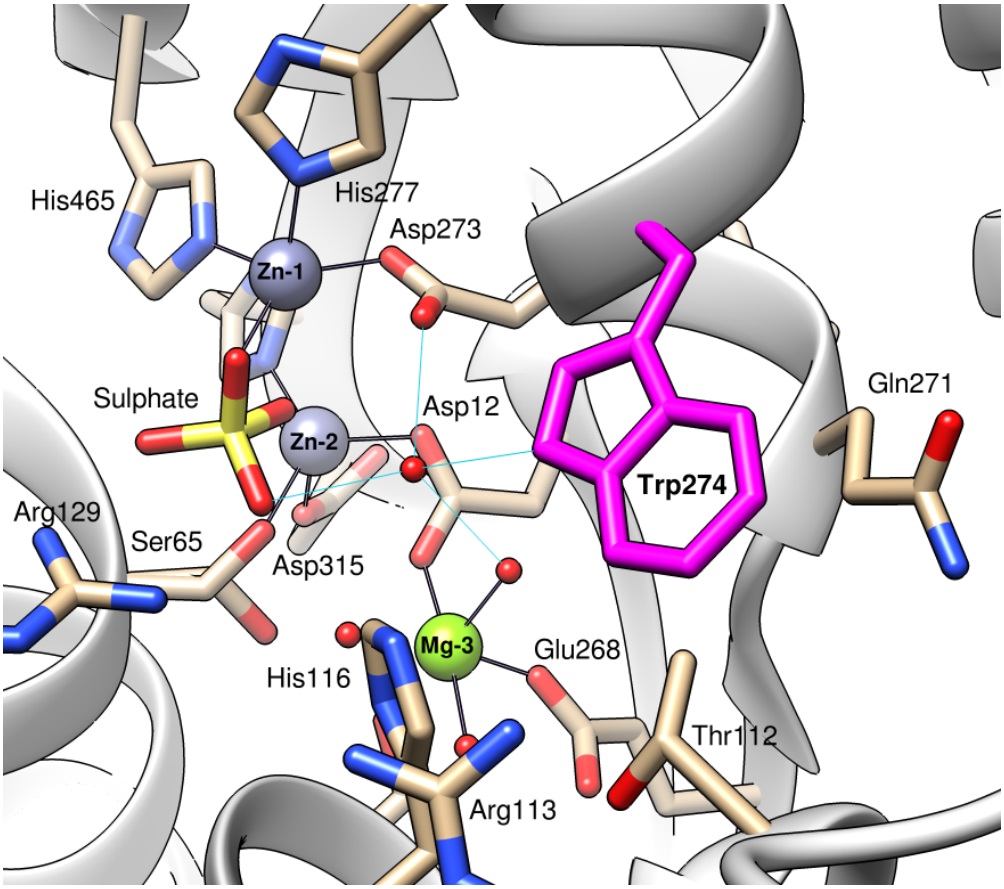

Figure 1.1. VAP active site. Zinc is shown as navy-blue spheres at the M1 and M2 sites (Zn-1 and Zn-2) and magnesium as a lime-green sphere at the M3 site (Mg-3). Water molecules are represented as red spheres and hydrogen bonds as aquamarine colored lines. A sulfate ion, binding as a competitive inhibitor, is shown in the active site. Note that Ser65 is shown as two crystallographic rotamers Figure is adapted from [6].

Zinc has high affinity towards binding to the M3 site occupied by Mg^{2+} in VAP (paper III) and the mammalian phosphatases [7, 8], where zinc is an inhibitor in the micromolar range while only ECAP is known to be tolerant to zinc in the millimolar range [9]. Furthermore, both VAP and the mammalian phosphatases are activated by Mg^{2+} while ECAP is not [9]. However, an ECAP variant resembling mammalian APs (D153H/K328H) showed similar properties as the mammalian APs towards Zn^{2+} inhibition. In the D153H ECAP variant, a tetrahedrally coordinated Zn^{2+} was bound in the M3 site in contrast to octahedral geometry when magnesium is bound there [9-11].

Gene inserts

There are several gene inserts of APs that give different structural characteristics (Figure 1.2).

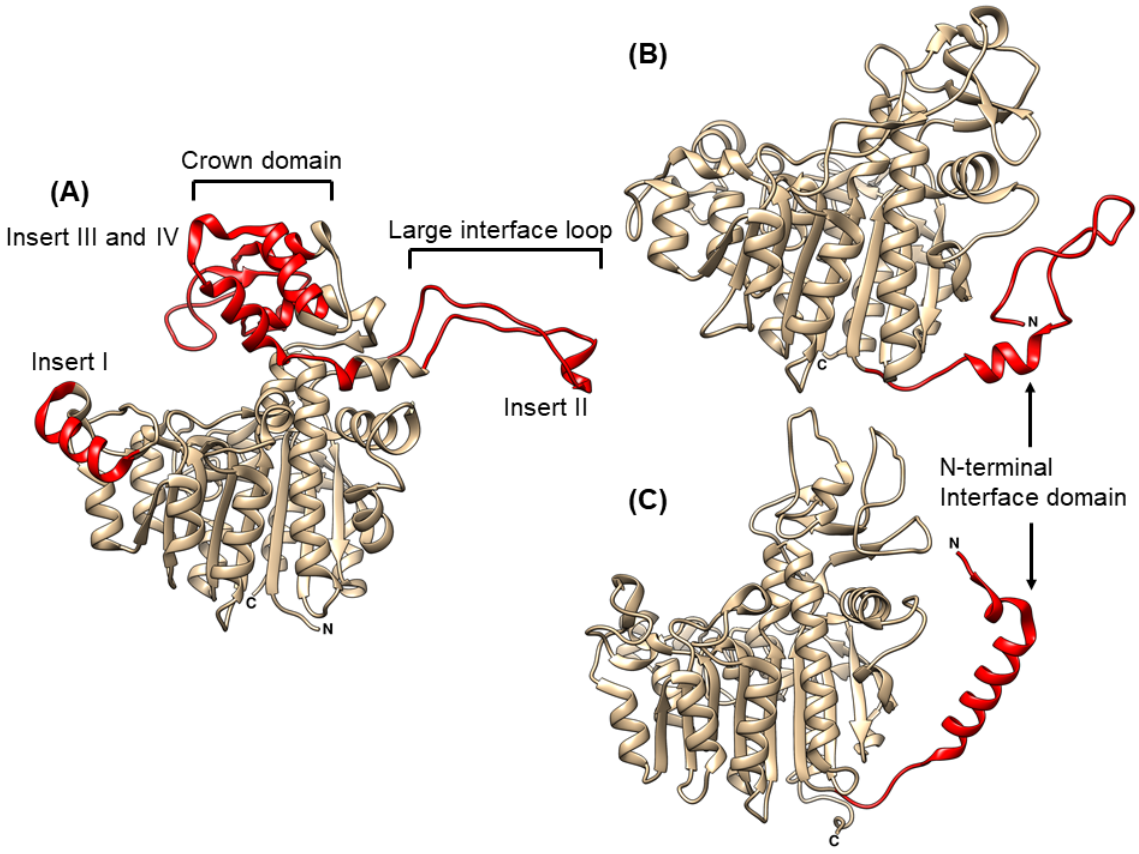

Figure 1.2. Alkaline phosphatase gene inserts. (A) VAP (PDB: 3E2D) showing the four gene inserts in red. (B) ECAP (PDB: 3TG0) and (C) PLAP (PDB:1ZEF), showing the N-terminal interface domain in red.

Inserts are mainly seen in the crown domain or at the N-terminus. VAP is one of the largest APs and has four inserts (Figure 1.2A). Two are located at the crown domain, resulting in considerably larger crown domains than found in ECAP (Figure 1.2B) or

human placental alkaline phosphatase (PLAP) (Figure 1.2C). VAP has a large interface loop with an unknown function (Insert II), but it is likely crucial for stability, since VAP is missing the N-terminal interface region that embraces the other subunit in the enzymes involved (discussed in Paper IV). The N-terminal interface domain of some other APs has either a large helical structure (mammalian phosphatases), or it is more disordered as seen for ECAP. This domain is important for ECAP catalytic activity and especially for stability [12, 13]. Furthermore, it might be important in the presumable half-of-sites reactivity mechanism [14] (see in 1.1.2). The role of the crown domain is largely unknown, but is likely not detrimental for the catalytic mechanism, since in some APs, for example the AP from the Antarctic bacterium TAB5 [15], the crown domain is missing. For mammalian phosphatases, a loop region in the crown domain has been shown to have an important role for stability [16] and to be essential for amino acid and small peptide inhibition. Furthermore, differences seen at the crown domain between PLAP and germ cell alkaline phosphatase (GCAP) are decisive towards L-Leu inhibition [17-20].

1.1.2 Reaction mechanism

Alkaline phosphatases catalyze the hydrolysis of phosphomonoesters, optimally at slightly alkaline to alkaline conditions. Phosphate esters are building blocks of life and have quite stable chemical bonds. The non-enzymatic hydrolysis of phosphoesters is slow unless heated at high temperatures and is highly dependent on pH. Hydrolysis rate is highest at pH 4-5 where the phosphate groups is monoanionic [21]. For enzymatic hydrolysis, the rate increases with pH giving V_{max} for para-nitrophenyl phosphate [pNPP] hydrolysis between pH 8.0 and 10.5. Furthermore, the basicity of the leaving group is more important for non-enzymatic hydrolysis than for enzymatic hydrolysis [22, 23].

Generally, APs are non-specific towards the nature of the leaving group and the rate of hydrolysis is similar for many small substrates, but for very bulky substrate, such as t-butyl phosphate and menthyl phosphate, the hydrolysis is slow due to higher K_M [24]. For many substrates the k_{cat} is similar, but K_M can vary greatly, up to 4 orders of magnitude [23]. The minimal reaction scheme for phosphoester hydrolysis or transphosphorylation by AP is shown below showing the fundamental rate constants. In addition, rate constants for conformational changes have been implicated as part of the overall mechanism (see below):

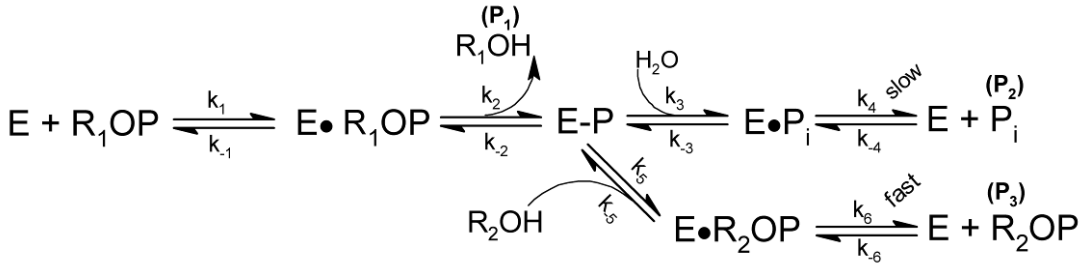

The rate limiting step for APs under alkaline conditions is generally the release of inorganic phosphate product (k_4) but becomes the hydrolysis (k_3) below pH 7.0. The presence of a suitable phosphate acceptor, such as amine alcohol, provides competition for water as a nucleophile to increase the reaction rate (k_5 and k_6), but they are needed at nonphysiological concentration (> 0.1 M) for efficient transphosphorylation. Thus, APs should rarely act as transphosphorylases *in vivo*.

The most plausible reaction mechanism involves a magnesium hydrate that activates the serine nucleophile towards nucleophilic attack (Figure 1.3). Arg166 and a zinc ion bound in the M1 site coordinate the binding of the substrate. A zinc ion bound in the M2 site stabilizes the Ser102 oxyanion towards nucleophilic attack. Hydrolysis of the Ser-P covalent intermediate takes place by an activated water Zn hydroxide (at the M1 site).

However, the role of the metal ion in the M3 site has been debated by some [25, 26]. These authors doubt that the magnesium ion in the M3 site acts as a general base to activate the nucleophilic Ser. Instead, they propose that the third metal ion stabilizes the transferred phosphoryl group in the transition state. This proposal was mainly based on the absence of a third metal ion, or a general base residue, in nucleotide pyrophosphatase/phospho- diesterase (similar active site geometry as APs), which mainly catalyzes phosphodiester hydrolysis. In fact, most zinc containing hydrolases work without a third metal, using a bimetallo center. It was also proposed that the magnesium served the role of increasing the specificity of APs for monophosphoryl esters rather than other types, such as sulfonylesters or diesters [27]. The negative charge on the phosphoryl group may be larger than on other similar esters, although it is not clear which ionic form is binding in the active site [28]. Two other mechanisms were proposed where Mg^{2+} stabilizes the transferred phosphoryl group on its way over the transition state during the reaction (Figure 1.4B and 1.4C) [25]. This, however, is not a rate-determining step overall under physiological pH conditions. Furthermore, a Mg^{2+} deficient variant E322Y has drastically reduced hydrolysis rates of monoesters but unchanged diester hydrolysis (promiscuous activity).

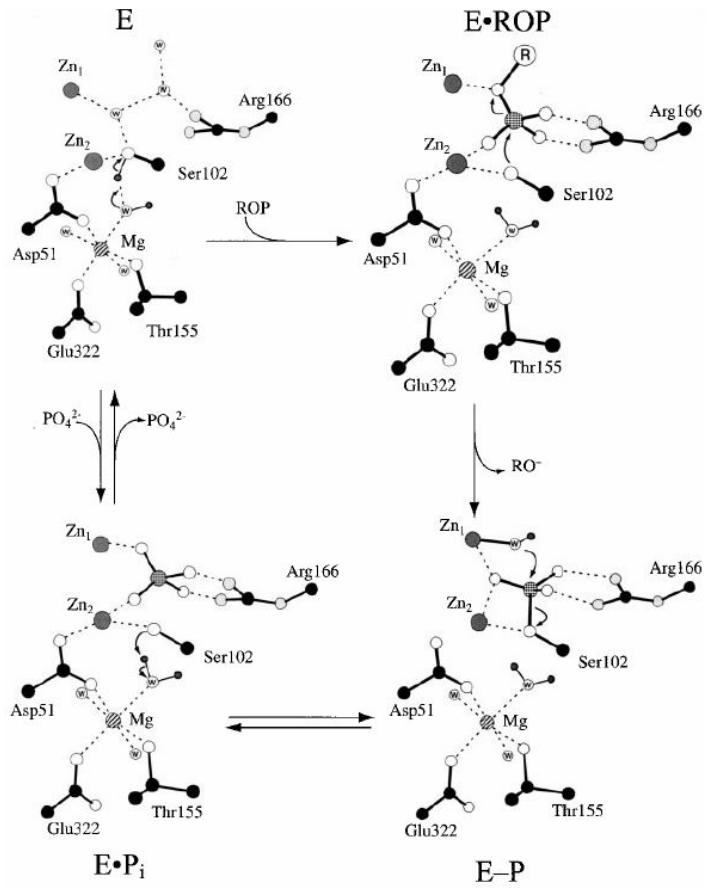

Figure 1.3. The "revised mechanism" proposed by Stec, Holzt and Kantrowitz (2000) [29], which shows how Mg^{2+} in the M3 site is important for catalysis and how Ser102 (ECAP) is activated towards nucleophilic attack. (see text for details) Adapted from [29].

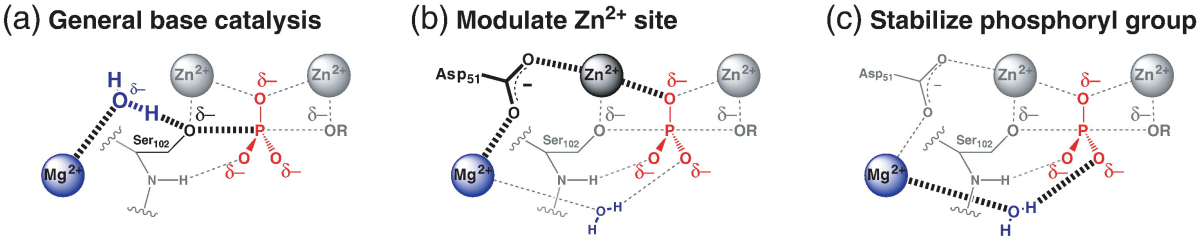

Figure 1.4. Role for Mg^{2+} in catalysis by APs. (a) General base catalysis where Mg^{2+} acts as a general base on the nucleophilic Ser102. (b) Modulated Zn^{2+} site where Mg^{2+} helps stabilize the transferring phosphoryl group via bimetallo Zn-coordination through Asp51. (c) Magnesium stabilized phosphoryl group via a water ligand. Figure adapted from [25].

1.1.3 Effect of ionic strength on catalysis

At acidic pH, the activity of ECAP is lower as the ionic strength increases [30, 31]. The chemical step (phosphorylation of the Ser) is the rate limiting step at acidic pH and the ionic strength is believed to affect the favorable electrostatics between the free enzyme and free substrate [32]. At pH above 7.5, the effect is reversed and an increase in activity is

seen for up to 1 M NaCl [31, 33]. Mammalian phosphatases are generally not activated by salt ions and in some cases the activity is lower at high NaCl concentration [34-36].

Since all the important active site features and the mechanism for hydrolysis are the same in mammalian APs as in other APs, it is not clear what causes the differences in ionic activation for APs. Some of these discrepancies can be explained by the use of high concentrations of ethanolamine phosphate acceptors, a transphosphorylation agent, in assays. For example, the use of 1 M Tris at pH 8.0 gives about 0.6 M of ionic strength. The NaCl concentration does not affect the dephosphorylation rate but is known to decrease the binding affinity for both substrate and inorganic phosphate [30, 37]. Therefore, when the rate-limiting step is the release of phosphate, then lower affinity for phosphate would be expected to increase the rate. For the mammalian phosphatases, the rate-limiting step (at pH 10.0) is also believed to be the release of phosphate [38]. If the ionic activation would simply involve charge neutralization of the phosphate product then the effect would likely be general for most APs. Some have theorized that the rate limiting step is not the release of phosphate, but rather a conformational change, where the enzyme switches between a low and high affinity state for substrate and product, respectively (half-of-sites flip-flop mechanism [39-42] (chapter 1.3.2). NaCl has been shown to have a strong effect on this presumed transition in ECAP [41].

An example of how complex the ionic activation can be, is seen for *Vibrio alginolyticus* AP which is highly homologous to VAP (93% sequence identity) and contains the large surface loop insert. At pH 8.0, the enzyme was highly activated by salt, but activation was not seen at pH 10 [43] (we observed similar results for VAP in paper II). The activation was shown to be dependent on the anion species, where chloride was shown to be the most activating anion. Furthermore, the effect of chloride activation was dependent on the concentration of a competitive inhibitor (SO_4^{2-}). Thus, the binding site for chloride and inhibitor was likely at the same site.

Another example comes from an AP from an extreme halophilic bacteria *Halomonas sp.* (HaAP) which has 70% sequence identity (Figure 1.5) and is highly structurally homologous to VAP, having the same gene inserts (Figure 1.6). The biggest difference is seen for surface residues where HaAP has 144 exposed Asp/Glu vs. 114 for VAP. In the crystal structure of HaAP, a chloride ion is bound in the substrate pocket where either a sulphate or a phosphate ion usually resides, coordinated by Arg129 and the Zn ion in the M1 site (Figure 1.6B). Unlike for VAP, no SO_4^{2-} was used in the crystallization conditions

of the halophilic AP (commonly used in high concentration in AP crystallization). Thus, SO_4^{2-} might have displaced a Cl^- during crystallization of VAP.

Figure 1.5. Sequence alignment of *Halomonas* sp. AP (3WBH) and VAP (3E2D). The signal sequence is denoted by a red box. The round mean square deviation (RMSD) of the alpha-carbons of the two structure is shown above the sequence as grey bars. The alignment was made using the Match-align plugin in UCSF Chimera.

Thus, APs that show increased activity with increased chloride concentration might all have a chloride competing for binding to the Zn in the M1 site, increasing the rate of phosphate product release. Moreover, chloride binding to Zn is further supported by Gettins and Coleman (1984) who observed Cl^- coordinated to Zn ion at the M1 site for ECAP using ^{35}Cl and ^{113}Cd nuclear magnetic resonance (NMR) [44]. Possibly, this binding is not facile in mammalian phosphatases because of steric constraints rather than direct interactions, since the Zn ligands show high conservation in identity and position.

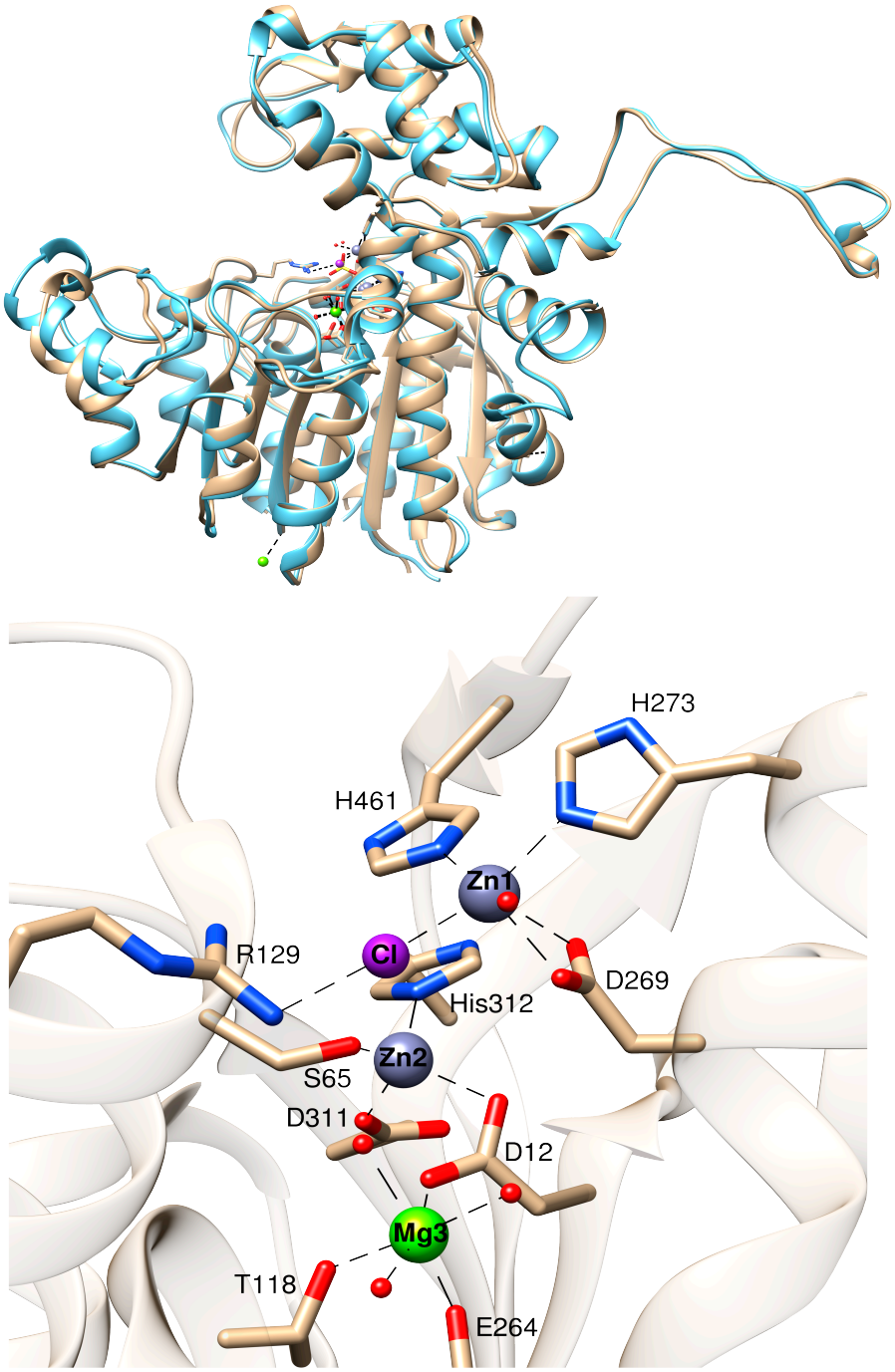

Figure 1.6 *Halomonas sp*. AP (PDB: 3WBH) structural alignment with VAP (PDB: 3E2D) shown above. Magnesium ion is shown as a green sphere and Zn ions as navy-blue spheres. Sulphate ion is shown in the active site (VAP) and a chloride ion in purple. Below: Active site of *Halomonas sp.* AP.

1.1.4 Role and distribution in nature

Due to the lack of substrate specificity of alkaline phosphatases towards phosphomonoester hydrolysis it has been difficult to determine their specific role. APs are widespread among organisms and are always found as ectozymes, that is an enzyme found outside of the inner membrane of a cell, or is secreted. Vertebrates express organ-specific isozymes, which can come in several isoforms (differently glycosylated). Most higher plants do not show alkaline phosphatase activity [45], instead they are rich of non-specific acid phosphatases and other substrate specific phosphatases. Alkaline phosphatase is also widely found in algae, molds, fungi, and all species of the animal kingdom [23].

Bacterial alkaline phosphatases

In bacteria, most APs are derived from the *phoA* gene (originally named *phoA* in *E. coli* and is the most common form of APs). The *phoA* gene in *E. coli* is a member of the *pho* regulon which contains 20 promoters which are inducible by phosphate starvation where *phoA* is regulated by *phoB* and *phoR* [46, 47]. Recently, an AP derived from the gene *phoX* has been characterized and shown to be far more common than initially thought [48], especially in marine bacteria [49]. In contrast to *phoA*, *phoX* is monomeric and is activated by Ca^{2+}. Since the AP under study in this thesis is of the *phoA* type, we will hereafter refer to APs as *phoA* alkaline phosphatases.

In bacteria, AP expression is induced by low phosphate in the medium. In Gram-negative bacterium, APs are secreted to the periplasmic space and are believed to function as phosphate scavengers while the phosphate pool is reserved in the cytoplasm [50]. Thus, the reason that the ECAP dimer is assembled in the periplasm is likely not due to stochastic chance but to protect the cell from active AP in the cytoplasm [51].

Since several bacterial alkaline phosphatases are affected by anionic strength (see in 1.1.3, 1.2.3 and Paper II), bacterial APs, among other hydrolases, might have a role in maintaining a constant ionic strength in the periplasm where the periplasm acts as a "homeostatic" compartment to protect the cytoplasm from changes in salt concentration. Originally, this was partially proposed by Stock et al. (1977) [52], where the volume and osmotic pressure of the periplasm were measured in different media for *E. coli* and *S. typhimurium*. The results indicated that the ionic composition of the periplasm can differ from that of the external medium, especially in a low-ionic strength medium. They

assumed that the outer membrane acts as a sieve permitting low molecular weight solutes to pass through but exclude larger molecules. It was proposed that polyanionic nucleic acids are the mayor source for the high negative charge inside the periplasmic space. Thus, here we propose that AP might dephosphorylate these nucleic acids to release inorganic phosphate, after nucleases would first digest the polyanionic nucleic acids, which could then penetrate out of the exoskeleton or be taken up into the cytoplasm. These enzymes, must then "sense" somehow the ionic strength where the activity of the hydrolases is tempered at low ionic strength (which is the case for ECAP and VAP). Thus, in low ionic strength medium, when AP activity is lower, large polyanionic nucleic acids would be retained in the periplasm, protecting the cytoplasm from osmotic shock. As the ionic strength increases the activity of AP is maximized and the ionic strength is kept constant by the release of inorganic phosphate. In fact, evidence for correlation between adaptation towards fresh water and AP activity has been shown for *A. castellanii [53]*, *Fundulus heterclitus [54]* and water eels. This concept could easily be tested by studying the effect on a *phoA-/-* phenotype of *E. coli* (such as strain LMG194). The knockout of *phoA* has normally no effect on the growth of *E. coli* in media rich of phosphate. However, the effect of changing the osmotic strength of the medium has not been tested on *phoA-/-* strains, to my knowledge.

Human AP

The properties and the role of human APs are in most cases very similar between mammalian species, with some exceptions [23]. Here, we will only discuss the role of the AP isozymes found in humans. APs are probably the most extensively studied enzymes in the human body. Four genes code for different organ specific APs, the placental (PLAP), intestinal (IAP), germ cell/placental like (GCAP) and tissue non-specific (TNAP) which is expressed in liver, bone, kidney and various tissues and are all a glycosylphosphatidyl-inositol (GPI) anchored. TNAP is also known to be differently glycosylated in the Golgi, where four isoforms are known in the bone [55]. In serum, AP activity is derived from TNAP (90% of total AP activity) where about half the TNAP activity comes from the bone isoform [56]. It is believed that a GPI specific phospholipase can release the GPI membrane-anchored AP to the bloodstream [57, 58].

Tissue non-specific AP (TNAP)

TNAP is functional as a homodimer (as all APs of the genotype *phoA*) and several mutations at the two-fold symmetric axis cause formation of inactive monomeric variants [59, 60]. Unlike the other isozymes, the crown domain of TNAP (see 1.1.2) has a low affinity to bind collagen [61]. Also, an N-terminal helical region stabilizes the dimer and has allosteric properties [62]. There is also some evidence that calcium modulates its activity by binding to a metal site normally occupied by Mg^{2+} or Zn^{2+} [63]. Thus, mutations located at the interface, on the N-terminal helix, in the crown domain or around the divalent metal ion binding sites can all cause defects in enzymatic activity.

Indications for the role of TNAP in bone and teeth mineralization have been accumulating for close to a century, first described by Robison (1923) [64]. Mutation in TNAP can lead to hypophosphatasia resulting in accumulation of inorganic pyrophosphate (PP_i), a substrate for TNAP and an inhibitor of mineralization of bones and teeth [65]. TNAP has also been shown to dephosphorylate osteopontin, an important calcium binding protein for bone mineralization and bone remodeling [66].

At least 300 mutations in TNAP are known to cause hypophosphatasia, which can be autosomal recessive or autosomal dominant [65]. The disease can cause stillbirths and be fatal for infants in the most severe cases. In the less severe cases, symptoms are not present until adulthood, usually involving dental problems [65]. However, in the more severe infantile cases, rickets, hypotonia and deformation of bones occurs. Recently, a recombinant form of TNAP (Asfotase alpha [or sALP-FcD_{10}]) has been administered intravenously to infants with severe hypophosphatasia with promising results (Figure 1.7) [67]. This variant of TNAP is produced in Chinese hamster ovary cells (CHO) as a fusion protein, excluding the C-terminal GPI anchoring motif of TNAP, but with the Fc region of human immunoglobulin G (IgG) gamma-1 attached to the C-terminus (for easy purification and prolonged serum half-life) and ten aspartate residues for drug delivery to the bone [68].

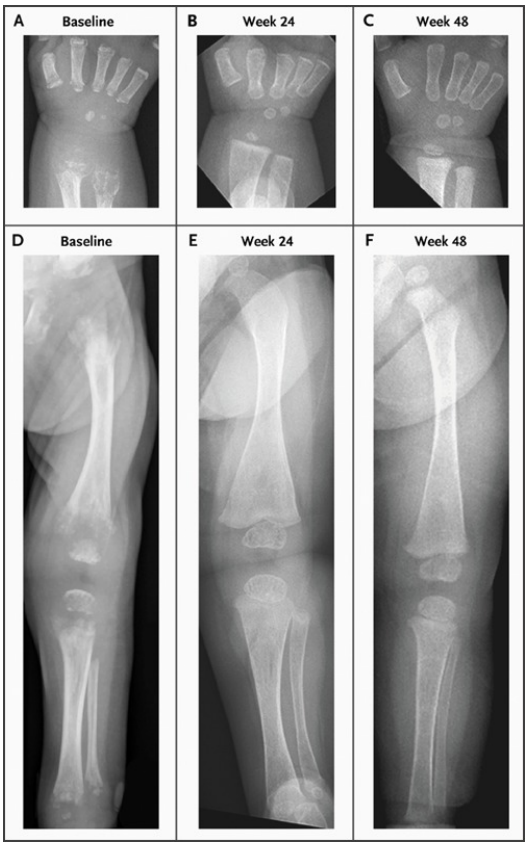

Figure 1.7. Radiograms of an infantile patient receiving recombinant TNAP intravenously, at baseline, 24 weeks after treatment and 48 weeks after treatment. Adapted from [67], support material.

In recent years, further roles of TNAP in several diseases, have been gaining a lot of attention, especially in cardiovascular diseases [55]. High serum levels of AP are linked to high mortality [69], especially when high phosphate and high AP activity are brought together [70]. Overexpression of TNAP has been linked to chronic kidney disease (CDK), especially in the vasculature which leads to vascular calcification and cardiac hypertrophy [55]. Since vascular calcification are linked to amounts of PP_i and phosphorylated osteopontin (both are potent calcification inhibitors), the link to TNAP activity and CDK is obvious, but what causes overexpression of TNAP is largely unknown. Vitamin D receptor activators have been used to downplay serum levels of phosphate and calcium (modulates AP activity) as a treatment in CDK [55]. Several potent small molecular drug inhibitors of TNAP have been synthesized, where the inhibitor SBI-425 inhibits vascular calcification in animal models [71].

Moreover, TNAP has been proposed to harbor “immuno-surveillance” mechanism [72, 73]. It is triggered by a nonspecific inflammatory signal (e.g. lipopolysaccharides [74] or ATP released due to cell/tissue damage) where TNAP ends up complexed to IgG. The

stimuli are shut down by dephosphorylation by TNAP. The TNAP-IgG complex is then finally taken up by endothelial cells or macrophages. Similar mechanism might exist at the blood-brain barrier [72, 75]. Furthermore, one study indicates that neuronal membrane bound TNAP is active in dephosphorylating the Alzheimer's-associated tau protein, possibly lessening its neuronal toxicity [76].

TNAP in kidney and liver is unknown, but possibly has a role in PP_i homeostasis and LPS inactivation [77].

Intestinal AP (IAP)

Intestinal AP contributes to gut mucosal defense and has a role in inflammatory responses and fat absorption [55, 65]. IAP is expressed in intestinal epithelial cells and is regulated by both nutritional and inflammatory factors [78]. It is believed to inactivate endotoxins produced by some bacteria such as LPS [79]. In animal models, IAP has been fed to mice and prevented metabolic stress when fed a high-fat diet [80]. Furthermore, IAP knockout mice have less diverse gut microbiome than wild type mice and when IAP was administered no difference was seen in gut microbiota compared to wild type mice. [81]. In zebrafish, IAP-deficient strains show hypersensitivity towards LPS toxicity. IAP activity was suggested to modulate optimal gut microbiota, normal homeostatic level of neutrophils and to promote mucosal tolerance to gut bacteria [82]. Moreover, IAP has possibly a role in bicarbonate segregation in rats where bicarbonate secretion increases the activity of IAP, locally, by an increase in pH which stimulates IAP activity. Purinergic receptors promote secretion of bicarbonate and are stimulated by ATP. The stimulation would be lessened by ATP dephosphorylation by IAP [83].

Curcumin (rich in turmeric) has long been thought to have a role in reducing inflammation. Its anti-inflammatory properties are believed to be caused by increased IAP expression in the gut, possibly explaining why the curcumin uptake does not need to be high for anti-inflammatory benefits to appear, since its effect is propagated in the gut [84].

Placental and germ cell APs (PLAP and GCAP)

Currently the roles of PLAP and GCAP are mostly unknown. These paralogous genes are highly homologous, with 98% sequence identity, where the only structural difference is seen in the crown domain. However, there are some speculations that these variants have a similar role in immunology as TNAP since they have also been found bound to IgG. PLAP and GCAP levels were determined to be higher during development of fetus than

postpartum. Mouse knockouts have shown PLAP and GCAP to be important for normal growth [85, 86].

1.1.5 Industrial use

Alkaline phosphatases from various sources have been used in industry and for research use. Alkaline phosphatase activity in cow milk is used as an indicator to assess the adequacy of pasteurization of milk, as the enzyme is thermally inactivated during pasteurization [87, 88]. In the research industry, APs have been widely used as an analytical reagent. APs have commonly been used for high precision detection in enzyme-linked immunosorbent assays (ELISA) to detect antigen concentrations in samples [89, 90], replacing radioactive assays. Horseradish peroxidase activity has also been used for the same purpose. In ELISA, AP is covalently linked to an antibody, and subsequently the turnover of a substrate is detected (usually with fluorescence) and then correlated to concentration of an antigen. It can be done directly where the enzyme-linked antibody binds the antigen (not common) or it can be done indirectly where an enzymatically-linked secondary antibody binds to a primary antibody which is bound to the antigen. APs have also been sold commercially for uses in molecular biology, mostly for dephosphorylating 5´phosphates of DNA to prevent unwanted ligation. Cold-active orthologs from Atlantic shrimp and the Antarctic bacterium TAB5 (NEB and Thermo) have been utilized for this purpose, due to the ease of their thermal inactivation.

Many enzyme-linked assays have been developed where the inorganic phosphate released is then usually assayed. Examples are assays for RNase [91] and UDP-glucuronic acid pyrophosphatase [92]. Generally, APs can be used for enzymatic assays if the molecule under study has a phosphomonoester group (except for highly bulky substrates). Recently, assays have been developed for the activities of nucleases, ribozymes and DNAzymes [93]. The drawback of using the APs in these assays is the need of assaying the inorganic phosphate which can be tedious. Several enzymatic linked phosphate assays have been developed such as the PiPer phosphate assay kit (Thermo) where maltose phosphorylase is linked to glucose oxidase and finally peroxidase is used to turn the fluorescence probe Amplex red to a fluorescent product which is detected by fluorometry [94]. Furthermore, a fluorescently labeled phosphate binding protein has been used successfully to detect inorganic phosphate in real-time in the nM range [95].

1.1.6 Cold-active alkaline phosphatases

Several cold-active APs have been purified and characterized, including the shrimp alkaline phosphatase (SAP), AP from the Antarctic bacterium TAB5 (TAP), *Shewanella* AP, AP from Atlantic cod and AP from *Vibrio splendidus* (VAP), the enzyme under study here and will be discussed more extensively in section 1.2. below.

Shrimp alkaline phosphatase (SAP)

This particular AP was purified and characterized by Olsen et al. [96] and later sequenced (amino acid and cDNA) by Nilsen et al. [97]. It was initially concluded that the monomers were functionally active using size-exclusion chromatography and activity staining of gels. [96]. Later, when the crystal structure was solved, the biologically active unit was shown to be a homodimer (Figure 1.8B) [98]. SAP has a predominately negatively charged surface, except for the active-site which has a positive potential surface. The SAP crystal was grown in 0.1 mM Zn^{2+} which caused displacement of Mg^{2+} from the M3 site for Zn^{2+}. Exchanging the Zn^{2+} in M3 with Mg^{2+} was shown to affect the rotameric position of the substrate binding Arg in the active site (equivalent to R166 in ECAP). Furthermore, the Arg residue was shown to adopt a "non-docked" position and "docked" conformation with ligand bound (phosphate) [99]. However, it could be disputed if SAP is truly cold-active, since it has similar T_{opt} as calf-intestinal AP (~40°C). Still, SAP has been sold commercially (NEB) to remove phosphorylated ends of DNA and RNA for subsequent use in cloning due to rapid inactivation. However, VAP is inactivated at even faster rate and lower temperatures and should be better suited for such applications.

Antarctic TAB5 alkaline phosphatase (TAP)

Rina et al. [100] first cloned and characterized this AP. The crystal structure was solved by Wang et. al [15]. TAP has the shortest polypeptide chain and the smallest dimer interface of known AP. The crystal structure shows that the interface is mainly stabilized by hydrophobic interactions (similar to VAP). The difference between this structure and other APs is that the crown domain is practically absent (Figure 1.8C). Furthermore, it has two additional magnesium ion binding sites (M4 and M5). The authors proposed that the Mg^{2+} ion in the M4 site stabilized the correct positions of R148 (the substrate binding Arg) and the Mg^{2+} in the M5 site might help release the negatively charged product. A glycine

cluster near the active site has been shown to be important for catalytic activity. The variant G262A (close to W260 in the active site) had a k_{cat} of less than 1% of the wild type, indicating that local flexibility around the active site is important. A directed evolution study of TAP revealed two mutations, H135E and H135E/G149D (H135 corresponds to D153 in ECAP), that increased k_{cat} by 2- and 3-fold and K_M increased by 10-fold in both cases [101]. Both these variants were also less thermostable. Crystal structures of H135E and H135D revealed only subtle changes in the active site, and the metal ion charge transfer network was not much altered. The authors promoted the idea of the magnesium ion not being important as a general base, but was necessary to stabilize the transitions state towards the phosphoryl transfer (as discussed in 1.2) [25, 26]. However, the authors used a puzzling approach in promoting Mg^{2+} binding to the third metal site by having first 0.1 mM Zn^{2+} in buffers and then afterwards exchanged the Zn^{2+} out of the M3 site with excess Mg^{2+}. Magnesium should have been retained in the active site from the beginning.

Shewanella AP (SCAP)

Ishida et al. (1998) [102] characterized and purified an AP from a Gram-negative proteobacteria *Shewanella sp.* isolated from intestines of shellfish living in the Antarctic ocean and subsequently cloned and expressed in *E. coli* [103]. The optimum temperature for catalysis was around 40°C during a 5-min assay period and the enzyme was unstable at room temperature on standing for several hours [102]. The crystal structure of SCAP shows similar active site properties as other cold-active APs. However, the Zn^{2+} ion was missing in the M2 site (possibly dissociated out during crystallization) and there was an additional Mg^{2+} binding site present at the dimer interface (Figure 1.8D) [104].

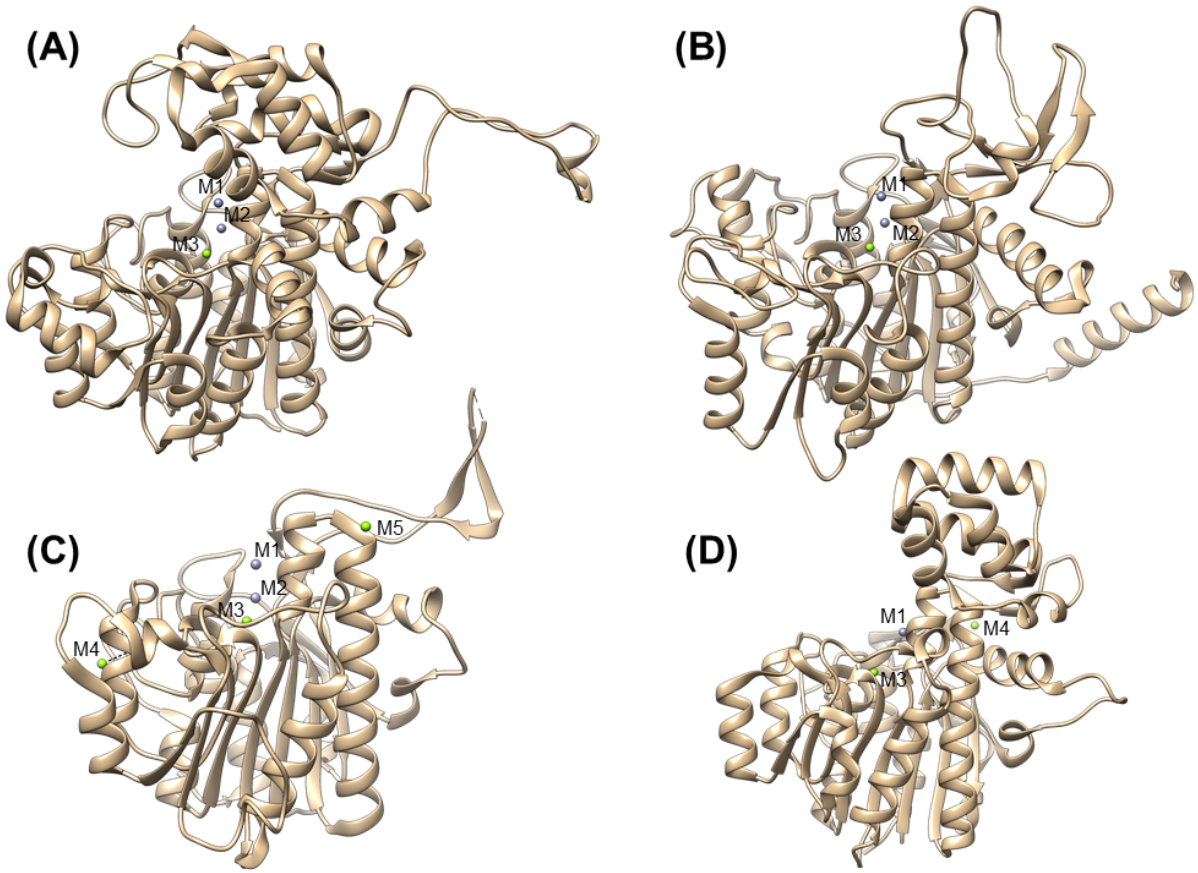

Figure 1.8. Cold-active alkaline phosphatases. (A) VAP (3E2D) from *Vibrio splendidus*, (B) SAP (1SHQ) from *Pandalus borealis*, (C) TAP (2IUC) from Antarctic bacterium and (D) SCAP (3A52) from *Shewanella sp.* Zinc ions are shown as navy-blue spheres and magnesium ions as lime-green spheres.

Atlantic cod AP

Atlantic cod AP has a high sequence similarity to human tissue non-specific AP (TNAP) [105]. It was originally purified from the pyloric caeca of the digestive tract [106] and from the small intestines [105]. Repeated attempts at its cloning and expression in *E. coli* have been unsuccessful (unpublished). It displayed significantly more activity at 5°C than calf intestinal AP, and was more stable than the bacterial cold-active orthologs, losing little activity at 45°C for 2.5 hours. Cod AP was also sensitive towards EDTA inactivation (pH 8.0), comparable to the mammalian phosphatases. An extensive study on dimer-monomer equilibrium was studied using GdmCl denaturation [107]. It revealed a three-state pathway: $N_2 \rightarrow 2M \rightarrow 2U$, where the active dimer (N2) transitioned to inactive monomers (M) which was then unfolded (U). The dimer to monomer transition had the major contribution to total free-energy of the process from the active enzyme towards the unfolded species. Inorganic phosphate at 1 mM was shown to destabilize the dimer, but

stabilize the monomers. Similar observations were made for VAP regarding the effect of phosphate on the dimer dissociation constant (paper II) [6]. When the measurements were repeated for cod AP using urea, the denaturation process was a four-state process: $N_2 \rightarrow I_2 \rightarrow 2I \rightarrow 2U$, where the enzyme went through a transition to an inactive dimer intermediate, (I_2) which then dissociated to inactive folded monomers which then finally unfolded [108]. However, the folded monomers were poorly populated. The enzyme could be reactivated by dilution, but the reactivation was dependent on the initial urea concentration, the incubation time and glycerol content in the reactivation buffer. The difference between the observations made using GdmCl and urea is likely due to stabilizing effect of chloride on the active site. An interesting observation was made where one zinc ion was shown to dissociate as the enzyme was inactivated. Similar observation has been made for VAP [6].

1.2 *Vibrio splendidus* alkaline phosphatase

1.2.1 Discovery and cloning of VAP gene for expression in *E. coli*

The first report of alkaline phosphatase from *Vibrio splendidus* described its purification from a strain that was designated *Vibrio splendidus II* strain 2 [109]. The last purification step was done on a tyraminyl-Sepharose affinity column (arsonate containing moiety) with a purification factor of 108. However, in this report, the enzyme was not further characterized.

The enzyme cloned by our group came from seawater bacterium collected from the coast around the city of Reykjavik (Iceland) during summer when water temperature was around 8°C [110]. Bacterial colonies were isolated and the colonies showing the highest AP activity (using 5-bromo-4-chloro-indolylphosphate) were selected and cultured. More than 200 bacterial clones were found. The following selection criteria were then applied: 1) maximal secretion of AP activity into the medium and 2) binding to an L-histidyldiazobenzylphosphonic acid agarose affinity column [111]. Eight strains showed high activity of secreted AP but only one strain bound to the affinity column. This strain was named G15-21 and 16S rRNA gene comparison showed it was of the genus *Vibrio*, most likely *Vibrio splendidus*. The gene was sequenced [112] and later confirmed by meta-genomic analysis to be of 100% identity to the strain *Vibrio splendidus* (NCBI reference: WP_017079505.1). The enzyme was purified in two steps, first on an affinity column (L-histidyldiazobenzylphosphonic acid agarose) followed by Sephadex S200 size exclusion column where the purification factor was 151-fold. It was later expressed in *E. coli* with a

StrepTag-II affinity tag attached to the C-terminus, where the tag was shown not to affect the kinetics or the stability of the enzyme [113].

1.2.2 Catalytic properties and stability

VAP showed high catalytic efficiency at 15°C, having similar alkaline pH optimum as ECAP [110]. However, this pH optimum can be altered by the conditions applied during measurements, such as buffer composition, ionic strength (chapter 1.2.3 and Paper II), substrate applied (and its concentration) and the presence of transphosphorylating agents such as ethanolamines (e.g. Tris or diethanolamine). The K_M of VAP is highly affected by pH, where it increases over 20-fold going from pH 8.0 to pH 10.5. Thus, the pH optimum (in terms of k_{cat}) was initially defined lower when using 1 mM pNPP substrate [110] than when repeated with 5 mM pNPP substrate (paper II) [6], the K_M at pH 10.0 being close to 1.0 mM compared with 0.05 mM at pH 8.0. In terms of VAP's role as a phosphate scavenger, VAP would function poorly at high pH.

VAP was shown to be extremely thermolabile (at low ionic strength), with half-life of 6 min at 40°C [110] and $T_{50\%}$ of 25.8 °C at pH 8.0. Furthermore, the enzyme proved extremely sensitive to urea, where the enzyme lost half of its activity in 0.4 M urea at pH 8.0 [113-115].

VAP has one Cys residue (Cys67) close to the active site. By introducing other Cys-residues near the native Cys, individual intrachain disulfide bonds were formed. All the Cys disulfide-linked variants showed ~10% of the wild type k_{cat} and all variants showed increased heat stability in terms of heat inactivation ($T_{50\%}$) indicating that local flexibility near the active site is important for optimal function. The global thermal stability of the folded state (T_m) was unaffected by the disulfide formation, indicating that the active conformation was not linked to stability of the native tertiary fold or dimer stability.

As for TAP, the non-conserved metal ion binding residues of VAP at the M3 site have been mutated towards their counterparts in ECAP [114]. These are the variants H116D, W274K and the double variant H116D/W274K. The Asp-Lys pair is present in ECAP, whereas a His-His pair is present in mammalian variants and other vertebrate APs.

The W274K and the H116D/W274K VAP variants showed increased thermal resistance towards inactivation and slight increase in global stability. The H116D showed a slight destabilization. All the variants showed increased K_M, the highest being for the double variant. Possibly a salt bridge was formed between D116 and K274 resulting in the

increased stability which could alter the coordination of the substrate binding Arg, or the zinc ligand.

1.2.3 Effect of ions on catalytic activity and stability

Paper II explains in details how ionic strength and how anions increase the turnover and stability of the enzyme [6]. The main result was that chloride was the most effective ion and that the effect of chloride was pH dependent. At 0.5 M NaCl and pH 8.0, the $T_{50\%}$ increased to 53.5°C from 25 °C in the absence of added salt. At pH 8.0 and 0.5 M NaCl, the k_{cat} increased approximately 4-fold with no increase in K_M. This rate enhancement was due to the enzyme having less affinity for the inorganic phosphate product (measured as an increase in K_i). At pH 10.5, NaCl had no effect on k_{cat} or stability but a large increase in K_M was observed. The possible mechanism of chloride activation is discussed in Paper II and III and chapter 1.1.3.

1.2.4 Crystal structure

VAP was initially believed to exist as a functional monomer, due to faulty analysis of activity stained native gels (similarly, SAP was thought to be a monomer on the same grounds as discussed in 1.1.7). Later, when the VAP crystal structure was solved, the biological unit was shown to be the homodimer [116]. The major difference seen for VAP, compared to other APs, was the large surface loop which hovers over the active site of the other monomer. Also, VAP has two inserts at the crown domain, making the crown domain the largest for APs (discussed in chapter 1.1.1). The surface of VAP does not have as large negative character as SAP, but has a relatively more negative surface than PLAP and ECAP. The active site has a net positive areal electrostatic potential (as most APs) and has a considerably narrower entrance due to the large crown domain. The monomers are mostly arranged by a rotational symmetry, but the catalytic Ser65 was found in two different conformers in the two monomers. The dimer interface has a similar set of non-covalent interactions as other APs except for having relatively more side-chain to side-chain hydrogen bonds. The dimer interface was found to have similar buried accessible surface area as other APs.

1.2.5 Promiscuous enzyme activity

Although the results of this thesis do not contain promiscuity data for VAP, this chapter was written due to ongoing work in the research group that revolves around VAPs

promiscuity, either towards sulphate monoesters, beta-lactams or peptide bonds (protease activity). These characteristics are intertwined with the properties under study here, such as the salt effects, and mechanistic discussions.

It is now well established that many enzymes show activity towards chemically distinct substrates, some of which are quite different from their native reactions. Jensen [117] first proposed this property of enzymes in 1976 and termed it “substrate ambiguity”. He proposed that a pathway would exist from one ancestral protein, where specificity evolved by subsequent gene duplication of the ancestral protein. Today, this property of enzymes is termed enzyme promiscuity, where enzymes catalyze a chemical reaction other than their native, albeit with much lower catalytic efficiency. Enzyme promiscuity should not to be confused with “protein moonlighting”, which is a term that describes newly discovered secondary functions of proteins with already defined roles.

The role of flexibility in evolution of enzymes towards new activities has been pointed out by several investigators [118-121], and has been termed “protein evolvability” (by Prof. Dan S. Tawfik [122]). By this approach enzymes are not considered as rigid entities with one functional state but rather as an ensemble of multiple states. Thus, promiscuous enzymes have the propensity towards more populations of catalytically relevant states. Tawfik et. al [123] found that mutations that are neutral towards activity and stability of an enzyme can increase the enzyme evolvability towards promiscuous activity. These mutations lie mostly in loop regions; thus, the term flexibility has been linked to evolvability. One example are serum paraoxonases (PON), which belong to a family of detoxifying enzymes in mammals [124]. The name comes from PON1 ability to hydrolyze the pesticide paraoxon with catalytic efficiency near the diffusion limit. This pesticide has not been around in nature for more than 60 years, so how can there exist an enzyme that hydrolyses this substance with such high specificity? It turns out that PONs are a group of highly promiscuous lactonases [125]. It seems that detoxifying enzymes such as PONs might need to be more evolvable and be able to adopt more states for a possible defense against new toxins.

Many hydrolases have been shown to be catalytically promiscuous for a wide range of substrates [119]. Promiscuity in phosphate and sulphate transfer enzyme has been widely established [126]. These enzymes have in many cases similar catalytic residues and active site topology regarding metal ion coordination. Figure 1.9 shows active sites and relative catalytic efficiencies of four hydrolases, each catalyzing its native function;

phospho monoester hydrolysis (AP), phosphodiester hydrolysis (nucleotide pyrophosphate phosphodiesterase [NPP]), phosphonatemonoester hydrolysis (phosphonatemonoester hydrolases [PMH]) and sulphatemonoester hydrolysis (arylsulphatases [AS]). No correlation has been found between charges or the type of ion in the active site, as means towards discrimination between these substrates.

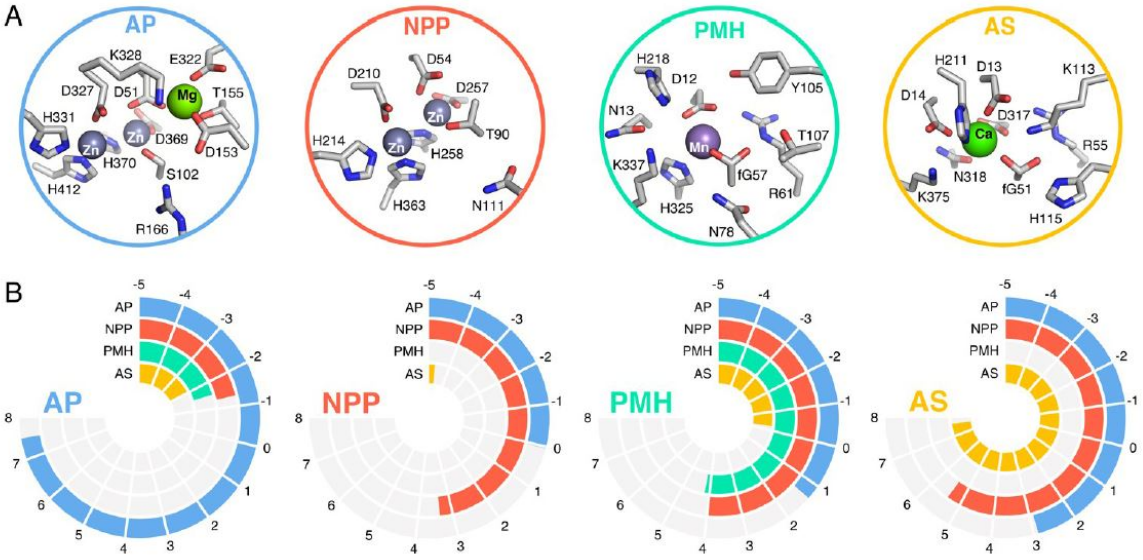

Figure 1.9 Active site of sulphonyl and phosphate esterases. (A) Active sites of ECAP (AP, PDB: 1ED9), *X. citri* nucleotide pyrophospodiesterase (NPP, PDB: 2GSN), *R. leguminosarum* phosphonatemonoester hydrolase (PMH, PDB: 2VQR) and *P. auruginosa arylsulphatase* (AS, PDB: 1HDH). (B) log10 (k_{cat}/K_M) for phosphomonoester hydrolase activity (blue bars), phospho diester hydrolysis activity (red bars), phosphonate monoester hydrolase activity (teal bars) and arylsulphatase activity (yellow bars). Data was taken from [127] and figure was adapted from [128].

Alkaline phosphatase promiscuity

ECAP has been shown to harbor substantial activity towards hydrolysis of sulphate monoesters [129] (also VAP, unpublished results). ECAP was also subsequently shown to have phosphodiesterase activity [130] (remains to be tested for VAP). The sulphate monoester hydrolysis of ECAP is about nine-orders of magnitude slower (pNPP vs para nitrophenyl sulphate [pNPS]) and the phosphodiesterase activity is five-order of magnitude slower (pNPP vs. methyl 2,4-dinotrophenyl phosphate [MDNPP]). The same residues are needed for efficient catalytic efficiency (R166 and S102) and inorganic phosphate is a competitive inhibitor for sulphatase activity [129] as well as phosphodiesterase activity [130]. Both experimental and computational approaches have been applied to answer how the enzymes evolve to catalytically discriminate between these substrates, mainly

regarding the difference of the transitions state of the chemical step [126, 131-133]. For APs, the rate limiting step is the release of the inorganic phosphate product. So, in order to be able to experimentally compare phosphomonoester hydrolysis with promiscuous activity, where the chemical step is the rate limiting step, some alterations to standard assays needed to be made. O'Brien and Herschlag [134] have employed an assay using alkyl phosphomonoesters under pre-steady-state conditions ([S] close to [E]) to determine k_{cat}/K_M with the chemical step as the rate-determining step [129, 130, 134]

The structural difference between sulphate monoesters and phosphate monoesters is small. Sulphate monoesters have a single negative charge and phosphate esters have a double negative charge at neutral pH. Aryl sulphatases (AS) have a bimetallo zinc center while APs have three divalent metal ions, all which are important for catalytic activity. Thus, the more negatively charged the substrate is, the more positively charged the active site might be. However, the charge difference can only partially explain the preference for each substrate for AP vs AS, since protein tyrosine phosphatases (PTPs), which do not contain metal ions and have close to neutrally charged active sites, do not show any preference for phosphate monoester hydrolysis over sulphate monoester hydrolysis [32]. Andrews et al. [32] proposed that positioning of dipolar hydrogen bond donors within the active site determines the specificity. Furthermore, the binding interaction(s) of R166 are possibly not only contributed by its charge but also the geometry of the guanidium group [135].

Is VAP functional as a protease?

Recently, we have found evidence of VAP being a functional protease (Bjarni Ásgeirsson, unpublished results). Initially, self-cleavage activity was only observed if the enzyme was incubated at low ionic strength. Figure 1.10 shows cleavage sites for VAP detected using MALDI-TOF-MS peptide mass fingerprinting of HPLC purified peptides from VAP autolysis experiment. Both the N- and C-terminus of the digested peptides mostly had a charged amino acid both positive and negatively charged, indicating the importance of a charged amino acid next to the cleavage site. However, the specificity of the enzyme as a protease is not clear and the enzyme seems to be rather unspecific towards protein digestion. Interestingly, the crown domain was nearly intact (or possibly over digested). Ongoing experiments are being conducted, e.g. towards the cleavage of typical protein substrates.

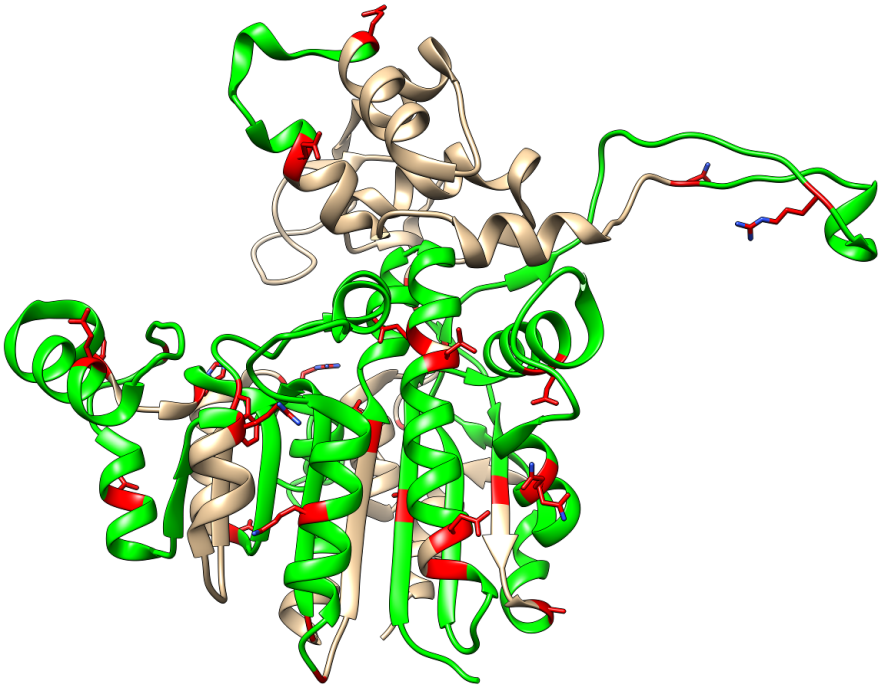

Figure 1.10. N- and C-terminal cleavage sites for VAP autolysis. Figure was rendered in UCSF Chimera using MALDI-TOF-MS data of cleaved fragments from VAP autolysis (Bjarni Ásgeirsson, unpublished results). The sample was diafiltrated into 10 mM Tris pH 8.0 using a YM30 centrifugal filter unit in the cold. The mass spectrometric analysis was both performed in-house as well as at the Proteome Factory AG (Berlin). Amount of protein in samples was 50 µg. The Mascot Search Service was used to identify peptides.

This is not the first case of reported protease activity of an AP. Chakraborty et al. [136] reported shrimp AP (SAP) having activity towards cleaving a protein substrate and towards self-cleavage. The latter activity was induced by the addition of EDTA. Neither ECAP or calf intestine AP showed any proteolytic activity. Here, a computational method termed catalytic active site prediction (CLASP) was used to predict the proteolytic activity of SAP. In this method, a motif of an enzyme with a known function is used where distances and potential differences of key residues (e.g. the catalytic triad for Ser proteases) are mapped and compared using a computer algorithm. This approach also indicated that VAP has potentially a β-lactamase activity and VAP was inhibited by the β-lactamase inhibitor imipenem [137]. However, VAP showed no detectable β-lactamase activity over relatively short incubation periods compared with several days that might be needed [137].

Another indication of proteolytic activity in an AP came from crystal structure studies of the rat intestinal AP [138]. The enzyme was expressed both in *E. coli* and Sf9 insect cells and subsequently crystallized. In both cases, the structure was the same, except

glycosylation did not occur in *E. coli* and the crown domain was missing for the *E. coli* expressed enzyme. The authors found that the crown domain was cleaved when the enzyme was kept at room temperature for prolonged periods. Since the cleavage was inhibited by protease inhibitors (Sigma protease cocktail) the authors concluded (possibly incorrectly) that the crown domain was cleaved by protease impurities, but the enzyme expressed in the insect cells was protected due to glycosylation. Possibly the proteolytic activity of the rat intestinal AP was inhibited by some of the inhibitors in the protease inhibitor cocktail or by metal chelation of EDTA (present in the cocktail). For example, 4-(2-aminoethyl) benzene sulfonyl fluoride (AEBSF) is a potent inhibitor for both VAP and ECAP. 10

1.3 Protein quaternary structures and symmetries

Protein symmetry has always fascinated me. However, it is the break of symmetry, or asymmetry, which is often relevant during a functional event. Quaternary structure (oligomerization) of proteins seems to be quite important for cellular functions. Most proteins in cells are found as symmetrical oligomeric complexes with two or more subunits. Crystallographic group symmetries are shown in Figure 1.11. The most common group symmetry is the cyclic C2 group where subunits are related by a twofold axis of rotational symmetry (homodimers). Higher order cyclic complexes exist as $C_{n(n>2)}$ with higher order rotational symmetries but are much rarer and typically involve proteins where directionality is needed, such as when one side interacts with a membrane or a hollow tube/chamber is formed (e.g. Porin). Dihedral complexes form $D_{n(n>1)}$ symmetry groups and have two symmetry axes, where one is a twofold rotational axis and the other of higher order. Thus, D_2 symmetry can be considered a dimer of dimers and D_3 symmetry a dimer of trimers etc. Dihedral groups are common for cytosolic enzymes (mostly D2 tetramers) and have more types of interfaces, therefore having higher propensity for allosteric control. Cubic complexes are the largest and can have tetrahedral (T), octahedral (O) or icosahedral (I) symmetries: For example, an octahedral homomer has 24 subunits with twofold, threefold and fourfold symmetries. Cubic complexes usually function as compartments for storage and transport [139, 140].

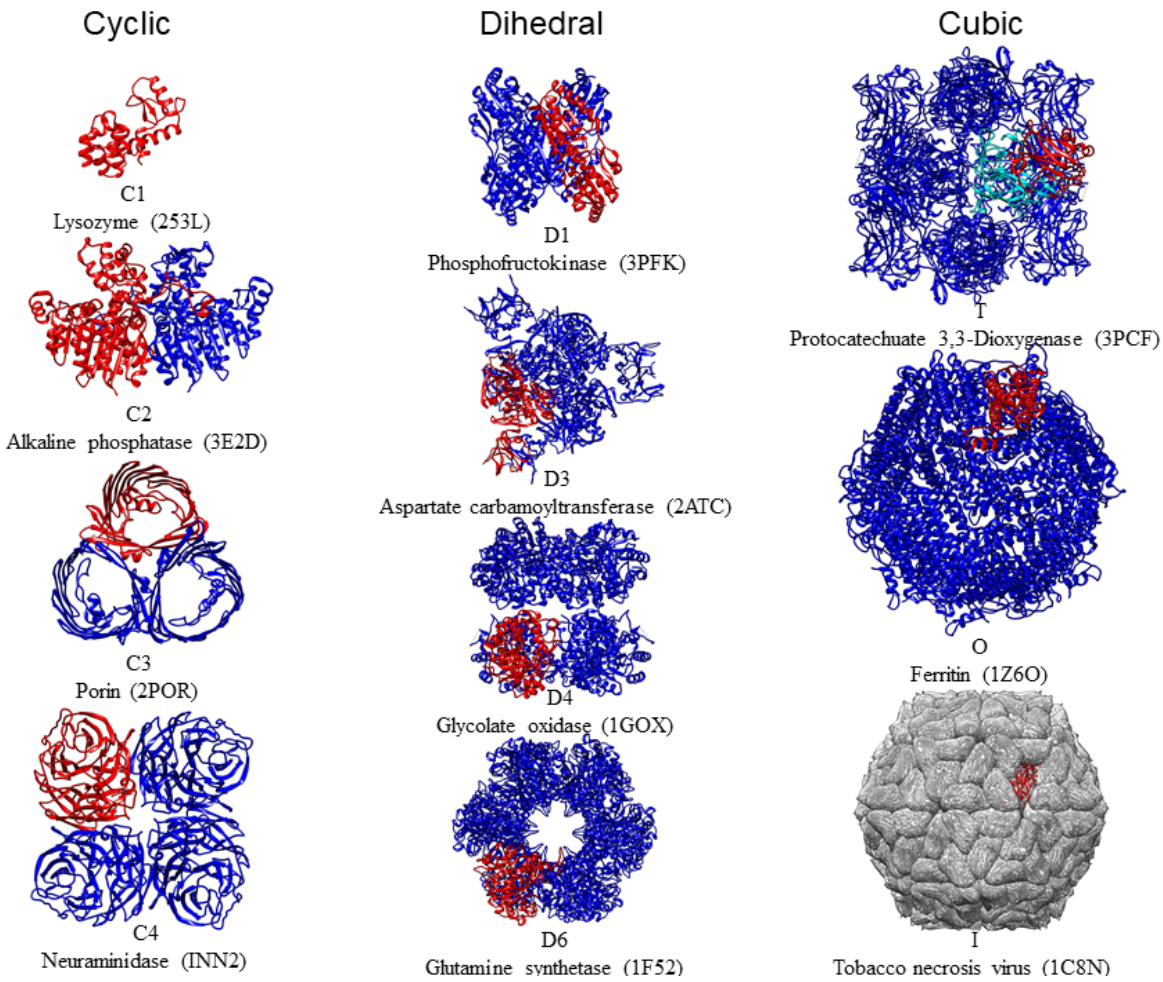

Figure 1.11. Crystallographic group symmetries. Point group symbols are shown below each protein structure. Note that higher cyclic symmetries are known, but are rare. This figure was inspired by Figure 1 in Goodsell and Olson [140].

A survey of all SWISS-PROT annotated proteins sequences in *E. coli* (year 1998) show that roughly 80% of the proteins are found as oligomers, where about 40% are dimeric and 20% are tetrameric [140]. Approximately 15% of the oligomers are heteromers. Generally, heteromeric proteins are regarded as being stable and purifiable entities. Weakly associated protein-protein interactions most likely exceed the number of stable homomeric complexes but many of these interactions have unknown function, are weak but still co-purify with a target protein in proteomic experiments [141]. Heteromers often adopt simple pseudo symmetries which resemble symmetric homomers, sometimes even with uneven stoichiometries [142]. It turns out that heteromers are much less evolutionary ancient than homomers, where the larger the heteromer the more “evolved” the protein has become [142]. Furthermore, there is evidence that the more evolved proteins become (less homology between subunits in a heteromeric complex) the more flexible the protein complexes tend to be. [142]. Also, the tendency is that the more ancient

interfaces of homodimers are, the larger they are [143, 144]. This may not be so surprising, giving the two most common mechanisms for heteromer evolution (Figure 1.12). Gene duplication or gene fusion always results in oligomeric complexes with smaller interfaces and which are more flexible. Gene duplication is more common in eukaryotic complexes while gene fusion is more common in prokaryotes. Examples for highly evolved heterocomplexes by gene duplication are the archaeal thermosome and proteasome, encoded by 8 and 14 paralogous genes, respectively [145].

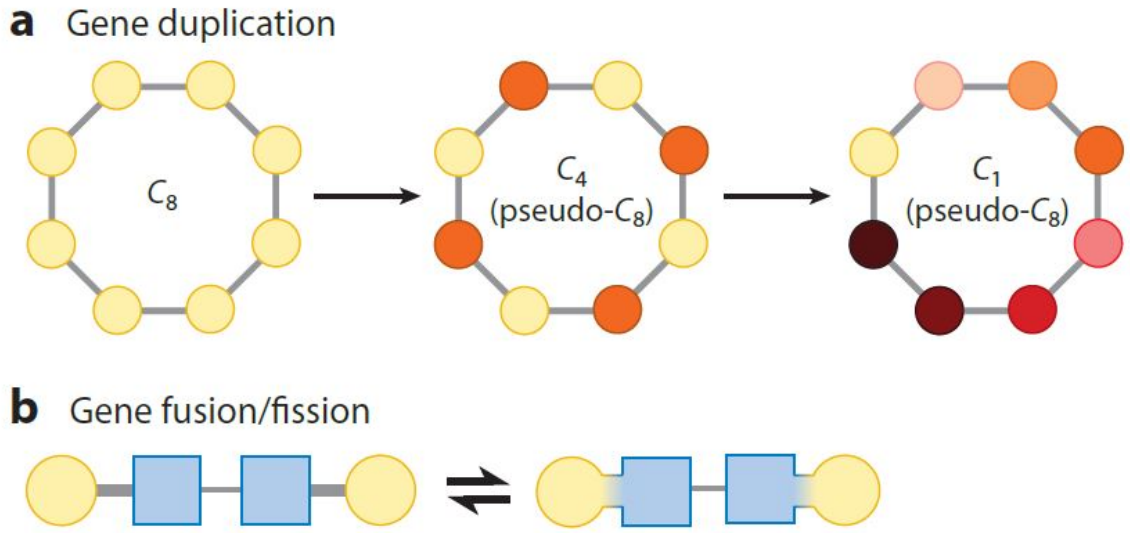

Figure 1.12. Mechanism for evolution of protein heterocomplexes. (a) Gene duplication. A gene duplication results in two proteins (yellow and orange circles) still interacting at the interface (here with C8 group symmetry). During separate evolution of each of the genes a C4 heterodimer (pseudo-C8) is formed. Further duplication events can occur where all subunits become distinct paralogs forming a complex where all subunits are derived by separate genes (here shown as C1 group symmetry and pseudo C8 symmetry). (b) Gene fusion/fission. Two different genes fuse together forming higher order heterodimeric complexes. The reverse (fission) happens rarely. Figure adapted from [139].

The function of proteins is usually driven towards larger proteins by evolution. However, the cost of protein synthesis limits the size. The average size of proteins is in the 30-50 kDa range, which seems to be a middle ground for these two factors (function and cost). [140]. However, being large is not always functionally beneficial. Secreted proteins are commonly monomeric since oligomeric complexes dissociate at low concentrations, except when the complexes are covalently linked via disulfide bonds. Furthermore, some proteins need to be small for rapid diffusion, such as hormones and toxins [140].

1.3.1 The importance of being dimeric

Since APs are dimeric enzymes we will focus the discussion about functionality of oligomeric structures towards homodimers.

The function of dimerization can simply be the formation of an active site at the interface. However, most homodimeric enzymes have two active sites, each located at the distinct subunit. Monod et al. [146], were among the first that emphasized the importance of dimerization, where isologous associations give closed structures with an increased stability due to smaller surface-to-volume ratio [147]. *In vivo,* formation of a dimer prevents the formation of unwanted interactions at the buried interface during folding. Saving of genetic material has also been mentioned as a factor favoring homodimer formation [148]. Furthermore, a shorter mRNA would need less energy to synthesize and possibly be easier to regulate than a larger mRNA. Even though allostery (binding to another site), which affects function of an enzyme or receptor, is more common in higher order oligomers [149], especially in complexes of dihedral symmetry [140], it is more common in homodimers than monomers [139]. However, the advantage of being dimeric might arise from a functional perspective i.e. cooperativity or allostery.

1.3.2 Cooperativity and allostery of dimeric enzymes

Allostery and cooperativity are different but related phenomena for enzymes. Allostery is generally thought of as a mechanism involving binding of a ligand at one site which influences the activity at a distant site. Heterotropic allostery involves a binding of a distinct ligand which affect the activity at the chemically active site, and which is different from the substrates of the enzyme. Homotropic allostery, on the other hand, involves interactions of a macromolecular system where two or more identical ligands (substrate) bind with different affinities. For example, a homodimer with two identical active sites can show negative cooperativity if binding to the first subunit induces a reduced affinity for the same ligand in the other subunit. Positive cooperativity, on the contrary, increases the affinity at the second site after binding of the first ligand. Two models are generally used to describe homotropic allostery (Figure 11.3A and B): the Monod-Wyman-Changeux (MWC) model [146] and the Koshland-Némethy-Filmer (KNF) model [149]. In MWC model, the receptor/active sites are identical and upon ligand binding a conformational change is observed simultaneously in both subunits. In the KNF model, the conformational change between high and low affinity state is only induced in one subunit at a time. It is likely that more complex equilibria exist in the unbound subunits which have led to more

complex models being proposed, such as by Hilser and Thomson (HT model) [150] (Figure 1.13C). The HT model was initially proposed for intrinsically disordered proteins, where the protein adopts several intermediate folded/misfolded states in the unbound form. However, this model could, in theory, also describe instances where preexisting asymmetry is present in subunits, such as rotameric flips. Examples of this are to be found in human caspase 9 [151], *E. coli* aspartate transcarbamoylase [152] and *Rhodopseudomonas palustris* fluoroacetate dehalogenase [153]. These enzymes all have experimentally confirmed half-of-sites reactivity. However, half-of-sites, or part-of-sites, reactivity (for higher order oligomers) has only been experimentally observed for about 1% of the homooligomeric structures in the PDB database [154]. This is likely to be underestimated (or undetermined).

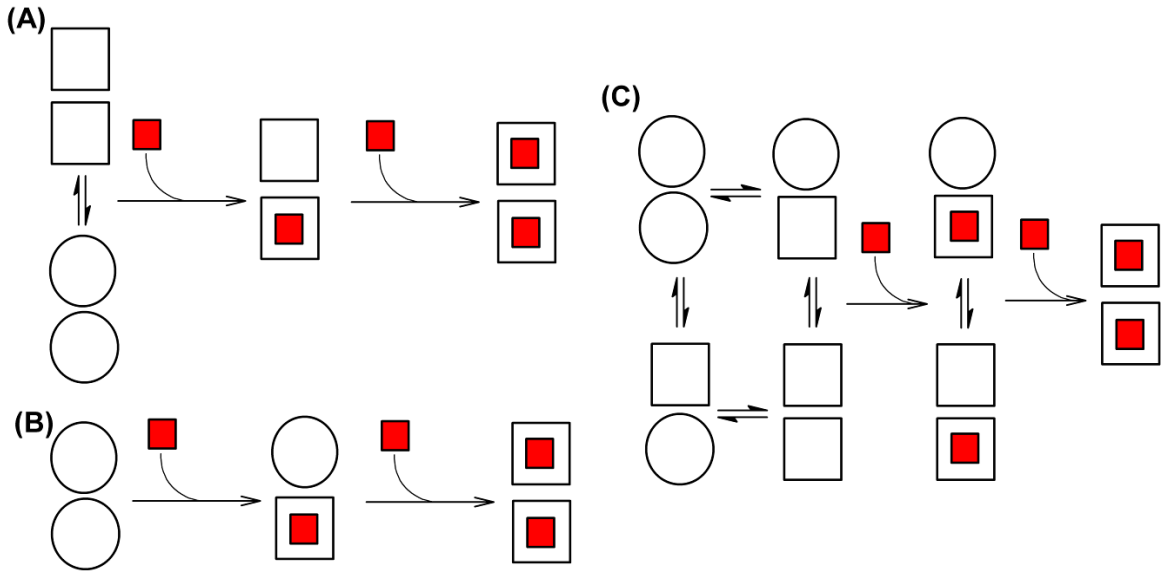

Figure 1.13. Homotropic allosteric models for dimers (A) the MWC model where binding of a ligand/substrate leads to simultaneous conformational changes affecting both sites. (B) KNF model where binding leads to conformational change at one subunit and the cooperativity is mediated through interface contacts. (C) HT model, where equilibrium exist between high and low affinity states of binding sites towards ligand substrate, where the conformations are pre-existent [155, 156]. This figure was inspired by Figure 1 in Freiburger et al. [157].

Half-of-sites activity is sometimes further characterized by separation into half-of-sites binding (HOSB) and half-of-sites reactivity (HOSR). [154]. HOSB and HOSR can be observed at the same time where only one subunit binds and catalyzes the reaction while the other subunit has only a stabilizing role for the structure of the enzyme. In this case the enzyme is found as E/E, ES/E and EP/E but never found in ES/ES, where E is the enzyme in the unbound state, ES the enzyme bound Michealis-complex and EP the enzyme-product complex (excluding covalent intermediates, for simplicity) with examples being found for cyclooxygenase-2 and microsomal prostaglandin E-synthase-1 [155, 156].

However, many homodimeric enzymes show all-of-the-sites binding (AOSB), where substrate analogs (inhibitors) bind to both active sites, usually detected by X-ray crystallography (which is the case for APs). These complexes can show negative cooperativity and HOSR, where only one active site performs catalysis with substrate still bound in the other subunit. Thus, the enzyme can be found as ES/E, ES/ES or ES/EP (or EP/EP when saturated with an inhibitor), but never visiting the E/E state in each cycle. Here, the binding to the second subunit might energetically facilitate the binding of the other subunit towards the substrate affecting the transition state barrier. There are fewer examples of this mechanism than for the HOSB/HOSR, but it seems to exist for dihydroorotate dehydrogenase A from *Lactococcus lactis* [158]. The last case of HOSR is the flip-flop mechanism where subunits reciprocally cycle between high and low affinity for substrate and product respectively (many have related the term half-of-sites only to this "two-piston" mechanism, but half-of-sites has a broader meaning as discussed above). Here, the enzyme cycles between ES/EP, ES/E or EP/ES, E/ES but is never found in either E/E or ES/ES during the catalytic cycle. Flip-flop mechanism is only observed in enzymes that show negative cooperativity.

Half-of-sites reactivity has been proposed for AP, but has never been fully confirmed. The dimer of ECAP shows negative cooperativity for both substrate and product binding [28, 31, 159-162]. VAP might show such negative cooperativity and half-of-sites reactivity. In Paper III we were interested to see if an inactive dimeric state resembled a “locked” conformation unable to perform a conformational change. However, we have currently no information regarding the type of half-of-sites reactivity in VAP as discussed above.

The work showing the third-of-the-sites reactivity (part-of-the-sites reactivity) of the trimeric calf purine nucleoside phosphorylase (PNP) is an excellent case which describes well the pitfalls when studying part-of-sites or half-of-sites reactivity. Initially, the enzyme was shown to have one-per-trimer binding stoichiometry of the reaction product hypoxanthine and a transition-state analogue inhibitor [163-165]. However, when the crystal structures, were soaked with the reaction product or inhibitor, ligand molecules were found bound to all three active sites [166, 167]. The presumed third-of-the-sites reactivity turned out to be the result of an assay artifact due to the presence of a “hitch-hiking” hypoxanthine product in a subset of active sites during purification, where in the end the enzyme was shown to have subunits that work independently [168, 169]. Another

example for faulty analysis came from the recombinant form of tryptophanyl-tRNA synthetase where Trp molecules were frequently found bound to the enzyme after purification [170]. Similarly, phosphate is found to occupy both active sites of ECAP during purification [162] and sulphates are present in the original VAP crystal structure. However, after removing the phosphate from the active site of ECAP by denaturation and subsequent refolding the subunits show clear negative cooperativity for inorganic phosphate [162].

1.3.3 Mechanisms for half-of-sites activity of dimeric enzymes

One method to detect half-of-sites reactivity is to engineer a subunit with an inactive active site and associate the native subunit with the inactive subunit to form a heterodimer. There are three possible outcomes for the effect of forming the heterodimer in this way: (i) the heterodimer has same activity as the native dimer, thus only one subunit catalyzes in each turnover, where the role of the other subunit is unknown (remember that individual subunits are inactive but interface contacts are needed for catalysis); (ii) the heterodimer has half the activity of the native enzyme per mole, therefore the enzyme shows independence of the other active site (not half-of-sites reactive) and (iii) the heterodimer has lower than half activity, where the subunit must reciprocally switch between low and high affinity state to bind substrate and release product (flip-flop). Example of case (i) was seen for castor Δ^9-18:0-acylcarrier protein desaturase [171]. Initially, it was thought that ECAP did not have half-of-sites-reactivity (case [ii]), based on an experiment where Bloch and Schlesinger [31] hybridized an inactive mutant variant with native subunits and observed that the activity was half of the native. Later, Hehir et al. [172] sequenced and expressed these variants and showed intragenic complementation for these heterodimeric variants (increased activity when combined). Most of the mutated variants were located at the active site and many were metal ion coordinates. When one subunit is rendered inactive, the need for dimerization to maintain function of the native subunit still exists for a yet unknown reason. The formation of a heterodimer is not always possible *in vitro* due to the difficulty of separating subunits without altering the active sites of the enzymes, so in many cases it can be beneficial to co-express both variants on different plasmids and then purify the heterodimer. To ease purification of the heterodimer, a charged tag (usually several charges) is sometimes attached to either the N- or C-terminus of one of the subunit to facilitate separation of the homodimers from the heterodimers on an ion exchange

column [172]. In fact, we have expressed a variant of VAP with 2xFLAG tag at the C-terminus, giving the enzyme extra eight negative charge [173, 174]. Attempts at forming heterodimers *in vitro* with wild type or Strep-tag VAP were unsuccessful, but are not fully exploited, and may be improved. In some cases, it has been possible to generate single chain versions of a dimeric enzyme where individual subunits are covalently linked by a linker sequence [175]. By this approach each subunit can be mutated to test for half-of-sites reactivity, giving that the enzyme is able to fold.

The examples mentioned above give no information about the mechanism for half-of-sites-reactivity at the structural level. Recently Kim et al. (2017) [153], studied the half-of-sites reactivity of fluoroacetate dehalogenase from *Rhodopseudomonas palustris* homodimer. This enzyme catalyzes one of the slowest reactions in nature (the hydrolysis of F-C bonds). The authors utilized the slow reaction using freeze trapping crystallography and NMR in a time-resolved manner. Using this approach, the structural mechanism of half-of-sites reactivity was revealed. This enzyme has only one subunit active in catalysis, binding and releasing substrate (HOSB and HOSR), while the other subunit facilitates catalysis by entropy compensation (Figure 1.14). As the substrate binds, bound water is released from the other subunit, resulting in an increase in dynamic mobility for the empty subunit. As the reaction proceeds a covalent intermediate is formed and water binds again after the hydrolysis step. Lastly, the product is released and asymmetry in dynamics of the subunits returns to a ground state. For APs, the mechanism could be similar with the exception that both subunits can bind substrate at the same time (substrate or product is found in both active sites in AP crystal structures). It is possible that conformational changes between ground states and a bound energy-rich state exist where water plays a key in the progress of decreasing the activation energy (Figure 1.14, below).

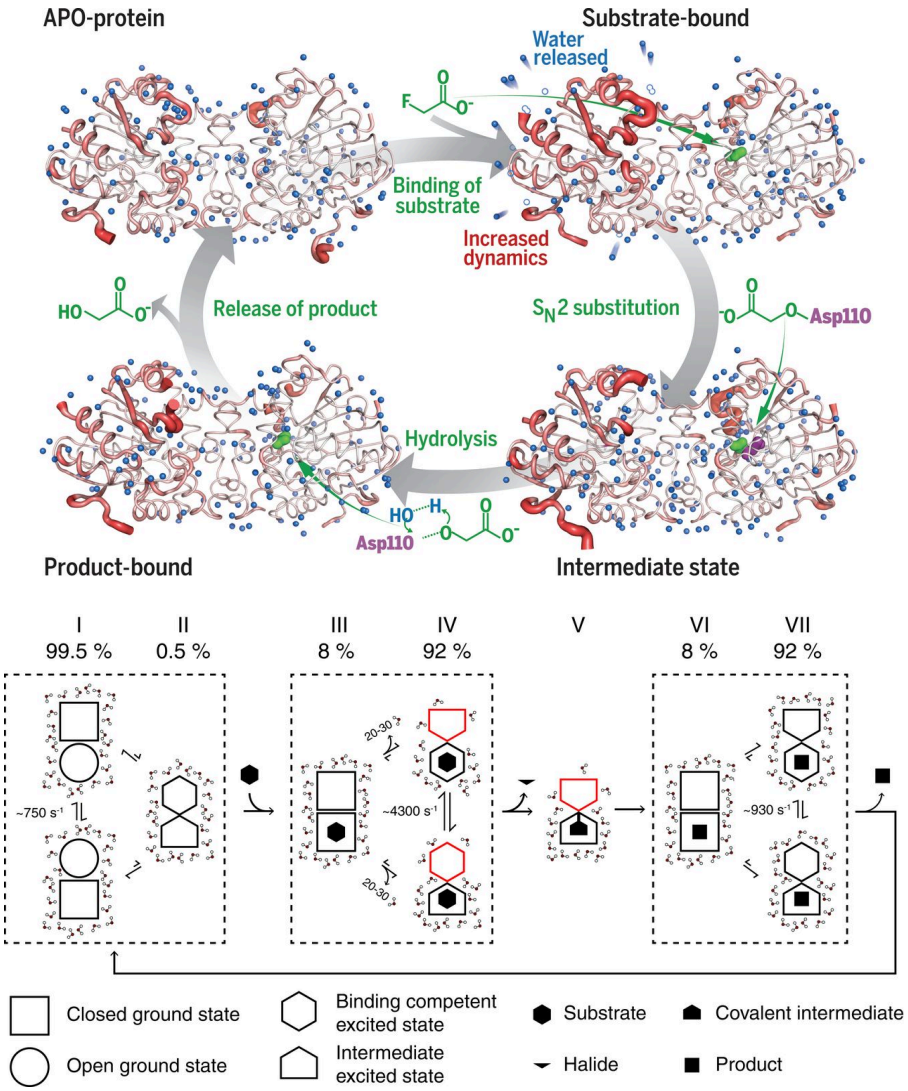

Figure 1.14. Half-of-sites reactivity of fluoroacetate dehalogenase. The binding of substrate to one subunit is facilitated by an increase in entropy brought about by the other subunit. As the hydrolysis progresses water binds again to the unbound subunit to facilitate the release of product. Fast dynamics occur between unbound and bound states where upon binding of substrate most of the molecules will adopt the excited state. Note the resemblance to the HT model in Figure 1.13C. Figure was adapted from Kim et al. (2017) [153].

1.4 Enzyme cold adaptation.

1.4.1 Thermodynamics

General considerations

All chemical reactions require kinetic energy to achieve the correct orientations of electron orbitals, that suffices to facilitate breaking or formation of chemical bonds. Temperature effects on chemical reactions do influence the equilibrium of the reaction, but more importantly the kinetics of the reactions, where energy is needed to pass the activation

energy barrier, E_a. The relationship of activation energy with rate of the reaction is described by the Arrhenius equation:

$$k = A\kappa e^{-E_a/RT} \tag{1.1}$$

where k is the rate, A is the pre-exponential factor, κ s the dynamic transmission coefficient (generally assumed to be 1), R the gas constant and T temperature in Kelvin.

From thermodynamical point of view, enzymes simply decrease the energy barrier needed to reach transition states. Yet, how enzymes achieve this can be diverse. In terms of Gibbs free energy (G) the diversity brought by enzyme comes from two components, the enthalpy (H) and the entropy (S) of the system where the free energy change at a constant temperature (T) is described as:

$$\Delta G = \Delta H - T\Delta S \tag{1.2}$$

As enzymes only affect the activation energy, but not the chemical equilibrium of a reaction, the activation free energy ($\Delta G^{\#}$) better describes how enzymes influence chemical reactions (Figure 1.15):

$$\Delta G^{\#} = \Delta H^{\#} - T\Delta S^{\#} \tag{1.3}$$

The enthalpy contribution, is a term of more tangible nature than the entropy and involves the bonding energy brought by enzyme residues or cofactors that are bound close to the active site pockets. Most of the enthalpy change occurs at the formation of the E•S complex. The E•S complex needs to assemble a form that resembles the transition state or a state which can be influenced by neighboring residues or cofactors towards the transition state. On the other hand, entropy is a phenomenon which is harder to fully account for. It describes the tendencies of matter to adopt states of maximum chaos. In other words, if a molecule in a system has a state where it interacts with other molecules (e.g. hydrogen bonds) and those bonds are broken, the tendency towards reforming the bonds will be less than towards breaking them, since the unbound state has higher entropy. Thus, processes that have a highly favorable increase in entropy, not compensated by enthalpy are often irreversible (very high kinetic barrier) or as Boltzmann puts it:

"Since a given system can never of its own accord go over into another equally probable state but into a more probable one, it is likewise impossible to construct a system of bodies that after traversing various states returns periodically to its original state, that is a

perpetual motion machine" Ludwig Boltzmann "On the second law of thermodynamics" delivered on 29 May 1886.

The formation of the E•S complex results in an entropy decrease; thus, the enthalpy change needs to be larger than the entropy decrease for the binding of substrate to be spontaneous (negative ΔG). However, the molecular size of enzymes, which is many times larger than just the residues that take part in binding of substrate, might act as an entropy "buffer", where upon binding of substrate a conformational change leads to a release of surface bound water molecules to increase the entropy of the system (such as shown in Figure 1.14) [153].

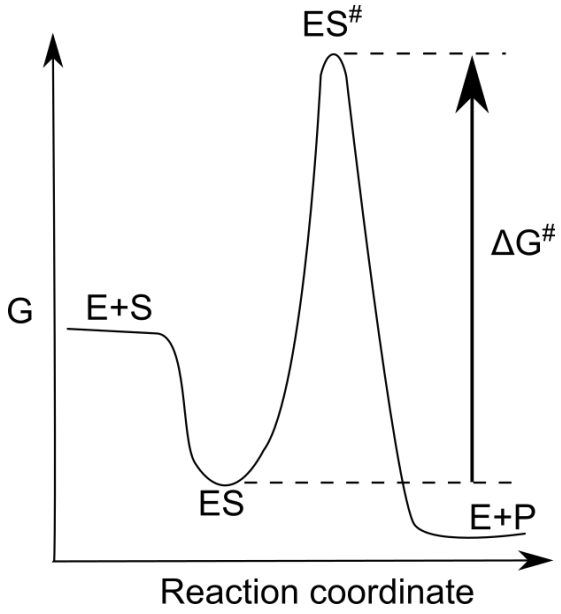

Figure 1.15. Free energy diagram of transition theory reaction coordinate.

According to the transitions state theory, k_{cat} is dependent on temperature and thermodynamic constants by the Eyring equation [176-179]:

$$k_{cat} = (k_B T / h) e^{-\Delta G^{\#}/RT} \tag{1.4}$$

where k_B is the Boltzmann constant and h the Planck constant. Substituting the ΔG term in eq. 1.3 to eq. 1.4 gives:

$$k_{cat} = (k_B T / h) e^{-[(\Delta H^{\#}/RT)+(\Delta S^{\#}/R)]} \tag{1.5}$$

According to eq. 1.5, k_{cat} can increase at lower temperature either by a decrease in $\Delta H^{\#}$ or an increase in $\Delta S^{\#}$. Most cold-adapted enzymes show decreased $\Delta H^{\#}$ and a consequential decrease in $\Delta S^{\#}$ compared to mesophilic enzymes [177, 179], sometimes termed the enthalpy-entropy compensation. Cold-adapted enzymes are more active than mesophilic enzymes and thus have lower $\Delta G^{\#}$. In the cases where decreased enthalpy results in an increase in entropy, increased flexibility of the active site has been proposed where the $ES^{\#}$ state is able to adopt a broader distribution of states. This could cause an increase in k_{cat} and an increase in K_M [180]. In the cases where evolutional pressure exists towards low K_M, such as for secreted marine enzymes where substrate concentrations are low, cold-adaptation does not necessarily result in increased k_{cat} [181-183].

Many enzymatic reactions involve multiple steps in each catalytic cycle, with several individual transitions states (Figure 1.16). Often, the breaking or forming of covalent bonds are not the rate-limiting step, but the release of products to reclaim the enzyme catalyst (multiple turnover) or other conformational changes in the reaction pathway. Thus, cold-adaptation might be involved in lowering multiple activation barriers. This (mainly entropy), has been frequently overlooked by computational scientist who often only address the transition state for the chemical step [126, 184, 185].

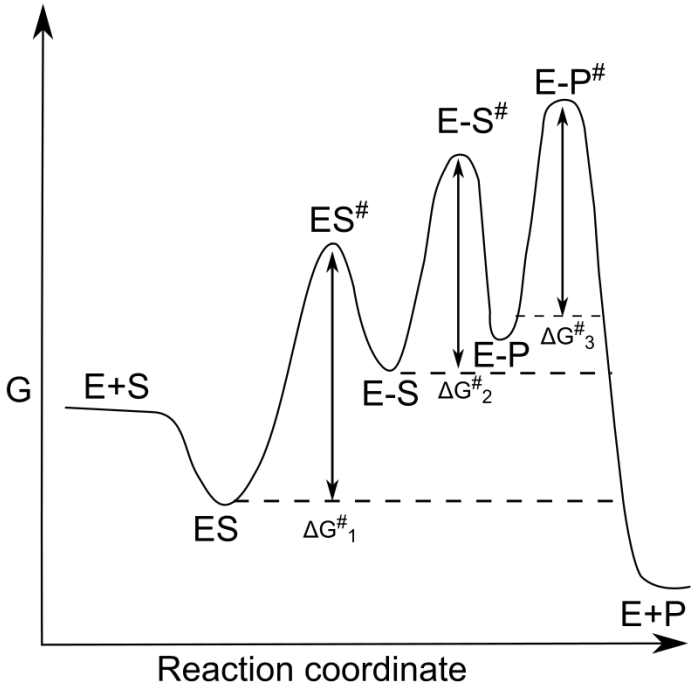

Figure 1.16. Free energy diagram of transition theory reaction coordinate with several enzymatic intermediates.

Macromolecular rate theory (MMRT)

Recently, Arcus et al. [186], described a new concept of temperature dependence of enzyme-catalyzed rates, the so called macromolecular rate theory (MMRT). It utilizes the heat capacity change for the ES to ES$^{\#}$ transition ($\Delta C_p^{\#}$). This is a parameter that quantifies the temperature dependence of the enthalpy and entropy of a system, and is often assumed to be constant with temperature (as in eq. 1.5). Implementation of $\Delta C_p^{\#}$ to eq. 1.3 gives:

$$\Delta G^{\#} = [\Delta H^{\#}_{T_0} + \Delta C^{\#}_p (T - T_0)] - T[\Delta S^{\#}_{T_0} + \Delta C^{\#}_p (\ln T - \ln T_0)] \qquad (1.6)$$

By implementing eq. 1.6 to the Eyring equation (eq. 1.5) gives:

$$\ln k = \ln \frac{k_B T}{h} - \left[\frac{\Delta H^{\#}_{T_0} + \Delta C^{\#}_p (T - T_0)}{RT} \right] + \left[\frac{\Delta S^{\#}_{T_0} + \Delta C^{\#}_p (\ln T - \ln T_0)}{R} \right] \qquad (1.7)$$

The $\Delta C_p^{\#}$ measures the capacity for the translational, rotational, vibrational and electronic modes to absorb energy. In water and at biologically relevant temperatures (-20 – 100 °C), electron modes above the ground state are inaccessible and the greatest contribution to heat capacity is the number of accessible vibrational modes [187]. For most enzymes, $\Delta C_p^{\#}$ is negative [188]. However, when we usually interpret the $\Delta G^{\#}$ as in eq. 1.3 we assume $\Delta C_p^{\#}$ is zero and that the enthalpy and entropy terms are temperature independent. Figure 1.17 shows the interpretation of enzymatic rate using eq. 1.5 (Eyring equation) vs. eq. 1.7 (MMRT equation) when the $\Delta C_p^{\#}$ is a known constant ($\Delta C_p^{\#}$ is assumed to be temperature independent). The former, shows an exponential temperature dependence for the enzymatic rate, while the latter shows a curved result resembling a typical enzymatic T_{opt} curve (Figure 1.17B). The increase in rate by temperature is first driven by the increase in enthalpy term ($-\Delta H^{\#}/RT$) but as the temperature reaches T_{opt} the rate slows down due to a decrease in the entropic term ($\Delta S^{\#}/R$) (Figure 1.17C). The MMRT theory predicts that the $\Delta H^{\#}$ for the enzyme catalyzed reaction at T_{opt} is near zero. Moreover, the most notable observation is the result that as the rate decreases at temperatures over T_{opt}, is due to the entropy decreasing with temperature, but not due to temperature denaturation of the active site. Here, the authors have carefully made sure that the kinetic data vs. temperature was denaturation independent, where the data was either corrected for denaturation rates or were of the so

called “zero time” nature [189].

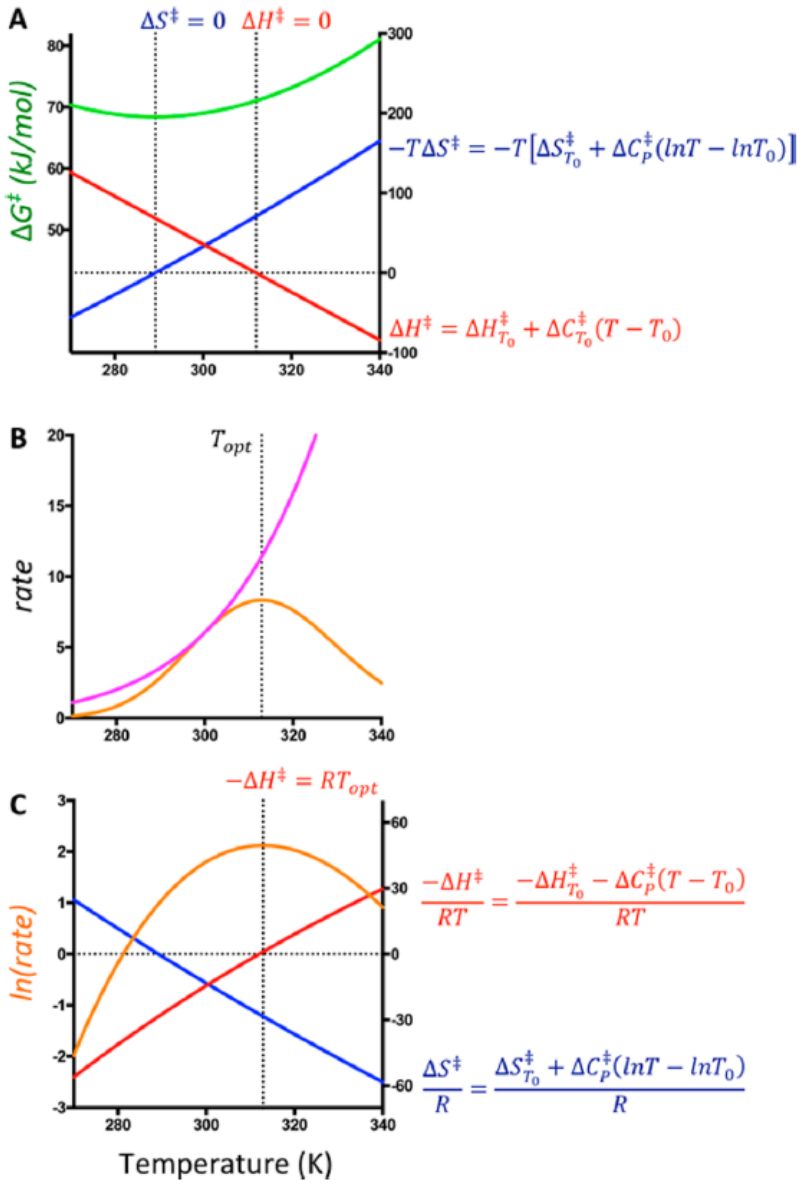

Figure 1.17. Temperature dependence of enzymatic catalytic rates with nonzero $\Delta C_p^{\#}$. (A) Temperature dependence of $\Delta G^{\#}$ (left axis shown in green) and the enthalpy and entropy contributions in red and blue respectively (right axis) when $\Delta C_p^{\#}$ is set to -3.0 kJ mol^{-1}K^{-1}. (B) Temperature dependence of enzymatic rate according to the Eyring function (in purple, eq. 1.5) and the MMRT (orange eq. 1.7) with $\Delta C_p^{\#}$ set to -3.0 kJ mol^{-1}K^{-1}. (C) Temperature dependence of the rate according to MMRT (orange line, left axis) and relative contributions of enthalpy (red line, right axis) and entropy (blue line, right axis). The vertical line shows T_{opt} and where $-\Delta H^{\#} = RT_{opt}$. This figure was adapted from Arcus et al. (2016) [186].

One further observation can be made using the MMRT equation. As the T_{opt} decreases, the curvature becomes more extreme. In other words, the lower the T_{opt} the more

sensitive the enzymatic rate is to temperature fluctuations (Figure 1.18). This is termed the "psychrophilic trap". To avoid this "trap", enzymes generally do not evolve to T_{opt} lower than ~20°C [190].

One of the main conclusions, when applying the MMRT to enzymatic rates, is that it provides a possible explanation why larger enzymes generally have a higher catalytic rate compared to the uncatalyzed reaction (k_{cat}/k_{non}) in relation to smaller enzymes, and why larger enzymes are able to decrease the activation energy of more complex reaction. Since the change in $\Delta C_p^{\#}$ is mainly due to vibrational modes, the larger the enzyme the more modes are available. Further experimentation is needed to generalize the correlation between $\Delta C_p^{\#}$ and T_{opt}, and to confirm if the correlation is strong. MMRT, in its simplicity, adds a new dimension to the transition state theory of enzymes, that is the $\Delta C_p^{\#}$.

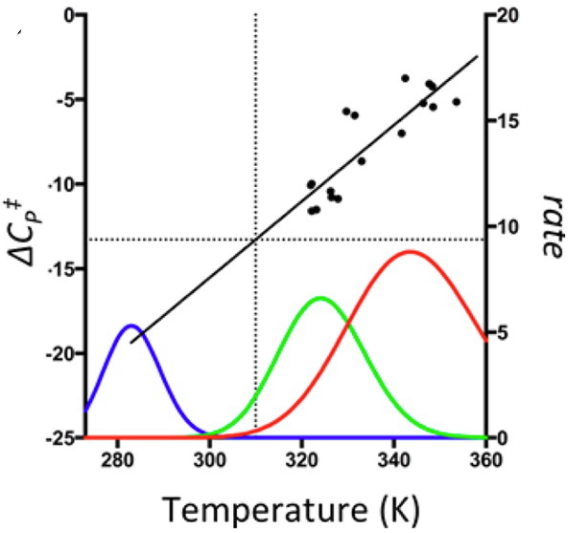

Figure 1.18. The psychrophilic trap. The correlation between $\Delta C_p^{\#}$ and T_{opt} for 10 homologous isopropyl malate dehydrogenase (IPMDH) from psychrophilic, mesophilic and thermophilic species of *Bacillus* and 7 mutants of MalL enzyme from *Bacillus subtilis*. The colored curves represent the rate vs. temperature for a hypothetical extreme psychrophilic (with T_{opt} of 10°C) in blue, mesophilic enzyme in green and thermophilic enzyme in red. This figure was adapted from Arcus et al. (2016) [186].

1.4.2 Flexibility and cold-adaptation

The role of flexibility and enzyme dynamics in cold-adaption has long been debated. Are cold adapted enzymes always more flexible than their mesophilic or thermophilic counterparts? "Flexibility" is an engineering term, implying that an object can reach former shape if bent. So, for a discussion of enzyme dynamics, it requires additional information regarding the range of such mobility and the time factor of its oscillations (how rigid

individual parts are). If we look at flexibility in terms of K_M, that is, if we assume higher K_M results in less rigid active sites, then cold-adapted enzymes that decrease the free energy barrier of the transition state by simply reducing the depth of the energy pit when ES is formed, might be termed more flexible. Many cold-adapted enzymes have been reported with larger and more open active sites, where bulky side chains have been replaced with smaller amino acids [191-193]. The broader active sites may show increased catalytic rate if the rate-limiting step is the release of product (as is the case for APs) [194].

One debate relating to cold-adapted enzymes revolves around the question if they generally have increased global flexibility, irrespective of the size of the enzyme, or if increased flexibility is only needed in certain loops or domains that are directly related to catalysis, while rigidity is kept unchanged or even increased in other domains for folding stability [178, 179, 181, 191, 193, 195-197]. For some enzymes, higher global flexibility has been attributed to higher catalytic rate at lower temperatures [198, 199]. Methods such as neutron scattering have been used to define local flexibility [200], revealing that fluctuations in amplitudes were similar near the physiological temperature of enzyme from different species [201]. Fluorescence quenching has also been widely used to study the flexibility indirectly [202-204], where acrylamide, which is known to be able to penetrate deep into protein core [205], quenches Trp residues by dynamic collision. The drawback of using this method to compare homologous enzymes is that there is no correlations between solvent accessibility of Trp residues and the fluorescence lifetime [206]. This means that the amount of relative quenching for each Trp residue is not just dependent on solvent exposure but also the close electrostatic environment around the fluorophore, which differs between enzymes.

Most of the literature supports that local flexibility is needed in certain domains or the active site while other less catalytically relevant domains can be kept more rigid [182, 207-209]. In these cases, the local flexibility has been uncoupled from thermal stability and correlates to activity [210-212]. Also, comparison of B-factors in crystal structures between psychrophilic and mesophilic structures as well as molecular dynamics analyses have indicated local flexibilities [116, 191, 211, 213-219]. However, in some cases there were no differences in flexibility when comparing a psychrophilic and a mesophilic counterpart, such as for trypsin [220, 221] and citrate synthase [222]. Recently, a 2 μs MD simulation of endonuclease A showed no difference in flexibility between the cold-adapted strain from *Aliivibrio salmonicida* and the mesophilic strain *Vibrio cholera* [223].

Thermal stability in cold-adaptation has not yet been mentioned here. Rigidity is undoubtedly needed at higher temperatures to stabilize the folded state of enzymes. However, rigidity needed at high temperature, does not irrefutably indicate that flexibility is needed at lower temperatures. In terms of evolution of thermophiles, stability is simply an indirect consequence of the need for function at high temperature. That is, stability has no evolutional meaning if it is not coupled to function. Thus, evolution towards cold-adaptation does not need to be coupled to low stability. Site-directed mutagenesis or directed evolution conducted on mesophilic or psychrophilic enzymes has resulted in enzymes with higher thermostability but unchanged or enhanced k_{cat} [224-231]. Cold-adapted enzymes are most often more intrinsically unstable due to lack of selection for stability, and the instability might simply result from stochastic genetic drift. However, in studies were random mutational libraries have been examined, improvement of both activity and stability is rare and in the cases where increased activity at low temperature was observed, stability was also decreased [225, 232].

Why has it been so hard to unravel in general terms the basis for temperature adaptation of enzymes? One thing that may have been overlooked is that enzymes are often a part of large synthesis or breakdown pathways that might be differently sensitive to temperature. Let's say that a "rate determining" enzyme in a pathway is more dependent on temperature than another enzyme later in the pathway, then the pressure on cold-adaptation is much higher on the former than the latter. Thus, the mechanism of a cell towards cold-adaptation is only applied when needed. Enzymologist who have been studying enzyme cold-adaption might need to ask the question more frequently; how important is the enzyme under study for the organism? Often the answer might be unknown.

When it comes to explaining why the role flexibility in enzyme catalysis has been difficult to generalize, perhaps one can start by proposing that the engineering terms "flexibility" and "dynamics" do not describe well enough how an enzyme functions. It looks as if there is some missing knowledge that could be the key towards these discrepancies. Bringing the mind to my second-year biochemistry course, the first thing that is usually focused on is how water affects proteins. The effect of water solvation on protein structures and substrates, and how entropy plays a part in catalysis, is in a way still too vague and difficult to formalize mathematically. Water and entropy are usually a problem for chemists, and it is difficult to predict solvent interactions in computer

simulations. This might be the missing link that could explain the role of flexibility where water/protein interactions are the key to explaining cold-adaptation rather than the protein singularly. Many cold-adapted enzymes have identical catalytic residues in the active sites as their more thermostable counterparts, thus cold-adaptation must involve amino acids far from the active site (as opposed to catalytic residues who are near each other). Isaksen et al [197], proposed that protein-solvent interfacial surfaces differ between cold-adapted and thermophilic enzymes due to point mutations that disrupt surface hydrogen bonding networks and bound water. This was observed using calculations of "high-precision" Arrhenius plots and thermodynamic activation parameters. It is experimentally challenging to prove this theory, but recently Kim et al. (2017) [153], used time-resolved crystallography and NMR to show that release of bound water network facilitated a conformational change to both bind substrate and release product in a homodimeric enzyme (Figure 1.14).

2 Aims of the studies

The general aim of this thesis work was to elucidate why VAP shows such a low thermal stability and if it relates to its enhanced low temperature kinetics. We wanted to study the mechanism of inactivation in detail and find out how salt ions affect kinetics and stability. Although AP is one of the most studied enzymes, relatively few studies have focused on events at the interface of the dimer. Initially, a method to study the dimer-monomer equilibrium was lacking, where the dissociation of weakly associated dimers was suspected to cause the loss of measured activity. It was soon realized, that the inactivation was a more complex process involving subtle conformational changes of the dimer, where more sophisticated methodology was needed to study the structural changes. Fluorescence spectroscopy was a key method used during this study. Furthermore, the effect of salt-ions on the enzyme was studied in detail revealing how salt dramatically affects the kinetics and stability of VAP.

Paper I

As a preparation for the employment of fluorometry, we made single Trp $\rightarrow$ Phe substitutions to reflect the effect of each Trp in the Trp fluorescence emission spectrum. The expectation was that this would elucidate local structural changes, and be a way to detect dimer dissociation. We were particularly interested in W460 which is close to the interface at the two-fold symmetric axis.

Paper II

We have known for some time that 0.5 M NaCl (and some other ions) in buffers both activated and stabilized the enzyme, but it had never been studied in detail. The ionic effect was shown to be of more complex nature than previously thought, where pH plays an important role. This paper reports in detail how ions affect VAP (and two other APs). Furthermore, an activity dilution assay was developed to study the dimer-monomer equilibrium as well as a metal ion assays to measure the metal occupancy in the inactive enzyme.

Paper III

In the previous listed papers, strong evidence supported the conclusion that upon inactivation the dimer is transformed to an inactive dimer intermediate. In this study a fluorescent probe, bimane, was attached on different locations at the interface and its fluorescence monitored as the enzyme was inactivated. We wanted to observe if the inactivated form showed any structural changes at the interface. In this paper, an effort was also made to explain half-of-sites reactivity of VAP and APs in general.

Paper IV

VAP has a large interface loop that hovers over the active site of the other monomer (Figure 1.2). Here, we studied the effect of breaking some extensive interfacial networks of hydrogen bonds, by kinetic assays, stability assays and molecular dynamics simulations. We wanted to define the role of the large loop, with respect to activity and stability.

3 Methodology

3.1 Protein overexpression in *E. coli*

An improvement in the methodology for overexpression of VAP was achieved by changing to a new T7 promoter system (pET11a) where previously a tetracycline inducible vector (pASK) was used [113]. The overlap extension PCR cloning method was used to subclone the VAP gene with StrepTag fused to the C-terminus via a two-amino acid linker, into the pET11a vector [6]. For this expression system, the T7 RNA polymerase gene is needed in the host strain (BL21(DE3)). For increased expression regulation, we used the Lemo21(DE3) *E. coli* strain. It harbors a plasmid containing the lysozyme gene *lys*Y which is modulated by L-rhamnose where lysozyme inhibits the T7-RNA polymerase. Thus, by adding L-rhamnose to the medium at levels from zero to 2 mM the expression can be fine-tuned [233]. Using this system, with proper aeration of the media, soluble VAP, up to 150 mg per liter LB culture could be obtained at 18° C. Optimal amount of soluble enzyme was achieved using 0.25 mM L-rhamnose. Using the older tetracycline expression system, the expression yield for VAP was in best cases 3 mg per liter LB culture. For some enzyme mutant variants, the expression yield using the T7 expression system was much lower than for the wild type where in some cases only 5-10 mg per liter LB culture was derived. Most of these were Cys variants (Paper III).

We have been using the StrepTactin affinity purification system with great success, purifying the enzyme to 99% purity in one step [6, 113]. The StrepTag is a short peptide (WSHPQFEK) which binds with μM affinity to StrepTactin resin, a genetic variant of streptavidin. By fusing the peptide to the N- or C-terminus (N-terminus not possible for VAP due to N-terminal signal export sequence), proteins bind to the StrepTactin resin and can be eluted in one step using desthiobiotin, which can be competed/exchanged out by the regenerating agent HABA (2-[4 -hydroxy-benzeneazo] benzoic acid) for multiple use of the resin.

3.2 Enzyme steady state kinetics

Throughout this thesis, all enzyme variants were characterized under steady-state conditions ([S]>>[E]) using p-nitro-phenyl phosphate (pNPP) as a substrate at pH 9.8 (see publication for further details). All kinetic curves were fitted with non-linear regression to the Michealis-Menten equation. In most cases, the rate limiting step for phoshoester-hydrolysis catalyzed by VAP was assumed to be the release of inorganic phosphate.

3.3 Urea denaturation and unfolding mechanism

To study the denaturation mechanism of VAP, urea was used as a denaturant. Since chloride is highly stabilizing for VAP (Paper II), GdmCl denaturation was not performed. The enzyme was incubated overnight at 10°C to make sure equilibrium was reached. Generally, 15-20 urea concentration points were used for each curve. Fluorescence of the six native Trp residues was monitored (excitation at 295 nm) for the detection of denaturation. In most cases λ_{max} was monitored to detect structural changes. In paper III, dissociation of the dimer and unfolding were shown to be linked. At pH 8.0, activity was used to monitor a transition towards inactive dimer intermediate but at pH 10.5 transition towards an inactive species was due to dissociation/unfolding of the dimer.

3.4 Thermal inactivation and thermal unfolding

Circular dichroism (CD) spectroscopy was used to monitor the global thermal stability (T_m) of the tertiary state (dimer dissociation likely as well, see paper III). The global thermal stability is dependent on pH, the concentration of Mg^{2+}, NaCl, and competitive inhibitor ions (sulphate and phosphate). To be able to compare T_m for new variants with older data, we have kept the same conditions throughout (25 mM Mops, 1 mM $MgSO_4$, pH 8.0).

The thermal stability of the active site was determined using the Arrhenius equation (ln k vs $1/T$) where the activation energy (E_a) was obtained and $T_{50\%}$ was then calculated from the Arrhenius equation, where the k for 50% loss of activity after 30 min gives $T_{50\%}$.

3.5 Fluorescence measurements and labeling

Tryptophan fluorescence was used to monitor changes in solvent accessibility to correlate to structural changes and folding. VAP has five native Trp residues and nineteen Tyr residues per monomer. By using 295 nm as excitation wavelength, the Tyr emission was

mostly excluded. Furthermore, the maximum emission of tyrosine is at 310 nm (except tyrosinate which has emission maximum at 340 nm), vs 355 nm for Trp, thus it is easy to discriminate between Tyr and Trp emission. It is generally impossible to resolve the contribution of each tryptophan in proteins that have more than one or two Trp. The reason is that Trp can exist in different rotameric states which fluctuate on the ns scale. Moreover, proteins switching between conformers on the ns scale could also be responsible for the heterogeneity of the emission lifetime. In fact, several single Trp containing proteins show three lifetimes [234, 235]. Thus, for VAP, it would be unrealistic to resolve the contribution of each Trp residue. However, using site-directed mutagenesis, the emission of the two Trp residues of triosephosphate isomerase has been resolved [236] and the three Trp of barnease [237]. Trp is then usually substituted to Phe or Tyr, which could affect the global tertiary hydrophobic packing, especially for buried Trp residues. Here, an attempt was made for VAP to gauge the contribution of each Trp to the total fluorescence where each Trp residue was mutated to Phe. Most of these mutations resulted in decreased catalytic efficiency and decreased global thermal stability (Paper I). A good example for the complexity of the emission decay can be seen in the support material of paper I (Figure S3), where very small changes can be seen in the decay time for the single substituted variants.

We turned our focus to the use of an extrinsic fluorescence label to detect local structural changes. Here, we used the small fluorescence label mono-bromo bimane (Figure 3.1) which reacts with free Cys groups. VAP has only one native Cys residues, so VAP is convenient to label. Furthermore, the native Cys was shown not to be accessible for labeling which was convenient, since the C67S variant, presumable needed to perform single labeling, affects the catalytic rate [113]. The reason we chose bimane was that it is quenched intrinsically by Trp or Tyr in a well-defined sphere of quenching [238, 239]. The sphere of quenching for bimane is up to 15 Å for Trp and 10 Å for Tyr. These are distance too short to be measured by Förster resonance energy transfer (FRET). The strategy was to introduce bimane near a Tyr or Trp residue present natively or incorporated using site-directed mutagenesis (Figure 3.2). We chose sites where bimane would be juxtaposing either a Trp or Tyr at the other subunit, to study structural changes at the dimer interface (Paper III), where a Phe residue at the relevant was used as a non-quencher control at the relevant positions.

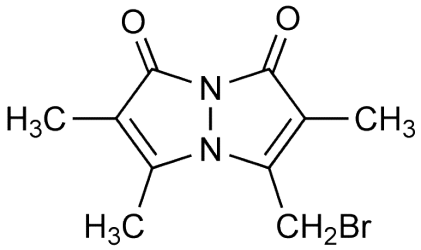

Figure 3.1. Monobromo-bimane.

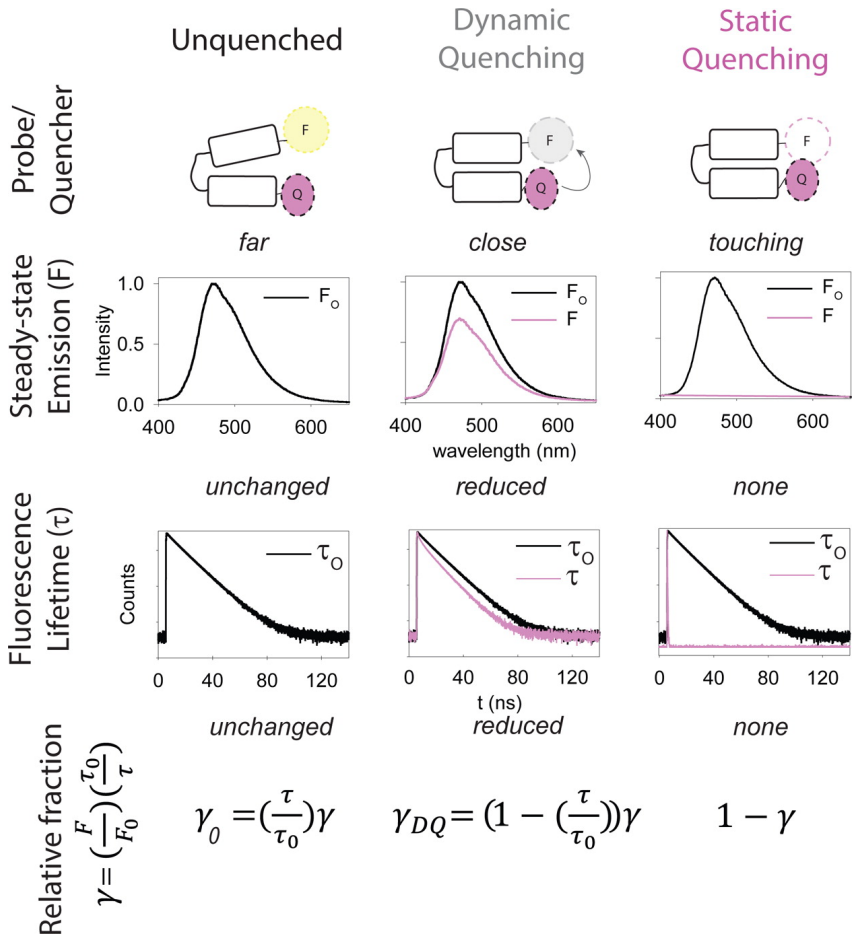

Figure 3.2. Tryptophan and tyrosine induced quenching (TrIQ, TyrIQ) of bimane. Phenylalanine at the quencher position is used as non-quenching control (F_0, τ_0) and Tyr or Trp as quenchers of bimane (F, τ). If dynamic quenching occurs, both the steady-state emission (F) and the fluorescence lifetime (τ) is affected. Static quenching only affects the steady-state emission. Thus, using the equation $\gamma = (F/F_0)(\tau_0/\tau)$ the relative fraction of non-static quenching can be derived and the static quenching component is simply 1-γ. The figure was adapted from [239].

3.6 Phosphorescence measurements

In Paper I, we discovered that one of the Trp residues (W460) was highly buried in the protein core and absent from static quenchers such as His, Tyr, Trp and Cys [240]. Since none of these residues are within 5 Å proximity to W460, and the fact that the residue is

highly buried, we suspected that the residue might show phosphorescence, similar to the highly phosphorescent W301 of ECAP. Phosphorescence of ECAP has been used to monitor negative cooperativity in phosphate binding [162] and structural role of metal ions [241]. Indeed, VAP was shown to be phosphorescent, having two lifetimes (Paper I). The W460F variant was also slightly phosphorescent, indicating that the second lifetime originated from a second Trp residue. However, phosphorescence measurements are extremely sensitive to oxygen, such that oxygen needs to be fully purged from samples before measurements. This proved to be technically difficult to make consistent. Thus, we were not able to answer the question which residue was the second phosphorescent active residue. Two purging methods were tried: 1) bubbling pure argon through a quartz flow cell; or: 2) directly applying vacuum to the sample in the cuvette and repressurize with oxygen free nitrogen in a homemade apparatus. The second method proved to be more successful, but repeatability was poor.

The value of using Trp phosphorescence is the rarity of Trp being phosphorescent in proteins generally. Proteins that are phosphorescent usually only have one Trp being phosphorescent. Thus, phosphorescence gives a local signal which is very sensitive to changes in solvent exposure and backbone movements. The next step in phosphorescence measurements of VAP would be finding a collaborator who is conducting phosphorescence measurements on a regular basis.

3.7 Metal ion assays

An improved sample preparation protocol before metal ion analysis was developed and is explained in Figure 3.3 (Paper II). We wanted to answer if the inactivation of the enzyme was due to metal ion dissociation from the active site. In the previously used method, the enzyme was inactivated in urea and the excess magnesium from the purification buffer removed by dialysis after incubation. Subsequently, the samples were assayed using atomic absorption spectroscopy. If the magnesium ions were loosely bound, then the dialysis step would likely result in further depletion of magnesium from the active site, giving rise to a systematic error. In the new method, the urea incubation step was performed straight after purification with lower magnesium used and with the enzyme still bound to the StrepTactin affinity resin. Urea does not affect the binding of the enzyme to the resin up to 1.0 M urea, whereas over 2.0 M urea the enzyme is unable to bind to the resin. After incubation in urea, the resin was rinsed with Chelex-treated buffer and the sample eluted with desthiobiotin. Lastly, the samples were assayed by atomic absorption

for Zn^{2+} and Mg^{2+} and the metal ion concentration was normalized to protein concentration (determined at A_{280}).

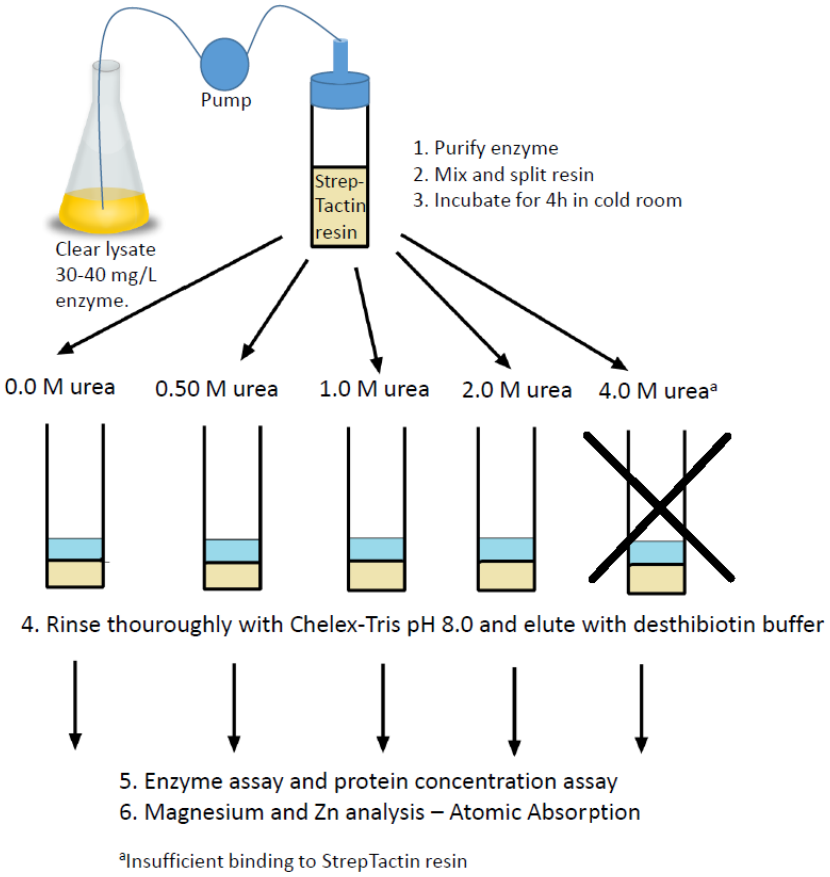

Figure 3.3. Sample preparation before metal ion analysis (Paper II).

3.8 Dimer-monomer equilibrium studies

Two methods were applied to study the dimer-monomer equilibrium. The first method involved measuring the specific activity of the enzyme after serial dilution (after incubation overnight, since dissociation is slow). By plotting specific activity vs. dimer concentration, a fit to a first-order dissociation curve gives K_d (Paper II). The second method simply involved a fit to the two-state urea denaturation curve ($I_2 \rightarrow 2U$) after incubation overnight, as measured by Trp fluorescence (see in Paper III).

3.9 Crystallization of VAP

We have previously sent enzyme variants for crystallization and subsequent X-ray diffraction analysis at the synchrotrons in Grenoble or Berlin to our collaborator at the University of Tromsø, (Dr. Ronny Helland). He originally solved the structure for VAP at

1.4 Å resolution [116], and the R336L variant (unpublished). A trip to Tromsø was made by the author of the present thesis to learn how to initiate crystallization screens. The initial screen involved a semi-automatic robot station for sitting drop samples of 0.2 µl in a 96 well plate. Most coarse optimizations were done using commercial screens (KCSG and SGF), while further optimization was done using 0.7-1.0 µl hanging drop samples in 48 well plates using the two-dimensional approach (varying two components at a time, e.g. pH and precipitant concentration). Several hits were discovered with wild type VAP which gave crystals, where the most promising condition was the same as for the one used in the published structure (0.1 M Tris, 0.2 M $LiSO_4$, 22.5-27.5% w/v PEG 3350, pH 7.0). Optimal concentration of enzyme for crystal formation was between 5-10 mg/ml. We were particularly interested in finding conditions for good crystal formation where the pH is ~10 (to see if the enzyme conformation at > pH 10 is different, see discussion in Paper II). Moreover, we wanted to find conditions devoid of competitive inhibitor ions (SO_4^{2-} and PO_4^{3-}). We have recently obtained a new X-ray machine (D8 venture, Bruker) at the Science Institute of the University of Iceland (Figure 3.4), which might be able to solve structures of highly diffracting protein crystals. We have successfully made in-house crystals (Figure 3.5). However, we have not been able to collect data successfully. We hope we will soon be able to solve structures of VAP enzyme variants in-house or alternatively for quality checks before further analysis at a synchrotron.

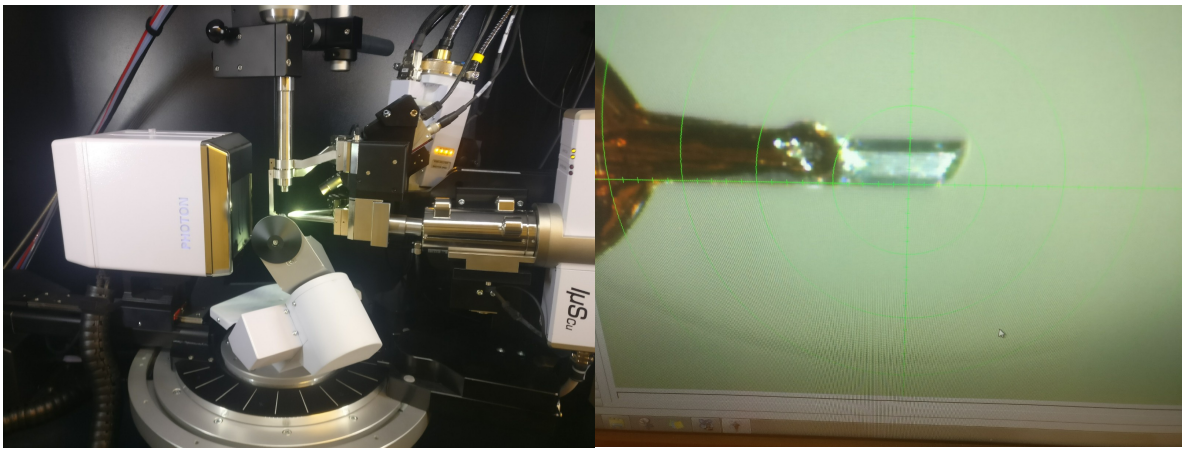

Figure 3.4. To the left: Single crystal X-ray diffraction using D8 venture (Bruker) at the Science Institute, University of Iceland. To the right: Crystal (from Figure 3.5) mounted on a micro loop under a stream of liquid nitrogen.

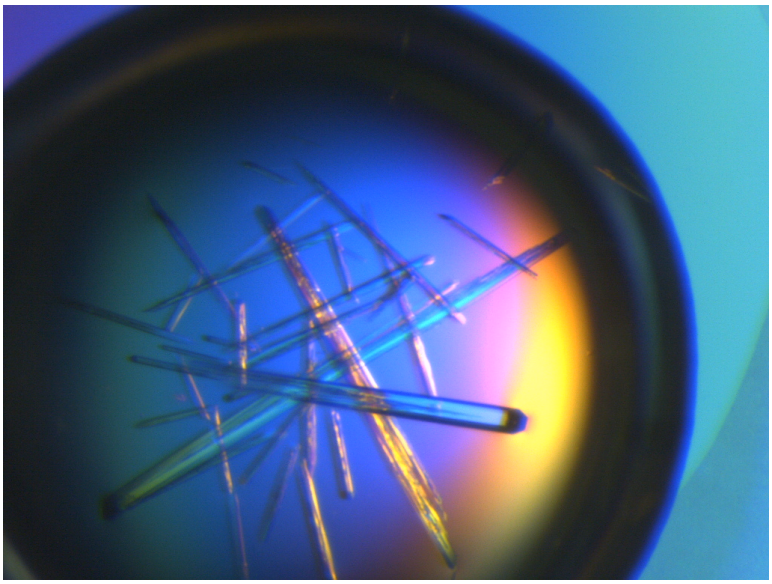

Figure 3.5. VAP crystal growth. Crystallization conditions using the hanging drop method: 0.1 M Tris, 0.2 M LiSO4, 25% w/v PEG 3350, pH 7.0, 10 mg/ml enzyme at 25°C.

4 Results and Discussion

Paper I

When the work of this thesis started, the unique ultra-sensitivity of VAP towards heat (room temperature) and urea had been known for some time [110, 113, 114], and that NaCl stabilized and activated the enzyme. However, little was known about the mechanism of inactivation of VAP. Three possibilities have been proposed for the thermal sensitivity: i) The dimers are very weakly associated and easily dissociate, ii) metal ions in the active site, needed for activity, are weakly bound to the enzyme, and iii) an irreversible conformational change, with a relatively low energy barrier, occurs. In this paper, the first possibility was addressed, by developing biophysical methods to study the dimer-monomer equilibrium.

Here Trp fluorescence was monitored as the enzyme was inactivated using urea. For the wild type, the Trp denaturation curve was of two state nature with no observable intermediates. However, the enzyme was inactivated before any structural transition was observed in the Trp fluorescence. This indicated that either, no major structural changes occur upon inactivation, or that dimer dissociation could not be detected due to placements of the Trp residues away from the interface. VAP has six Trp residues, where only one is located close to the dimer interface (W460), facing towards the protein core 10 Å away from the active site. Single Trp $\rightarrow$ Phe substitutions were made in order to elucidate the contribution of each Trp residue in the fluorescence emission signal. Results indicated that W460 and W301, both highly buried residues, where responsible for more than 80% of the emission signal. Furthermore, W274, located at the outer rim of the active site, close to the magnesium ion coordination site, was shown to be highly quenched and gave almost no signal. In fact, when substituted to Phe (W274F) the emission increased compared to wild type, indicating that W274 might be an acceptor for resonance energy transfer for the other Trp residues (discussed in paper II, in relations to effect of pH on Trp fluorescence) [6]. When acrylamide was used for collisional quenching studies, W460 was shown to be much more buried than the other Trp residues. This lead us to think that W460 might be in an environment optimal for phosphorescence (excited triplet state formation).

Relatively few studies have been conducted, using phosphorescence as a probe, but it has the advantage that it is rare and enzymes generally do not have more than one Trp in optimum environment for phosphorescence, that is protected from solvent and excited state quenchers [240]. Thus, phosphorescence could give an isolated signal coming from one distinct site of the enzyme. The drawback of phosphorescence studies, is that it requires rather sophisticated equipment to measure samples in absolute absence of oxygen which is a potent quencher of phosphorescence (discussed in chapter 3.6). Using a rather primitive in-house made equipment, it was found that W460 was highly phosphorescent. Furthermore, it was clear that the life time distribution was not of a single component nature. Thus, the signal was coming from a second state of the same molecule or another molecule. By mutagenesis, we found that the other signal was coming from another Trp residue with a 17% relative amplitude. We could however not derive which residue it was due to high noise in the measurements (double Trp substitutions would have to be made).

In theory, it is challenging to resolve the contribution of each Trp residue for multi-tryptophan containing protein by this method (discussed in chapter 3.5), since Trp are often conserved residues and important for structure or activity. Indeed, most Trp $\rightarrow$ Phe substitutions in VAP resulted in lower T_m values than the wild type, especially for Trp located at a buried site. The effect of the Trp $\rightarrow$ Phe substitutions was even more pronounced for activity, where W460F had only 10% of the catalytic efficiency of the wild type. Moreover, W460I was shown to be close to inactive (Hjörleifsson, unpublished), but W460Y had the same catalytic properties as the wild type (the effect of these mutations on activity is discussed in detail in Paper III).

An attempt was made to study the dimer-monomer equilibrium by introducing Trp at the dimer interface at site F355W. The variant showed similar kinetic properties and stability (T_m) as the wild type. A minor difference could be seen in the Trp fluorescence denaturation curve for F355W as the enzyme was inactivated, but the effect was too small to be used for quantification or to elucidate the correct unfolding model (see unfolding models in chapter 3.3). Size-exclusion chromatography (SEC) was used to detect oligomeric states at several urea concentrations. The results showed that as the enzyme was inactivated the enzyme transitioned to an inactive dimer intermediate at 1.0 M urea. It was not clear if folded monomers were populated. SEC indicated vaguely that the dimer peak splits, but initial separation of dimers from the monomers on the column sets up another

equilibrium driven movement, possibly forming monomers during the duration of the experimental run. Therefore, the unfolding model could either be of the nature:

$$N_2 \rightleftharpoons I_2 \rightleftharpoons 2I \rightleftharpoons 2U \text{ or } N_2 \rightleftharpoons I_2 \rightleftharpoons 2U.$$

Paper II

The effect of salt ions on VAP activity and stability was evaluated in the molar range 0-1 M, following a lead from older studies that had not given a comprehensive explanation for this as regards of/to mechanism, or which types of salt ions were effective. Increased ionic strength (using NaCl or other salts) was shown to lead to an increase in the activity of VAP, with a peak of activation at 0.5-0.6 M. The nature of the cation had no effect, while chloride was shown to be the most efficient anion in activating the enzyme. The effect of NaCl activation was shown to be pH dependent, where at pH 8.0, a 4-fold activation was seen, but no activation was present at pH 10.5. Salt activation as a function of pH gave a sigmoidal curve, an indication of a single protonation event with a pK_a of 8.7. Activity profiles as a function of pH showed two maxima, at pH 9.0 and 10.2, unique amongst APs. Only the former peak showed increased activity in the presence of 0.5 M NaCl. Thus, in the pH range 8.0 – 10.5, we propose there is a conformational change where both K_M and K_i (inorganic phosphate) increase greatly.

The effect on thermal stability was also pH dependent. $T_{50\%}$ was 25.8 °C without NaCl and 53.5°C with 0.5 M NaCl present, at pH 8.0. At pH 10.5, NaCl had no stabilizing effect. Magnesium showed no specific stabilizing effect towards inactivation, but the inorganic competitive inhibitor ions SO_4^{2-} and PO_4^{3-} increased thermal stability by specific binding to the active site. The thermal stability of the tertiary structure (T_m) increased linearly with NaCl, most likely by destabilization of the unfolded state.

Trp fluorescence was used to monitor structural changes as a function of pH. Distinctive states could be detected, which correlated with changes in activity. Most likely W274, an exposed Trp residue in the active site was affected by pH. This observation strengthened the double-peak pH profile observed for activity

An assay was developed to study the metal-ion content of the enzyme as it was inactivated by urea. The enzyme was treated during purification, bound to the StrepTactin affinity column, with buffers devoid of metal ions (Chelex® treated). After treating the enzyme with urea in the range 0-2 M, it was eluted and subsequently assayed for specific activity and metal-ion content. Results indicated that as the enzyme was inactivated by

urea there was no change in magnesium or zinc content. Thus, the inactivated state was a fully metallated dimer.

Lastly, an assay to study the dimer-monomer equilibrium was developed. This was done by serial dilution of the enzyme and by monitoring specific activity as a function of the dimer concentration (specific activity should be constant unless dissociation occurs). The dissociation constant of the dimer (K_d) could then be derived and subsequently the free energy change for the dissociation event. The K_d was shown to be in the nM range, where the dimer was showed to be stabilized in going from pH 8.0 to 10.5. Furthermore, phosphate and sodium chloride were shown to increase the K_d at pH 8.0.

Paper III

We believe that the inactive dimeric state of VAP (in terms of phosphatase activity) has an interesting shift in the functional properties (see 1.2.6 Promiscuous activity). We have not been able to detect any structural changes accompanying the inactivation event. The presumable half-of-sites mechanism, where one subunit binds the substrate while the other releases products (or drive a conformational change at the other subunit to release product) might occur for VAP, and is possibly general for APs (see chapter 1.3.3). Thus, we proposed that the inactive dimer might have lost a connection at the dimeric interface that drives phosphate release in each catalytic cycle. This making another conformer dominating in the equilibrium ensemble of molecules.

In paper III, we introduced the fluorescence probe bimane at selected sites on the dimer interface to detect subtle structural changes upon inactivation. Bimane is known to be intrinsically quenched by Trp and Tyr in a well-defined sphere of quenching (5-15 Å range) [238, 239]. Compared to Förster resonance energy transfer (FRET), this method, termed tryptophan and tyrosine induced quenching (TrIQ/TyrIQ), can detect changes in distances much closer than FRET based methods (20-100 Å).

Two areas were chosen for labeling, on the short loop comprising amino acid residues 58-61 and residue K486. Either Trp or Tyr where introduced, juxtaposing a bimane label at the other monomer, to serve as intermolecular quenchers of bimane fluorescence. A Phe residue was used as a control (non-quencher). Cys substitutions, needed to attach the probe, affected greatly the catalytic efficiency of the enzyme at position 58-61 (E58C, D59C, A60C, I61C), while the K486C substitution had a lesser effect. Bimane labeling further affected the activity. The variant A60C/F355W showed the

greatest drop in catalytic efficiency, only 1% of the wild type. Interestingly, the F355W mutation had no effect on catalytic efficiency whereas the A60C variant had 20% catalytic efficiency compared to the wild type. The loop 58-61 extends to the helix containing the catalytic Ser (S65). Presumably, there exist networks close to this area that might mediate asymmetric interactions across the interface.

When the labelled A60C variant was inactivated by urea, subtle changes in bimane fluorescence could be detected, giving three-state denaturation curves, while the Trp denaturation curve was always of a two-state nature. At both labeled sites, the three-state curve could only be derived if Trp or Tyr was present at the other monomer within the so-called sphere of quenching. Thus, we concluded that as the enzyme was deactivated by urea, an interaction network mediated through the interface is lost, resulting in a failure of the enzyme to release the phosphate. Using this data and by evaluating the enzyme concentration dependence of each urea denaturation step, we confirmed that the denaturation mechanism at pH 8.0 was of the nature: $(N_2 \rightleftharpoons I_2 \rightleftharpoons 2U)$, where N_2 is the native dimer, I_2 the inactivated dimer intermediate and U the unfolded protein. Thus, folded monomers were not populated, showing that there exists a close link between dissociation and unfolding of the enzyme. In other words, the folding and association of VAP is a cooperative process, as has been reported for several homodimers and heterodimers [242, 243]. At pH 10.5, the native state was stabilized towards inactivation (urea, heat) and the loss of activity coincides with the unfolding event. Here, the denaturation simplifies to a two-state process $(N_2 \rightleftharpoons 2U)$. NaCl was shown to increase the stability of the native state at pH 8.0, but had no effect at pH 10.5.

An attempt was made to summarize the effect of several interface mutations by reference to local specific areas of the interface. Four regions were compared where it was shown that mutations at the marginal areas of the interface where relatively neutral compared to mutations at the central twofold-rotational axis. An antiparallel β-sheet at the two-fold rotational axis is conserved in all APs. This point of symmetry resides between W460 and G461 in VAP. Mutations in this region are known to cause hypophosthatasia in humans, presumably by formation of an inactive variant. This antiparallel sheet is not fully unidirectional. A kink is seen between W460 and G461. We propose that half-of-sites reactivity might be mediated through this symmetry point, possibly by main chain rotations that allow the W460 residue to flip/flop to an inwards/outwards position relative to the

other W460 at the other subunit. Similar long-range flip/flop rotameric transitions are known for a Phe residue in the half-of-sites reactive enzyme caspase 9 [151].

Paper IV

In this paper, the possible role in catalysis and structural stabilization of the long interface loop insert was in focus. This particular loop characterizes VAP and hovers over the active site of the other monomer. It is structurally disordered, with one turn helix at its end, but makes several stabilizing interactions that are unequally distributed along its length. There are eleven intermolecular hydrogen bonds and several intramolecular hydrogen bonds involved in the loop interface region. R336 is located in a central position of the loop and is involved in extensive intra- (with loop-residue Q344) and intermolecular (with residues S79 and S80) hydrogen bonding network. R336 is also bound to several crystallized water molecules. Furthermore, R336 forms a weak intermolecular salt-bridge (4.8 Å) with D59 in the other subunit. Y346F, on the large loop, is interchain hydrogen bonded to S79 (main chain) and S80 of the other subunit as well as to the crystalline water network which R336 also binds.

In our first version of the paper, the variants R336L, Y346F and F355Y were tested for activity and stability ($T_{50\%}$ and T_m). Furthermore, 1-µs all-atom molecular dynamics (MD) simulations where performed for all the variants.

Initial results indicated that disruption the hydrogen bonding network by introducing leucine to position R336 increased k_{cat} and lowered $K_{M.}$ resulting in a 40% increase in catalytic efficiency. The F355Y substitution had no effect on kinetics while the k_{cat} of the Y346F variant decreased to 46% of wild type. K_M also decreased to 40% of wild type resulting in unchanged catalytic efficiency.

MD simulations of the R336L variant indicated an increased flexibility of the large loop and further indicated that this change affected rotameric states of the nucleophilic S65 and the conserved R166, which binds the phosphate moiety. However, when we repeated the kinetic measurements in buffer devoid of ethylene glycol (ethylene glycol was thought to be crucial in stabilizing the enzyme on ice, which later was proven unnecessary), they were not consistent with R336L being an activating mutation. Thus, we repeated all the kinetic measurements where we measured the kinetics with or without the addition of 0.5 M NaCl, excluding ethylene glycol (Table 4.1). We also introduced new variants; the Q334L, S79A, S87A and the S79A/S87A double-variant. Q334 is part of the large loop

and is hydrogen bonded to R336 within the same loop as well as binding to residues S79 and S87 on the other monomer over the interface.

Results for R336L indicated that k_{cat} is only 30% of wild type without addition of salt but 78% of the wild type with the addition of 0.5 M NaCl (Table 4.1). The k_{cat} was unchanged for Q334L, Y346F and F355Y compared to wild type. S79A showed a 70% higher k_{cat} with no salt addition but 35% increase with 0.5 M NaCl compared to the wild type, resulting in almost 4-fold increase in catalytic efficiency. The S87A variant showed a decrease in k_{cat} being 40% and 60% of the wild type with no addition and with 0.5 M NaCl, respectively. Interestingly, the double variant S79A/S87A was notably catalytically impaired. A large decrease in k_{cat} caused catalytic efficiency to drop to 17% and 8% of wild type, measured with no addition of NaCl or 0.5 M NaCl, respectively. These results indicate that the presence of at least one intersubunit hydrogen bond to R336 is needed to maintain the integrity of the active site. Thus, the double-alanine change S79A/S87A is not tolerated, presumably due to loss of hydrogen bonding opportunities.

Interestingly, K_M was significantly lower than for the wild type for all loop connecting variants (except Y346F). This was not the case at 0.5 M NaCl, where there was a significant change for K_M compared to the wild type, except for S79A and S79A/S87A. In most cases there was not much change in active site stability seen for the loop variants except for R336L and Q334L where $T_{50\%}$ was 12.8 °C and 16.5°C respectively compared 25.8 °C for the wild type. However, at 0.5 M NaCl (pH 8.0), both these variants were stabilized and had similar stability as the wild type (Table 4.1). This strengthens the argument that the stabilization induced by NaCl is based on ion binding near the active site. The increase in K_M seen when 0.5 M NaCl is introduced can likely be explained by charge neutralization of the substrate by the salt ions resulting in less facile binding to the positively charged Arg and Zn in the active site.

Table 4.1. The effect of sodium chloride on the temperature stability and kinetic constants of VAP variants. Activity measurements were performed using p-nitrophenyl phosphate as substrate at 10°C in 0.1 M Caps, 1 mM $MgCl_2$, pH 9.8 in the presence of 500 mM NaCl or without added salt. n= number of independent experiments each performed in triplicate.

	k_{cat}, s^{-1}	K_m, (μM^-)	k_{cat}/K_m, ($\mu M^{-1}s^{-1}$)	$T_{50\%}$ (°C)	T_m (°C)
VAP no salt (n=6)	171 ±11	52 ±9	3.4 ±0.5	25.8 ±1.4	50.8 ±0.6
VAP with NaCl (n=8)	240 ±23	211 ±11	1.1 ±0.1	53.5 ±1.1	58.5 ±1.7
Q334L no salt (n=2)	170 ±10	44 ±17	3.9 ±0.1	16.5 ±0.8	51.0 ±1.8
Q334L with NaCl (n=2)	252 ±8	220 ±18	1.1 ±0.1	ND	ND
R336L no salt (n=7)	49 ±13	48 ±10	1.0 ±0.5	12.8 ±1.2	45.0 ±5.1
R336L with NaCl (n=4)	188 ±14	212 ±33	0.9 ±0.3	53.0 ± 0.1	ND
Y346F no salt (n=2)	220 ±4	88 ±16	2.5 ±0.6	21.4 ±1.4	53.1 ±1.6
Y346F with NaCl (n=2)	251 ±6	218 ±5	1.2 ±0.2	ND	ND
F335Y no salt (n=2)	176 ±6	40 ±10	4.4 ±1.1	20.3 ±1.1	50.2 ±1.3
F335Y9 with NaCl (n=2)	270 ±32	260 ±42	1.0 ±0.3	52.2 ±0.1	ND
S79A no salt (n=3)	271 ± 44	42 ±7	6.5 ±1.7	27.9 ±1.7	44.1 ±3.4
S79A with NaCl (n=3)	325 ±38	193 ±45	1.8 ±0.5	ND	ND
S87A no salt (n=3)	57 ±6	22 ±3	2.6 ±0.6	20.1 ±1.8	47.5 ±1.1
S87A with NaCl (n=4)	77 ±13	62 ±15	1.3 ±0.4	ND	ND
S79A/S87A no salt (n=4)	12 ±4	35 ±4	0.34 ±0.05	25.2 ±3.6	57.0 ±4.9
S79A/S87A with NaCl (n=4)	15 ±4	159 ±13	0.09 ±0.01	49.1 ±5.1	ND

A crystal structure for R336L has been solved (unpublished). It shows no major main-chain changes, and has an identical active site as the wild type. The only significant change is in the relative B-factors which are on average higher in the Ser cluster region (S79 and S87) opposite the large-loop, but the large interface loop itself is on average similarly mobile (Figure 4.1). However, B-factor comparisons between structures can be perplexing due to variable diffraction resolution and packing of the crystals.

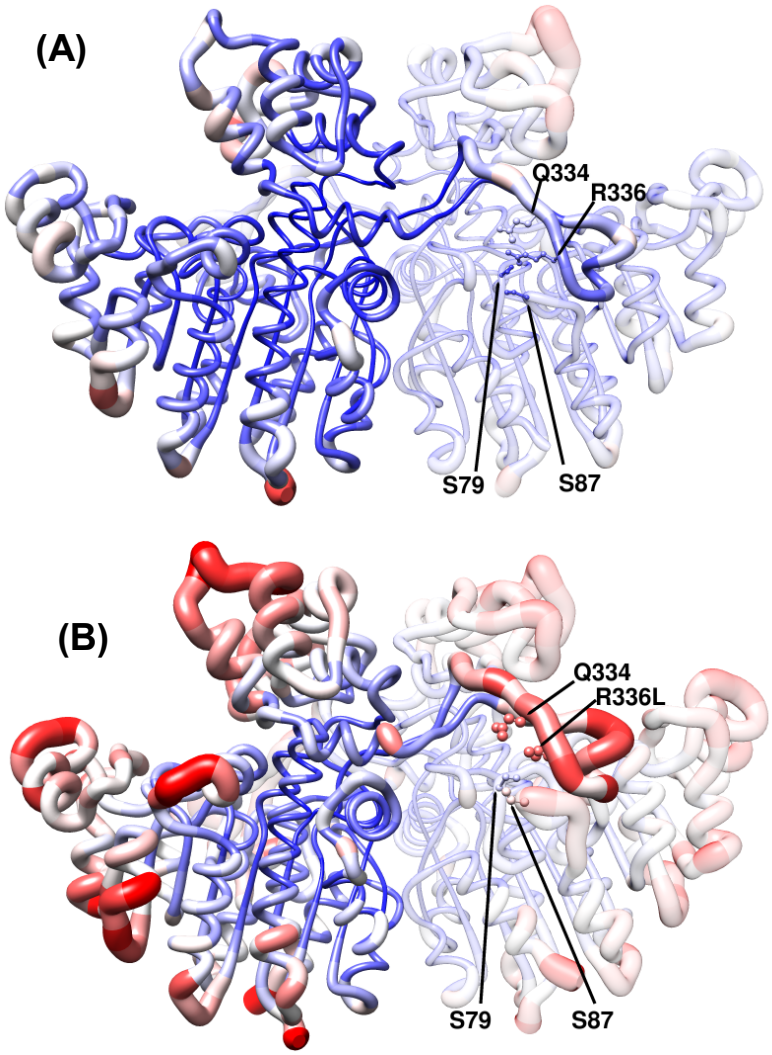

Figure 4.1. Average B-factor comparison of residues for VAP wild type structure (PDB: 3E2D) (A) and the R336L variant (unpublished) (B). The comparison was made in UCSF Chimera using the "render by attribute" plugin. The color coding is relative for each structure, blue for the lowest B-factors and red for the highest (white is set for the average). The resolution and crystal lattices are not the same for each structure, thus the comparison can only be applied relatively for each structure. Note the increased mobility of the helix at position S87 for R336L.

5 Conclusions

Paper I

The results indicated that the dimer interface of VAP is not the most sensitive part of the enzyme, where the inactivated form is likely an inactive dimeric intermediate. We ascertained that the measurement of Trp fluorescence is not a possible route to monitor dimer-monomer equilibrium, likely due to folded monomers not being populated in the denaturation process. However, we discovered that the region where the buried W460 resides close to the interface is important for modulating catalytic activity. Furthermore, discovering that W460 is a phosphorescent residue opens new possibilities to use phosphorescence to probe subunit heterogeneity and structural changes.

Paper II

Ionic strength, and chloride, have a large effect on activity and stability of VAP. We propose that the chloride ion binds specifically to the active site in a pH dependent fashion. It is likely that the chloride ions are coordinated to Zn^{2+} where the phosphate group usually binds (see Figure 1.6). The chloride both decreases the affinity of the enzyme for the substrate and increases the rate of phosphate release (the rate limiting step) by competing with the Zn^{2+} coordination site. Results indicated that as the enzyme was inactivated at low ionic strength, it is transformed to an inactive dimer which retains both the magnesium and two zinc ions in the active site. By bringing the pH from neutral to basic (7 – 10.5), a conformational change occurs (measured by Trp fluorescence), so that salt no longer has effect on activity or stability.

Paper III

Here we have shown using the intrinsic fluorescence probe bimane that as the enzyme is inactivated, subtle changes are detected at the interface. We have also confirmed that folded monomers are not populated in the denaturation pathway (at least in *in vitro)*. This was debated in Paper I, where size-exclusion chromatography (SEC) indicated a split of the dimeric peak revealing an intermediate species. Perhaps the inactivated dimer has a slightly different mobility, resulting in splitting of the dimer in the SEC diagram. The

effect of pH and NaCl on stability of VAP was also put in numbers for the first time in terms of free energy. The native state is remarkably unstable at low ionic strength (at pH 8.0), with a ΔG of 2-3 kJ/mol, which is an energy significantly less than for one hydrogen bond. In the last part of the discussion, speculations about the half-of-sites reactivity of VAP and APs are put forward. It is suggested that there might exist networks of interactions which are mediated through the interface and where entropy might play a big role in mediating product release, presumable by release of bound water in a cooperative fashion from each subunit alternatively (as shown for fluoroacetate dehalogenase in Figure 1.14).

Paper IV

Results show that the role of the large interface loop is mostly to stabilize the active site by an unknown mechanism. Both intra- and interchain hydrogen at the loop were shown to be important for important for stability. It remains to be tested how much the R336L mutation affects the K_d of the dimer. With regards to catalytic efficiency, the hydrogen network linking the large loop with the active site of the opposite monomer, seems to be important. However, the intramolecular hydrogen bonds are not as important as the interchain hydrogen bonds involving S79A and S87A. Possibly, the loops where S79 and S87 are located need to have some degree of restriction to maintain the correct positions of catalytic residues (S65 and R129). Disrupting these hydrogen bonds gives increased mobility of the two small loops connected with the active site (residues 50-54 and 78-80) which is catalytically unfavorable. These results indicate that high mobility of loops in the active site does not always result in increased k_{cat}, especially for enzymes that have a large active site, where nucleophilic residues and substrate binding metal ions need to be orchestrated towards the catalytically active state.

References

[1] Wojciechowski, C. L., Cardia, J. P., and Kantrowitz, E. R. (2002) Alkaline phosphatase from the hyperthermophilic bacterium *T. maritima* requires cobalt for activity, *Protein Sci 11*, 903-911.

[2] Hulett, F. M., Kim, E. E., Bookstein, C., Kapp, N. V., Edwards, C. W., and Wyckoff, H. W. (1991) *Bacillus subtilis* alkaline phosphatases III and IV. Cloning, sequencing, and comparisons of deduced amino acid sequence with *Escherichia coli* alkaline phosphatase three-dimensional structure, *J Biol Chem 266*, 1077-1084.

[3] Simpson, R. T., and Vallee, B. L. (1968) Two differentiable classes of metal atoms in alkaline phosphatase of *Escherichia coli*, *Biochemistry 7*, 4343-4350.

[4] Applebury, M. L., and Coleman, J. E. (1969) *Escherichia coli* Co(II) alkaline phosphatase, *J Biol Chem 244*, 709-718.

[5] Wang, J., Stieglitz, K. A., and Kantrowitz, E. R. (2005) Metal specificity is correlated with two crucial active site residues in *Escherichia coli* alkaline phosphatase, *Biochemistry 44*, 8378-8386.

[6] Hjorleifsson, J. G., and Asgeirsson, B. (2017) pH-dependent binding of chloride to a marine alkaline phosphatase affects the catalysis, active site stability, and dimer equilibrium, *Biochemistry 56*, 5075-5089.

[7] Cathala, G., and Brunel, C. (1975) Bovine kidney alkaline phosphatase. Catalytic properties, subunit interactions in the catalytic process, and mechanism of Mg^{2+} stimulation, *J Biol Chem 250*, 6046-6053.

[8] Hung, H. C., and Chang, G. G. (2001) Differentiation of the slow-binding mechanism for magnesium ion activation and zinc ion inhibition of human placental alkaline phosphatase, *Protein Sci 10*, 34-45.

[9] Murphy, J. E., Xu, X., and Kantrowitz, E. R. (1993) Conversion of a magnesium binding site into a zinc binding site by a single amino acid substitution in *Escherichia coli* alkaline phosphatase, *J Biol Chem 268*, 21497-21500.

[10] Janeway, C. M., Xu, X., Murphy, J. E., Chaidaroglou, A., and Kantrowitz, E. R. (1993) Magnesium in the active site of *Escherichia coli* alkaline phosphatase is important for both structural stabilization and catalysis, *Biochemistry 32*, 1601-1609.

[11] Murphy, J. E., Tibbitts, T. T., and Kantrowitz, E. R. (1995) Mutations at positions 153 and 328 in *Escherichia coli* alkaline phosphatase provide insight towards the structure and function of mammalian and yeast alkaline phosphatases, *J Mol Biol 253*, 604-617.

[12] Roberts, C. H., and Chlebowski, J. F. (1984) Trypsin modification of *Escherichia coli* alkaline phosphatase, *J Biol Chem 259*, 729-733.

[13] Tyler-Cross, R., Roberts, C. H., and Chlebowski, J. F. (1989) Proteolytic modification of *Escherichia coli* alkaline phosphatase, *J Biol Chem 264*, 4523-4528.

[14] Olafsdottir, S., and Chlebowski, J. F. (1989) A hybrid *Escherichia coli* alkaline phosphatase formed on proteolysis, *J Biol Chem 264*, 4529-4535.

[15] Wang, E., Koutsioulis, D., Leiros, H. K., Andersen, O. A., Bouriotis, V., Hough, E., and Heikinheimo, P. (2007) Crystal structure of alkaline phosphatase from the Antarctic bacterium TAB5, *J Mol Biol 366*, 1318-1331.

[16] Hoylaerts, M. F., and Millan, J. L. (1991) Site-directed mutagenesis and epitope-mapped monoclonal-antibodies define a catalytically important conformational difference between human placental and germ-cell alkaline phosphatase, *Eur J Biochem 202*, 605-616.
[17] Hoylaerts, M. F., Manes, T., and Millan, J. L. (1992) The molecular basis of the uncompetitive inhibition of placental and germ-cell alkaline phosphatase, *FASEB J 6*, A334-A334.
[18] Bossi, M., Hoylaerts, M. F., and Millan, J. L. (1993) Modifications in a flexible surface loop modulate the isozyme-specific properties of mammalian alkaline phosphatases, *J Biol Chem 268*, 25409-25416.
[19] Hummer, C., and Millan, J. L. (1991) Gly429 is the major determinant of uncompetitive inhibition of human germ cell alkaline phosphatase by L-leucine, *Biochem J 274*, 91-95.
[20] Watanabe, T., Wada, N., Kim, E. E., Wyckoff, H. W., and Chou, J. Y. (1991) Mutation of a single amino acid converts germ cell alkaline phosphatase to placental alkaline phosphatase, *J Biol Chem 266*, 21174-21178.
[21] Barnard, P. W. C., Bunton, C. A., Llewellyn, D. R., Vernon, C. A., and Welch, V. A. (1961) 523. The reactions of organic phosphates. Part V. The hydrolysis of triphenyl and trimethyl phosphates, *J Chem Soc (Resumed) 0*, 2670-2676.
[22] Heppel, L. A., Harkness, D. R., and Hilmoe, R. J. (1962) A study of the substrate specificity and other properties of the alkaline phosphatase of *Escherichia coli*, *J Biol Chem 237*, 841-846.
[23] McComb, R. B., Bowers, G. N., and Posen, S. (1979) *Alkaline phosphatase*, Plenum Press, New York
[24] Williams, A., and Naylor, R. A. (1971) Evidence for $Sn_2(P)$ mechanism in phosphorylation of alkaline phosphatase by substrates, *J Chem Soc B*, 1973-&.
[25] Zalatan, J. G., Fenn, T. D., and Herschlag, D. (2008) Comparative enzymology in the alkaline phosphatase superfamily to determine the catalytic role of an active-site metal ion, *J Mol Biol 384*, 1174-1189.
[26] Koutsioulis, D., Lyskowski, A., Maki, S., Guthrie, E., Feller, G., Bouriotis, V., and Heikinheimo, P. (2010) Coordination sphere of the third metal site is essential to the activity and metal selectivity of alkaline phosphatases, *Protein Sci 19*, 75-84.
[27] Kamerlin, S. C. L., and Wilkie, J. (2007) The role of metal ions in phosphate ester hydrolysis, *Org Biomol Chem 5*, 2098-2108.
[28] Orhanovic, S., and Pavela-Vrancic, M. (2003) Dimer asymmetry and the catalytic cycle of alkaline phosphatase from *Escherichia coli*, *Eur J Biochem 270*, 4356-4364.
[29] Stec, B., Holtz, K. M., and Kantrowitz, E. R. (2000) A revised mechanism for the alkaline phosphatase reaction involving three metal ions, *J Mol Biol 299*, 1303-1311.
[30] Fernley, H. N., and Walker, P. C. (1968) Effect of sodium chloride on *Escherichia coli* alkaline phosphatase, *Biochem J 110*, 11P-12P.
[31] Bloch, W., and Schlesinger, M. J. (1974) Kinetics of substrate hydrolysis by molecular variants of *Escherichia coli* alkaline phosphatase, *J Biol Chem 249*, 1760-1768.
[32] Andrews, L. D., Zalatan, J. G., and Herschlag, D. (2014) Probing the origins of catalytic discrimination between phosphate and sulfate monoester hydrolysis: comparative analysis of alkaline phosphatase and protein tyrosine phosphatases, *Biochemistry 53*, 6811-6819.

[33] Wilson, I. B., Dayan, J., and Cyr, K. (1964) Some properties of alkaline phosphatase from *Escherichia coli*. Transphosphorylation, *J Biol Chem 239*, 4182-4185.
[34] Harkness, D. R. (1968) Studies on human placental alkaline phosphatase. II. Kinetic properties and studies on the apoenzyme, *Arch Biochem Biophys 126*, 513-523.
[35] McComb, R. B., and Bowers, G. N. (1972) Study of optimum buffer conditions for measuring alkaline phosphatase activity in human serum, *Clin Chem 18*, 97-104.
[36] Chappelet-Tordo, D., Fosset, M., Iwatsubo, M., Gache, C., and Lazdunski, M. (1974) Intestinal alkaline phosphatase. Catalytic properties and half-of-the-sites reactivity, *Biochemistry 13*, 1788-1795.
[37] Applebury, M. L., Johnson, B. P., and Coleman, J. E. (1970) Phosphate binding to alkaline phosphatase. Metal ion dependence, *J Biol Chem 245*, 4968-4976.
[38] Hoylaerts, M. F., Ding, L., Narisawa, S., Van Kerckhoven, S., and Millan, J. L. (2006) Mammalian alkaline phosphatase catalysis requires active site structure stabilization via the N-terminal amino acid microenvironment, *Biochemistry 45*, 9756-9766.
[39] Halford, S. E., Bennett, N. G., Trentham, D. R., and Gutfeund, H. (1969) A substate-induced conformation change in the reaction of alkaline phosphatase from *Escherichia coli*, *Biochem J 114*, 243-251.
[40] Reid, T. W., and Wilson, I. B. (1971) Conformational isomers of alkaline phosphatase in the mechanism of hydrolysis, *Biochemistry 10*, 380-387.
[41] Halford, S. E. (1972) *Escherichia coli* alkaline phosphatase. Relaxation spectra of ligand binding, *Biochem J 126*, 727-738.
[42] Bloch, W., and Schlesinger, M. J. (1973) The phosphate content of *Escherichia coli* alkaline phosphatase and its effect on stopped flow kinetic studies, *J Biol Chem 248*, 5794-5805.
[43] Hayashi, M., Unemoto, T., and Hayashi, M. (1973) pH- and anion-dependent salt modifications of alkaline phosphatase from a slightly halophilic *Vibrio alginolyticus*, *Biochim Biophys Acta 315*, 83-93.
[44] Gettins, P., and Coleman, J. E. (1984) Chloride binding to alkaline phosphatase. ^{113}Cd and ^{35}Cl NMR, *J Biol Chem 259*, 11036-11040.
[45] Naganna, B., Venugopal, B., and Sripathi, C. E. (1955) Occurrence of alkaline pyrophosphatase in vegetable tissues, *Biochem J 60*, 224-225.
[46] Wanner, B. L., and Chang, B. D. (1987) The *phoBR* operon in *Escherichia coli* K-12, *J Bacteriol 169*, 5569-5574.
[47] Garen, A., and Echols, H. (1962) Properties of two regulating genes for alkaline phosphatase, *J Bacteriol 83*, 297-300.
[48] Majumdar, A., Ghatak, A., and Ghosh, R. K. (2005) Identification of the gene for the monomeric alkaline phosphatase of *Vibrio cholerae* serogroup O1 strain, *Gene 344*, 251-258.
[49] Sebastian, M., and Ammerman, J. W. (2009) The alkaline phosphatase *PhoX* is more widely distributed in marine bacteria than the classical *PhoA*, *ISME J 3*, 563-572.
[50] Malamy, M., and Horecker, B. L. (1961) The localization of alkaline phosphatase in *E. coli* K12, *Biochem Biophys Res Commun 5*, 104-108.
[51] Schlesinger, M. J. (1968) Secretion of alkaline phosphatase subunits by spheroplasts of *Escherichia coli*, *J Bacteriol 96*, 727-733.
[52] Stock, J. B., Rauch, B., and Roseman, S. (1977) Periplasmic space in *Salmonella typhimurium* and *Escherichia coli*, *J Biol Chem 252*, 7850-7861.

[53] Bowers, B., and Korn, E. D. (1973) Cytochemical identification of phosphatase activity in the contractile vacuole of *Acanthamoeba castellanii*, *J Cell Biol 59*, 784-791.
[54] Pettengill, O. (1947) Phosphatase activity in the chloride cells in the gill of *Fundulus heteroclitus*, *Biol Bull 93*, 224.
[55] Haarhaus, M., Brandenburg, V., Kalantar-Zadeh, K., Stenvinkel, P., and Magnusson, P. (2017) Alkaline phosphatase: a novel treatment target for cardiovascular disease in CKD, *Nat Rev Nephrol 13*, 429-442.
[56] Magnusson, P., Degerblad, M., Saaf, M., Larsson, L., and Thoren, M. (1997) Different responses of bone alkaline phosphatase isoforms during recombinant insulin-like growth factor-I (IGF-I) and during growth hormone therapy in adults with growth hormone deficiency, *J Bone Miner Res 12*, 210-220.
[57] Anh, D. J., Eden, A., and Farley, J. R. (2001) Quantitation of soluble and skeletal alkaline phosphatase, and insoluble alkaline phosphatase anchor-hydrolase activities in human serum, *Clin Chim Acta 311*, 137-148.
[58] Magnusson, P., Sharp, C. A., and Farley, J. R. (2002) Different distributions of human bone alkaline phosphatase isoforms in serum and bone tissue extracts, *Clin Chim Acta 325*, 59-70.
[59] Makita, S., Al-Shawafi, H. A., Sultana, S., Sohda, M., Nomura, S., and Oda, K. (2012) A dimerization defect caused by a glycine substitution at position 420 by serine in tissue-nonspecific alkaline phosphatase associated with perinatal hypophosphatasia, *FEBS J 279*, 4327-4337.
[60] Sultana, S., Al-Shawafi, H. A., Makita, S., Sohda, M., Amizuka, N., Takagi, R., and Oda, K. (2013) An asparagine at position 417 of tissue-nonspecific alkaline phosphatase is essential for its structure and function as revealed by analysis of the N417S mutation associated with severe hypophosphatasia, *Mol Genet Metab 109*, 282-288.
[61] Tsonis, P. A., Argraves, W. S., and Millan, J. L. (1988) A putative functional domain of human placental alkaline phosphatase predicted from sequence comparisons, *Biochem J 254*, 623-624.
[62] Hoylaerts, M. F., Manes, T., and Millan, J. L. (1997) Mammalian alkaline phosphatases are allosteric enzymes, *J Biol Chem 272*, 22781-22787.
[63] Hoylaerts, M. F., Van Kerckhoven, S., Kiffer-Moreira, T., Sheen, C., Narisawa, S., and Millan, J. L. (2015) Functional significance of calcium binding to tissue-nonspecific alkaline phosphatase, *PLoS One 10*, e0119874.
[64] Robison, R. (1923) The possible significance of hexosephosphoric esters in ossification, *Biochem J 17*, 286-293.
[65] Millan, J. L., and Whyte, M. P. (2016) Alkaline phosphatase and hypophosphatasia, *Calcif Tissue Int 98*, 398-416.
[66] Jono, S., Peinado, C., and Giachelli, C. M. (2000) Phosphorylation of osteopontin is required for inhibition of vascular smooth muscle cell calcification, *J Biol Chem 275*, 20197-20203.
[67] Whyte, M. P., Greenberg, C. R., Salman, N. J., Bober, M. B., McAlister, W. H., Wenkert, D., Van Sickle, B. J., Simmons, J. H., Edgar, T. S., Bauer, M. L., Hamdan, M. A., Bishop, N., Lutz, R. E., McGinn, M., Craig, S., Moore, J. N., Taylor, J. W., Cleveland, R. H., Cranley, W. R., Lim, R., Thacher, T. D., Mayhew, J. E., Downs, M., Millan, J. L., Skrinar, A. M., Crine, P., and Landy, H. (2012) Enzyme-replacement therapy in life-threatening hypophosphatasia, *N Engl J Med 366*, 904-913.

[68] Nishioka, T., Tomatsu, S., Gutierrez, M. A., Miyamoto, K., Trandafirescu, G. G., Lopez, P. L., Grubb, J. H., Kanai, R., Kobayashi, H., Yamaguchi, S., Gottesman, G. S., Cahill, R., Noguchi, A., and Sly, W. S. (2006) Enhancement of drug delivery to bone: characterization of human tissue-nonspecific alkaline phosphatase tagged with an acidic oligopeptide, *Mol Genet Metab 88*, 244-255.

[69] Kunutsor, S. K., Apekey, T. A., and Khan, H. (2014) Liver enzymes and risk of cardiovascular disease in the general population: a meta-analysis of prospective cohort studies, *Atherosclerosis 236*, 7-17.

[70] Tonelli, M., Curhan, G., Pfeffer, M., Sacks, F., Thadhani, R., Melamed, M. L., Wiebe, N., and Muntner, P. (2009) Relation between alkaline phosphatase, serum phosphate, and all-cause or cardiovascular mortality, *Circulation 120*, 1784-1792.

[71] Sheen, C. R., Kuss, P., Narisawa, S., Yadav, M. C., Nigro, J., Wang, W., Chhea, T. N., Sergienko, E. A., Kapoor, K., Jackson, M. R., Hoylaerts, M. F., Pinkerton, A. B., O'Neill, W. C., and Millan, J. L. (2015) Pathophysiological role of vascular smooth muscle alkaline phosphatase in medial artery calcification, *J Bone Miner Res 30*, 824-836.

[72] Pike, A. F., Kramer, N. I., Blaauboer, B. J., Seinen, W., and Brands, R. (2015) An alkaline phosphatase transport mechanism in the pathogenesis of Alzheimer's disease and neurodegeneration, *Chem Biol Interact 226*, 30-39.

[73] Pike, A. F., Kramer, N. I., Blaauboer, B. J., Seinen, W., and Brands, R. (2013) A novel hypothesis for an alkaline phosphatase 'rescue' mechanism in the hepatic acute phase immune response, *Biochim Biophys Acta 1832*, 2044-2056.

[74] Grabarek, J., Du, L. T., Johnson, G. L., Lee, B. W., Phelps, D. J., and Darzynkiewicz, Z. (2002) Sequential activation of caspases and serine proteases (serpases) during apoptosis, *Cell Cycle 1*, 124-131.

[75] Deracinois, B., Lenfant, A. M., Dehouck, M. P., and Flahaut, C. (2015) Tissue non-specific alkaline phosphatase (TNAP) in vessels of the brain, *Subcell Biochem 76*, 125-151.

[76] Diaz-Hernandez, M., Gomez-Ramos, A., Rubio, A., Gomez-Villafuertes, R., Naranjo, J. R., Miras-Portugal, M. T., and Avila, J. (2010) Tissue-nonspecific alkaline phosphatase promotes the neurotoxicity effect of extracellular tau, *J Biol Chem 285*, 32539-32548.

[77] Whyte, M. P. (2016) Hypophosphatasia - aetiology, nosology, pathogenesis, diagnosis and treatment, *Nat Rev Endocrinol 12*, 233-246.

[78] Lalles, J. P. (2014) Intestinal alkaline phosphatase: novel functions and protective effects, *Nutr Rev 72*, 82-94.

[79] Bilski, J., Mazur-Bialy, A., Wojcik, D., Zahradnik-Bilska, J., Brzozowski, B., Magierowski, M., Mach, T., Magierowska, K., and Brzozowski, T. (2017) The role of intestinal alkaline phosphatase in inflammatory disorders of gastrointestinal tract, *Mediators Inflamm 2017*, 9074601.

[80] Kaliannan, K., Hamarneh, S. R., Economopoulos, K. P., Nasrin Alam, S., Moaven, O., Patel, P., Malo, N. S., Ray, M., Abtahi, S. M., Muhammad, N., Raychowdhury, A., Teshager, A., Mohamed, M. M., Moss, A. K., Ahmed, R., Hakimian, S., Narisawa, S., Millan, J. L., Hohmann, E., Warren, H. S., Bhan, A. K., Malo, M. S., and Hodin, R. A. (2013) Intestinal alkaline phosphatase prevents metabolic syndrome in mice, *Proc Natl Acad Sci U S A 110*, 7003-7008.

[81] Malo, M. S., Alam, S. N., Mostafa, G., Zeller, S. J., Johnson, P. V., Mohammad, N., Chen, K. T., Moss, A. K., Ramasamy, S., Faruqui, A., Hodin, S., Malo, P. S., Ebrahimi, F., Biswas, B., Narisawa, S., Millan, J. L., Warren, H. S., Kaplan, J. B.,

Kitts, C. L., Hohmann, E. L., and Hodin, R. A. (2010) Intestinal alkaline phosphatase preserves the normal homeostasis of gut microbiota, *Gut 59*, 1476-1484.
[82] Bates, J. M., Akerlund, J., Mittge, E., and Guillemin, K. (2007) Intestinal alkaline phosphatase detoxifies lipopolysaccharide and prevents inflammation in zebrafish in response to the gut microbiota, *Cell Host & Microbe 2*, 371-382.
[83] Akiba, Y., Mizumori, M., Guth, P. H., Engel, E., and Kaunitz, J. D. (2007) Duodenal brush border intestinal alkaline phosphatase activity affects bicarbonate secretion in rats, *Am J Physiol Gastrointest Liver Physiol 293*, G1223-1233.
[84] Ghosh, S. S., Gehr, T. W., and Ghosh, S. (2014) Curcumin and chronic kidney disease (CKD): major mode of action through stimulating endogenous intestinal alkaline phosphatase, *Molecules 19*, 20139-20156.
[85] Millán, J. L. (2006) The *in vivo* role of TNAP, In: *Mammalian Alkaline Phosphatases*, pp. 105-129, Wiley-VCH Verlag GmbH & Co. KGaA.
[86] Millán, J. L. (2006) Knockout mouse models, In: *Mammalian Alkaline Phosphatases*, pp 131-164, Wiley-VCH Verlag GmbH & Co. KGaA.
[87] Scharer, H. (1938) A rapid phosphomonoesterase test for control of dairy pasteurization, *J Dairy Sci 21*, 21-34.
[88] Shahani, K. M. (1966) Milk enzymes: their role and significance, *J Dairy Sci 49*, 907-920.
[89] Engvall, E., Jonsson, K., and Perlmann, P. (1971) Enzyme-linked immunosorbent assay. II. Quantitative assay of protein antigen, immunoglobulin G, by means of enzyme-labelled antigen and antibody-coated tubes, *Biochim Biophys Acta 251*, 427-434.
[90] Engvall, E., and Perlmann, P. (1971) Enzyme-linked immunosorbent assay (ELISA). Quantitative assay of immunoglobulin G, *Immunochemistry 8*, 871-874.
[91] Stern, R., and Wilczek, J. (1973) An alkaline phosphatase-linked assay for ribonucleases, *Anal Biochem 54*, 419-428.
[92] Puhakainen, E., Saarinen, A., and Hanninen, O. (1977) UDPglucuronic acid pyrophosphatase assay with the aid of alkaline phosphatase, *Acta Chem Scand B B31*, 125-129.
[93] Eriksson, J., and Langel, U. (2016) Quantitative microplate assay for real-time nuclease kinetics, *PLoS One 11*, e0154099.
[94] Zhou, M., Diwu, Z., Panchuk-Voloshina, N., and Haugland, R. P. (1997) A stable nonfluorescent derivative of resorufin for the fluorometric determination of trace hydrogen peroxide: Applications in detecting the activity of phagocyte NADPH oxidase and other oxidases, *Anal Biochem 253*, 162-168.
[95] Brune, M., Hunter, J. L., Corrie, J. E., and Webb, M. R. (1994) Direct, real-time measurement of rapid inorganic phosphate release using a novel fluorescent probe and its application to actomyosin subfragment 1 ATPase, *Biochemistry 33*, 8262-8271.
[96] Olsen, R. L., Overbo, K., and Myrnes, B. (1991) Alkaline phosphatase from the hepatopancreas of shrimp (*Pandalus borealis*) - a dimeric enzyme with catalytically active bubunits, *Comp Biochem Phys B 99*, 755-761.
[97] Nilsen, I. W., Overbo, K., and Olsen, R. L. (2001) Thermolabile alkaline phosphatase from Northern shrimp (*Pandalus borealis*): protein and cDNA sequence analyses, *Comp Biochem Physiol B Biochem Mol Biol 129*, 853-861.

[98] de Backer, M., McSweeney, S., Rasmussen, H. B., Riise, B. W., Lindley, P., and Hough, E. (2002) The 1.9 Ångstrom crystal structure of heat-labile shrimp alkaline phosphatase, *J Mol Biol 318*, 1265-1274.
[99] de Backer, M. M. E., McSweeney, S., Lindley, P. F., and Hough, E. (2004) Ligand-binding and metal-exchange crystallographic studies on shrimp alkaline phosphatase, *Acta Crystallogr D 60*, 1555-1561.
[100] Rina, M., Pozidis, C., Mavromatis, K., Tzanodaskalaki, M., Kokkinidis, M., and Bouriotis, V. (2000) Alkaline phosphatase from the Antarctic strain TAB5. Properties and psychrophilic adaptations, *Eur J Biochem 267*, 1230-1238.
[101] Koutsioulis, D., Wang, E., Tzanodaskalaki, M., Nikiforaki, D., Deli, A., Feller, G., Heikinheimo, P., and Bouriotis, V. (2008) Directed evolution on the cold adapted properties of TAB5 alkaline phosphatase, *Protein Eng Des Sel 21*, 319-327.
[102] Ishida, Y., Tsuruta, H., Tsuneta, S. T., Uno, T., Watanabe, K., and Aizono, Y. (1998) Characteristics of psychrophilic alkaline phosphatase, *Biosci Biotechnol Biochem 62*, 2246-2250.
[103] Murakawa, T., Yamagata, H., Tsuruta, H., and Aizono, Y. (2002) Cloning of cold-active alkaline phosphatase gene of a psychrophile, *Shewanella sp*., and expression of the recombinant enzyme, *Biosci Biotechnol Biochem 66*, 754-761.
[104] Tsuruta, H., Mikami, B., Higashi, T., and Aizono, Y. (2010) Crystal structure of cold-active alkaline phosphatase from the psychrophile *Shewanella sp.*, *Biosci Biotechnol Biochem 74*, 69-74.
[105] Asgeirsson, B., Nielsen, B. N., and Hojrup, P. (2003) Amino acid sequence of the cold-active alkaline phosphatase from Atlantic cod (*Gadus morhua*), *Comp Biochem Physiol B Biochem Mol Biol 136*, 45-60.
[106] Asgeirsson, B., Hartemink, R., and Chlebowski, J. F. (1995) Alkaline-Phosphatase from Atlantic Cod (*Gadus morhua*) - Kinetic and Structural-Properties Which Indicate Adaptation to Low-Temperatures, *Comp Biochem Phys B 110*, 315-329.
[107] Asgeirsson, B., Hauksson, J., and Gunnarsson, G. (2000) Dissociation and unfolding of cold-active alkaline phosphatase from Atlantic cod in the presence of guanidinium chloride, *Eur J Biochem 267*, 6403-6412.
[108] Asgeirsson, B., and Guojonsdottir, K. (2006) Reversible inactivation of alkaline phosphatase from Atlantic cod (*Gadus morhua*) in urea, *Biochim Biophys Acta 1764*, 190-198.
[109] Woolkalis, M. J., and Baumann, P. (1981) Evolution of alkaline phosphatase in marine species of *Vibrio*, *J Bacteriol 147*, 36-45.
[110] Hauksson, J. B., Andresson, O. S., and Asgeirsson, B. (2000) Heat-labile bacterial alkaline phosphatase from a marine *Vibrio sp.*, *Enzyme Microb Technol 27*, 66-73.
[111] Landt, M., Boltz, S. C., and Butler, L. G. (1978) Alkaline phosphatase: affinity chromatography and inhibition by phosphonic acids, *Biochemistry 17*, 915-919.
[112] Asgeirsson, B., and Andresson, O. S. (2001) Primary structure of cold-adapted alkaline phosphatase from a *Vibrio sp*. as deduced from the nucleotide gene sequence, *Biochim Biophys Acta 1549*, 99-111.
[113] Heidarsson, P. O., Sigurdsson, S. T., and Asgeirsson, B. (2009) Structural features and dynamics of a cold-adapted alkaline phosphatase studied by EPR spectroscopy, *FEBS J 276*, 2725-2735.
[114] Gudjonsdottir, K., and Asgeirsson, B. (2008) Effects of replacing active site residues in a cold-active alkaline phosphatase with those found in its mesophilic counterpart from *Escherichia coli*, *FEBS J 275*, 117-127.

[115] Hjorleifsson, J. G., and Asgeirsson, B. (2016) Cold-active alkaline phosphatase is irreversibly transformed into an inactive dimer by low urea concentrations, *Biochim Biophys Acta 1864*, 755-765.
[116] Helland, R., Larsen, R. L., and Asgeirsson, B. (2009) The 1.4 Å crystal structure of the large and cold-active *Vibrio sp*. alkaline phosphatase, *Biochim Biophys Acta 1794*, 297-308.
[117] Jensen, R. A. (1976) Enzyme recruitment in evolution of new function, *Annu Rev Microbiol 30*, 409-425.
[118] Tokuriki, N., and Tawfik, D. S. (2009) Protein dynamism and evolvability, *Science 324*, 203-207.
[119] Khersonsky, O., and Tawfik, D. S. (2010) Enzyme promiscuity: A mechanistic and evolutionary perspective, *Ann Rev Biochem 79*, 471-505.
[120] Pabis, A., Risso, V. A., Sanchez-Ruiz, J. M., and Kamerlin, S. C. L. (2018) Cooperativity and flexibility in enzyme evolution, *Curr Opin Struc Biol 48*, 83-92.
[121] Campbell, E., Kaltenbach, M., Correy, G. J., Carr, P. D., Porebski, B. T., Livingstone, E. K., Afriat-Jurnou, L., Buckle, A. M., Weik, M., Hollfelder, F., Tokuriki, N., and Jackson, C. J. (2016) The role of protein dynamics in the evolution of new enzyme function, *Nat Chem Biol 12*, 944-950.
[122] Aharoni, A., Gaidukov, L., Khersonsky, O., Mc, Q. G. S., Roodveldt, C., and Tawfik, D. S. (2005) The 'evolvability' of promiscuous protein functions, *Nat Genet 37*, 73-76.
[123] Amitai, G., Gupta, R. D., and Tawfik, D. S. (2007) Latent evolutionary potentials under the neutral mutational drift of an enzyme, *HFSP J 1*, 67-78.
[124] Bar-Rogovsky, H., Hugenmatter, A., and Tawfik, D. S. (2013) The evolutionary origins of detoxifying enzymes: the mammalian serum paraoxonases (PONs) relate to bacterial homoserine lactonases, *J Biol Chem 288*, 23914-23927.
[125] Khersonsky, O., and Tawfik, D. S. (2005) Structure-reactivity studies of serum paraoxonase PON1 suggest that its native activity is lactonase, *Biochemistry 44*, 6371-6382.
[126] Pabis, A., Duarte, F., and Kamerlin, S. C. (2016) Promiscuity in the enzymatic catalysis of phosphate and sulfate transfer, *Biochemistry 55*, 3061-3081.
[127] Pabis, A., and Kamerlin, S. C. (2016) Promiscuity and electrostatic flexibility in the alkaline phosphatase superfamily, *Curr Opin Struct Biol 37*, 14-21.
[128] Petrovic, D., Szeler, K., and Kamerlin, S. C. L. (2018) Challenges and advances in the computational modeling of biological phosphate hydrolysis, *Chem Commun (Camb)*.
[129] O'Brien, P. J., and Herschlag, D. (1998) Sulfatase activity of *E. coli* alkaline phosphatase demonstrates a functional link to arylsulfatases, an evolutionarily related enzyme family, *J Am Chem Soc 120*, 12369-12370.
[130] O'Brien, P. J., and Herschlag, D. (2001) Functional interrelationships in the alkaline phosphatase superfamily: phosphodiesterase activity of *Escherichia coli* alkaline phosphatase, *Biochemistry 40*, 5691-5699.
[131] Duarte, F., Amrein, B. A., and Kamerlin, S. C. (2013) Modeling catalytic promiscuity in the alkaline phosphatase superfamily, *Phys Chem Chem Phys 15*, 11160-11177.
[132] Allen, K. N., and Dunaway-Mariano, D. (2016) Catalytic scaffolds for phosphoryl group transfer, *Curr Opin Struct Biol 41*, 172-179.

[133] Duarte, F., Barrozo, A., Aqvist, J., Williams, N. H., and Kamerlin, S. C. (2016) The competing mechanisms of phosphate monoester dianion hydrolysis, *J Am Chem Soc 138*, 10664-10673.
[134] O'Brien, P. J., and Herschlag, D. (2002) Alkaline phosphatase revisited: hydrolysis of alkyl phosphates, *Biochemistry 41*, 3207-3225.
[135] O'Brien, P. J., Lassila, J. K., Fenn, T. D., Zalatan, J. G., and Herschlag, D. (2008) Arginine coordination in enzymatic phosphoryl transfer: evaluation of the effect of Arg166 mutations in *Escherichia coli* alkaline phosphatase, *Biochemistry 47*, 7663-7672.
[136] Chakraborty, S., Minda, R., Salaye, L., Bhattacharjee, S. K., and Rao, B. J. (2011) Active site detection by spatial conformity and electrostatic analysis--unravelling a proteolytic function in shrimp alkaline phosphatase, *PLoS One 6*, e28470.
[137] Chakraborty, S., Asgeirsson, B., Minda, R., Salaye, L., Frere, J. M., and Rao, B. J. (2012) Inhibition of a cold-active alkaline phosphatase by imipenem revealed by in silico modeling of metallo-beta-lactamase active sites, *FEBS Lett 586*, 3710-3715.
[138] Ghosh, K., Mazumder Tagore, D., Anumula, R., Lakshmaiah, B., Kumar, P. P., Singaram, S., Matan, T., Kallipatti, S., Selvam, S., Krishnamurthy, P., and Ramarao, M. (2013) Crystal structure of rat intestinal alkaline phosphatase--role of crown domain in mammalian alkaline phosphatases, *J Struct Biol 184*, 182-192.
[139] Marsh, J. A., and Teichmann, S. A. (2015) Structure, dynamics, assembly, and evolution of protein complexes, *Annu Rev Biochem 84*, 551-575.
[140] Goodsell, D. S., and Olson, A. J. (2000) Structural symmetry and protein function, *Annu Rev Biophys Biomol Struct 29*, 105-153.
[141] Tarassov, K., Messier, V., Landry, C. R., Radinovic, S., Serna Molina, M. M., Shames, I., Malitskaya, Y., Vogel, J., Bussey, H., and Michnick, S. W. (2008) An *in vivo* map of the yeast protein interactome, *Science 320*, 1465-1470.
[142] Marsh, J. A., and Teichmann, S. A. (2014) Protein flexibility facilitates quaternary structure assembly and evolution, *PLoS Biol 12*, e1001870.
[143] Kim, W. K., Henschel, A., Winter, C., and Schroeder, M. (2006) The many faces of protein-protein interactions: A compendium of interface geometry, *PLoS Comput Biol 2*, e124.
[144] Dayhoff, J. E., Shoemaker, B. A., Bryant, S. H., and Panchenko, A. R. (2010) Evolution of protein binding modes in homooligomers, *J Mol Biol 395*, 860-870.
[145] Archibald, J. M., Logsdon, J. M., and Doolittle, W. F. (1999) Recurrent paralogy in the evolution of archaeal chaperonins, *Curr Biol 9*, 1053-1056.
[146] Monod, J., Wyman, J., and Changeux, J. P. (1965) On the nature of allosteric transitions: A plausible model, *J Mol Biol 12*, 88-118.
[147] Bershtein, S., Mu, W., and Shakhnovich, E. I. (2012) Soluble oligomerization provides a beneficial fitness effect on destabilizing mutations, *Proc Natl Acad Sci U S A 109*, 4857-4862.
[148] Mei, G., Di Venere, A., Rosato, N., and Finazzi-Agro, A. (2005) The importance of being dimeric, *FEBS J 272*, 16-27.
[149] Koshland, D. E., Jr., Nemethy, G., and Filmer, D. (1966) Comparison of experimental binding data and theoretical models in proteins containing subunits, *Biochemistry 5*, 365-385.
[150] Hilser, V. J., and Thompson, E. B. (2007) Intrinsic disorder as a mechanism to optimize allosteric coupling in proteins, *Proc Natl Acad Sci U S A 104*, 8311-8315.

[151] Renatus, M., Stennicke, H. R., Scott, F. L., Liddington, R. C., and Salvesen, G. S. (2001) Dimer formation drives the activation of the cell death protease caspase 9, *Proc Natl Acad Sci U S A 98*, 14250-14255.
[152] Jin, L., Stec, B., Lipscomb, W. N., and Kantrowitz, E. R. (1999) Insights into the mechanisms of catalysis and heterotropic regulation of *Escherichia coli* aspartate transcarbamoylase based upon a structure of the enzyme complexed with the bisubstrate analogue N-phosphonacetyl-L-aspartate at 2.1 A, *Proteins 37*, 729-742.
[153] Kim, T. H., Mehrabi, P., Ren, Z., Sljoka, A., Ing, C., Bezginov, A., Ye, L., Pomes, R., Prosser, R. S., and Pai, E. F. (2017) The role of dimer asymmetry and protomer dynamics in enzyme catalysis, *Science 355*.
[154] Wielgus-Kutrowska, B., Grycuk, T., and Bzowska, A. (2018) Part-of-the-sites binding and reactivity in the homooligomeric enzymes - facts and artifacts, *Arch Biochem Biophys 642*, 31-45.
[155] Yuan, C., Rieke, C. J., Rimon, G., Wingerd, B. A., and Smith, W. L. (2006) Partnering between monomers of cyclooxygenase-2 homodimers, *Proc Natl Acad Sci U S A 103*, 6142-6147.
[156] He, S., Wu, Y., Yu, D., and Lai, L. (2011) Microsomal prostaglandin E synthase-1 exhibits one-third-of-the-sites reactivity, *Biochem J 440*, 13-21.
[157] Freiburger, L. A., Baettig, O. M., Sprules, T., Berghuis, A. M., Auclair, K., and Mittermaier, A. K. (2011) Competing allosteric mechanisms modulate substrate binding in a dimeric enzyme, *Nat Struct Mol Biol 18*, 288-294.
[158] Shi, J., Dertouzos, J., Gafni, A., Steel, D., and Palfey, B. A. (2006) Single-molecule kinetics reveals signatures of half-sites reactivity in dihydroorotate dehydrogenase A catalysis, *Proc Natl Acad Sci U S A 103*, 5775-5780.
[159] Bale, J. R., Chock, P. B., and Huang, C. Y. (1980) The nature of negative cooperativity in alkaline phosphatase. Kinetic patterns contrary to the flip-flop model, *J Biol Chem 255*, 8424-8430.
[160] Del Arco, A., Burguillo, F. J., Roig, M. G., Usero, J. L., Izquierdo, C., and Herraez, M. A. (1982) Negative cooperativity in alkaline phosphatase from *E. coli*: new kinetic evidence from a steady-state study, *Int J Biochem 14*, 127-140.
[161] Cioni, P., Piras, L., and Strambini, G. B. (1989) Tryptophan phosphorescence as a monitor of the structural role of metal ions in alkaline phosphatase, *Eur J Biochem 185*, 573-579.
[162] Sun, L., Kantrowitz, E. R., and Galley, W. C. (1997) Room temperature phosphorescence study of phosphate binding in *Escherichia coli* alkaline phosphatase, *Eur J Biochem 245*, 32-39.
[163] Kline, P. C., and Schramm, V. L. (1992) Purine nucleoside phosphorylase. Inosine hydrolysis, tight binding of the hypoxanthine intermediate, and third-the-sites reactivity, *Biochemistry 31*, 5964-5973.
[164] Miles, R. W., Tyler, P. C., Furneaux, R. H., Bagdassarian, C. K., and Schramm, V. L. (1998) One-third-the-sites transition-state inhibitors for purine nucleoside phosphorylase, *Biochemistry 37*, 8615-8621.
[165] Wang, F., Miles, R. W., Kicska, G., Nieves, E., Schramm, V. L., and Angeletti, R. H. (2000) Immucillin-H binding to purine nucleoside phosphorylase reduces dynamic solvent exchange, *Protein Sci 9*, 1660-1668.
[166] Bzowska, A., Koellner, G., Wielgus-Kutrowska, B., Stroh, A., Raszewski, G., Holy, A., Steiner, T., and Frank, J. (2004) Crystal structure of calf spleen purine nucleoside phosphorylase with two full trimers in the asymmetric unit: important implications for the mechanism of catalysis, *J Mol Biol 342*, 1015-1032.

[167] Chojnowski, G., Breer, K., Narczyk, M., Wielgus-Kutrowska, B., Czapinska, H., Hashimoto, M., Hikishima, S., Yokomatsu, T., Bochtler, M., Girstun, A., Staron, K., and Bzowska, A. (2010) 1.45 Å resolution crystal structure of recombinant PNP in complex with a pM multisubstrate analogue inhibitor bearing one feature of the postulated transition state, *Biochem Biophys Res Commun 391*, 703-708.

[168] Breer, K., Wielgus-Kutrowska, B., Girstun, A., Staron, K., Hashimoto, M., Hikishima, S., Yokomatsu, T., and Bzowska, A. (2010) Overexpressed proteins may act as mops removing their ligands from the host cells: a case study of calf PNP, *Biochem Biophys Res Commun 391*, 1203-1209.

[169] Wielgus-Kutrowska, B., Breer, K., Hashimoto, M., Hikishima, S., Yokomatsu, T., Narczyk, M., Dyzma, A., Girstun, A., Staron, K., and Bzowska, A. (2012) Trimeric purine nucleoside phosphorylase: exploring postulated one-third-of-the-sites binding in the transition state, *Bioorg Med Chem 20*, 6758-6769.

[170] Han, G. W., Yang, X. L., McMullan, D., Chong, Y. E., Krishna, S. S., Rife, C. L., Weekes, D., Brittain, S. M., Abdubek, P., Ambing, E., Astakhova, T., Axelrod, H. L., Carlton, D., Caruthers, J., Chiu, H. J., Clayton, T., Duan, L. A., Feuerhelm, J., Grant, J. C., Grzechnik, S. K., Jaroszewski, L., Jin, K. K., Klock, H. E., Knuth, M. W., Kumar, A., Marciano, D., Miller, M. D., Morse, A. T., Nigoghossian, E., Okach, L., Paulsen, J., Reyes, R., van den Bedem, H., White, A., Wolf, G., Xu, Q. P., Hodgson, K. O., Wooley, J., Deacon, A. M., Godzik, A., Lesley, S. A., Elsliger, M. A., Schimmel, P., and Wilson, I. A. (2010) Structure of a tryptophanyl-tRNA synthetase containing an iron-sulfur cluster, *Acta Crystallogr F 66*, 1326-1334.

[171] Liu, Q., Chai, J., Moche, M., Guy, J., Lindqvist, Y., and Shanklin, J. (2015) Half-of-the-sites reactivity of the castor delta^{9}-18:0-acyl carrier protein desaturase, *Plant Physiol 169*, 432-441.

[172] Hehir, M. J., Murphy, J. E., and Kantrowitz, E. R. (2000) Characterization of heterodimeric alkaline phosphatases from *Escherichia coli*: An investigation of intragenic complementation, *J Mol Biol 304*, 645-656.

[173] Sigurður Rafn, Þ. (2015) Hraðafræði einliðuflakks hjá alkalískum fosfatasa úr kuldakærri bakteríu undirbúin með gerð FLAG-afbrigðis, B.Sc. thesis, University of Iceland.

[174] Ólafur Ármann, S. (2016) Characterization of FLAG-tagged *Vibrio* alkaline phosphatase, B.Sc. thesis, University of Iceland.

[175] Lanfranco, M. F., Garate, F., Engdahl, A. J., and Maillard, R. A. (2017) Asymmetric configurations in a reengineered homodimer reveal multiple subunit communication pathways in protein allostery, *J Biol Chem 292*, 6086-6093.

[176] Eyring, H., and Stearn, A. E. (1939) The application of the theory of absolute reaction rates to proteins, *Chem Rev 24*, 253-270.

[177] Lonhienne, T., Gerday, C., and Feller, G. (2000) Psychrophilic enzymes: revisiting the thermodynamic parameters of activation may explain local flexibility, *Biochim Biophys Acta 1543*, 1-10.

[178] Feller, G. (2003) Molecular adaptations to cold in psychrophilic enzymes, *Cell Mol Life Sci 60*, 648-662.

[179] Siddiqui, K. S., and Cavicchioli, R. (2006) Cold-adapted enzymes, *Annu Rev Biochem 75*, 403-433.

[180] D'Amico, S., Claverie, P., Collins, T., Georlette, D., Gratia, E., Hoyoux, A., Meuwis, M. A., Feller, G., and Gerday, C. (2002) Molecular basis of cold adaptation, *Philos Trans R Soc Lond B Biol Sci 357*, 917-925.

[181] Kim, S. Y., Hwang, K. Y., Kim, S. H., Sung, H. C., Han, Y. S., and Cho, Y. (1999) Structural basis for cold adaptation. Sequence, biochemical properties, and crystal structure of malate dehydrogenase from a psychrophile *Aquaspirillium arcticum*, *J Biol Chem 274*, 11761-11767.
[182] Bentahir, M., Feller, G., Aittaleb, M., Lamotte-Brasseur, J., Himri, T., Chessa, J. P., and Gerday, C. (2000) Structural, kinetic, and calorimetric characterization of the cold-active phosphoglycerate kinase from the antarctic *Pseudomonas sp*. TACII18, *J Biol Chem 275*, 11147-11153.
[183] Hoyoux, A., Jennes, I., Dubois, P., Genicot, S., Dubail, F., Francois, J. M., Baise, E., Feller, G., and Gerday, C. (2001) Cold-adapted beta-galactosidase from the Antarctic psychrophile *Pseudoalteromonas haloplanktis*, *Appl Environ Microbiol 67*, 1529-1535.
[184] Roston, D., and Cui, Q. (2016) Substrate and transition state binding in alkaline phosphatase analyzed by computation of oxygen isotope effects, *J Am Chem Soc 138*, 11946-11957.
[185] Sunden, F., AlSadhan, I., Lyubimov, A. Y., Ressl, S., Wiersma-Koch, H., Borland, J., Brown, C. L., Jr., Johnson, T. A., Singh, Z., and Herschlag, D. (2016) Mechanistic and evolutionary insights from comparative enzymology of phosphomonoesterases and phosphodiesterases across the alkaline phosphatase superfamily, *J Am Chem Soc 138*, 14273-14287.
[186] Arcus, V. L., Prentice, E. J., Hobbs, J. K., Mulholland, A. J., Van der Kamp, M. W., Pudney, C. R., Parker, E. J., and Schipper, L. A. (2016) On the temperature dependence of enzyme-catalyzed rates, *Biochemistry 55*, 1681-1688.
[187] Seewald, M. J., Pichumani, K., Stowell, C., Tibbals, B. V., Regan, L., and Stone, M. J. (2000) The role of backbone conformational heat capacity in protein stability: temperature dependent dynamics of the B1 domain of *Streptococcal* protein G, *Protein Sci 9*, 1177-1193.
[188] Hobbs, J. K., Jiao, W., Easter, A. D., Parker, E. J., Schipper, L. A., and Arcus, V. L. (2013) Change in heat capacity for enzyme catalysis determines temperature dependence of enzyme catalyzed rates, *ACS Chem Biol 8*, 2388-2393.
[189] Daniel, R. M., and Danson, M. J. (2010) A new understanding of how temperature affects the catalytic activity of enzymes, *Trends Biochem Sci 35*, 584-591.
[190] Cipolla, A., Delbrassine, F., Da Lage, J. L., and Feller, G. (2012) Temperature adaptations in psychrophilic, mesophilic and thermophilic chloride-dependent alpha-amylases, *Biochimie 94*, 1943-1950.
[191] Russell, R. J., Gerike, U., Danson, M. J., Hough, D. W., and Taylor, G. L. (1998) Structural adaptations of the cold-active citrate synthase from an Antarctic bacterium, *Structure 6*, 351-361.
[192] Jung, S. K., Jeong, D. G., Lee, M. S., Lee, J. K., Kim, H. K., Ryu, S. E., Park, B. C., Kim, J. H., and Kim, S. J. (2008) Structural basis for the cold adaptation of psychrophilic M37 lipase from *Photobacterium lipolyticum*, *Proteins 71*, 476-484.
[193] Feller, G. (2013) Psychrophilic enzymes: from folding to function and biotechnology, *Scientifica (Cairo) 2013*, 512840.
[194] De Vos, D., Collins, T., Nerinckx, W., Savvides, S. N., Claeyssens, M., Gerday, C., Feller, G., and Van Beeumen, J. (2006) Oligosaccharide binding in family 8 glycosidases: crystal structures of active-site mutants of the beta-1,4-xylanase pXyl from *Pseudoaltermonas haloplanktis* TAH3a in complex with substrate and product, *Biochemistry 45*, 4797-4807.

[195] Feller, G., Payan, F., Theys, F., Qian, M., Haser, R., and Gerday, C. (1994) Stability and structural analysis of alpha-amylase from the antarctic psychrophile *Alteromonas haloplanctis* A23, *Eur J Biochem 222*, 441-447.
[196] Karshikoff, A., Nilsson, L., and Ladenstein, R. (2015) Rigidity versus flexibility: the dilemma of understanding protein thermal stability, *FEBS J 282*, 3899-3917.
[197] Isaksen, G. V., Aqvist, J., and Brandsdal, B. O. (2016) Enzyme surface rigidity tunes the temperature dependence of catalytic rates, *Proc Natl Acad Sci U S A 113*, 7822-7827.
[198] D'Amico, S., Gerday, C., and Feller, G. (2001) Structural determinants of cold adaptation and stability in a large protein, *J Biol Chem 276*, 25791-25796.
[199] Tindbaek, N., Svendsen, A., Oestergaard, P. R., and Draborg, H. (2004) Engineering a substrate-specific cold-adapted subtilisin, *Protein Eng Des Sel 17*, 149-156.
[200] Tehei, M., Franzetti, B., Madern, D., Ginzburg, M., Ginzburg, B. Z., Giudici-Orticoni, M. T., Bruschi, M., and Zaccai, G. (2004) Adaptation to extreme environments: macromolecular dynamics in bacteria compared in vivo by neutron scattering, *EMBO Rep 5*, 66-70.
[201] Somero, G. N. (1995) Proteins and temperature, *Annu Rev Physiol 57*, 43-68.
[202] Collins, T., Meuwis, M. A., Gerday, C., and Feller, G. (2003) Activity, stability and flexibility in glycosidases adapted to extreme thermal environments, *J Mol Biol 328*, 419-428.
[203] Georlette, D., Damien, B., Blaise, V., Depiereux, E., Uversky, V. N., Gerday, C., and Feller, G. (2003) Structural and functional adaptations to extreme temperatures in psychrophilic, mesophilic, and thermophilic DNA ligases, *J Biol Chem 278*, 37015-37023.
[204] Huston, A. L., Haeggstrom, J. Z., and Feller, G. (2008) Cold adaptation of enzymes: structural, kinetic and microcalorimetric characterizations of an aminopeptidase from the Arctic psychrophile *Colwellia psychrerythraea* and of human leukotriene A(4) hydrolase, *Biochim Biophys Acta 1784*, 1865-1872.
[205] Strambini, G. B., and Gonnelli, M. (2010) Protein phosphorescence quenching: distinction between quencher penetration and external quenching mechanisms, *J Phys Chem B 114*, 9691-9697.
[206] Lakowicz, J. R. (2007) *Principles of Fluorescence Spectroscopy*, Springer US.
[207] Feller, G., d'Amico, D., and Gerday, C. (1999) Thermodynamic stability of a cold-active alpha-amylase from the Antarctic bacterium *Alteromonas haloplanctis*, *Biochemistry 38*, 4613-4619.
[208] Smalas, A. O., Leiros, H. K., Os, V., and Willassen, N. P. (2000) Cold adapted enzymes, *Biotechnol Annu Rev 6*, 1-57.
[209] Siddiqui, K. S., Feller, G., D'Amico, S., Gerday, C., Giaquinto, L., and Cavicchioli, R. (2005) The active site is the least stable structure in the unfolding pathway of a multidomain cold-adapted alpha-amylase, *J Bacteriol 187*, 6197-6205.
[210] Svingor, A., Kardos, J., Hajdu, I., Nemeth, A., and Zavodszky, P. (2001) A better enzyme to cope with cold. Comparative flexibility studies on psychrotrophic, mesophilic, and thermophilic IPMDHs, *J Biol Chem 276*, 28121-28125.
[211] Olufsen, M., Smalas, A. O., Moe, E., and Brandsdal, B. O. (2005) Increased flexibility as a strategy for cold adaptation: a comparative molecular dynamics study of cold- and warm-active uracil DNA glycosylase, *J Biol Chem 280*, 18042-18048.

[212] Chiuri, R., Maiorano, G., Rizzello, A., del Mercato, L. L., Cingolani, R., Rinaldi, R., Maffia, M., and Pompa, P. P. (2009) Exploring local flexibility/rigidity in psychrophilic and mesophilic carbonic anhydrases, *Biophys J 96*, 1586-1596.
[213] Brandsdal, B. O., Heimstad, E. S., Sylte, I., and Smalås, A. O. (1999) Comparative molecular dynamics of mesophilic and psychrophilic protein homologues studied by 1.2 ns simulations, *J Biomol Struct Dyn 17*, 493-506.
[214] Tsuruta, H., Mikami, B., and Aizono, Y. (2005) Crystal structure of cold-active protein-tyrosine phosphatase from a psychrophile, *Shewanella sp.*, *J Biochem 137*, 69-77.
[215] Papaleo, E., Riccardi, L., Villa, C., Fantucci, P., and De Gioia, L. (2006) Flexibility and enzymatic cold-adaptation: a comparative molecular dynamics investigation of the elastase family, *Biochim Biophys Acta 1764*, 1397-1406.
[216] Leiros, H. K., Pey, A. L., Innselset, M., Moe, E., Leiros, I., Steen, I. H., and Martinez, A. (2007) Structure of phenylalanine hydroxylase from *Colwellia psychrerythraea* 34H, a monomeric cold active enzyme with local flexibility around the active site and high overall stability, *J Biol Chem 282*, 21973-21986.
[217] Merlino, A., Russo Krauss, I., Castellano, I., De Vendittis, E., Rossi, B., Conte, M., Vergara, A., and Sica, F. (2010) Structure and flexibility in cold-adapted iron superoxide dismutases: the case of the enzyme isolated from *Pseudoalteromonas haloplanktis*, *J Struct Biol 172*, 343-352.
[218] Tiberti, M., and Papaleo, E. (2011) Dynamic properties of extremophilic subtilisin-like serine-proteases, *J Struct Biol 174*, 69-83.
[219] Papaleo, E., Renzetti, G., Invernizzi, G., and Asgeirsson, B. (2013) Dynamics fingerprint and inherent asymmetric flexibility of a cold-adapted homodimeric enzyme. A case study of the *Vibrio* alkaline phosphatase, *Biochim Biophys Acta 1830*, 2970-2980.
[220] Smalås, A. O., Heimstad, E. S., Hordvik, A., Willassen, N. P., and Male, R. (1994) Cold adaption of enzymes: structural comparison between salmon and bovine trypsins, *Proteins 20*, 149-166.
[221] Isaksen, G. V., Aqvist, J., and Brandsdal, B. O. (2014) Protein surface softness is the origin of enzyme cold-adaptation of trypsin, *PLoS Comput Biol 10*, e1003813.
[222] Bjelic, S., Brandsdal, B. O., and Aqvist, J. (2008) Cold adaptation of enzyme reaction rates, *Biochemistry 47*, 10049-10057.
[223] Michetti, D., Brandsdal, B. O., Bon, D., Isaksen, G. V., Tiberti, M., and Papaleo, E. (2017) A comparative study of cold- and warm-adapted Endonucleases A using sequence analyses and molecular dynamics simulations, *PLoS One 12*, e0169586.
[224] Akanuma, S., Yamagishi, A., Tanaka, N., and Oshima, T. (1998) Serial increase in the thermal stability of 3-isopropylmalate dehydrogenase from *Bacillus subtilis* by experimental evolution, *Protein Sci 7*, 698-705.
[225] Giver, L., Gershenson, A., Freskgard, P. O., and Arnold, F. H. (1998) Directed evolution of a thermostable esterase, *Proc Natl Acad Sci U S A 95*, 12809-12813.
[226] Zhao, H., and Arnold, F. H. (1999) Directed evolution converts subtilisin E into a functional equivalent of thermitase, *Protein Eng 12*, 47-53.
[227] Gershenson, A., Schauerte, J. A., Giver, L., and Arnold, F. H. (2000) Tryptophan phosphorescence study of enzyme flexibility and unfolding in laboratory-evolved thermostable esterases, *Biochemistry 39*, 4658-4665.
[228] Gonzalez-Blasco, G., Sanz-Aparicio, J., Gonzalez, B., Hermoso, J. A., and Polaina, J. (2000) Directed evolution of beta -glucosidase A from *Paenibacillus polymyxa* to thermal resistance, *J Biol Chem 275*, 13708-13712.

[229] Miyazaki, K., Wintrode, P. L., Grayling, R. A., Rubingh, D. N., and Arnold, F. H. (2000) Directed evolution study of temperature adaptation in a psychrophilic enzyme, *J Mol Biol 297*, 1015-1026.
[230] Bae, E., and Phillips, G. N., Jr. (2006) Roles of static and dynamic domains in stability and catalysis of adenylate kinase, *Proc Natl Acad Sci U S A 103*, 2132-2137.
[231] Oskarsson, K. R., Nygaard, M., Ellertsson, B. O., Thorbjarnardottir, S. H., Papaleo, E., and Kristjansson, M. M. (2016) A single mutation Gln142Lys doubles the catalytic activity of VPR, a cold adapted subtilisin-like serine proteinase, *Biochim Biophys Acta 1864*, 1436-1443.
[232] Cherry, J. R., Lamsa, M. H., Schneider, P., Vind, J., Svendsen, A., Jones, A., and Pedersen, A. H. (1999) Directed evolution of a fungal peroxidase, *Nat Biotechnol 17*, 379-384.
[233] Wagner, S., Klepsch, M. M., Schlegel, S., Appel, A., Draheim, R., Tarry, M., Hogbom, M., van Wijk, K. J., Slotboom, D. J., Persson, J. O., and de Gier, J. W. (2008) Tuning *Escherichia coli* for membrane protein overexpression, *Proc Natl Acad Sci U S A 105*, 14371-14376.
[234] Beechem, J. M., and Brand, L. (1985) Time-resolved fluorescence of proteins, *Annu Rev Biochem 54*, 43-71.
[235] Tanaka, F., Tamai, N., Mataga, N., Tonomura, B., and Hiromi, K. (1994) Analysis of internal motion of single tryptophan in *Streptomyces subtilisin* inhibitor from its picosecond time-resolved fluorescence, *Biophys J 67*, 874-880.
[236] Pattanaik, P., Ravindra, G., Sengupta, C., Maithal, K., Balaram, P., and Balaram, H. (2003) Unusual fluorescence of W168 in *Plasmodium falciparum* triosephosphate isomerase, probed by single-tryptophan mutants, *Eur J Biochem 270*, 745-756.
[237] Loewenthal, R., Sancho, J., and Fersht, A. R. (1991) Fluorescence spectrum of barnase: contributions of three tryptophan residues and a histidine-related pH dependence, *Biochemistry 30*, 6775-6779.
[238] Mansoor, S. E., Dewitt, M. A., and Farrens, D. L. (2010) Distance mapping in proteins using fluorescence spectroscopy: the tryptophan-induced quenching (TrIQ) method, *Biochemistry 49*, 9722-9731.
[239] Jones Brunette, A. M., and Farrens, D. L. (2014) Distance mapping in proteins using fluorescence spectroscopy: tyrosine, like tryptophan, quenches bimane fluorescence in a distance-dependent manner, *Biochemistry 53*, 6290-6301.
[240] Gonnelli, M., and Strambini, G. B. (1995) Phosphorescence lifetime of tryptophan in proteins, *Biochemistry 34*, 13847-13857.
[241] Cioni, P., Piras, L., and Strambini, G. B. (1989) Tryptophan phosphorescence as a monitor of the structural role of metal-ions in alkaline phosphatase, *Eur J Biochem 185*, 573-579.
[242] Neet, K. E., and Timm, D. E. (1994) Conformational stability of dimeric proteins: quantitative studies by equilibrium denaturation, *Protein Sci 3*, 2167-2174.
[243] Shieh, Y.-W., Minguez, P., Bork, P., Auburger, J. J., Guilbride, D. L., Kramer, G., and Bukau, B. (2015) Operon structure and cotranslational subunit association direct protein assembly in bacteria, *Science 350*, 678-680.

Paper I

Biochimica et Biophysica Acta 1864 (2016) 755–765

Contents lists available at ScienceDirect

Biochimica et Biophysica Acta

journal homepage: www.elsevier.com/locate/bbapap

Cold-active alkaline phosphatase is irreversibly transformed into an inactive dimer by low urea concentrations

Jens Guðmundur Hjörleifsson *, Bjarni Ásgeirsson *

Department of Biochemistry, Science Institute, University of Iceland, Dunhagi 3, 107 Reykjavik, Iceland

ARTICLE INFO

Article history:
Received 21 December 2015
Received in revised form 8 March 2016
Accepted 28 March 2016
Available online xxxx

Keywords:
Alkaline phosphatase
Dimer
Enzyme kinetics
Protein fluorescence
Phosphorescence
Cold adaption

ABSTRACT

Alkaline phosphatase is a homodimeric metallo-hydrolase where both Zn^{2+} and Mg^{2+} are important for catalysis and stability. Cold-adapted alkaline phosphatase variants have high activity at low temperatures and lower thermal stability compared with variants from mesophilic hosts. The instability, and thus inactivation, could be due to loose association of the dimers and/or loosely bound Mg^{2+} in the active site, but this has not been studied in detail for the cold-adapted variants. Here, we focus on using the intrinsic fluorescence of Trp in alkaline phosphatase from the marine bacterium *Vibrio splendidus* (VAP) to probe for dimerization. Trp → Phe substitutions showed that two out of the five native Trp residues contributed mostly to the fluorescence emission. One residue, 15 Å away from the active site (W460) and highly solvent excluded, was phosphorescent and had a distant role in substrate binding. An additional Trp residue was introduced to the dimer interface to act as a possible probe for dimerization. Urea denaturation curves indicated that an inactive dimer intermediate, structurally equivalent to the native state, was formed before dimer dissociation took place. This is the first example of the transition of a native dimer to an inactive dimer intermediate for alkaline phosphatase without using mutagenesis, ligands, or competitive inhibition.

1. Introduction

Alkaline phosphatase (AP) is one of the most extensively studied enzymes and yet its role is still not fully understood [1–3]. It catalyzes the hydrolysis of phosphomonoesters and is generally believed to be only active as a homodimer. The active site in each monomer consists of three conserved metal ion sites. The M1 and M2 sites are occupied by Zn^{2+} whereas the M3 site is generally occupied by Mg^{2+} and in some cases exchanged by Co^{2+} [4–6].

The role of the metal ions in catalysis and substrate binding has been extensively studied in *Escherichia coli* AP [7–10] and mammalian APs [11,12]. For *E. coli* AP (ECAP), the generally proposed reaction mechanism has the Zn^{2+} ions in M1 and M2 coordinating the binding of the monophosphate substrate, as well as activating the Ser102 nucleophile [13].

The role of Mg^{2+} is not fully clear. In crystallographic structures, the Mg^{2+} is usually octahedrally bound where a water molecule is coordinated between the Ser102 and Mg^{2+} [8,13,14]. The Mg^{2+} has been postulated to act as a general base, activating the nucleophilic Ser102. Earlier reports have also suggested a stabilizing role of Mg^{2+} for ECAP against inactivation during storage [15,16]. Clearly, the role of Mg^{2+} is different for many alkaline phosphatases, where the Mg^{2+} can have activating role [17] as well as stabilizing role, or simply no effect [18]. Lastly, Mg^{2+} may be the deciding factor in bringing about discrimination between phosphoryl-hydrolysis from different substrates, e.g. monoesters and diesters [19].

The alkaline phosphatase studied here (VAP) was originally isolated from *Vibrio splendidus* [20], a Gram negative and cold-adapted marine bacterium closely related to *E. coli*. It has one of the highest reported catalytic activity for APs, being adapted to work at cold temperatures [20,21]. Furthermore, it has the lowest reported thermal stability of known APs with half-life less than 10 min at 40 °C [20,22] as well as the activity being very sensitive to urea [22,23]. By replacing active-site residues involved in Mg^{2+} coordination with corresponding residues in the mesophilic ECAP, namely D153 and K328, thermo-stability as well as resistance to urea increased [22]. Thus, it has been postulated that VAP binds magnesium weaker than other APs, hence the thermo-instability when activity is being monitored. Another possibility is that the active dimers in VAP are very weakly associated, leading to enzyme inactivation via dimer dissociation (VAP has inactive monomers). Recently, we made the enzyme variant R336L, where at least two hydrogen bonds at the interface should be broken. This mutant showed extreme thermo-instability and its activity dropped by half at 0.1 M of urea within half an hour (unpublished results). Thus, at present, it has not been established if VAP instability is governed by a weakly bound Mg^{2+} at the M3 site or by an instable dimer. Another possibility is that dimer association is cooperatively linked to Mg^{2+} binding.

To better understand the inactivation and unfolding pathway of VAP, a method to study the dimer dissociation event is needed. Many

* Corresponding authors.
E-mail addresses: jgh4@hi.is (J.G.ð Hjörleifsson), bjarni@hi.is (B. Ásgeirsson).

http://dx.doi.org/10.1016/j.bbapap.2016.03.016
1570-9639/

methods have been applied to study dimerization of various APs where the most common methods are size-exclusion chromatography (SEC) [24] and sedimentation velocity [25,26]. Our group previously used SEC to study dimer dissociation in AP from Atlantic cod where the dimer dissociation was shown to be linked to loss of activity in the 2–3 M urea range [27]. SEC however has several drawbacks to study homodimer/monomer equilibrium. 1) In many cases SEC data has poor resolution leading to biased assignment of peaks, making data usually only qualitatively reliable, 2) resin interaction with proteins is known to occur, and 3) local concentration and solubility on SEC columns during runs can affect the dimer/monomer dissociation equilibrium. Shrimp AP was initially believed to be active as a monomer judged by SEC data as well as by native PAGE activity staining [28], but was later found to crystallize as a dimer [8]. The same conclusion was initially drawn for VAP for the same reasons [20], before the crystal structure was obtained [21].

Fluorescence of proteins is the most preferable real-time method to study quaternary structure dissociation due to its sensitivity and ability to work at physiological conditions. In addition to fluorescence, phosphorescence has been utilized to study metal ion binding [7] and phosphate binding [29] in ECAP. Only deeply buried Trp residues, like Trp109 in ECAP, have the propensities to have an electron transition to the long-lived triplet state. The absence of quenching residues nearby, or protein backbone interference, is a crucial factor as well [30]. Chemical incorporation of fluorescence probes can also be used to study homodimer dissociation, such as by fluorescence resonance energy transfer (FRET), however using extrinsic probes can affect either activity and/or stability of subunit association.

In order to report on the folded state of proteins, Tyr or Trp need to be in a position in the native fold so that upon dissociation a change in fluorescence signal is detected, e.g. residues are relieved of quenching by a nearby group, or a change in local polarity around the fluorophore is observed (spectral shifts). VAP has five Trp residues where no residue is located at the dimer interface. Thus, upon dissociation of dimers, the change in fluorescence signal due to monomer dissociation is insignificant, since it has been shown in the case of ECAP that the structure change of monomers upon dissociation is minimal [31].

In this study, all of the tryptophan residues of VAP were characterized with respect to fluorescence by making tryptophan to phenylalanine substitutions. An additional tryptophan residue was also introduced at the dimer interface. Urea induced fluorescence redshift and size exclusion chromatography were used to study the mechanism of inactivation and unfolding, in addition to the assessment of activity and global stability of the variants.

2. Materials and methods

2.1. Materials

Chemicals were generally obtained from Sigma-Aldrich (Schnelldorf, Germany) or Merck (Darmstadt, Germany). Strep-Tactin Sepharose, (2-(4′-hydroxy-benzene-azo) benzoic acid (HABA), desthiobiotin and anhydrotetracyclin (AHTC) were from IBA GmbH (Germany). Bacto Yeast extract was obtained from Becton, Dickinson and Company (France). Primers were obtained from TAG (Copenhagen). Pfu polymerase, DnpI nuclease and markers were from Fermentas (St. Leon-Rot, Germany). Alkaline phosphatase from *E. coli* and other proteins were purchased from Sigma-Aldrich.

2.2. Generation of enzyme variants

VAP was sub-cloned from an original pBluescript vector to a pASK3-plus StrepTactin vector (IBA, Gottingen, Germany). *Bsa*I site overhangs were introduced in a PCR reaction using the forward oligonucleotide primer: 5′TAATGA**GGTCTCna**ATGAAACCAATTGT TACCGCA-3′ and reverse primer: 5′-CAAAAA**GGTCTCngcgc**GTTTACTTG TTGTTTAATGT-3′, where the *Bsa*I binding site is shown in bold (cleavage sites in bold/lower letters) and the gene complimentary region is underlined. The PCR product was ligated into pASK3-plus digested with *BsaI* giving a two amino acid linker between the gene C-terminus and the C-terminally linked StrepTag (WSHPQFEK).

Site-directed mutagenesis was performed using the QuikChange® kit (Stratagene) following the manufacturer's protocol. Oligonucleotide primers were synthesized by TAG (Copenhagen, Denmark). All plasmids were propagated in *E. coli* TOP10 cells and plasmids were purified using NucleoSpin® plasmid purification kit (Macherey-Nagel, Germany) following the manufacturers protocol, or by co-precipitation with glycogen (Fermentas R0561 molecular biology grade) in ethanol following the manufacturer's protocol. Generally, three clones were sent for sequencing (Beckman Genomics, United Kingdom) and a positive clone selected and further expressed in the *E. coli* LMG194 strain (lacking an AP gene).

2.3. Protein expression and purification

A single colony of LMG194 cells, previously transformed with mutated plasmid, was added to a 20 ml LB medium containing 0.1 mg/ml ampicillin (LAMP medium) and incubated at 37 °C until a saturated culture was obtained (no more than 16 h). Approximately 2 ml of this starter culture was added to 450 ml of freshly prepared sterilized LAMP medium in total of nine bottles (4 l). Cells were grown at 18 °C on an orbital shaker at 150 rpm until OD600 was 0.5–0.7. Then, anhydrotetracyclin was added to a final concentration of 20 ng/ml to induce expression. Cells were harvested 24 h later by centrifugation. The cell pellet was re-suspended in lysis buffer (25 mM Tris, 10 mM $MgCl_2$, 0.5 mg/ml hen egg lysozyme, 0.01% Triton X-100, pH 8.0) and incubated at 2–4 h at 4 °C before being frozen at −20 °C. The cell lysate was allowed to slowly thaw and DNAse added to a final concentration of 0.050–0.10 mg/ml. The lysate was further incubated for 1–2 h at 4 °C and finally centrifuged at 15.000 × *g* for 15 min to obtain a clear lysate.

For all variants except the W512F, where the tryptophan is located within the StrepTag sequence, the clear lysate was loaded onto a Strep-Tactin® affinity column (previously equilibrated in binding buffer: 25 mM Tris, 10 mM $MgCl_2$, pH 8.0) overnight at 4 °C with a flow-rate of less than 0.1 ml/min. Nonspecifically bound proteins were washed off with 25 mM Tris, 10 mM $MgCl_2$, 150 mM NaCl, pH 8.0. The column was then equilibrated with binding buffer before eluting with elution buffer (25 mM Tris, 10 mM $MgCl_2$, 15% (v/v) ethylene glycol, 2.5 mM desthiobiotin, pH 8.0). Typical protein yield was between 3 and 5 mg of pure enzyme.

The W512F variant with a non-functional StrepTag was purified directly on L-histidyldiazobenzylphosphonic acid agarose column specific for alkaline phosphatases (Sigma-Aldrich) using the same conditions as for Strep-Tactin purification, except elution was done in 100 mM Na_2HPO_4, pH 9.1. Active fractions were pooled and dialyzed overnight in 2.0 L of 25 mM Tris, 10 mM $MgCl_2$, pH 8.0.

The W301F variant required further purification after Strep-Tactin column elution. The eluted enzyme from the Strep-Tactin purification was loaded onto a Mono-Q ion-exchange column and eluted using a 0–1 M NaCl gradient on a FPLC apparatus (GE-Healthcare).

Purity was analyzed by SDS-PAGE on 4–12% bis-Tris NUPAGE® (Invitrogen) gels. All purified enzyme samples contained 15% (v/v) ethylene glycol and were snap-frozen in liquid nitrogen before storing at −20 °C.

2.4. Fluorescence measurements

All enzyme variants were diluted from approximately 0.4–0.5 mg/ml stock solutions to 0.02 mg/ml in buffer containing 20 mM Mops, 1 mM $MgSO_4$, pH 8.0 (10 °C). Emission spectra were recorded at 10 °C on a FluoroMax4 (Horiba) with 0.5 nm increments and consisted of three

averaged scans. An excitation wavelength of 295 nm was selected and a slit-width of 5.0 nm was used for both excitation and emission. The relatively high excitation slit-width of 5 nm did not cause significant photo-bleaching during measurements. A blank solution spectrum was measured under the same conditions and subtracted from the other spectra. The wavelength of maximum emission intensity (λ_{max}) was determined by fitting the spectra to a 3rd degree polynomial in the range 315–370 nm ($y = ax^3 + bx^2 + cx + d$, where y is the intensity and x is the wavelength. The roots of the first derivative were solved by solving the quadratic equation for the polynomial.

Acrylamide was chosen for collisional quenching studies for three reasons: Acrylamide quenching efficiency (f_Q) of tryptophan is near unity [32], acrylamide is uncharged, so charge effects are absent, and acrylamide is capable of long-range interactions with tryptophan in proteins, so quenching can be observed without direct penetration [33,34]. Collisional quenching of fluorescence is described by the Stern–Volmer equation:

$$F_0/F = 1 + k_q\tau_0[Q] = 1 + K_{sv}$$

where F_0 and F are the fluorescence intensities in the absence and presence of quencher, respectively, k_q is the bimolecular quenching constant, t_0 is the lifetime of fluorescence without quencher, Q is the concentration of quencher and K_{sv} is the Stern–Volmer constant for collisional quenching.

Fluorescence measurement for acrylamide quenching was done as described above after adding aliquots from a 5.0 M stock solution of acrylamide giving concentrations in the range 0–0.3 M acrylamide (sample dilution by each added aliquot was corrected for). By plotting F_0/F against [acrylamide], the slope of the linear fit is the Stern–Volmer constant, K_{sv}.

2.5. Urea denaturation and inactivation measurements

Samples were incubated for 4 h at 10 °C with varying concentration, of urea ranging from 0–8 M in 25 mM Mops, 1 mM $MgSO_4$, pH 8.0. Tryptophan fluorescence was monitored as described above, where the wavelength of maximum emission intensity (λ_{max}) was determined. For enzyme inactivation experiments, samples were incubated in urea in the range of 0–2 M. Activity was measured under transphosphorylating conditions using 2.0 mM p-nitrophenyl phosphate (p-NPP) in 1.0 M diethanolamine with 1.0 mM $MgCl_2$ at pH 9.8 and 10 °C. The change in absorbance was followed at 405 nm over a 30 s period in a temperature regulated Evolution 220 spectrophotometer (Thermo Scientific). An extinction coefficient of 18.5 M^{-1} cm^{-1} was used at pH 9.8. The unfolding curves were fitted to a two state model for the wild-type VAP (N → D) and a three state model for the F355 W variant (I_2 → 2I → 2D) using the open-source graphical freeware CDpal [35].

2.6. Phosphorescence measurements

Phosphorescence of samples was measured in 20 mM Tris, 10 mM $MgCl_2$, pH 8.0 at 10 °C on a Horiba Fluormax4-P using a xenon pulsed lamp equipped with a R928P photon-counting detector. Samples were degassed by argon-purging in a closed flow-cell cuvette for 1 h on ice before performing measurements. Concentration was 5–6 μM for VAP and ECAP, and 8 μM for W460F. Phosphorescence spectra were measured using excitation at 292 nm with 5 nm slit width for both excitation and emission. A gate-and-delay generator was used to measure phosphorescence decay by increasing the initial delay from 1 ms to 180 ms in 2 ms intervals using 290 nm and 440 nm for excitation and emission, respectively. The excitation and emission slit-widths were 5 nm and 10 nm, respectively. Each interval consisted of 50 measured pulses with a sample window of 200 ms. The data were initially fitted to a single-exponential curve $I(t) = \alpha \cdot e^{-t/\tau}$, where I is the intensity, α is the pre-exponential factor, t is time and τ is the lifetime. While this analysis was sufficient for ECAP, wild-type VAP and the VAP-W460F variant required a double-exponential fit, $I(t) = \alpha_1 \cdot e^{-t/\tau 1} + \alpha_2 \cdot e^{-t/\tau 2}$.

2.7. Enzyme kinetics

Enzyme kinetic rate constants were determined at 10 °C by measuring the turnover-rate under hydrolyzing conditions using varying concentrations of p-nitrophenyl phosphate (p-NPP) in 0.1 M CAPS, 1 mM $MgCl_2$, 0.5 M NaCl, pH 9.8 (corrected for 10 °C) over 30 s period in a temperature regulated Evolution 220 spectrophotometer (Thermo Scientific). For exact determination of the initial pNPP concentration for each measurement, the sample was allowed to fully hydrolyze and its concentration determined by measuring the absorbance at 405 nm (using extinction coefficient 18.5 mM^{-1} cm^{-1}). Enzyme concentration was measured by absorption at 280 nm using extinction coefficient of 61,310 M^{-1} cm^{-1}, 55,935 M^{-1} cm^{-1} and 66,810 M^{-1} cm^{-1} for wild-type, Trp → Phe variants and Phe → Trp variants respectively, [36].

K_M and k_{cat} were determined by non-linear regression fit to the Michaelis–Menten equation using GraphPad Prism®.

2.8. Thermal unfolding measurements

Enzyme samples with absorbance at 280 nm between 0.1 and 0.2 were dialyzed overnight in 25 mM Mops, 1 mM $MgSO_4$ at pH 8.0 (20 °C). T_m determination was performed on a JASCO J-810 circular dichroism (CD) spectropolarimeter by measuring a melting curve at 222 nm in the range 15–85 °C in a 2 mm cuvette with 1 °C/min temperature rise. A two-state pathway was assumed for monomer unfolding N ⇆ U, where N is the native and U is the unfolded enzyme. The traces were normalized and T_m determined at F_U by a direct fit to a sigmoidal curve using the program Kaleidagraph®.

2.9. Size exclusion chromatography

Chromatography was performed on a Pharmacia FPLC apparatus equipped with a Superose 12 column (GE Healthcare). The column was pre-equilibrated at 0.5 ml/min and temperature of 4–5 °C with three column volumes of the same denaturant solution as used for pre-incubating the samples. The buffer was 25 mM Mops, 1 mM $MgSO_4$ (pH 8.0) containing urea where indicated. The final enzyme concentration was ≈1.5 mg/ml (25 μM) and the samples were applied in a volume of 0.5 ml. The column was calibrated with the following standard proteins: immunoglobulin G (150 kDa), egg albumin (45 kDa), pepsin (35 kDa), myoglobin (16 kDa), and cytochrome c (11.6 kDa).

3. Results

3.1. Trp substitutions in VAP

Vibrio alkaline phosphatase (VAP) has five native Trp residues and one extra Trp located on the StrepTag® purification tag which is likely fully exposed and mobile. The StrepTag variant of the wild-type VAP gave an identical x-ray structure to the one previously published without a C-terminal tag (Fig. 1A) and no diffractions were observed from the tag (Helland & Asgeirsson, unpublished results). All of the Trp residues in VAP are highly conserved in known bacterial APs, except W475 and W155 (Fig. 1B). None of the Trp residues are located on the four designated non-homologous inserts previously reported in VAP [21]. W155, W301 and W475 are all located in the typical αβα-folded center and are buried, or partially buried, between the strands and helices in the fold (Fig. 1C–H). The environment is highly non-polar for W155, while for W301, W460 and W475 the environment has a distinctive amphipathic character with one side surrounding the tryptophan residue non-polar and the other polar. The W460 residue is located on a short loop at a conserved site buried below the roots of

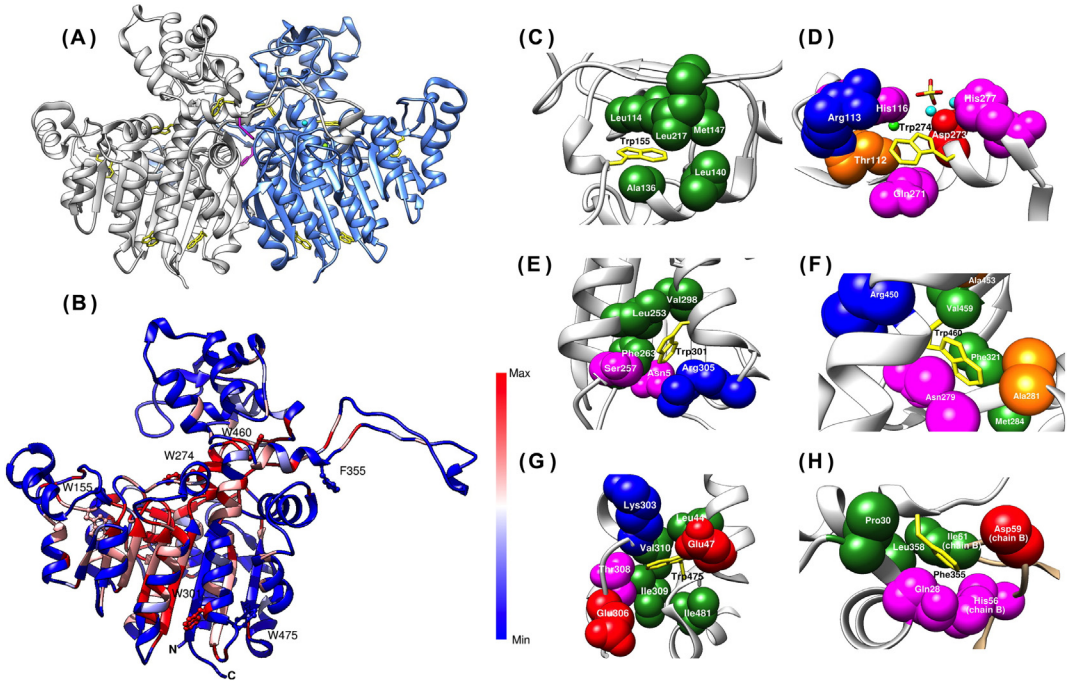

Fig. 1. VAP crystal structure (PDB: 3E2D). (A) VAP dimeric structure. Tryptophan residues are colored in yellow, residue F355 in magenta, and Zn and Mg ions in cyan and green, respectively. (B) Conservation of residues in the VAP monomer. Conserved sites are shown in red and non-conserved in blue. The five native tryptophans and F355 are shown as balls and sticks. Conservation calculations were done using ConSurf server (UNIREF90 and MAFFT) and the structure rendered in Chimera. (C–H) The environment within 5 Å around the chosen native tryptophan residues (C–G), and Phe355 (H). Tryptophan residues and Phe355 are shown in yellow sticks and neighboring residues as spheres. Hydrophobic residues are shown in green, small non-polar residues in orange, polar residues in magenta, negatively charged residues in red and positively charged residues in blue. Zn and Mg ions are shown in teal and green respectively and sulfate ion as sticks in yellow and red (D).

the so-called crown domain, 15 Å away from the active site and 5 Å away from the backbone of the other monomer. Even so, W460 is not counted here as an interface residue in the usual sense, since the residue points inwards toward the tertiary core. W274 is located in the active site and nearly fully exposed. It binds a water molecule that is additionally hydrogen bonded to another water molecule bound to the active-site Mg^{2+}.

Single Trp substitutions to phenylalanine were made to study the role of each Trp in VAP emission spectrum. All variants were expressed as soluble enzymes with yields comparable to wild-type expression yield, except for W301F, where the yield for soluble enzyme was 10–20 times lower, and the enzyme was possibly precipitated as inclusion bodies to some extent. W301F required further purification after affinity purification to remove two extra bands seen in SDS-PAGE that were consistently present as co-eluents.

A new Trp residue was introduced by forming the F355W variant as a strategy to introduce a Trp residue at the dimer interface to serve as a probe for dimerization. F355 is located at the root of the long surface loop that characterizes this particular AP in comparison with ECAP (Fig. 1B and H). This site was chosen for further studies, since we found that a mutation to a Tyr at this site had no effect on kinetics or thermal stability, indicating structural neutrality at this site.

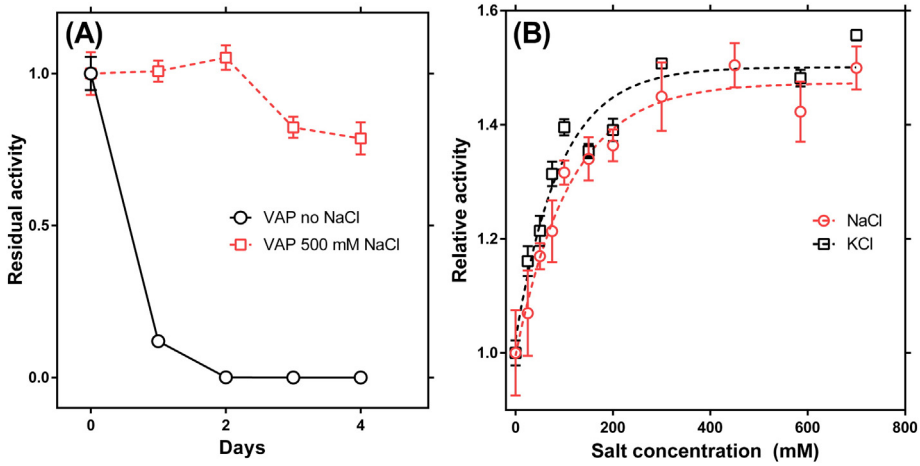

Fig. 2. Effect of NaCl on VAP activity and stability. (A) Effect of NaCl on VAP storage at room temperature. Samples were incubated in 25 mM Mops, pH 8.0 and activity measured under trans-phosphorylation of 2.0 mM p-nitrophenyl phosphate (p-NPP) at 25 °C in 1.0 M diethanolamine with 1.0 mM $MgCl_2$ at pH 9.8. (B) Effect of NaCl and KCl on catalytic turnover. Activity was measured under hydrolyzing conditions with 5 mM PNPP, 100 mM Caps, 1 mM $MgCl_2$ with NaCl or KCl ranging from 0–700 mM at pH 9.8 and 10 °C.

3.2. Kinetic constants and stability of the Trp → Phe variants

Enzyme kinetics were performed under hydrolyzing conditions. Recently, we have added 500 mM NaCl to our kinetic sample buffer since it has a stabilizing effect for storage, both on ice and at room temperature. Fig. 2A shows the high stabilizing effect 500 mM NaCl has on VAP at room temperature, where activity does not drop for two days. After 4 days with NaCl present the activity was still 75% of initial activity. Without NaCl the activity dropped steadily and after 1 day 10% of activity remained. Furthermore, NaCl increased the enzymes catalytic turnover, where the activity peaked at a salt concentration of 500 mM (Fig. 2B). Concurrently, K_M was increased approximately twofold at 500 mM NaCl (data not shown). This activity enhancement is believed to come from the chloride anion since the same effect is seen using KCl.

The W512F variant (tryptophan located on the C-terminal StrepTag) showed no significant change for either k_{cat} or K_M compared with the wild-type VAP that showed a k_{cat} and K_M of 302 ± 20 s^{-1} and 194 ± 30 μM, respectively (Table 1). The W274F mutant, where an exposed Trp was removed from the active site, maintained the same activity as the wild-type. The k_{cat} decreased for all the other variants, being 125 ± 2 s^{-1}, 137 ± 8 s^{-1}, 65 ± 4 s^{-1} and 44 ± 2 s^{-1} for W155F, W301F, W460F and W475F, respectively. The K_M values remained unchanged compared with wild-type, except for W460F and W274F, where the K_M was 1.8-fold and 2.5-fold higher than the wild-type value, respectively. Overall, W460F had the lowest catalytic efficiency (k_{cat}/K_M) of 184 s^{-1} mM^{-1} compared to 1460 s^{-1} mM^{-1} for the wild-type.

In order to understand better the role of W460 in catalysis, the W460Y (Tyr or Trp is conserved at this position) and W460I (non-polar branched residue) variants were made. The W460Y variant showed only minimal decrease in k_{cat} (275 ± 4 s^{-1}) and a slight increase in K_M (252 ± 46 μM) compared to the wild-type, while the W460I variant was completely inactive.

Melting temperatures (T_m) were determined by CD spectroscopy as an indication of monomer unfolding (Table 1 and Figure S1-A). Magnesium and the competitive inhibitor-ion sulfate affected the stability of the monomers (Figure S1-B), so we used a moderate concentration of 1 mM $MgSO_4$ in the sample buffer for melting temperature experiments. No change in T_m was observed for the W512F (51.0 ± 0.6 °C) variant compared to wild-type (51.0 ± 0.3 °C). For all the other variants, a decrease in T_m was seen at 49.8 ± 2.2 °C, 47.1 ± 0.7 °C, 44.6 ± 1.7 °C, 48,7 ± 1.3 °C and 48.1 ± 0.1 for W155F, W274F, W301F, W460F and W475F, respectively. The large decrease in T_m observed for the W301F variant indicated a loosening of the globular fold.

3.3. Trp → Phe variant emission spectra and acrylamide quenching

Tryptophan emission spectra for all the enzyme variants are shown in Fig. 3A. The W512F change located on the StrepTag had no effect on the emission spectra, indicating that W512 is completely solvent exposed and likely quenched by a nearby group, possibly the histidine residue in the tag (residue number 3). It is clear, that the dominant fluorescence signal comes from W460 and W301, as variants W460F and W301F showed a close to 50% decrease in fluorescence intensity individually compared to the wild-type VAP. The W274F variant showed increased fluorescence compared to the wild-type VAP. This can be explained by a change in conformation around one or more remaining Trp, where static quenching by nearby residue has been relieved. The W155F variant had a slightly lower emission signal than the wild-type, while W475F showed a moderate decrease.

From the data in Fig. 3A, it is also apparent that one or more of the Trp → Phe alterations affected the packing and/or structure of the enzyme, since the sum of the difference spectra for the Trp → Phe variants compared to wild-type VAP emission was higher than the emission of wild-type VAP. This was most noticeable at the blue edge of the emission spectra (W274F was excluded since the difference there < 0).

To examine solvent exposure of Trp-residues in VAP, the wavelength of maximum emission (λ_{max}) was determined (Table 2). Overall, the Trp-substitutions had only a moderate effect on λ_{max}. For the wild-type VAP, the λ_{max} was 340.1 ± 0.1 nm while the exposed Trp residue mutants, W274F and W512F, showed a modest blue-shift to λ_{max} 339.3 ± 0.2 nm and 339.5 ± 0.3 nm, respectively. This correlates with removal of a Trp residue that is more exposed than the average of the set of tryptophans. Removal of the residues that showed decreased emission upon removal, W155F, W301F, W460F and W475F, resulted in a moderate red-shift in all cases with λ_{max} of 341.1 ± 0.1 nm, 341.0 ± 0.1 nm, 341.4 ± 0.8 nm and 342.0 ± 0.1 nm, respectively. This correlates with the removal of a residue more buried than the average.

To further examine solvent exposure of the Trp residues, acrylamide collisional studies were conducted. Measurements were plotted as Stern–Volmer plots (Fig. 3B) and the calculated Stern–Volmer constants, K_{sv} are shown in Table 2. In the concentration range of 0–0.3 M acrylamide, none of the variants showed deviation from linearity in the Stern–Volmer plots. All variants had similar Stern–Volmer constants as wild-type VAP (2.4 ± 0.3 M^{-1}), except W460F, which showed a striking 3.3 fold increase in the Stern–Volmer constant (7.9 ± 0.2 M^{-1}). This indicated that upon W460 removal, the remaining residues became more prominent in their contribution to the signal. In other words, W460 is likely almost completely shielded from the solvent. Not even acrylamide, which is known to have long range quenching effect deep into protein cores [36], is able to reach W460 and quench its emission.

Table 1
Kinetic measurements and temperature unfolding. For kinetic measurements the rate of hydrolysis of p-NPP in 0.1 M CAPS, 500 mM NaCl, 1 mM $MgCl_2$, pH 9.8 was measured at 10 °C. Temperature unfolding (T_m) was monitored by CD spectroscopy in 25 mM Mops, 1 mM $MgSO_4$, pH 8.0 (20 °C) by measuring a melting curve at 222 nm in the range 15–85 °C. The average data with standard deviations were obtained from several independent experiments (n = 3–5).

Enzyme variant	k_{cat} (s^{-1})	K_m (μM)	k_{cat}/K_m (s^{-1} mM^{-1})	T_m (°C)
Wild-type	302 ± 20	194 ± 30	1560 ± 260	51.0 ± 0.6
W155F	125 ± 2	218 ± 8	573 ± 23	49.8 ± 2.2
W274F	300 ± 4	462 ± 25	650 ± 36	47.1 ± 0.7
W301F	137 ± 8	239 ± 23	573 ± 64	44.6 ± 1.7
W460F	65 ± 4	354 ± 56	184 ± 31	48.7 ± 1.3
W475F	44 ± 2	194 ± 22	230 ± 28	48.1 ± 0.1
W512F	313 ± 36	212 ± 29	1480 ± 260	51.0 ± 0.3
F355W	255 ± 56	218 ± 20	1170 ± 280	52.0 ± 0.9
W460Y	275 ± 41	252 ± 46	869 ± 240	N/A

3.4. Room-temperature phosphorescence measurements

Only Trp residues buried deeply away from the solvent in protein-cores are capable of having long emission lifetimes in aqueous buffer solutions at room temperature. Such excited state is the result of inter-state crossing from the singlet state to the long-lived triplet state. It is also well known, that oxygen is a very efficient collisional quencher of phosphorescence. Thus, samples need to be deoxygenated efficiently before measurements can proceed. Furthermore, phosphorescence is often quenched statically by a nearby intrinsic quencher, mainly His, Tyr, Trp and Cys residues [30]. None of these residues are within 5 Å proximity of W460, which is a likely candidate to be phosphorescent at room temperature in VAP.

Indeed, VAP was found to be phosphorescent at 20 °C, having a typical red-shifted phosphorescence emission spectrum (Fig. 4A) with two maxima at 418 nm and 443 nm, similar in shape as the ECAP phosphorescence spectrum at room temperature [7,29]. Phosphorescence decay curves are shown in Fig. 3B where VAP wild-type phosphorescence decay fitted best to a double exponential decay with one long lifetime of 140 ms and one short lifetime of 40 ms. The latter had a 17% relative amplitude. To define whether the two lifetimes originated

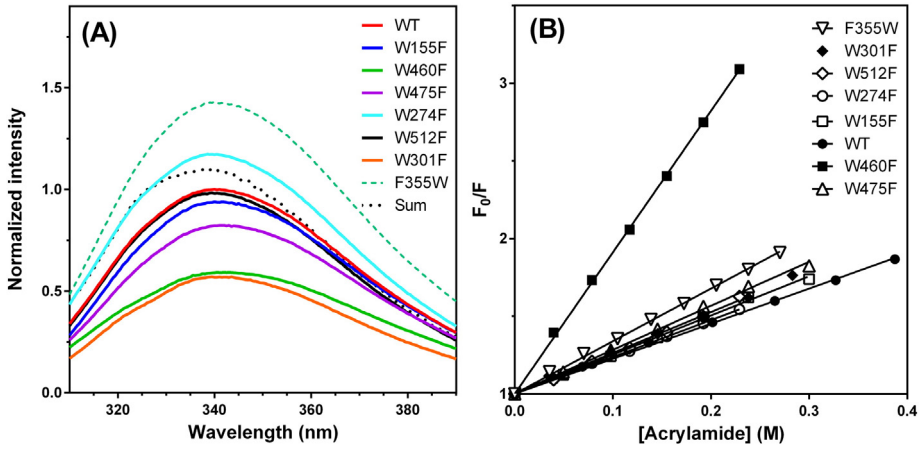

Fig. 3. Emission spectra of single tryptophan variants of VAP and acrylamide quenching. (A) Emission spectra were recorded at 10 °C in the range 310–390 nm using excitation at 295 nm (5 nm slit-width for both emission and excitation). Blank was measured under the same conditions and subtracted from the spectra. Measurements came from several independent experiments (n = 2–4). The sum spectrum shown is the total of the added difference spectra of Trp → Phe mutants compared to the wild-type VAP spectrum, but excluding the W274F spectrum (black dotted line). Emission intensity was normalized to the wild-type maximum emission intensity (B) Stern–Volmer plots. Emission intensity at 340 nm was measured under the same conditions as in (A) after addition of aliquots of acrylamide giving F_0/F, where F_0 is the emission without acrylamide and F the emission after each added aliquot. The Stern–Volmer constant was derived by linear regression in Graphpad Prism.

from the same Trp molecule, phosphorescence decay of W460F was recorded. W460F also showed phosphorescence, although the signal was roughly 10 times less intense than for the wild-type VAP and correlated well with the low relative amplitude of the shorter 40 ms lifetime. The W460F decay curve was fitted to a double exponential decay equation, where the lifetimes were 6 ms and 65 ms, The shorter lifetime of W460F might arise from background during acquisition due to higher signal to noise ratio, or a third phosphorescent tryptophan with very a low phosphorescence quantum yield not detectable when W460 is present.

As a control, ECAP phosphorescence was also recorded. In our hands, the ECAP phosphorescence decay was fitted to a single exponential decay function and had a lifetime of 230 ms which is considerably shorter than published values [37]. Thus, it was clear that our oxygen purging system, by slowly blowing argon gas through a quartz flow-cell, was not working to fully remove all oxygen from the sample. We calculated that the oxygen concentration after purging for 1 h in our system was ~3 μM.

3.5. Introducing a tryptophan to the dimer interface

The F355W dimer interface variant showed the same kinetic properties and thermal stability as the wild-type VAP (Table 1). It displayed an increase in fluorometric emission intensity compared to wild-type VAP and a slight red-shift, where λ_{max} was 340.9 ± 0.2 nm (Table 2). The Stern–Volmer constant increased to 3.2 ± 0.2 M^{-1}, indicating that a Trp at position F355 is more exposed on average than the other Trp residues. It was also relatively unquenched in the native state of VAP as judged by its high contribution in the emission spectrum.

Table 2
Fluorescence emission maxima and acrylamide quenching data for VAP variants. All samples were prepared in 20 mM Mops, 1 mM $MgSO_4$, pH 8.0 (corrected for 10 °C) to a final enzyme concentration of 0.02 mg/ml. The emission spectra were recorded at 10 °C for 310–400 nm using 295 nm as excitation wavelength. Stern–Volmer constants (K_{sv}) were derived as the slope of F_0/F plotted against [acrylamide] quencher. The data represent the average and standard deviation from 2–4 independent experiments.

Enzyme variant	λ_{max} (nm)	K_{sv} (M^{-1})
Wild-type	340.1 ± 0.1	2.4 ± 0.3
W155F	341.1 ± 0.1	2.6 ± 0.1
W274F	339.3 ± 0.2	2.4 ± 0.1
W301F	341.0 ± 0.1	2.3 ± 0.1
W460F	341.4 ± 0.8	7.9 ± 0.2
W475F	342.0 ± 0.1	2.9 ± 0.1
W512F	339.5 ± 0.3	2.8 ± 0.2
F355W	340.9 ± 0.2	3.2 ± 0.2

3.6. Urea induced denaturation/inactivation for wild-type and F355W

Urea denaturation and inactivation curves for the wild-type VAP and F355W are shown in Fig. 5A. Inactivation was an irreversible step while the unfolding step was partially reversible as monitored by the peak of fluorescence emission (data not shown). The denaturation curve for the wild-type VAP showed the characteristics of a two-state unfolding pathway in the 2–4 M urea range with no detectable intermediates. It can also be seen, that the activity fell rapidly with increasing concentration of urea, where half of the activity was lost at 0.3–0.4 M urea. The F355W inactivation curve was identical to the curve for the wild-type VAP. However, the unfolding curve occurring at higher urea concentrations was somewhat different. For the wild-type VAP, unfolding seems to be occurring in the 2–4 M range, but for W355 a larger curvature (red-shift) was seen in the unfolding curve starting at around 0.8 M urea. This could be due to solvent exposure of W355 upon dimer dissociation, since the activity had dropped down to less than 15% at 0.8 M urea. This suggested the possibility that an inactive dimeric intermediate was formed before its dissociation took place. Thus, the unfolding scheme is either of the two following cases:

Case 1. $N_2 \rightarrow I_2 \rightarrow 2I \rightarrow 2U$

Case 2. $N_2 \rightarrow I_2 \rightarrow 2U$

The unfolding curve for the F355W variant could be fitted a four state model (Case 1), where first the inactive dimer is formed $N_2 \rightarrow I_2$ (inactivation is not seen using fluorescence since no dissociation happens). Then, the fluorescence unfolding curve could be fitted with the $I_2 \rightarrow 2I \rightarrow 2D$ model, or $I_2 \rightarrow 2D$, where no folded monomer intermediate accumulates (Case 2). The signal for the possible $I_2 \rightarrow 2I$ conversion (seen by a red-shift) is low and partially merges with the $2I \rightarrow 2D$ conversion, making this observation qualitative at most, and making it difficult to distinguish between Case 1 and Case 2 using F355W fluorescence for detection.

In an attempt to resolve between Case 1 and Case 2, we incubated VAP in 8-Anilinonaphthalene-1-sulfonic acid (ANS), which is widely used to detect structural changes resulting in solvent exposure of

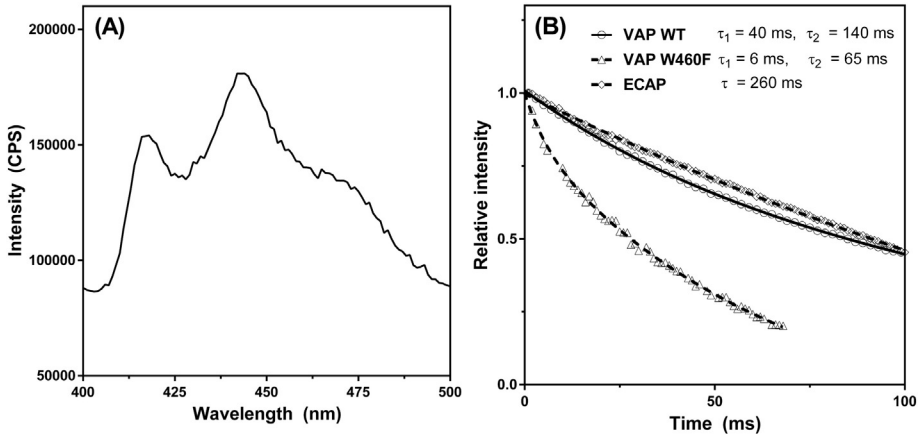

Fig. 4. VAP phosphorescence. (A) Phosphorescence emission spectrum of VAP. (B) Phosphorescence decay for VAP wild-type, VAP-W460F or ECAP. Data for VAP wild-type and VAP-W460F were fitted to a two exponential decay model, whereas the ECAP data was fitted to a single exponential model using Graphpad Prism.

hydrophobic residues. Surprisingly, VAP showed no increase in fluorescence of ANS over blank measurements in the range 0–5 M urea (Figure S2-A) and the signal was not protein concentration dependent (Figure S2-B). Bovine serum albumin (BSA) which is known to readily bind ANS in the native state [38] was used as a control for the experiment and showed the expected increase in ANS fluorescence.

Size exclusion chromatography (SEC) was used to detect the oligomeric state of VAP at 0 M, 1 M, and 2 M urea (Fig. 5B). At 0 M urea the enzyme migrates as a 110 kDa protein on the column which fits well to the calculated mass of 112 kDa. At 1 M urea, the dimeric peak is present and starts to split toward a species with lower molecular mass (the monomer). Thus, the observation that dimer dissociation starts around 0.8 M urea using F355W fluorescence (Fig. 5A) seems to be correct. In Fig. 5A, it can be seen that approximately 10–20% of the enzyme should be unfolded at 2 M urea (if two-state monomer unfolding is assumed). Thus, Case 2 ($N_2 \rightarrow I_2 \rightarrow 2I \rightarrow 2$ U) seems to be the correct model as two states were seen at 2 M urea, folded monomer and unfolded monomer, where the latter migrates as a larger species than the dimer. However, the molecular mass of the folded monomer in SEC did not fit exactly the calculated mass of 56 kDa, but migrates as a 79 kDa species. It is possible that the folded monomers are partially unfolded to some extent at 2 M urea, thus they migrate as a larger protein.

4. Discussion

The aim of this study was to clarify the inactivation and unfolding mechanism of VAP to understand better what factors makes this cold-adapted enzyme so susceptible to heat and urea. The global stability of the enzyme to heat (usually measured by melting temperature) is much greater than the stability of the active-site, but it was not clear if inactivation was due to dissociation of the active dimer or other causes. Here, our goal was to use fluorescence to study subtle structural changes upon enzyme inactivation induced by urea. We first characterized the role of each tryptophan in the emission spectrum together with solvent accessibility to define which parts of the enzyme reflected most of the emission spectrum. However, our results showed that none of the native tryptophan residues could serve as a probe for oligomeric structural changes in the urea induced denaturation experiment. Introducing a tryptophan residue at the dimer interface, indicated that an inactive dimer intermediate was formed and this was confirmed by size exclusion chromatography.

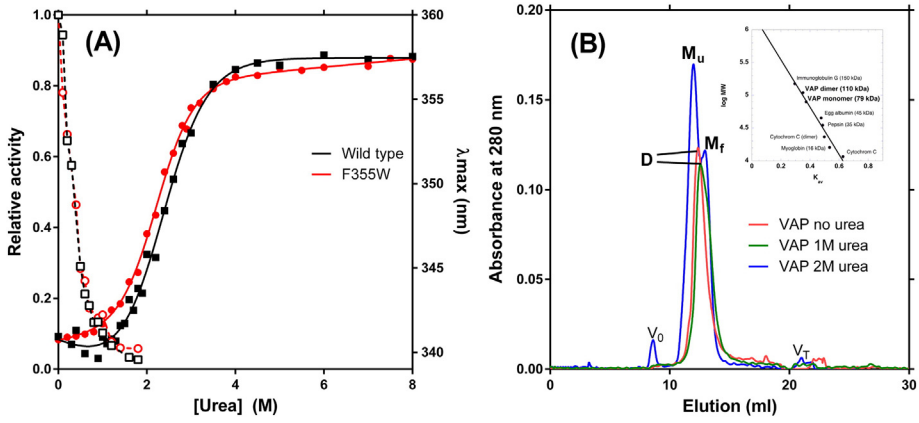

Fig. 5. Urea denaturation of VAP. (A) Urea induced fluorescence red-shift and inactivation. Samples were incubated in 0–8 M urea for 4 h at 10 °C before measurements were made. Data for the wild-type VAP are plotted in black with closed and open squares for inactivation and denaturation, respectively. Data for F355W are plotted in red with closed and open circles for inactivation and denaturation, respectively. The unfolding curves were fitted to a two-state model for wild-type VAP (N → U) and a three-state model for the F355W variant ($I_2 \rightarrow 2I \rightarrow 2$ U). (B) Size exclusion chromatography. VAP samples of approximately 1.5 mg/ml were pretreated with 0, 1 or 2 M urea for 4 h at 10 °C in 25 mM Mops, 1 mM $MgSO_4$, pH 8.0 before loading on a Superose 12 column (GE Healthcare) pre-equilibrated in the same denaturant buffer. Protein standard curve is shown as an inset. $V_t = 20.67$ ml and $V_o = 8.33$ ml. R_f dimer $= 12.67 \pm 0.39$ ($n = 3$) ml; R_f monomer $= 12.97 \pm 0.25$ ml; R_f unfolded monomer $= 10.20$ ml. V_t, V_o, D, M_f and M_u denote the total volume, void volume, native dimer, folded monomer and unfolded monomer, respectively.

4.1. Using tryptophan fluorescence to detect structural changes in VAP

For proteins having multiple Trp residues, it is sometimes feasible to make the Trp fewer by site-directed mutagenesis to decrease the complexity of their fluorescence emission signal. Tyrosine emission is used to a much lesser extent to examine protein folding and dynamics due its higher abundance and lower emission. In order to be able to resolve fluorescence decay spectra, the number of Trp must in most cases be reduced to either one or two, since each Trp is frequently observed having more than one lifetime (e.g. due to rotameric states). For a multi-tryptophan containing protein, the lifetime distribution can be examined as was done with β-glycosidase from the thermophile *Sulfolobus solfataricus* containing 17 Trp per subunit [39]. In such cases, the relative amplitude of lifetimes of the components is often categorized to a short and long lifetime component by distribution functions. For the fluorescence decay of VAP, it was possible to see a slight decrease in the relative amplitude of the shorter mean-lifetime using Top-hat distribution model (Figure S3) for the removal of the two exposed W274 (in the active site) and W512 (located on StrepTag), indicating that these two residues have shorter lifetimes on average than the rest of the tryptophans.

It would be ideal to reduce the number of Trp residues to either one or two residues and characterize the effect of each on the steady state fluorescence emission of VAP dimers. For *E. coli* cystathionine β-lyase, the complex urea unfolding curve of this homo-tetramer containing six Trp residues was resolved by site-directed mutagenesis. Thus, one Trp residue located at the interface could be used to probe local conformational changes [40]. The urea unfolding curve of native VAP had much less complexity and showed a typical two-state unfolding. Either the dissociation event of dimers was not "felt" by any of the native Trp residues, or no folded monomeric intermediate exist in the unfolding pathway. It is widely accepted that alkaline phosphatases dissociate to inactive monomers. Examples can be seen for ECAP [31] and another cold-active AP from cod [27,41].

Here we found, using single Trp substitution variants, that two of the conserved Trp residues, W301 and W460, are mostly responsible for the Trp fluorescent emission from VAP. Surprisingly, replacing the tryptophan in the active site (W274F), increased emission compared to the wild-type VAP, indicating that some rearrangement around its Trp residues was taking place. Most likely, another Trp residue was relieved of static quenching. Prior experiments have indicated that W274 plays an indirect role in substrate binding, since W274K [22], W274H [23], W274A (unpublished results) and W274F all caused an approximately two-fold increase in K_M.

It was apparent from the acrylamide quenching studies, that W460 was highly buried in the protein core. Knowing that W460 is a highly buried residue, and produces almost half of the fluorescence emission, it was unexpected to see that the red-shift upon the W460F replacement was not more than approximately 1 nm. However, a high increase in the Stern–Volmer constant, as observed, is either a sign of the loss of highly buried tryptophan emission, or due to a conformational change allowing better access of the quencher.

4.2. Most tryptophan residues in VAP are important for activity and stability

All the Trp to Phe substitutions in VAP resulted in lower T_m values, an indication of monomer destabilization. Substituting a buried Trp with a Phe residue should leave a hole where the Trp pyrrole ring has been "removed". The lost hydrophobic contacts will likely result in some local alteration of the tertiary structure that may affect distal parts too. The most buried tryptophans, namely W155 (as judged by the crystal structure) and W460, displayed a decreased T_m value by 2–3 °C. Trp to Phe substitutions for solvent exposed Trp should not affect protein stability, at least not when Trp is variably introduced at non-conserved, solvent exposable sites [42,43]. This is true for the W512F substitution of the highly exposed Trp located on the C-terminal StrepTag. However, a larger decrease in T_m of 4 °C was observed for the W274F variant, located at an exposed spot in the active site, than the buried W155F or W460F. The W475F variant had a T_m of 3 °C lower than the wild-type, while W301F had a T_m of 6 °C lower. These differences can be regarded as very large compared with our previous experience with VAP variants [22,23]. The W301F mutation clearly affected the folding process in an unknown way resulting in very low expression yields for that variant.

We found that a correlation between solvent exposure of the various Trp in VAP, as estimated from the crystal structure, and the effect on protein stability of Trp-Phe substitutions was not always consequential. A recent example can be found in the literature where the replacement of a highly exposed Trp at a dimer interface with phenylalanine increased stability [44].

All the Trp to Phe substitutions resulted in decreased k_{cat} values, except in case of the solvent exposed W274F and W512F. However, K_M was generally not affected, except for W274F and W460F, where it was increased. It is not clear why k_{cat} is so highly reduced by the replacement of W475F, since W475F is located far from the active site. A loosening of the global fold would be expected going from a larger residue, having more contacts, to a smaller residue having fewer contacts. However, it is likely that the packing of the hydrophobic core is affected by the Trp → Phe substitutions, since the sum of the difference spectra was not identical to the wild-type VAP and was blue-shifted. This could reach afar through networks shaping distribution of intra- and intermolecular interactions [45].

K_M was increased for the active-site W274F variant (and other W274 variants) but k_{cat} was unaffected. W274, which is equivalent to K328 in ECAP, has no direct contacts with the substrate but coordinates a water molecule which is a part of tight water molecule network around the M3 site. The coordinated waters in the active site might help accommodate the hydrated substrate when it binds.

The W460F replacement caused a lower affinity for the substrate despite the fact that this residue is located 15 Å away from the active site. Furthermore, the W460Y VAP variant had only a slight effect on k_{cat} and K_M, showing that either Trp or Tyr is preferred at this site as the W460I variant was completely inactive. The unexpected increase in K_M for W460F could be rationalized by the consideration that a phenylalanine in that position is unable to have favorable polar–polar interactions with Asn279. Asn279 is located on a helix-turn-helix loop in the active site, close to His277 and Asp273 that are both M1 coordinates for Zn (Fig. 6). Furthermore, His465, another M1 coordinate, is located on a short ß-strand upstream of the loop where W460 is located. Thus, increased mobility of this short loop (magenta in Fig. 6) could allow for movement of zinc ion coordinates and disfavor substrate binding by the zinc ion.

For APs in general, an aromatic residue is conserved at the corresponding site occupied by Trp460. For ECAP and human placenta alkaline phosphatase (PLAP), there is a Tyr residue at this site. For cold-adapted APs, the residue corresponding to W460 is also a Trp residue in *Shewenella* AP [46–48] and *Cobetia marina* AP [49], while it is a Tyr residue in APs from Antarctic shrimp [8] and the Antarctic bacterium TAB5 AP [14,50]. Notably, all of the cold adapted variants mentioned here have an Asn residue at same position as Asn279 in VAP.

4.3. Phosphorescence of VAP

All proteins that contain Trp are phosphorescent if the viscosity and/or temperature is lowered to 77 K [51]. The radiation-less decay of the excited triplet state in solvents is very dependent on solvent viscosity. Thus, a very low triplet state lifetime at room temperature is observed for solvent exposed Trp, while deeply buried Trp can have a lifetime of several orders of magnitude higher (reviewed in [52]). In a survey, where protein phosphorescence at room temperature was tested for 39 proteins, the

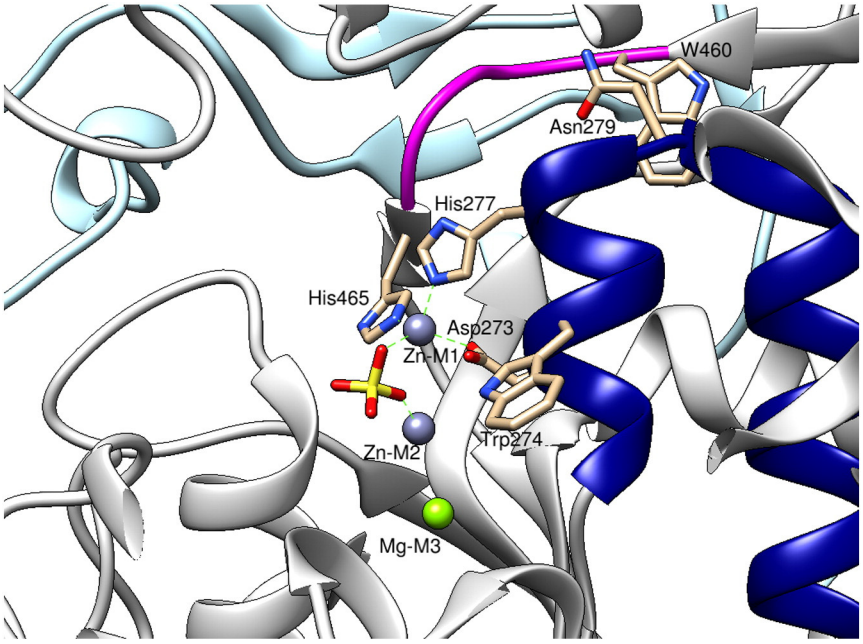

Fig. 6. Distal linkage of Trp460 to the active-site. The short loop where Trp460 is located is shown in magenta and the helix-turn-helix where Asn279 and zinc coordinates are located is shown in navy blue. A sulfate ion is shown bound to the active site pocket. It should be noted that not all substrate and metal-ion ligands are shown here for simplicity.

phosphorescence lifetimes in the range 0.5 ms to 2 s were observed for three-fourths of the proteins tested [53]. Only nine proteins had no detected phosphorescence, while seven proteins had lifetimes greater than 100 ms.

Here, VAP was shown to be phosphorescent at room temperature, having two lifetimes, where the longer lifetime was 140 ms and due to W460 phosphorescence. It was not possible to resolve which Trp residue was responsible for the shorter lifetime, since the margins of repeated measurements were around 30%. We believe that this can be explained by less than optimal deoxygenation of the samples, letting argon gas bubble slowly through a 500 μl quartz flow cell. To test the efficiency of deoxygenation, a protein sample with a known bimolecular quenching constant was measured using the same purging conditions. Alkaline phosphatase from *E. coli* (ECAP) has a well-known bimolecular quenching constant, where Trp 109 in ECAP has the highest reported phosphorescence lifetimes for a protein at room temperature. Measuring ECAP under an identical condition to that used for VAP showed that ECAP had one phosphorescence lifetime of 230 ms. The reported lifetime without any oxygen is close to 2 s at room temperature in the literature [30]. We are currently optimizing a new deoxygenation method, since having a phosphorescent protein at room temperature opens up many possibilities to study dynamics and conformational changes on the millisecond to second timescale which is the timescale of protein collective domain motions. As an example, protein phosphorescence has been useful in studying affinities for inorganic phosphate in ECAP, where the phosphorescent Trp109 is located near the active site [29]. The structural role of metal ion binding in ECAP [7], slow structure rearrangement upon reactivation of ECAP [54], and hydrogen exchange in the core of ECAP [55], were also studied by measuring phosphorescence. The phosphorescence of several proteins was used to elegantly show that acrylamide was capable of long range quenching without the requirement of direct penetration, and also shown how conformational fluctuations can be probed by quenchers of different sizes [56].

Returning to VAP, we would like to see if the phosphorescence of W460 could serve as a more sensitive probe than fluorescence probe for reporting on the dissociation of dimers, since its backbone position is facing the subunit interface. The two phosphorescence lifetimes reported here for VAP, could be used to study VAP subunit heterogeneity in the millisecond to second timescale with reference to the heterogeneous activity of subunits [57–61] and asymmetric flexibility [45] reported for other APs.

4.4. Detection of a dimer intermediate and mechanism for inactivation and unfolding

We have shown here, that the effect on kinetics and thermal stability was too great for single Trp substitutions to make it possible to leave either one or two Trp intact and expect the variant to reflect the state of the native VAP structure.

Introducing a new Trp residue by site directed mutagenesis at the subunit interface (position F355) was shown to have no effect on the steady-state kinetic constants or stability of the enzyme. Furthermore, an emission red-shift in the 0.8–1.8 M urea range was observed as a small curvature in the urea denaturation curve for F355W, an indication of an increased polarity around the F355W residue. For F355W (as well as the wild-type VAP), almost all activity of the enzyme was lost at 1 M urea concentration. Thus, if the red-shift seen at around 1–2 M urea was the dimer dissociation event, the inactivation induced by urea was a consequence of formation of an inactive dimer or a dimeric state with trace activity present. We have previously reported on an increase in the mobility of a spin probe in the 1–2 M urea range when located on the only native Cys67 residue close to the active site [23]. The wild-type VAP did not show as distinct a red-shift curvature at this range before unfolding took place. SEC data indicated that the enzyme was still in the dimeric form at 1 M urea and completely monomeric at 2 M urea. Thus, the correct model for inactivation and unfolding involves an inactive dimeric intermediate and a folded monomeric state before the monomers unfold: $N_2 \rightarrow I_2 \rightarrow 2I \rightarrow 2D$. This is the first example of an inactive alkaline phosphatase dimeric state induced by a denaturant. In the literature, there are not many examples of inactive dimer intermediate states induced by denaturants for other enzymes. Some examples include guanidine hydrochloride mediated denaturation of *E. coli* alanyl-tRNA synthetase [62] and organophosphorus

hydrolase from *Pseudomonas diminuta* [63]. Commonly, the active-site is usually more stable to denaturants than the dimer interface, and cold-adapted enzymes are probably more prone to form inactive dimer intermediates than mesophilic ones.

The inactivation event in VAP might be facilitated by a dissociation of Mg^{2+} from the active site or rearrangement of key residues involved in substrate activation such as Arg129 (homologous to Arg166 in *E. coli*). Arg129 is crucial for substrate binding [64], activation and possibly for modulation of negative cooperativity in half-of-sites reactivity [65].

VAP has one of the highest catalytic activities at lower temperatures found in APs, which is likely promoted by more loop mobility around the active site. Therefore, it does not come by surprise that the active-site might be more prone to adapt kinetically unfavorable rearrangements of key residue compared with more heat-tolerant APs, especially the ones that coordinate the active site metal ions. Thus, low concentration of a chaotropic denaturant might facilitate the transition to this inactive and kinetically trapped state. More experiments need to be conducted to evaluate the nature of this inactive dimeric state, such as conducting crystallographic experiments at low urea concentrations. We strongly believe that magnesium might be absent in the inactive dimeric structure. We are currently optimizing magnesium dissociation assays for VAP. However, it is very challenging to measure the dissociation of magnesium from the active site where a bias for magnesium dissociation exists, since leakage of magnesium during sample preparation and handling of the enzyme is common (e.g. dialysis or desalting).

5. Conclusion

In this study, we have characterized all the tryptophan residues in VAP with respect to fluorescence, activity and stability. One residue close to the active site, excluded from the solvent (W460), is highly phosphorescent and plays a distant role in modulating substrate binding. By studying the inactivation and unfolding mechanism using urea as a denaturant, the enzyme was found to form an inactive dimeric intermediate state that is structurally similar to the active state. This is the first time to our knowledge that alkaline phosphatase is shown to have an inactive dimeric state not promoted by mutagenesis or chemical inhibition.

Transparency document

The Transparency document associated with this article can be found in the online version.

Acknowledgments

Financial support from the Icelandic Research Fund (project 141619-051) and the Science Institute of the University of Iceland is gratefully acknowledged. The authors also extend their gratitude to Tinna Pálmadóttir for performing the experiment of Fig. 2B.

Appendix A. Supplementary data

Supplementary data to this article can be found online at http://dx.doi.org/10.1016/j.bbapap.2016.03.016.

References

[1] A. Shurki, E. Derat, A. Barrozo, S.C. Kamerlin, How valence bond theory can help you understand your (bio)chemical reaction, Chem. Soc. Rev. 44 (2015) 1037–1052.
[2] F. Duarte, J. Aqvist, N.H. Williams, S.C. Kamerlin, Resolving apparent conflicts between theoretical and experimental models of phosphate monoester hydrolysis, J. Am. Chem. Soc. 137 (2015) 1081–1093.
[3] F. Sunden, A. Peck, J. Salzman, S. Ressl, D. Herschlag, Extensive Site-directed Mutagenesis Reveals Interconnected Functional Units in the Alkaline Phosphatase Active Site, Elife, 4, 2015.
[4] M. Gottesman, R.T. Simpson, B.L. Vallee, Kinetic properties of cobalt alkaline phosphatase, Biochemistry 8 (1969) 3776–3783.
[5] J. Wang, K.A. Stieglitz, E.R. Kantrowitz, Metal specificity is correlated with two crucial active site residues in *Escherichia coli* alkaline phosphatase, Biochemistry 44 (2005) 8378–8386.
[6] N. Gong, C. Chen, L. Xie, H. Chen, X. Lin, R. Zhang, Characterization of a thermostable alkaline phosphatase from a novel species *Thermus yunnanensis* sp. nov. and investigation of its cobalt activation at high temperature, Biochim. Biophys. Acta 1750 (2005) 103–111.
[7] P. Cioni, L. Piras, G.B. Strambini, Tryptophan phosphorescence as a monitor of the structural role of metal ions in alkaline phosphatase, Eur. J. Biochem. 185 (1989) 573–579.
[8] M. de Backer, S. McSweeney, H.B. Rasmussen, B.W. Riise, P. Lindley, E. Hough, The 1.9 Ångstrom crystal structure of heat-labile shrimp alkaline phosphatase, J. Mol. Biol. 318 (2002) 1265–1274.
[9] C.L. Wojciechowski, E.R. Kantrowitz, Altering of the metal specificity of *Escherichia coli* alkaline phosphatase, J. Biol. Chem. 277 (2002) 50476–50481.
[10] L. Ma, T.T. Tibbitts, E.R. Kantrowitz, *Escherichia coli* alkaline phosphatase: X-ray structural studies of a mutant enzyme (His-412– > Asn) at one of the catalytically important zinc binding sites, Protein Sci. 4 (1995) 1498–1506.
[11] M. Bortolato, F. Besson, B. Roux, Role of metal ions on the secondary and quaternary structure of alkaline phosphatase from bovine intestinal mucosa, Proteins Struct. Funct. Genet. 37 (1999) 310–318.
[12] G. Cathala, C. Brunel, D. Chappelettordo, M. Lazdunski, Bovine kidney alkaline-phosphatase — catalytic properties, subunit interactions in catalytic process, and mechanism of Mg^{2+} stimulation, J. Biol. Chem. 250 (1975) 6046–6053.
[13] B. Stec, K.M. Holtz, E.R. Kantrowitz, A revised mechanism for the alkaline phosphatase reaction involving three metal ions, J. Mol. Biol. 299 (2000) 1303–1311.
[14] E. Wang, D. Koutsioulis, H.K. Leiros, O.A. Andersen, V. Bouriotis, E. Hough, P. Heikinheimo, Crystal structure of alkaline phosphatase from the Antarctic bacterium TAB5, J. Mol. Biol. 366 (2007) 1318–1331.
[15] A. Garen, C. Levinthal, A fine-structure genetic and chemical study of the enzyme alkaline phosphatase of *E. coli*. I. Purification and characterization of alkaline phosphatase, Biochim. Biophys. Acta 38 (1960) 470–483.
[16] M.H. Malamy, B.L. Horecker, Purification and crystallization of the alkaline phosphatase of *Escherichia coli*, Biochemistry 3 (1964) 1893–1897.
[17] X.J. Tian, X.H. Song, S.L. Yan, Y.X. Zhang, H.M. Zhou, Study of refolding of calf intestinal alkaline phosphatase, J. Protein Chem. 22 (2003) 417–422.
[18] R.B. McComb, G.N. Bowers, S. Posen, Alkaline Phosphatase, Plenum Press, 1979 198–199 (330-332).
[19] J.G. Zalatan, T.D. Fenn, D. Herschlag, Comparative enzymology in the alkaline phosphatase superfamily to determine the catalytic role of an active-site metal ion, J. Mol. Biol. 384 (2008) 1174–1189.
[20] J. Hauksson, O. Andresson, B. Asgeirsson, Heat-labile bacterial alkaline phosphatase from a marine *Vibrio* sp. Enzym. Microb. Technol. 27 (2000) 66–73.
[21] R. Helland, R.L. Larsen, B. Asgeirsson, The 1.4 Ångstrom crystal structure of the large and cold-active *Vibrio* sp. alkaline phosphatase, Biochim. Biophys. Acta, Proteins Proteomics 1794 (2009) 297–308.
[22] K. Gudjonsdottir, B. Asgeirsson, Effects of replacing active site residues in a cold-active alkaline phosphatase with those found in its mesophilic counterpart from *Escherichia coli*, FEBS J. 275 (2008) 117–127.
[23] P.O. Heidarsson, S.T. Sigurdsson, B. Asgeirsson, Structural features and dynamics of a cold-adapted alkaline phosphatase studied by EPR spectroscopy, FEBS J. 276 (2009) 2725–2735.
[24] I.S. Krull, H.H. Stuting, S.C. Krzysko, Conformational studies of bovine alkaline phosphatase in hydrophobic interaction and size-exclusion chromatography with linear diode array and low-angle laser light scattering detection, J. Chromatogr. 442 (1988) 29–52.
[25] M.L. Applebury, J.E. Coleman, *Escherichia coli* alkaline phosphatase. metal binding, protein conformation, and quaternary structure, J. Biol. Chem. 244 (1969) 308–318.
[26] M.J. Schlesinger, K. Barrett, The reversible dissociation of the alkaline phosphatase of *Escherichia coli*. I. Formation and reactivation of subunits, J. Biol. Chem. 240 (1965) 4284–4292.
[27] B. Asgeirsson, K. Gudjonsdottir, Reversible inactivation of alkaline phosphatase from Atlantic cod (*Gadus morhua*) in urea, Biochim. Biophys. Acta, Proteins Proteomics 1764 (2006) 190–198.
[28] R.L. Olsen, K. Overbo, B. Myrnes, Alkaline-phosphatase from the hepatopancreas of shrimp (*Pandalus borealis*) — a dimeric enzyme with catalytically active subunits, Comp. Biochem. Physiol. B 99 (1991) 755–761.
[29] L. Sun, E.R. Kantrowitz, W.C. Galley, Room temperature phosphorescence study of phosphate binding in *Escherichia coli* alkaline phosphatase, Eur. J. Biochem. 245 (1997) 32–39.
[30] M. Gonnelli, G.B. Strambini, Phosphorescence lifetime of tryptophan in proteins, Biochemistry 34 (1995) 13847–13857.
[31] R.R. Boulanger Jr., E.R. Kantrowitz, Characterization of a monomeric *Escherichia coli* alkaline phosphatase formed upon a single amino acid substitution, J. Biol. Chem. 278 (2003) 23497–23501.
[32] M.R. Eftink, C.A. Ghiron, Exposure of tryptophanyl residues and protein dynamics, Biochemistry 16 (1977) 5546–5551.
[33] G.B. Strambini, M. Gonnelli, Acrylonitrile quenching of trp phosphorescence in proteins: a probe of the internal flexibility of the globular fold, Biophys. J. 99 (2010) 944–952.
[34] G.B. Strambini, M. Gonnelli, Protein phosphorescence quenching: distinction between quencher penetration and external quenching mechanisms, J. Phys. Chem. B 114 (2010) 9691–9697.
[35] M. Niklasson, C. Andresen, S. Helander, M.G. Roth, A. Zimdahl Kahlin, M. Lindqvist Appell, L.G. Martensson, P. Lundstrom, Robust and convenient analysis of protein thermal and chemical stability, Protein Sci. (2015) 2055–2062.

[36] C.N. Pace, F. Vajdos, L. Fee, G. Grimsley, T. Gray, How to measure and predict the molar absorption coefficient of a protein, Protein Sci. 4 (1995) 2411–2424.
[37] P. Cioni, G.B. Strambini, Pressure/temperature effects on protein flexibility from acrylamide quenching of protein phosphorescence, J. Mol. Biol. 291 (1999) 955–964.
[38] D.M. Togashi, A.G. Ryder, A fluorescence analysis of ANS bound to bovine serum albumin: binding properties revisited by using energy transfer, J. Fluoresc. 18 (2008) 519–526.
[39] E. Bismuto, G. Irace, S. D'Auria, M. Rossi, R. Nucci, Multitryptophan-fluorescence-emission decay of beta-glycosidase from the extremely thermophilic archaeon *Sulfolobus solfataricus*, Eur. J. Biochem. 244 (1997) 53–58.
[40] A.F. Jaworski, S.M. Aitken, Exploration of the six tryptophan residues of *Escherichia coli* cystathionine beta-lyase as probes of enzyme conformational change, Arch. Biochem. Biophys. 538 (2013) 138–144.
[41] B. Asgeirsson, J. Hauksson, G. Gunnarsson, Dissociation and unfolding of cold-active alkaline phosphatase from Atlantic cod in the presence of guanidinium chloride, Eur. J. Biochem. 267 (2000) 6403–6412.
[42] H. Gu, N. Doshi, D.E. Kim, K.T. Simons, J.V. Santiago, S. Nauli, D. Baker, Robustness of protein folding kinetics to surface hydrophobic substitutions, Protein Sci. 8 (1999) 2734–2741.
[43] A. Vallee-Belisle, S.W. Michnick, Visualizing transient protein-folding intermediates by tryptophan-scanning mutagenesis, Nat. Struct. Mol. Biol. 19 (2012) (731-+).
[44] Z. Markovic-Housley, B. Stolz, R. Lanz, B. Erni, Effects of tryptophan to phenylalanine substitutions on the structure, stability, and enzyme activity of the IIAB(Man) subunit of the mannose transporter of *Escherichia coli*, Protein Sci. 8 (1999) 1530–1535.
[45] B. Asgeirsson, G. Renzetti, G. Invernizzi, E. Papaleo, Asymmetric flexibility of a homodimeric enzyme as shown by molecular dynamics computations. A case study of the cold-active *Vibrio* alkaline phosphatase, FEBS J. 280 (2013) 157.
[46] H. Tsuruta, B. Mikami, T. Higashi, Y. Aizono, Crystal structure of cold-active alkaline phosphatase from the psychrophile *Shewanella sp*, Biosci. Biotechnol. Biochem. 74 (2010) 69–74.
[47] T. Murakawa, H. Yamagata, H. Tsuruta, Y. Aizono, Cloning of cold-active alkaline phosphatase gene of a psychrophile, *Shewanella* sp., and expression of the recombinant enzyme, Biosci. Biotechnol. Biochem. 66 (2002) 754–761.
[48] Y. Suzuki, Y. Mizutani, T. Tsuji, N. Ohtani, K. Takano, M. Haruki, M. Morikawa, S. Kanaya, Gene cloning, overproduction, and characterization of thermolabile alkaline phosphatase from a psychrotrophic bacterium, Biosci. Biotechnol. Biochem. 69 (2005) 364–373.
[49] V. Golotin, L. Balabanova, G. Likhatskaya, V. Rasskazov, Recombinant production and characterization of a highly active alkaline phosphatase from marine bacterium *Cobetia marina*, Mar. Biotechnol. (NY) 17 (2015) 130–143.
[50] M. Rina, C. Pozidis, K. Mavromatis, M. Tzanodaskalaki, M. Kokkinidis, V. Bouriotis, Alkaline phosphatase from the Antarctic strain TAB5. Properties and psychrophilic adaptations, Eur. J. Biochem. 267 (2000) 1230–1238.
[51] M.L. Saviotti, W.C. Galley, Room temperature phosphorescence and the dynamic aspects of protein structure, Proc. Natl. Acad. Sci. U. S. A. 71 (1974) 4154–4158.
[52] P. Cioni, G.B. Strambini, Tryptophan phosphorescence and pressure effects on protein structure, Biochim. Biophys. Acta 1595 (2002) 116–130.
[53] J.M. Vanderkooi, D.B. Calhoun, S.W. Englander, On the prevalence of room-temperature protein phosphorescence, Science 236 (1987) 568–569.
[54] V. Subramaniam, N.C. Bergenhem, A. Gafni, D.G. Steel, Phosphorescence reveals a continued slow annealing of the protein core following reactivation of *Escherichia coli* alkaline phosphatase, Biochemistry 34 (1995) 1133–1136.
[55] C.J. Fischer, J.A. Schauerte, K.C. Wisser, A. Gafni, D.G. Steel, Hydrogen exchange at the core of *Escherichia coli* alkaline phosphatase studied by room-temperature tryptophan phosphorescence, Biochemistry 39 (2000) 1455–1461.
[56] G.B. Strambini, M. Gonnelli, Influence of denaturants on native-state structural fluctuations in azurin probed by molecular size-dependent quenching of Trp phosphorescence, J. Phys. Chem. B 115 (2011) 13755–13764.
[57] D. Chappelet-Tordo, M. Fosset, M. Iwatsubo, C. Gache, M. Lazdunski, Intestinal alkaline phosphatase. Catalytic properties and half of the sites reactivity, Biochemistry 13 (1974) 1788–1795.
[58] D. Chappelet-Tordo, M. Iwatsubo, M. Lazdunski, Negative cooperativity and half of the sites reactivity. Alkaline phosphatases of *Escherichia coli* with Zn^{2+}, Co^{2+}, Cd^{2+}, Mn^{2+}, and Cu^{2+} in the active sites, Biochemistry 13 (1974) 3754–3762.
[59] S. Orhanovic, M. Pavela-Vrancic, Dimer asymmetry and the catalytic cycle of alkaline phosphatase from *Escherichia coli*, Eur. J. Biochem. 270 (2003) 4356–4364.
[60] P. Gettins, J.E. Coleman, ^{31}P nuclear magnetic resonance of phosphoenzyme intermediates of alkaline phosphatase, J. Biol. Chem. 258 (1983) 408–416.
[61] M.F. Hoylaerts, T. Manes, J.L. Millan, Mammalian alkaline phosphatases are allosteric enzymes, J. Biol. Chem. 272 (1997) 22781–22787.
[62] B. Banerjee, R. Banerjee, Guanidine hydrochloride mediated denaturation of *E. coli* alanyl-tRNA synthetase: identification of an inactive dimeric intermediate, Protein J. 33 (2014) 119–127.
[63] J.K. Grimsley, J.M. Scholtz, C.N. Pace, J.R. Wild, Organophosphorus hydrolase is a remarkably stable enzyme that unfolds through a homodimeric intermediate, Biochemistry 36 (1997) 14366–14374.
[64] A. Chaidaroglou, D.J. Brezinski, S.A. Middleton, E.R. Kantrowitz, Function of arginine-166 in the active site of *Escherichia coli* alkaline phosphatase, Biochemistry 27 (1988) 8338–8343.
[65] N.M. Rao, R. Nagaraj, Anomalous stimulation of *Escherichia coli* alkaline phosphatase activity in guanidinium chloride. Modulation of the rate-limiting step and negative cooperativity, J. Biol. Chem. 266 (1991) 5018–5024.

Supplementary material

Cold-active alkaline phosphatase is irreversibly transformed into an inactive dimer by low urea concentrations.

Jens Guðmundur Hjörleifsson[1]* and Bjarni Ásgeirsson[1]*

[1]Department of Biochemistry, Science Institute, University of Iceland, Dunhagi 3, 107 Reykjavik, Iceland.

* Corresponding authors: Bjarni Ásgeirsson, email: bjarni@hi.is and Jens Guðmundur Hjörleifsson, email: jgh4@hi.is

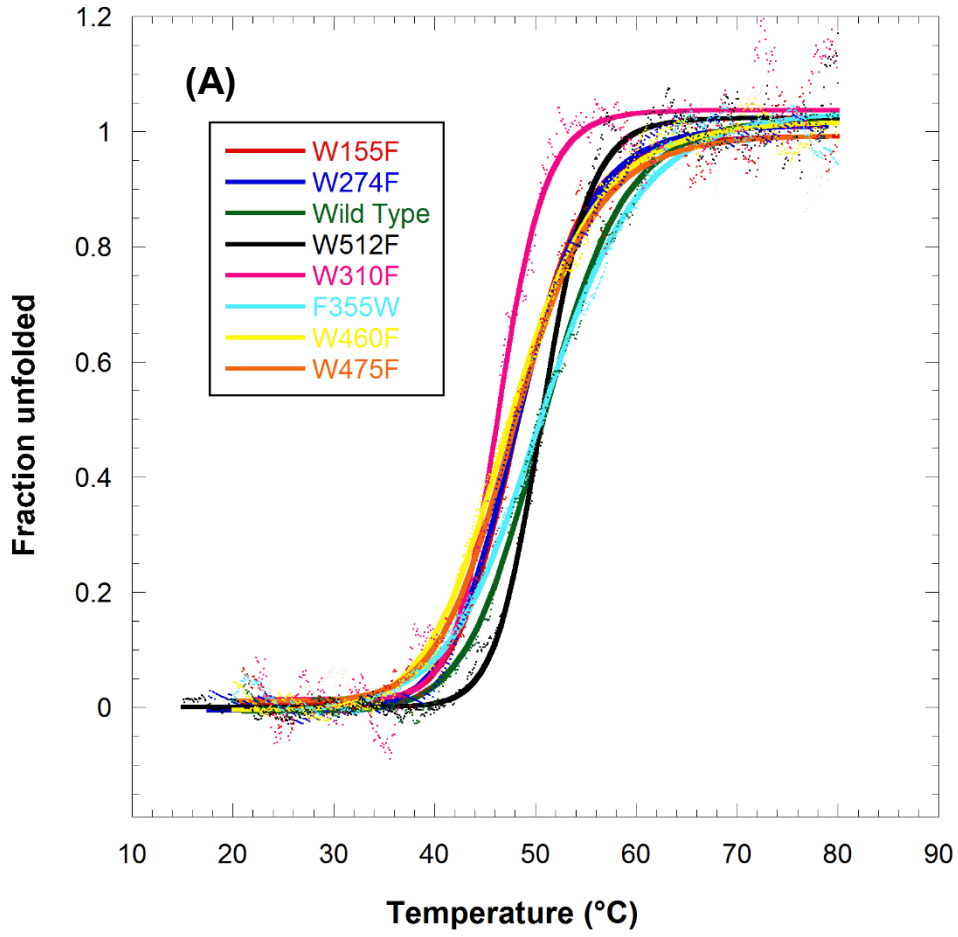

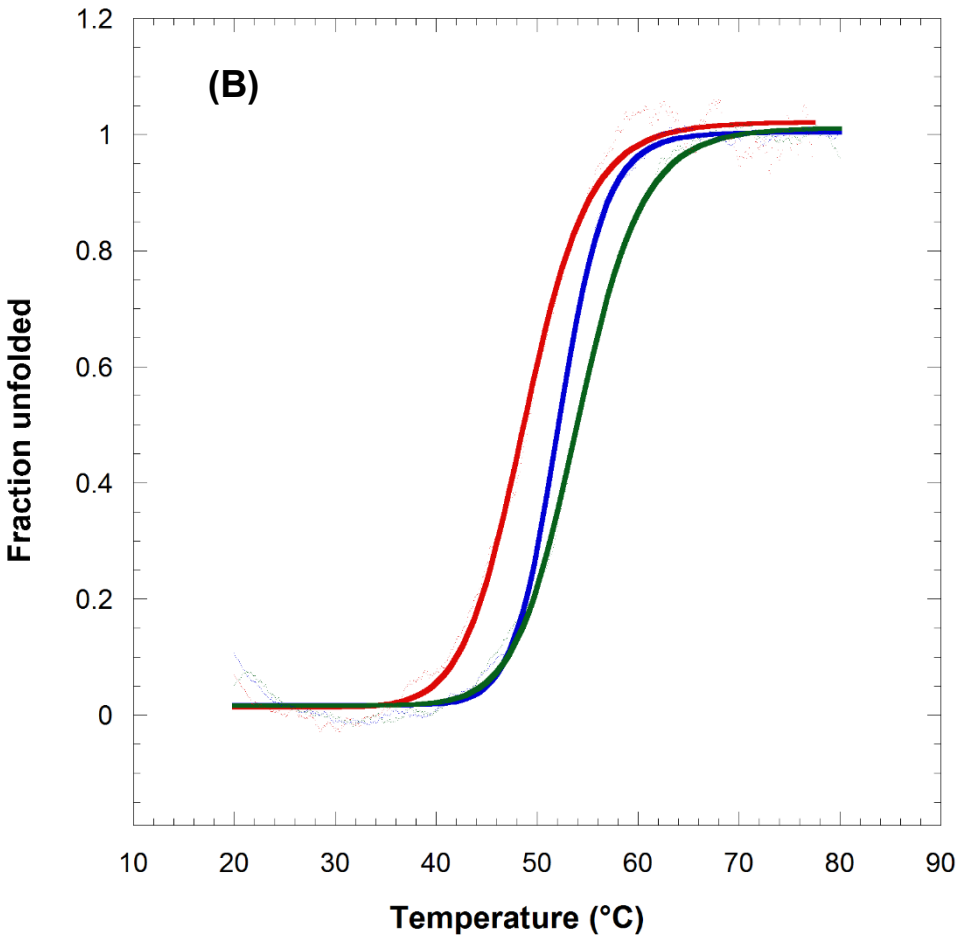

Figure S1: **(A)** Normalized melting temperature (T_m) traces of VAP variants. T_m determination was performed on a JASCO J-810 circular dichroism (CD) spectropolarimeter by measuring a melting curve at 222 nm in the range 15-85 °C in a 2 mm cuvette with 1°C/min temperature rise. The traces where first normalized to fraction unfolded and then fitted with a two state S curve to define the T_m (results shown in table 2). **(B)** Effect of magnesium on VAP global heat stability. All samples were measured in 25 mM Mops, pH 8.0 (20°C) with no added magnesium (black curve), 1 mM $MgCl_2$ (red curve) and 1 mM $MgSO_4$ (Blue line). Melting temperature (T_m) was 48.9 °C, 52.2 °C and 54.2 °C for no Mg^{2+}, 1 mM $MgCl_2$ and 1 mM $MgSO_4$, respectively.

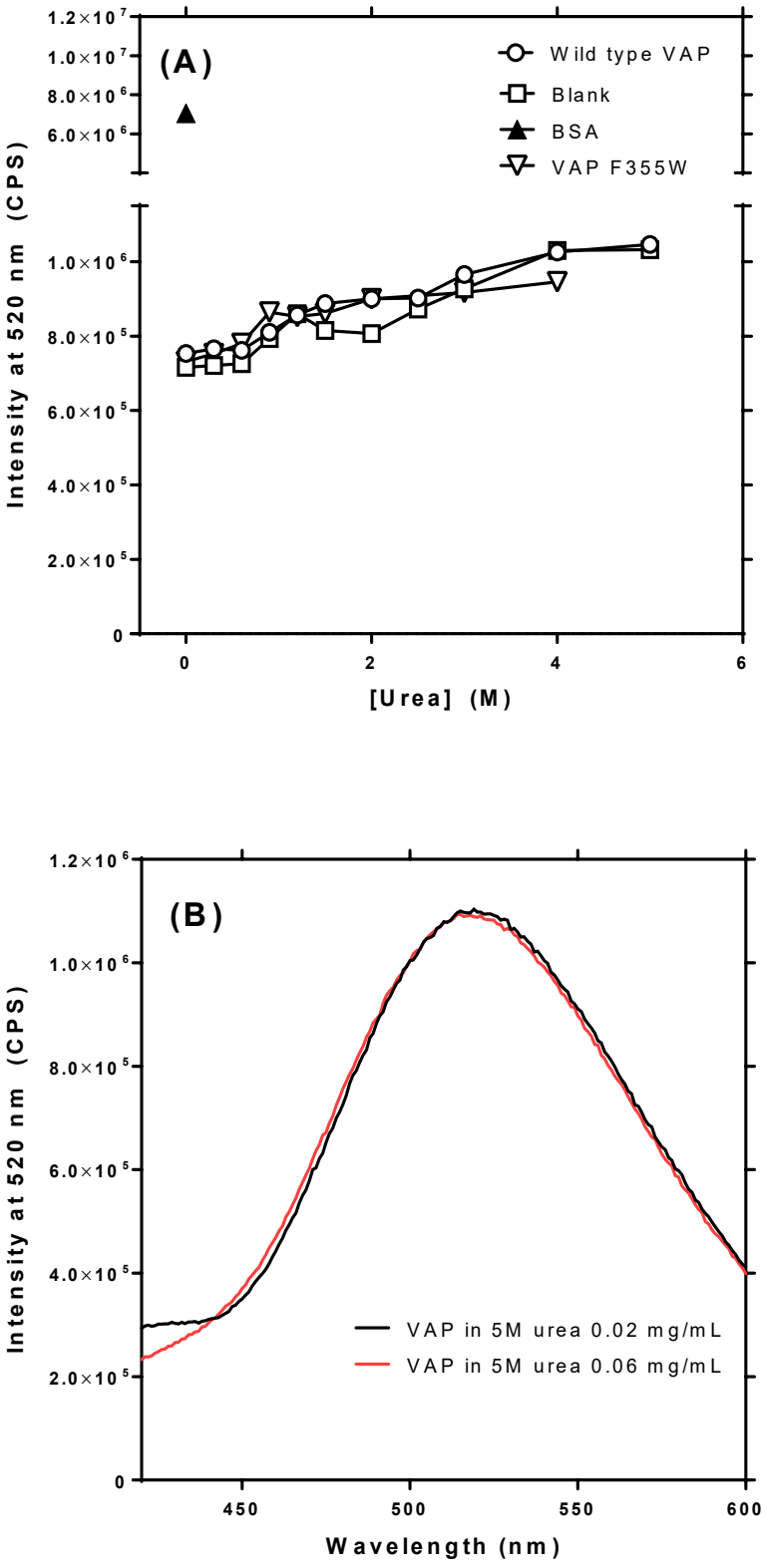

Figure S2. ANS fluorescence measurements. **(A)** ANS fluorescence vs. urea concentration. The samples were incubated at 10 °C with urea ranging from 0-5 M in 25 mM Mops, 1 mM MgSO4, pH 8.0 for 4 hours with a protein concentration of 0.02 mg/ml. ANS was then added from 2 mM stock solution to a final concentration of 20 µM and an emission curve was recorded from 420 – 600 nm (8 nm slit width) with an excitation wavelength fixed at 390 nm (5 nm slit width). Blank measurements were made under the same conditions without adding enzyme. **(B)** Effect of VAP concentration on ANS emission. ANS and BSA were purchased from Sigma.

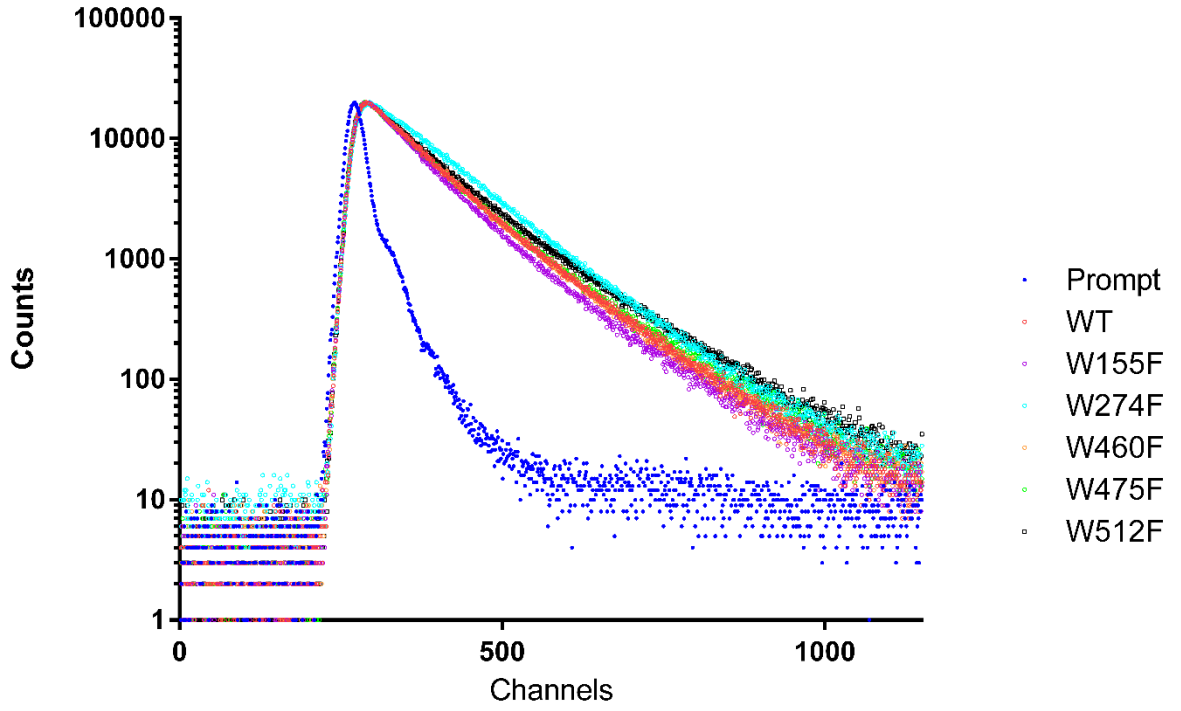

Figure S3: Fluorescence decay curves for VAP tryptophan mutants. Time resolved decay curves were measured on a Fluoromax4-P (Horiba) equipped with a single photon counting system (FluoroHub, Horiba). The detector photomultiplier tube was maintained at 900 V and the sample excited using NanoLED 280 nm (Horiba) using a 7 nm slit width for emission monochromator fixed at 340 nm. The stop count rate was not allowed to exceed 2% of the excitation rate. A prompt was measured under the same settings to define the instrument response time using LUDOX TM-40 colloidal silica (Sigma) scattering agent. Acquisition was stopped when the signal peaked at 20.000 counts. The sample was measured at 10 °C in 25 mM Mops, 1 mM $MgSO_4$ pH 8.0. Each channel was automatically calibrated to 0.0548 ns by the instrument.

Paper II

Biochemistry

Article

pubs.acs.org/biochemistry

pH-Dependent Binding of Chloride to a Marine Alkaline Phosphatase Affects the Catalysis, Active Site Stability, and Dimer Equilibrium

Jens G. Hjörleifsson* and Bjarni Ásgeirsson*

Department of Biochemistry, Science Institute, University of Iceland, Dunhagi 3, 107 Reykjavik, Iceland

Supporting Information

ABSTRACT: The effect of ionic strength on enzyme activity and stability varies considerably between enzymes. Ionic strength is known to affect the catalytic activity of some alkaline phosphatases (APs), such as *Escherichia coli* AP, but how ions affect APs is debated. Here, we studied the effect of various ions on a cold-adapted AP from *Vibrio splendidus* (VAP). Previously, we have found that the active form of VAP is extremely unstable at low ionic strengths. Here we show that NaCl increased the activity and stability of VAP and that the effect was pH-dependent in the range of pH 7−10. The activity profile as a function of pH formed two maxima, indicating a possible conformational change. Bringing the pH from the neutral to the alkaline range was accompanied by a large increase in both the K_i for inorganic phosphate (product inhibition) and the K_M for *p*-nitrophenyl phosphate. The activity transitions observed as the pH was varied correlated with structural changes as monitored by tryptophan fluorescence. Thermal and urea-induced inactivation was shown to be accompanied by neither dissociation of the active site metal ions nor dimer dissociation. This would suggest that the inactivation involved subtle changes in active site conformation. Furthermore, the VAP dimer equilibrium was studied for the first time and shown to highly favor dimerization, which was dependent on pH and NaCl concentration. Taken together, the data support a model in which anions bind to some specific acceptor in the active site of VAP, resulting in great stabilization and catalytic rate enhancement, presumably through a different mechanism.

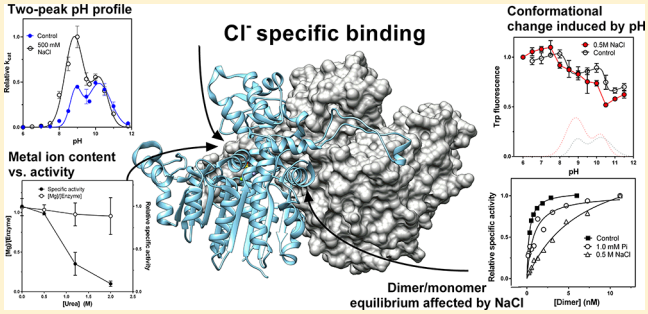

Environmental factors, such as heat, pH, and ionic strength, place enzymes under evolutionary pressure to adapt by residue replacements.[1−3] For multicellular organisms, the ionic strength is kept relatively constant both inside cells and in extracellular spaces. However, bacteria have evolved to withstand environments of various ionic strengths. In sea ice, for example, microbes are found in habitats created by pores and channels in the sea ice, where salinity can vary from 0 to 200%.[4,5]

The effects of ions on the function and stability of enzymes have been extensively studied but vary depending on the enzyme. Different effects may be observed at low concentrations (salting in), where effects may be due to semispecific binding of the ions to the enzyme, or higher concentrations (salting out), where the properties of the water medium might be affected (Hofmeister effects). The intricacies of these interactions are not yet fully understood.[6,7]

The alkaline phosphatase (AP) superfamily is well-suited to studying the evolution of enzymes due to environmental factors, because it is found only as an extracellular enzyme, either secreted or membrane-bound. APs are homodimeric metalloenzymes containing two zinc ions and one magnesium ion in each active site. The Zn^{2+} ions have both a substrate binding role and a role in hydrolysis, while the Mg^{2+} ion is believed to activate the nucleophilic Ser in the active site.[8] In Gram-negative bacteria, APs are secreted to the periplasmic space where they are believed to act mostly as phosphate scavengers. In one study, the volume and osmotic pressure of the periplasm were measured in different media for *Escherichia coli* and *Salmonella typhimurium*. The results indicated that the ionic composition of the periplasm can differ from that of the external medium, especially in a low-ionic strength medium. The concentration of chloride was found to be around 200−400 mM inside the periplasmic space using a medium with an ionic strength of approximately 100 mM.[9] Furthermore, using a pH-sensitive green fluorescence protein variant (TorA-GFPmut3) fused to a periplasmic protein, the pH of the periplasm of *E. coli* was found to equal the pH of the medium. Thus, the pH is likely not regulated in the periplasmic space.[10]

An AP from the Gram-negative, cold-adapted bacterium *Vibrio* sp. (VAP) is an interesting case, because it has been found to be very intolerant to heat at low ionic strengths.[11,12] Furthermore, VAP has been shown to be remarkably stabilized and activated by 0.5 M NaCl.[12] The mechanism for this ionic effect is unknown and is explored in this study. Some APs are known to be activated by high ionic strengths, such as the *E. coli* AP (ECAP)[13−15] and the AP from *Vibrio alginolyticus*.[16] The latter is closely related to VAP. Other APs, such as the human placental AP (PLAP),[17] are

Received: July 19, 2017
Revised: August 22, 2017
Published: August 22, 2017

DOI: 10.1021/acs.biochem.7b00690
Biochemistry 2017, 56, 5075−5089

not activated by high ionic strengths. The rate of phosphomonoester hydrolysis by APs increases with an increase in pH, where the rate-limiting step becomes the release of the inorganic phosphate (P_2) from the phospho-enzyme complex at pH >8.0 (Scheme 1). This pH dependence of the rate-limiting step causes

Scheme 1

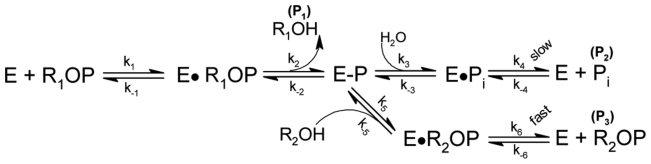

a shift of the slowest step from dephosphorylation (k_3) to phosphate release (k_4) at higher pH values.[18] Furthermore, the presence of a suitable phosphate acceptor, such as amine alcohols, provides competition for water as a nucleophile and increases the reaction rates.

It has been postulated that ionic strength decreases the affinity of the enzyme for the phosphate product, leading to the increased rate of phosphate release (k_4). This has been directly measured by an increase in the inhibition constant (K_i) with inorganic phosphate at high ionic strengths, where the rate of dephosphorylation of E-P is only marginally affected by ionic strength.[15] Another aspect is the possibility that the ionic strength might be affecting rate-limiting conformational changes. A conformational change in AP between active and inactive states has been postulated previously,[19,20] and asymmetric binding of phosphate or substrate has been directly observed for ECAP.[21,22] The reaction cycle in the dimeric enzyme is believed to be half-of-sites in nature, where a conformational change between low and high affinity for the substrate is the driving force for catalysis by facilitating release of the product.[22] It is not fully understood how pH affects catalysis for APs and why some APs are not affected by ionic strength. In this study, we sought to answer how ionic strength influences the chemical and physical properties of VAP and, more specifically, how anions affect both the activity and stability. Furthermore, we wanted to answer how and why the enzyme is deactivated at a moderate temperature at low ionic strengths.

Our results indicate that anions, rather than cations, both activate and stabilize VAP. The ionic effect was shown to be pH-dependent. The pH−activity curves had two maxima, which is unique among APs, and we propose that is caused by a conformational change involving a deprotonation event in the pH range of 9.0−10.5. Conformational changes were detected using tryptophan fluorescence, which correlated with changes in activity and phosphate binding. Both NaCl and pH were further shown to affect the monomer−dimer equilibrium, suggesting their involvement in a conformational change. Interestingly, the decrease in enzyme activity was not linked to dimer dissociation or depletion of metal ions from the active site.

MATERIALS AND METHODS

Materials. Chemicals were obtained from Sigma-Aldrich (Schnelldorf, Germany) or Merck (Darmstadt, Germany) unless stated otherwise. L-Rhamnose and isopropyl β-D-1-thiogalactopyranoside (IPTG) were obtained from AppliChem. Bacto yeast extract and Bacto tryptone were purchased from Becton, Dickinson, and company. Triton X-100 was obtained from BPH chemicals and chloramphenicol from Ampresco. Primers were obtained from TAG (Copenhagen, Denmark). Phusion polymerase was obtained from NEB and DpnI from Fermentas. Alkaline phosphatase from *E. coli* and calf intestines were purchased from Sigma-Aldrich.

Subcloning of the VAP Gene to pET11a. The VAP gene containing the original N-terminal export sequence (MKPIVT-AVVTSTLSFNVLS), previously generated with a StrepTag II (WSHPQFEK) at the C-terminus,[12] was subcloned from the pASK3-plus StrepTag vector (IBA, Gottingen, Germany) to a pET11a vector using the overlap extension polymerase chain reaction (PCR) cloning method.[23,24] Details of the cloning procedure can be found in the Supporting Information. Positive *E. coli* Top10 clones were selected, and the plasmid was subsequently purified on a GeneJET Plasmid Miniprep Kit (Fermentas) and sequenced (Genewiz) to confirm 100% sequence identity. The VAP gene in the pET11a vector contained the StrepTag II sequence at the C-terminus with a two-amino acid linker (Ser-Ala) between the polypeptide chain and the tag, upstream of the stop codon.

Enzyme Expression and Purification. *E. coli* Lemo21-(DE3) cells (NEB) were transformed with the VAP-pET11a plasmid and clones selected on an LB-agar containing 100 μg/mL ampicillin and 30 μg/mL chloramphenicol. A single colony was inoculated into 20 mL of LB medium starter culture containing 100 μg/mL ampicillin and 30 μg/mL chloramphenicol and shaken overnight at 300 rpm in a 100 mL Erlenmeyer flask at 37 °C. The overnight culture was back diluted 1:100 into 200−250 mL of the same medium containing an addition of 0.50 mM L-rhamnose and grown at room temperature in 1 L Erlenmeyer flask at 220 rpm until the OD_{600} was 0.4−0.6, at which point the cells were induced by adding isopropyl β-D-1-thiogalactopyranoside (IPTG) to a final concentration of 400 μM. After induction, cells were grown at 18−20 °C at 220 rpm until they were harvested 16−18 h later by centrifugation. Cells were resuspended in 100 mL (1:10) of lysis buffer [20 mM Tris, 10 mM $MgCl_2$, 0.1% (w/v) Triton X-100, 0.1 mg/mL hen egg lysozyme, and 10 units/mL DNase I (Sigma) (pH 8.0)] and incubated for 3−4 h at 4−8 °C under gentle agitation and then quick-frozen under liquid N_2.

Purification of VAP, tagged with StrepTag, has been described elsewhere.[12] The active fractions of the elution peak were collected and analyzed for purity using sodium dodecyl sulfate−polyacrylamide gel electrophoresis (NuPAGE, 4 to 20%) and then snap-frozen in liquid N_2. The enzyme was not allowed to go through more than two freeze−thaw cycles before being used in analyses. The snap-freezing had no effect on the specific activity for a few freezing cycles if the enzyme was supplemented with at least 15% (v/v) ethylene glycol.

Standard Activity Assay. For standard activity assays, 10 μL of the enzyme solution was mixed with 990 μL of reaction buffer [5 mM *p*-nitrophenyl phosphate, 1.0 M diethanolamine, and 1 mM $MgCl_2$ (pH 9.8)], and the formation of *p*-nitrophenol (pNP) was monitored at 405 nm and 25 °C, using an extinction coefficient of 18.5 mM^{-1} cm^{-1} for 30 s on a Peltier temperature-regulated Evolution 220 spectrophotometer (Thermo Fisher).

Effect of Ionic Strength and pH on Activity. Activity assays were performed under pseudo-zero-order conditions ([S] close to V_{max}) using 5 mM *p*-nitrophenyl phosphate at 25 °C unless stated otherwise. Salt solutions were added from 1.2−4.0 M stocks (depending on the solubility of the respective salt species). Buffers were diluted to a final concentration of 50 mM from 0.2 M stock solutions. All buffers were titrated with HCl or NaOH to the respective target pH value. For pH dependence

DOI: 10.1021/acs.biochem.7b00690
Biochemistry 2017, 56, 5075−5089

experiments, Mops was used as a buffer for pH 6.0−7.0, Tris for pH 7.0−9.0, and Caps for pH 9.0−11.5.

Ionic strength did not affect the measured pH values up to 1.0 M salt. Furthermore, ionic strength did not greatly affect the molar extinction coefficient of pNP up to 1.0 M salt. Of all the conditions tested, the molar extinction coefficient of pNP was only marginally affected by pH in the range used here (Figure S3). Thus, an average molar extinction coefficient of 18.1 mM^{-1} cm^{-1} was used for pH 8.0 measurements, 18.9 mM^{-1} cm^{-1} for pH 9.0, and 19.0 mM^{-1} cm^{-1} for pH 10.5.

Enzyme Kinetics and Competitive Inhibition Measurements. Enzyme kinetics were performed at 25 °C for pNPP concentrations ranging from 0.0 to 2.0 mM at pH 8.0, 9.0, and 10.5 using 50 mM Tris for pH 8.0−9.0 and 50 mM Caps for pH 10.5. NaCl was added from a 3.0 M stock solution and mixed with the respective buffer diluted from a 0.2 M stock solution. In the case in which 1.0 M Tris or 1.0 M diethanolamine (DEA) were used, no additional buffer was added, and the pH was titrated to the respective value used in the experiments. For addition of 1.0 M Tris or diethanolamine, the total ionic strength was set to 0.59 M by adding NaCl.

For K_i measurements, inorganic phosphate was added from a 100 mM Na_2PO_4 stock. The enzyme solution was diluted to 0.05−0.10 mg/mL, a 10 μL solution mixed with 990 μL of buffer, and A_{405} assayed for 30 s at 23 °C on a Peltier temperature-regulated Evolution 220 spectrophotometer (Thermo Fisher). For the exact determination of the *p*-nitrophenyl phosphate concentration, each sample was allowed to hydrolyze fully and the concentration determined by measuring the absorbance at 405 nm using the appropriate extinction coefficient. K_M and V_{max} were determined by a nonlinear regression fit to the Michaelis−Menten equation using GraphPad Prism. To evaluate k_{cat} ($k_{cat} = V_{max}/[E]_t$), the enzyme concentration was measured at A_{280} using a calculated molar extinction coefficient of 61310 M^{-1} cm^{-1} for each monomer as described by Pace et al.[25]

The competitive inhibitor constant K_i for inorganic phosphate (PO_4^{2-}) was determined by a global nonlinear regression fit to the equation $Y = V_{max}[S]/[K_M(1 + [I]/K_i + [S])]$, where Y is the activity, [S] is the substrate concentration, and [I] is the inhibitor concentration, using GraphPad Prism. The fit was applied to 0, 0.5, and 1.0 mM PO_4^{2-}.

Effect of Sucrose on Activity. For sucrose experiments and enzyme dilution studies, the enzyme activity assays were performed on a SpectraMax 2 (Molecular Probes) plate reader by monitoring the formation of pNP at 450 nm for 10−30 min (depending on the enzyme concentration), or until the absorbance reached 0.4−0.5. All plate reads were performed in 96-well plates, in duplicate or triplicate at ambient room temperature. A wavelength of 450 nm was chosen to maintain the absorbance change during the reaction inside the linear range.

For sucrose experiments, the enzyme was diluted at a 4× buffer concentration (0.20 M) and 50 μL mixed with 150 μL of 6.7 mM *p*-nitrophenyl phosphate, giving a final concentration of 5 mM and a respective final concentration of NaCl, sucrose (diluted from a 4× stock), or nucleophile (Tris or diethanolamine) as denoted for each experiment.

Enzymatic Assays after Dilution. For enzyme dilution studies, the enzyme was incubated in 50 mM Tris buffer at pH 8.0−9.0 and 50 mM Caps at pH 10.5, starting from 2.15 μM enzyme stock solution (measured at 280 nm using an extinction coefficient of 122620 M^{-1} cm^{-1} for dimer). Inorganic phosphate was added from a 100 mM stock solution and NaCl from a 3.0 M stock solution where indicated. The enzyme was serially diluted from a 0.015−0.50 μM enzyme solution (dimer concentration) by diluting 650 μL of the sample to 350 μL of the same buffer. Samples were incubated for 18−20 h at 25 °C. The activity was then assayed at 25 °C by mixing 180 μL of the enzyme sample with 20 μL of an aqueous 50 mM pNPP substrate solution. This 10% enzyme dilution, upon being assayed, did not affect the outcome of the experiments because the rate toward enzyme dissociation equilibrium was found to be reached within several hours.

Inorganic Phosphate Assay. Phosphate release during enzyme turnover (P_2) was measured using the PiPer phosphate assay kit (Thermo Fisher) following the manufacturer's protocol for the inorganic phosphate assay. An end point analysis was performed at five different time points during the enzyme reaction under the same conditions that were used for the enzyme pNPP kinetic assay. No more than 10% of the substrate was allowed to hydrolyze during the time course to guarantee the initial rate conditions. The rate of pNP release was also monitored for the same assay batch under identical conditions for comparison. At the defined time points, the enzyme reaction was stopped by pipetting 100 μL of the enzyme sample into 100 μL of a 10 mM EDTA solution (pH 8.0) previously warmed to 90 °C and kept at 90 °C for 5 min before the samples were placed on ice. The samples were then frozen at −20 °C until they were further analyzed. The typical inactivation method using 5% trichloroacetic acid to stop the enzyme reaction was shown to affect the formation of the fluorescent product resorufin in the phosphate assay (data not shown), whereas EDTA had no effect (at the concentration tested in the assay). All samples were diluted 10-fold in a black, clear bottom 96-well plate in 1× reaction buffer [0.1 M Tris (pH 7.5)] to a final volume of 50 μL, and then 50 μL of the working reaction solution was added (100 μM Amplex Red reagent, 4 units/mL maltose phosphorylase, 0.4 mM maltose, 2 units/mL glucose oxidase, and 0.4 unit/mL horseradish peroxidase) and incubated for 45 min at 37 °C.

Fluorescence was monitored on a Spectramax M3 (Molecular Probes) fluorescence plate reader using an excitation wavelength of 530 nm and an emission wavelength of 590 nm in top read mode and an average read of 12 flashes. A standard curve was generated from the provided phosphate standard diluted in 1× reaction buffer in the range of 0−50 μM phosphate. A blank was subtracted (1× reaction buffer) from all samples. By plotting the phosphate concentration versus time, we obtained the initial rate of phosphate formation from the initial slope of the linear regression fit.

Enzyme Thermal Stability Measurements. Thermal inactivation experiments were conducted in a digitally regulated heat block using a heat probe for accurate temperature measurements. The enzyme was diluted 100-fold into 500−1000 μL of buffer with various added ions, giving a solution with an enzyme content of ∼10 units/mL, and allowed to incubate for 60−120 s before the assay was started by pipetting 10 μL of the enzyme sample into 990 μL of standard assay buffer [5 mM pNPP, 1 M diethanolamine, and 1 mM $MgCl_2$ (pH 9.8) at 25 °C] and collecting at least five data points until the activity had fallen to 20−30% of the initial activity. The rate of inactivation was determined by plotting ln(activity) versus time, where the slope gives the rate constant, k, of inactivation. The half-life was then calculated using the relationship $t_{1/2} = 0.693/k$.

For Arrhenius plots and $T_{50\%}$ determinations, five temperature points were measured at approximately $T_{50\%} \pm 5$ °C. From an Arrhenius plot (ln k vs $1/T$), the activation energy (E_a) was

DOI: 10.1021/acs.biochem.7b00690
Biochemistry 2017, 56, 5075−5089

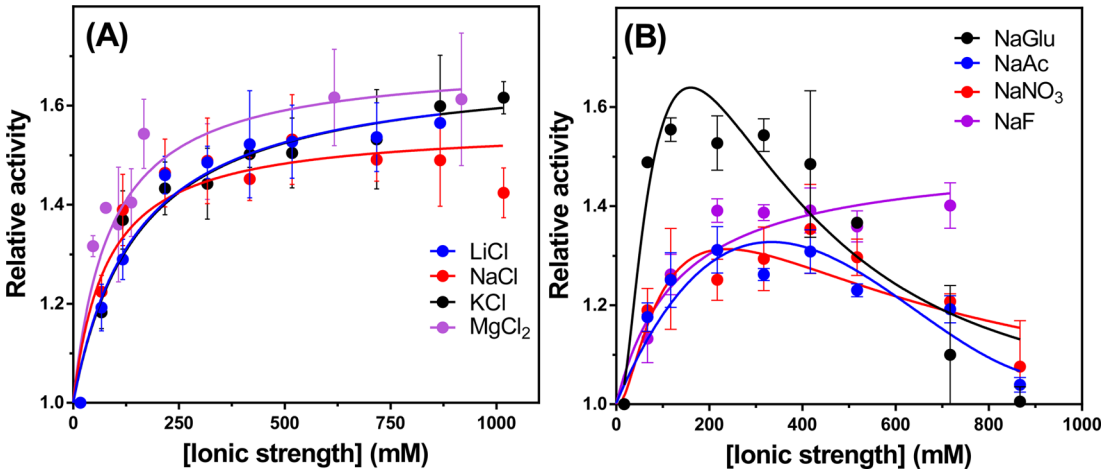

Figure 1. Salt activation of VAP at pH 9.8. Effect of (A) chloride salts and (B) sodium salts on activity. Activity was measured for pNPP hydrolysis in 50 mM Caps and 5 mM pNPP (pH 9.8) at 25 °C. Data points were normalized to activity measured with no salt added. Data were fitted to a hyperbolic function [$y = 1 + B_{max} \times x/(K_D + x)$] or a log-Gaussian function ($y = 1 +$ amplitude $\times \exp\{0.5 \times [\ln(x/\text{center})/\text{width}]^2\}$), whichever fitted best, only to aid the eye. Measurements consisted of several independent experiments in which activity was measured in duplicate ($n = 2-5$).

obtained. $T_{50\%}$ was then calculated from the Arrhenius equation, where the k for 50% loss of activity after 30 min was used in each case ($k = \ln 2/30$ min $\times$ 60 s/min) to give $T_{50\%} = (E_a \times 1000)/R(\ln A - \ln k)$.

The thermal denaturation midpoint measurements (T_m) were determined in 25 mM Mops and 1 mM $MgSO_4$ (pH 8.0) using circular dichroism (CD) in a 2 mm cuvette at 222 nm over the temperature range of 15−90 °C with a rate of increase in temperature of 1 °C/min. The enzyme concentration was ∼0.2−0.3 mg/mL. For monomer unfolding, a two-state pathway was assumed (N → U, where N is native and U is unfolded). T_m was determined by a direct fit to a normalized sigmoid curve using GraphPad Prism.

Sample Preparation for the Metal Ion Assay. Lemo21(DE3) *E. coli* cells, transformed with the VAP-pET11a plasmid, were cultivated in a total of 1.0 L of LB medium. Purification was performed as described above on columns using 6 mL of fresh StrepTactin resin except the lysis buffer contained 100 times less $MgCl_2$ (0.1 mM). The column was washed extensively with Chelex-treated 10 mM Tris buffer (pH 8.0). Then, the resin was divided into two columns, and 3 mL of either 0.1 or 0.5 M NaCl in 10 mM Tris (pH 8.0) was added to each column and incubated at 37 °C for 16 h under gentle agitation. The resin was then washed with 3 × 5 mL of Chelex-treated 10 mM Tris before the enzyme was eluted with 3 mL of Chelex-treated 15 mM desthiobiotin in 10 mM Tris elution buffer (pH 8.0). The eluted samples were then assayed for activity (see Standard Activity Assay), protein concentration (A_{280}), and Zn^{2+} and Mg^{2+} content using atomic absorption spectroscopy (see below).

The metal ion analysis was also performed after incubating the enzyme, bound to StrepTactin, in urea. The resin was divided into four columns and incubated in 3 mL of 10 mM Tris buffer (pH 8.0) containing 0.0, 0.5, 1.2, or 2.0 M urea for 4 h at 4 °C under gentle agitation (the urea stock solution was also Chelex-treated). The resin was then washed with 3 × 5 mL of Chelex-treated 10 mM Tris, and the enzyme was eluted and assayed as previously described.

Atomic Absorption Spectroscopy. Atomic absorption spectroscopy was performed on a Varian (Crawley, England) Spectra220 FS atomic absorption spectrometer. Standard curves for Mg^{2+} were made from 9949 Titrisol (Merck) diluted to the range of 0.00−1.00 mg/L in Milli-Q water, and Zn^{2+} standards were made from 9953 Titrisol (Merck) diluted to the range of 0.00−1.00 mg/L in Milli-Q water. The measurement time was 1 s for each read, and each measurement contained five reads for each of the standards and three reads for the samples. Milli-Q water was used as a blank for the standards and the elution buffer as a blank for the samples.

Tryptophan Fluorescence Measurements. The intrinsic tryptophan fluorescence was monitored at 20 °C on a Fluoromax 4P (Horiba) instrument using a 500 μL quartz cuvette with a 4 mm path length. The enzyme sample from a 2.5 mg/mL stock was diluted to 0.040 mg/mL with a solution containing 1 mM $MgSO_4$ (for stabilization) and 50 mM buffer, using Mops for pH 6.0−7.0, Tris for pH 7.5−9.0, and Caps for pH 9.5−11.5. Slits were set to 3 and 5 nm for excitation and emission, respectively, using 295 nm for excitation, recording emission from 310 to 450 nm in 0.5 nm increments. The wavelength of maximum emission (λ_{max}) was determined mathematically using Excel Solver (LINEST function) by fitting the spectra from 320 to 380 nm with a third-degree polynomial ($y = ax^3 + bx^2 + cx + d$, where y is the intensity and x is the wavelength). By solving the roots for the first derivative of the equation, we determined λ_{max}.

RESULTS

Activation of VAP by Salt. Because we have previously observed both stabilizing and activation effects on VAP by using NaCl at 0.5 M,[12] we sought to study in detail the effect of various ions on the enzyme's structure, stability, and function. First, we wanted to determine if the effect was specific for a particular type of ion(s) or followed the Hofmeister series effect.[26,27] Figure 1A shows the effect of chloride salts and Figure 1B the effect of sodium salts on the activity at pH 9.8. VAP was activated similarly in the concentration range of 0.0−1.0 M using four different chloride salt species (Figure 1A) with a plateau observed at a 50−60% increase in activity. Using the sodium salts of various anions, a difference in activation was seen. Glutamate is one of the main osmolytes in *E. coli* and has been shown to be highly kosmotropic (ranks between F^- and SO_4^{2-}).[28] Thus, we decided it would be an interesting comparison with inorganic ions. Sodium glutamate was, in fact, the most effective additive we tested in promoting the activity of VAP at ionic strengths in the range of 0−200 mM.

DOI: 10.1021/acs.biochem.7b00690
Biochemistry 2017, 56, 5075−5089

However, at higher concentrations of glutamate, the activity dropped sharply. Sodium acetate, sodium nitrate, and sodium fluoride were all less effective than the chloride salts in activating the enzyme. At concentrations above 300 mM, fluoride stimulation reached a plateau similar to those of the chloride salts, whereas the activity diminished in the presence of acetate or nitrate. It may be concluded that ionic strength rather than the type of anion governed the salt activation of VAP at low salt concentrations (0−200 mM), whereas at higher salt concentrations, an anion-dependent inhibition was produced by some of the anion types. Chloride and fluoride were not inhibitory to VAP, whereas glutamate, acetate, and nitrate did inhibit VAP.

VAP Activation by NaCl Is Dependent on pH. The activity of VAP with pNPP was measured in the pH range of 7.0−10.5 with NaCl concentrations ranging from 0.0 to 1.0 M (Figure 2A). The relative increase in activity induced by addition of NaCl was 4-fold greater at pH 7.0−8.0 than at pH 9.8 (typical assay conditions). Changing the pH from 8.0 to 10.5 gradually decreased the ionic effect to near no effect at pH 10.5. The dependence of activity as a function of NaCl concentration exhibited a hyperbolic dependence. By fitting the data to a hyperbolic equation for each pH, we could derive two coefficients. One is the I_{max} salt coefficient, which denotes the maximum level of activation induced by NaCl at the respective pH. The second is $I_{1/2}$, the salt activation coefficient, which is the concentration of salt needed to reach half of I_{max} at the respective pH.

The dependence of I_{max} on pH in the pH range of 7.0−10.5 gave a sigmoidal curve, which is an indication of the enzyme occupying two states in this pH range (Figure 2B): one form that was activated by NaCl and another that is not affected by NaCl. The pK_a of a group responsible for the transition between the two states was found to be 8.7 under the conditions tested. Interestingly, the $I_{1/2}$ constant showed a near-linear negative dependence on pH in the range of pH 7.0−10.5. Thus, as the pH increased, the enzyme was less activated, e.g., >100 mM NaCl, and required less salt to reach the respective maximum activity that could be attained through NaCl activation. NaCl had no effect on the activity of VAP once the pH reached 10.5.

The pH−Activity Profile of VAP Gave Two Maxima. To better understand the salt activation of VAP, the pH−activity profile was measured from pH 6.0 to 11.5, without adding salt (control) and after the addition of 500 mM NaCl (Figure 3A).

The pH−activity profile showed two maxima at approximately pH 9.0 and 10.2. The addition of 500 mM NaCl increased the activity at pH 9.0 considerably but had hardly any effect on the maximum at pH 10.2. At pH 10.5, NaCl greatly increased the K_M for pNPP (see in Table S2) to such an extent that the concentration of the substrate used was not enough to achieve V_{max}. Thus, the second maximum was slightly shifted toward a lower pH value using 500 mM NaCl.

To address if these two maxima and the specific ionic activation around pH 9.0 for VAP were due to a systematic assay error, or substrate activation, and thus not a unique property of VAP, calf intestinal alkaline phosphatase (CIP) and *E. coli* alkaline phosphatase (ECAP) activity profiles were measured using the same conditions that were used for VAP (Figure 3B,C). Only one pH maximum was observed for both CIP and ECAP. CIP was not activated by NaCl, in agreement with previous observations.[29] However, the pH optimum shifted from pH 10.0 to 9.5 in 500 mM NaCl, possibly by affecting activity coefficients for pK_a values of groups responsible for activity (Debye−Hückel).

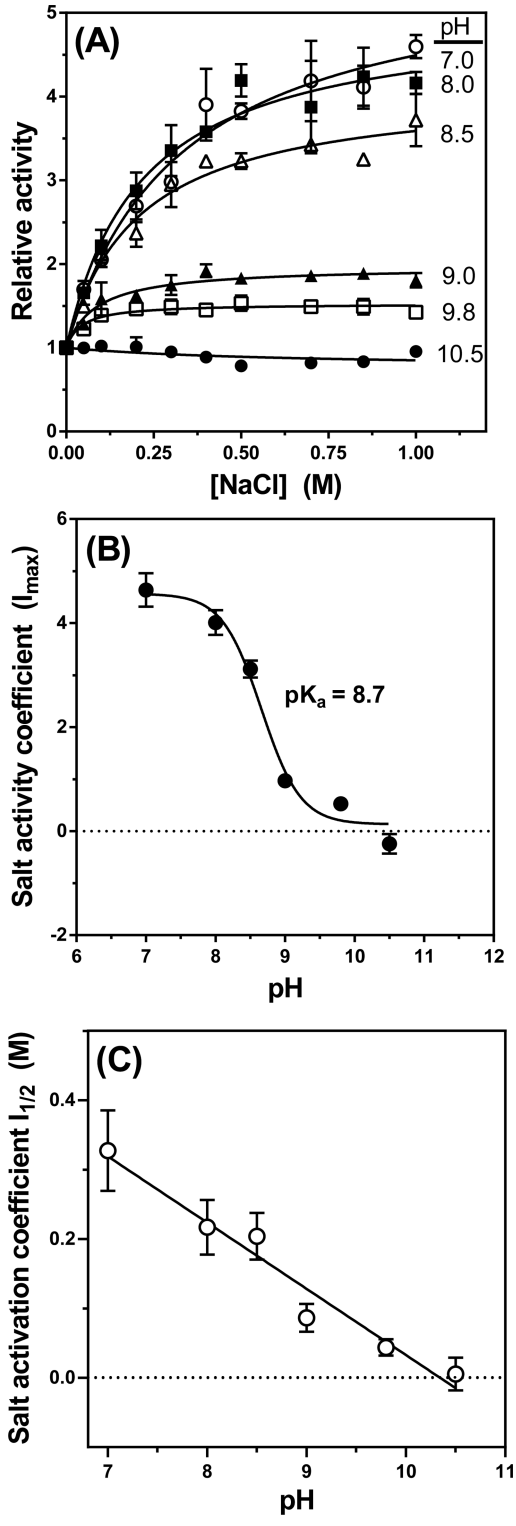

Figure 2. Effect of pH on NaCl activation for VAP. (A) Activity as a function of NaCl concentration. Activity was normalized at each pH value to activity measured with no NaCl added. Data were fitted to a hyperbolic function [$y = 1 + I_{max} \times x/(I_{1/2} + x)$, where y is activity, x the salt concentration, I_{max} the salt coefficient, and $I_{1/2}$ the salt activation constant]. (B) Salt coefficient I_{max} as a function of pH. Data were fitted with a variable-slope sigmoidal curve (GraphPad Prism). (C) Near-linear relationship of salt activity constant $I_{1/2}$ as a function of pH in the pH range of 7.0−10.5. Data were taken from several independent experiments during which activity was measured in duplicate (n = 2−4).

DOI: 10.1021/acs.biochem.7b00690
Biochemistry 2017, 56, 5075−5089

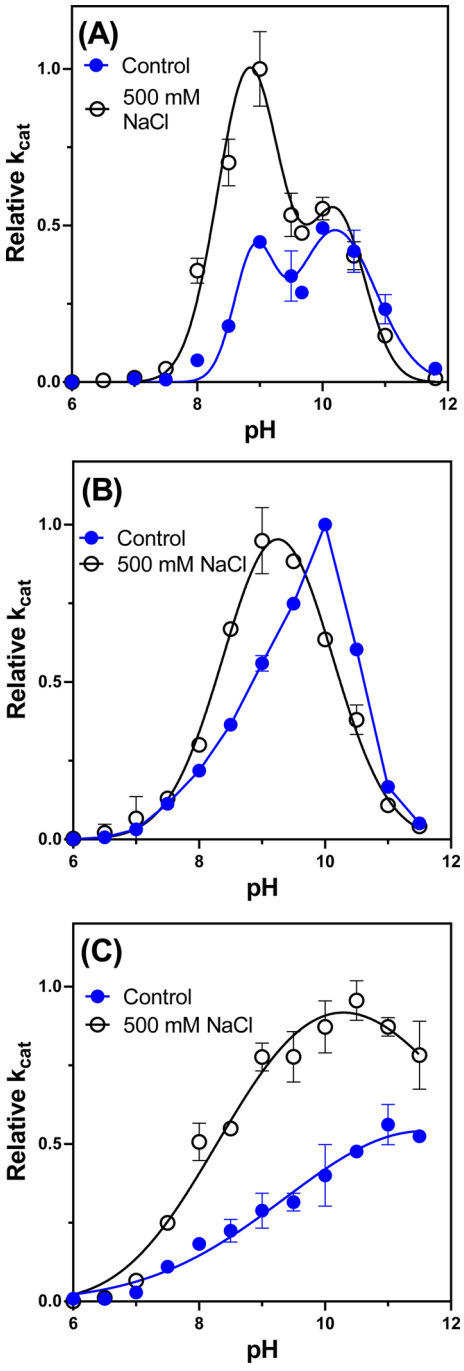

Figure 3. Activity profiles as a function of pH for three alkaline phosphatases: (A) VAP, (B) calf intestinal alkaline phosphatase, and (C) *E. coli* alkaline phosphatase. The pH−activity profiles were measured either without any addition (control) or with 500 mM NaCl. Activity was normalized to the highest k_{cat} point measured for each enzyme activity profile. To aid the eye, curves were fitted with Gaussian, the sum of two Gaussian or Lorentzian functions, whichever gave the best fit. Data were taken from several independent experiments during which activity was measured in duplicate (n = 2−4).

The activity of ECAP is known to be influenced by ionic strength.[13,30] Here, NaCl was shown to increase the activity of ECAP at all pH values tested from 6.0 to 11.5. Furthermore, the pH optimum of ECAP was lowered by two pH units in the presence of NaCl.

Effect of pH, Ionic Strength, and Transphosphorylation on VAP Enzyme Kinetics. To study further the effect of pH, ionic strength, and the presence of a transphosphorylation substrate on VAP activity, Michaelis−Menten kinetics were measured, as well as a competitive inhibition assay with inorganic phosphate, at pH 8.0, 9.0, and 10.5, together with the addition of 0.5 M NaCl or 1.0 M nucleophilic phosphate acceptor (Table S2).

The stimulating effect of NaCl on k_{cat} was pH-dependent. Only the peak in Figure 3A at pH 9.0 was sensitive to NaCl, while the other peak at pH 10−10.5 was not. Further analysis showed that the affinity for the substrate and product was greatly reduced at pH 10.5 (both K_M and K_i increased), while k_{cat} was unchanged by NaCl. In the presence of an organic phosphate acceptor (Tris or DEA), both k_{cat} and K_M were greatly increased. In most cases, the addition of 20% (w/v) sucrose decreased the activity substantially, indicating that the release of the inorganic phosphate product was the rate-limiting step at pH 8.0 and 9.0. At pH 10.5, sucrose had a weaker effect on k_{cat}, and via the addition of 0.5 M NaCl, sucrose had no effect on activity, indicating a possible shift in the rate-limiting step toward a step not affected by diffusion rates.

Thermal Inactivation and Denaturation of VAP Are Affected by Ionic Strength and pH. Inorganic phosphate and sulfate are well-documented competitive inhibitors of AP activity.[31−33] Phosphate binds approximately 10 times more tightly to VAP than sulfate does and provides much more protection against thermal inactivation than sulfate does. Figure 4A shows that VAP had a half-life of <1 min when heated at 30 °C with no additional ions in the buffer. The half-life at 30 °C increased to ∼10 and 50 min for 1 mM sulfate and 1 mM phosphate, respectively (Figure 4A). The cation added with the sulfate salts had no effect on VAP stabilization. Magnesium ions added as a chloride salt did not provide any specific stabilization and performed equally well as NaCl.

The effect of NaCl on thermal inactivation of VAP was further studied at 55 °C in the range of 0.0−1.0 M NaCl (Figure 4B). The half-lives (for activity) at 55 °C were 0.2 and 38.5 min with 0.0 and 1.0 M NaCl, respectively. It was noted that the rate of inactivation at 55 °C did not decrease linearly with NaCl concentration (Figure 4C), which is possibly due to thermal denaturation occurring when the temperature increases above 54 °C and a stability plateau is reached. Figure 4D shows that NaCl increased the thermal midpoint for unfolding from 54.2 to 62.2 °C for 0.0 M and 1.0 M NaCl respectively, and the increase was linear with NaCl concentration (Figure 4E). The thermal denaturation curves using CD showed that, upon addition of NaCl from zero to 0.1 M, there was an increase in cooperativity for unfolding (steeper slope between the transition). This cooperativity might be due to the binding of a chloride ion to a high-affinity site of as yet unknown identity.

The linear dependence of NaCl on stabilization of the folded state observed here is likely due to salting-out effects of the denatured state, which have been observed for many proteins.[34] However, it is unclear how salt affects the stabilization of the structural form with maximal activity. Table 1 shows the effect of 0.50 M NaCl on $T_{50\%}$. It can be seen that the effect of NaCl was pH-dependent. At pH 8.0, the $T_{50\%}$ was greatly increased, from 25.8 to 53.5 °C, from the control to 0.50 M NaCl, respectively. Increasing the pH to 9.0 increased the thermal resistance of VAP as the $T_{50\%}$ increased to 30.6 °C for the control. On the contrary, the effect of NaCl diminished where $T_{50\%}$ with 0.50 M NaCl was

DOI: 10.1021/acs.biochem.7b00690
Biochemistry 2017, 56, 5075−5089

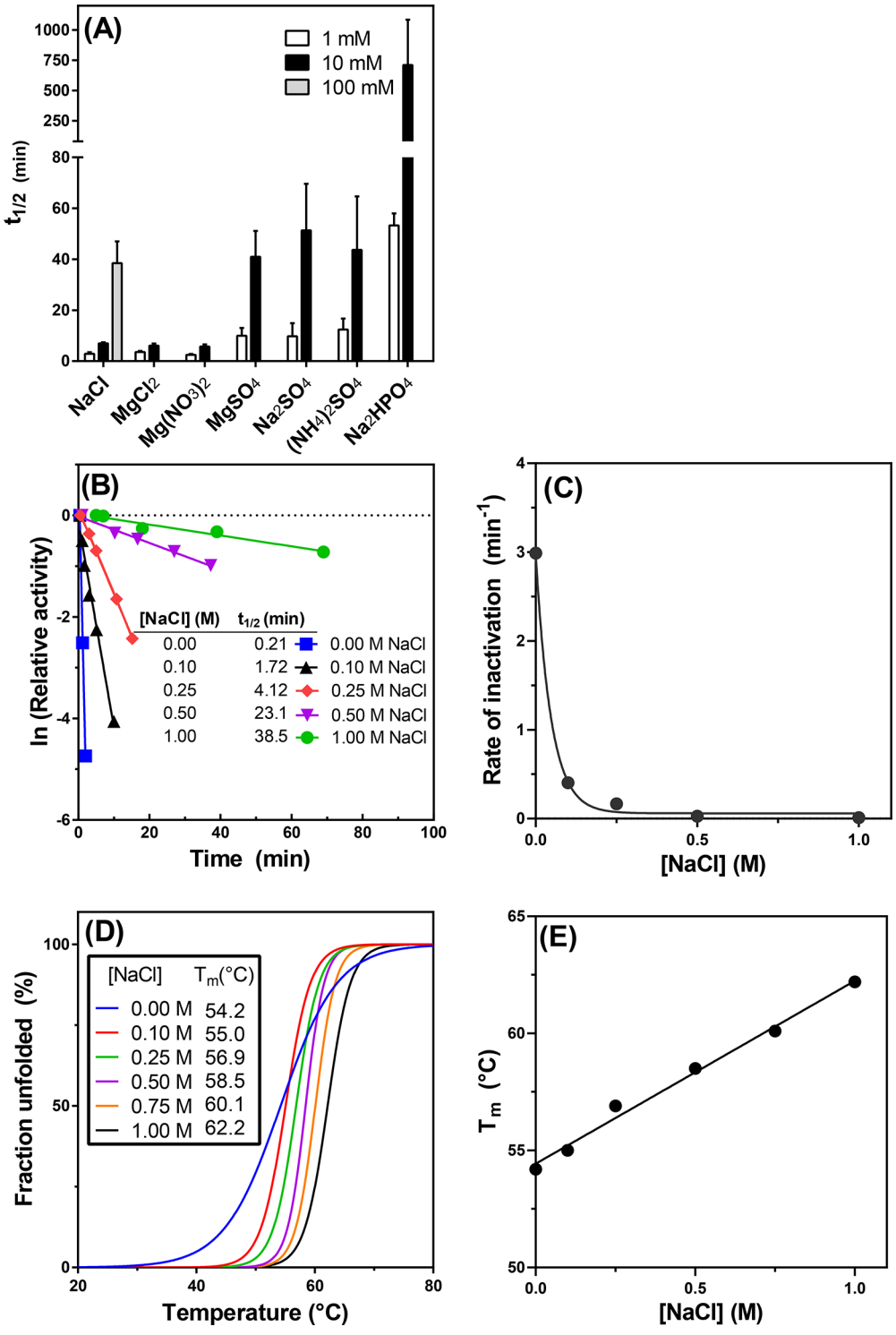

Figure 4. Effect of ions on VAP thermal stability. (A) Effect of NaCl, magnesium, and competitive inhibitor salts on stability at 30 °C in 20 mM Tris (pH 8.0). Aliquots of the enzyme were taken at different time points and assayed using the standard activity assay, and the half-life at 30 °C ($t_{1/2}$) was determined. (B) Rate of inactivation at 55 °C vs NaCl concentration in 20 mM Tris and 10 mM $MgCl_2$ (pH 8.0). (C) Rate of inactivation at 55 °C (k) as a function of NaCl concentration using the data from panel B. (D) Thermal denaturation of VAP vs NaCl concentration. The fraction of folded VAP was determined using CD spectroscopy at 222 nm in 25 mM Mops and 1 mM $MgSO_4$ (pH 8.0). The traces were normalized and fitted to a sigmoidal variable slope equation using GraphPad Prism. (E) Linear dependence of T_m with NaCl concentration using the data from panel D.

50.5 °C at pH 9.0. At pH 10.5, the $T_{50\%}$ had increased to 33.2 °C, but NaCl had no stabilizing effect at pH 10.5.

The Inactive State of VAP Is Dimeric and Still Contains Zn^{2+} and Mg^{2+}. We previously found that urea-induced inactivation of VAP produced an inactive dimeric state.[12] We sought to answer the question if the inactivation of the enzyme involved Zn^{2+} or Mg^{2+} dissociation. We expected that ion dissociation might accompany or be the main cause of inactivation. In particular, loss of the Mg^{2+} ion could result in failure to activate the nucleophilic Ser in the active site. Our VAP

DOI: 10.1021/acs.biochem.7b00690
Biochemistry 2017, 56, 5075−5089

Table 1. Effect of Sodium Chloride on Thermal Inactivation

	$T_{50\%}$ (°C)[a]	
pH	control	0.50 M NaCl
8.0	25.8 ± 1.4	53.5 ± 1.5
9.0	30.6 ± 0.6	50.5 ± 0.5
10.5	33.2 ± 1.0	31.7 ± 1.1

[a]Samples were incubated in 20 mM Tris and 10 mM $MgCl_2$ (pH 8.0 or 9.0) or in 20 mM Caps and 10 mM $MgCl_2$ (pH 10.5) with or without the addition of 0.50 M NaCl on a heat plate over time at various temperatures, and the $T_{50\%}$ values were determined by assaying the remaining activity in the standard assay at pH 9.8 and 25 °C. The mean and standard deviations reflect two to five independent experiments.

storage buffers contain a rather high concentration of $MgCl_2$ (10 mM), and therefore, decreasing the extraneous Mg^{2+} concentration to a value sufficiently below the enzyme sample concentration (10−20 μM) by filtration or dialysis, without possibly promoting its dissociation from the active site, has proven to be difficult. As mentioned above, the initial hypothesis was that inactivation observed in low-salt buffer solutions was due to dissociation of the Mg^{2+} from the active site. Thus, we reduced the Mg^{2+} content of the lysis buffer 100-fold (0.1 mM) and used Chelex-treated, 10 mM Tris buffer in all purification steps. Furthermore, the enzyme was immobilized on StrepTactin resin (Figure S4) and inactivated while still bound to the resin at 37 °C for 16 h in 0.1 or 0.5 M NaCl (Figure 5A). The latter condition prevents inactivation observed in low-ionic strength buffers and served as a control. At 37 °C, 0.1 M NaCl was not enough to protect the enzyme against inactivation, the specific activity being 75% lower than in the sample with 0.5 M NaCl. There was not a statistically significant difference in the Mg^{2+} content of VAP treated in 0.1 M NaCl buffers (1.8 ± 0.4) compared with VAP when 0.5 M NaCl was present (1 ± 0.8). The large standard deviation is due to the lower binding affinity of the StrepTag to the affinity column at 37 °C compared to that at 4 °C, especially for the 0.1 M NaCl sample, leading to a lower concentration of enzyme eluted, and thus a higher signal-to-noise ratio for both atomic absorption and protein concentration assay. Interestingly, there was a significant difference in Zn^{2+} content depending on salt concentration, being 2.0 ± 0.7 per monomer for 0.5 M NaCl and 1.0 ± 0.1 per monomer for 0.1 M NaCl. Thus, VAP lost one of its two Zn^{2+} ions when the NaCl concentration was decreased from 0.5 to 0.1 M. However, the magnesium ion content was unchanged. It should be noted that because of the loss of protein content from the columns under the latter condition, the reason for which is being studied, the error in the data was relatively large.

After immobilization of the enzyme to the StrepTactin resin, we also applied the resin to four separate columns and incubated the resins in 0.0−2.0 M urea for 4 h. After being rinsed with Chelex-treated Tris buffer, the enzyme was eluted as described above (Figure S4). The samples were then assayed for Mg^{2+} content (Figure 5B), Zn^{2+} content (Figure 5C), and specific activity. The inactivation occurred without changes in the metal content.

VAP Adopts Several Structural States with Respect to pH. It is unclear how many deprotonation events occurred in Figure 3A. If we assume each ascending and descending limb in the bell-shaped activity curve is due to a single protonation event, then there are possibly four deprotonation events that affect VAP activity. The second maximum might also be due to a conformational change resulting in a change in the rate-limiting step toward the hydrolysis step.

This would explain why salt had no effect on the second maximum, because dephosphorylation of the covalent inter-

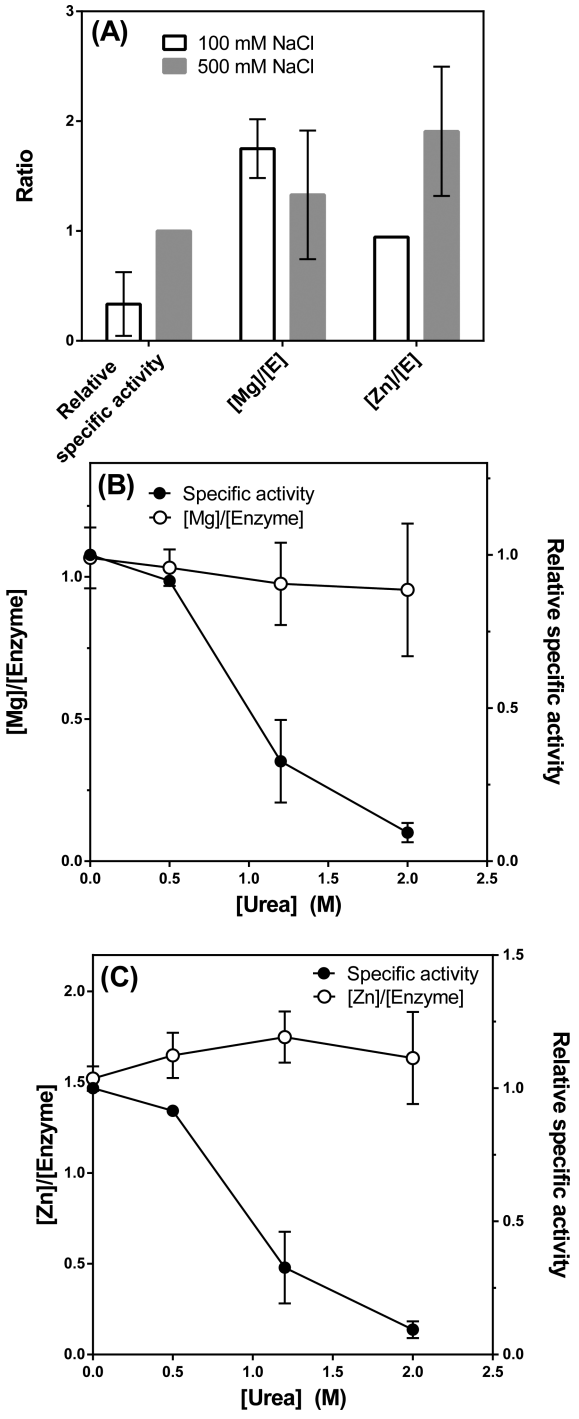

Figure 5. Determination of the Zn^{2+} and Mg^{2+} ion contents during VAP inactivation. (A) Zn^{2+} and Mg^{2+} contents were normalized to the enzyme monomer concentration after thermal inactivation at 37 °C for 16 h at pH 8.0 in the presence of 100 or 500 mM NaCl. (B) Mg^{2+} content and (C) Zn^{2+} content of VAP after incubation of the enzyme in urea at pH 8.0 for 4 h at 4 °C. Data were normalized to the enzyme monomer concentration. Means and standard deviations reflect several independent measurements (n = 2−5). Note that some error bars are smaller than the borders of the symbols or columns and, thus, are not visible.

DOI: 10.1021/acs.biochem.7b00690
Biochemistry 2017, 56, 5075−5089

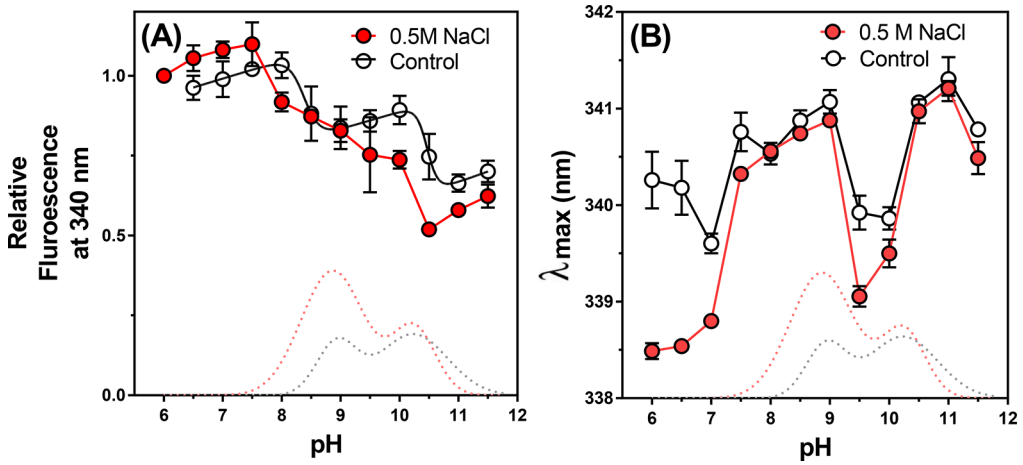

Figure 6. VAP tryptophan fluorescence as a function of pH. (A) Relative tryptophan emission at 340 nm as a function of pH. (B) Wavelength of maximum emission (λ_{max}) as a function of pH. The dotted line curve is adopted from VAP pH−activity profiles in Figure 3A for control (black) and 0.5 M NaCl (red) for comparison.

mediate, within the active site, would be minimally affected by ionic strength. The activity presented on the *y*-axis in Figure 3B was assayed at a saturating substrate concentration (>10K_M). At pH >10.0, the affinity for the product (measured as K_i) was greatly decreased. This is likely reflected in the second maximum at pH 10.2, because the release of the product is the rate-limiting step in the reaction pathway at alkaline pH. The limb of the second peak may decrease sharply with an increase in pH (Figure 3) because the activity measured no longer represented V_{max} (at 5 mM substrate) as K_M was also increasing as the pH increased pH 10.0.

To address the question of whether pH changes might be inducing structural changes, we monitored tryptophan fluorescence for VAP under conditions identical to those used in Figure 3. We used two fluorescence methods to represent the structural changes, (i) the absolute tryptophan fluorescence intensity at 340 nm (Figure 6A) and (ii) the wavelength of maximal fluorescence, λ_{max} (Figure 6B). The absolute intensity value (and the changes in intensity) is sensitive to the distance and orientation of electron-deficient residues in the proximity of the indole group(s). On the other hand, the λ_{max} is more an indicator of solvent accessibility to the indole group(s), and not as sensitive to intrinsic quenching events. Three distinctive states could be detected from the absolute fluorescence intensity at 340 nm with a change in pH. Figure 6A shows where the fluorescence decreased between pH 8.0 and 9.0, correlating with activation of the enzyme (dotted lines are adopted from the activity profile in Figure 3 for comparison). Another drop in fluorescence was seen at pH 10.0−11.0, correlating with the large increase in K_M and K_i (Table S2). In the presence of 0.5 M NaCl, the trend in fluorescence was similar except the transition was shifted toward lower pH values. A similar shift was seen for the pH−activity profile (Figure 3). The fluorescence at 0.5 M NaCl was also slightly lower at pH 10.0−11.5 than for the control.

The emission wavelength shift (Figure 6B) showed pH-dependent transitions in VAP structure presumably due to subtle changes in solvent accessibility of certain Trp residue(s). Four transitions were observed (between pH 7.0 and 8.0, pH 9.0 and 9.5, pH 10.0 and 10.5, and pH 11.0 and 11.5). The first transition did not correlate with any activity change, but the second and third transitions did correlate with a decrease and a subsequent increase in activity, respectively. Thus, they correlated well with the two maxima in Figure 3. The last transition correlated with the large increase in K_M and K_i that occurs when the pH becomes high. Interestingly, the λ_{max} was quite different at pH 6.0 when 0.5 M NaCl was added, being 338.5 and 340.5 nm for 0.5 M NaCl and the control, respectively (Figure 6A). Apart from that, the λ_{max} followed the same trend as the control. The native fold is possibly not as stable without NaCl present at pH 6.0−6.5 and is partially unfolded, leading to a higher λ_{max} value. This would explain the drop in λ_{max} for the control going from pH 6.5 to 7.0.

Effect of Buffer Conditions on the Dimer−Monomer Equilibrium. We have observed an effect of NaCl on both the activity and thermal stability of the active site ($T_{50\%}$), as well as on the native fold (T_m). Because the monomers of APs are generally inactive, no information about the effect of ionic strength on the dimer−monomer equilibrium could be obtained from the earlier experiments. Therefore, we attempted to induce dissociation of dimers to monomers by dilution. The dimer to monomer dissociation was detected using the specific activity of the enzyme.

If the K_d is high, activity as a measurement can be problematic, because of difficulties in measuring the initial rate at high enzyme concentrations. This problem can be overcome by assaying the activity by an additional dilution into a reaction buffer and assuming the equilibrium does not shift during the assay (not a problem if the dissociation rate is slow).

We performed dilution of VAP to test for dissociation and found dissociation occurring below 50 nM dimer. Instead of applying a further dilution to a reaction assay buffer, we mixed a concentrated solution of pNPP with the samples to a final concentration of 5.0 mM to initiate the activity assay, thus resulting in only an additional 10% dilution.

The rate of dissociation was measured by dilution at pH 8.0 using different initial concentrations of VAP (Figure 7A−C). Equilibrium was reached in approximately 8−10 h. The rates of dissociation at 15 nM dimer were 0.004 and 0.003 min^{-1} in buffer containing 1 mM inorganic phosphate and 0.50 M NaCl, respectively. Without these stabilizing additives, the activity of the enzyme fell too quickly to reflect the state of the dimer−monomer equilibrium. To rule out the possibility that the enzyme concentration dependence of the specific activity was due to magnesium dissociation, the enzyme was diluted at 15 nM dimer with an addition of 10 mM $MgCl_2$ (Figure 7D). Magnesium did not affect the dissociation equilibrium.

DOI: 10.1021/acs.biochem.7b00690
Biochemistry 2017, 56, 5075−5089

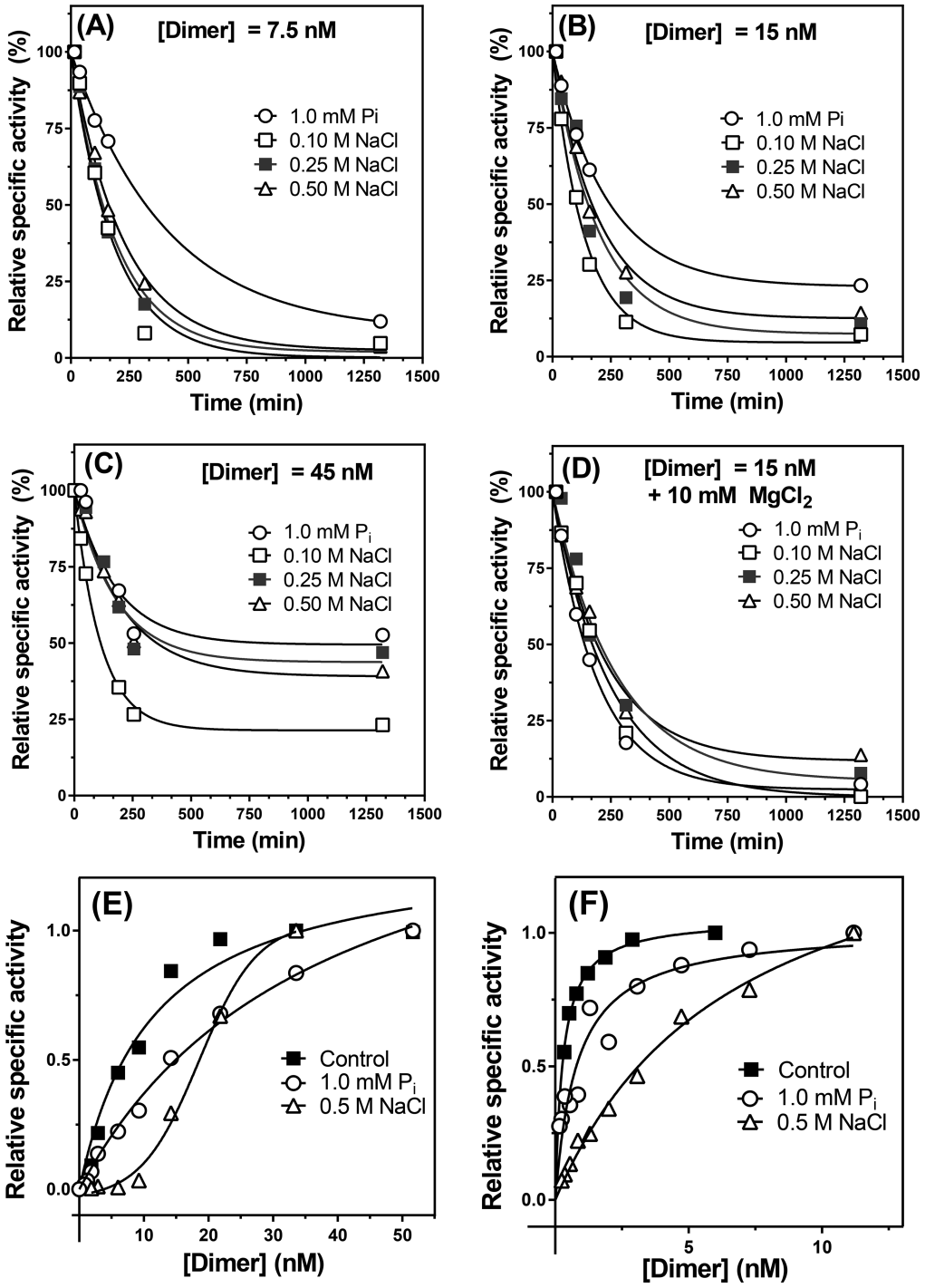

Figure 7. VAP dissociation induced by dilution. The rate of dissociation was determined as a function of enzyme concentration at pH 8.0 and 25 °C for different initial concentrations: (A) 7.5 nM dimer, (B) 15 nM dimer, and (C) 45 nM dimer. (D) The effect of magnesium was tested by incubating 15 nM dimer (as in panel B) in 10 mM $MgCl_2$. (E and F) Examples of enzyme dilution curves used for K_d analysis (summarized in Table 2) at pH 8.0 and 10.5, respectively, after incubation for 18 h. Curves in panels A–D were fitted to a single-exponential decay function, and curves in panels E and F were fitted to a one-site binding hyperbola except for the addition of 0.5 M NaCl at pH 8.0, for which a sigmoidal fit was applied.

The dimer dissociation constant, K_d, was derived by applying serial dilutions in the range of 0–100 nM at pH 8.0 (Figure 7E) and pH 10.5 (Figure 7F) and the activity assayed 18 h later. It can be seen that phosphate ions increased the K_d from 7.3 ± 5.9 nM for the control to 23 ± 7.5 nM in the presence of 1 mM phosphate. Interestingly, at pH 8.0 using 0.50 M NaCl, the K_d increased to 20 ± 8.6 nM with a distinctive sigmoidal character (S-shaped curve) not seen at pH 10.5. When the pH was increased to 10.5, the K_d was greatly decreased to 0.4 ± 0.3 nM, where there was no significant difference for 1.0 mM P_i, or 0.7 ± 0.2 nM. For 0.50 M NaCl at pH 10.5, the K_d was similar to values obtained at pH 8.0, 11.1 ± 6.3 (Table 2).

The stability of the dimer was shown to be relatively high with a dimer dissociation free energy in the range of 40–50 kJ/mol. Thus, VAP's low thermal resistance is not due to an unstable dimer but some other transition to an inactivated state that is not

DOI: 10.1021/acs.biochem.7b00690
Biochemistry 2017, 56, 5075–5089

Table 2. pH Dependence of the VAP Dimer−Monomer Equilibrium

	K_d[c] (nM)	ΔG_d (kJ/mol)
pH 8.0[a]		
control	7.3 ± 5.9	46 ± 2
1.0 mM P_i	23 ± 7.5	44 ± 1
0.50 M NaCl	20 ± 8.6	44 ± 1
pH 10.5[b]		
control	0.4 ± 0.3	54 ± 2
1.0 mM P_i	0.7 ± 0.2	52 ± 1
0.50 M NaCl	11 ± 6.3	45 ± 1

[a]Samples were incubated for 18 h at 25 °C and activity assays performed in 50 mM Tris and 5 mM pNPP at 25 °C. [b]Samples were incubated for 18 h at 25 °C and activity assays performed in 50 mM Caps and 5 mM pNPP at 25 °C. [c]Data from panels E and F of Figure 7 were either fitted to a hyperbolic function [ν_{spec} = top × [E]/(K_d + [E])] or a sigmoidal function (ν_{spec} = bottom + (top − bottom)/{1 + $10^{[\log(K_d)-[E]]\times \text{Hill slope}}$}, where ν_{spec} is the specific activity, [E] is the enzyme dimer concentration, K_d is the dissociation constant, top is the maximum specific activity, bottom is the background specific activity, and the Hill slope is the slope for the transition between the two states. K_d represents the dissociation constant for the dimer species; K_d = $[M]^2/[D]$, where M denotes the monomer and D the dimer.

dependent on enzyme concentration. Thermal inactivation at 25 °C for VAP was not dependent on concentration. This can be observed in the dilution experiments in which absolute specific activity was much lower for the control than when phosphate or NaCl was added. After incubation at 25 °C for 18 h, >90% of the enzyme was inactivated. However, the remaining population of active enzyme residues was still affected by dilution. The thermal inactivation should not affect the K_d value obtained because only the remaining active dimer subunits are being measured relative to enzyme concentration. Adding 1.0 mM phosphate or 0.50 M NaCl protected the enzyme against thermal inactivation. Thus, thermal inactivation was not due to concentration-dependent dimer dissociation.

DISCUSSION

Effect of Ions on VAP Activation. It is well-known that anions dominate the Hofmeister effect over cations for both stability and activity.[35] If the effects of chosen ions on VAP observed in this study were due to general solvent effects, then the anions should follow the Hofmeister sequence from being stabilizing/activating to being destabilizing/inhibitory as follows: $Glu^- > F^- > CH_3COO^- > Cl^- > NO_3^-$. The cations should follow this order: $K^+ > Na^+ > Li^+ > Mg^{2+}$. The anionic effect seen here did not follow a typical Hofmeister series, making it unlikely that the ions were changing the VAP's behavior by affecting the solvent. More likely, the anions were interacting specifically with a charged residue on the protein surface, most likely near or in the active site.

There are many examples of ions not following the Hofmeister effect when affecting the function of enzymes, which is likely due to relevant positions of the surface charges and polarity of the main chain in the folded protein.[36,37] A good example is the fact that salting out of lysozyme followed the Hofmeister series only at high ionic strengths or alkaline pH. Under acidic or neutral conditions, the Hofmeister series was reversed for lysozyme.[38] Another example was the reversing of the Hofmeister series for the salting out of tripeptide GGG when the N-terminal amine was capped.[6]

A study of ECAP activity using 17 chloride and sodium salts showed that the salt-induced activation followed mostly the Hofmeister series. The activation did not involve any structural changes, and the conclusion was that the ionic strength weakened the electrostatic interactions in substrate binding and product release.[30] Another study of calf intestinal alkaline phosphatase (CIP) showed a similar trend. Overall, for CIP, the salts mostly affected K_M and the pH optimum (as observed in Figure 3B), but the V_{max} was only slightly affected.[39]

Dependence of VAP Activity on pH and Ionic Strength. In the work presented here, we found that the activation by NaCl was highly pH-dependent (Figures 2 and 3), forming two maxima in the pH−activity profile. It can be suggested that the enzyme may adopt two structural states, one that is affected by NaCl and one that is not. Applying this assumption, we derived a pK_a of 8.7 from a deprotonation event (Figure 2B). It is possible that the chloride ions were directly involved in an ionic bond with a particular charged group in the first maximum that was being deprotonated in the second maximum. Otherwise, the increase in pH could lead to a conformational change involving several residues that is affected by ionic strength. A direct binding of Cl^- to ECAP has been observed using ^{35}Cl nuclear magnetic resonance (NMR), where it was proposed that Cl^- might bind to a charged amino acid with a high exchange rate.[40] Another more detailed study, using both ^{35}Cl and ^{113}Cd NMR (by studying the Zn- and Cd-saturated enzyme, respectively), showed that Cl^- binds to the Zn ion in the M1 site. The Zn ion had five ligands in the E-P state with three histidyl groups and either two Cl^- ions or two water molecules.[41] These authors also reported different affinities of the two monomers for phosphate ions, implying two different conformational states.

The candidate ionizable charged groups causing a change in activity in the pH range being studied here would be His (pK_a = 6.0), Lys (pK_a = 10.5), or Arg (pK_a = 12.5). Most of the titratable side chains in the active site of VAP take part in ligation of the metal ions. One candidate in VAP would be Arg129 that binds two of the nonbridging oxygens of the phosphate group in substrates. Other candidates would be Arg113, His465, His277 or His116, the latter two being zinc binding histidyl ligands. However, even though pK_a values of amino acids can be offset by proximity to charged or polar groups, it is more likely that deprotonation of a hydrated metal ion is taking place as has been proposed for ECAP rather than involvement of these positively charged residues.[41,42]

O'Brien and Herschlag[42] evaluated k_{cat}/K_M as a function of pH under pre-steady-state conditions for ECAP using alkyl phosphate substrates, which have a poor leaving group. The rate-limiting step over the pH range tested, for the alkyl phosphates, was the initial phosphorylation of the nucleophilic Ser. An ascending activity limb around pH 5 was believed to be caused by deprotonation of the substrate monoanion and the nucleophilic Ser in the active site. The descending limb was linked to the deprotonation of a Zn-coordinated water molecule with a pK_a of 8.0, leading to inactivity. Under steady-state conditions, using pNPP as a substrate, the pK_a of the ascending limb for ECAP was reported to be in the pH range of 7.1−7.4.[43,44] This was attributed to a basic group. However, the pK_a of 8.6−9.2 of the descending limb was attributed to a deprotonation step of an acidic group involved in substrate binding (possibly a Zn-coordinated water molecule as previously discussed). In our hands, the pH optimum of ECAP under steady-state conditions was shifted toward a higher pH value by a factor of approximately 1.0 pH unit, compared to results in previous reports[43,44] (Figure

DOI: 10.1021/acs.biochem.7b00690
Biochemistry 2017, 56, 5075−5089

3B), although a similar "alkaline" pH optimum has previously been reported for ECAP.[45] The most probable explanation for this inconsistency is the different assay conditions used (buffer species and substrate concentration), and whether the pH optimum is reported using k_{cat} or k_{cat}/K_M. For VAP, evaluation of V_{max} needed to be performed at a high substrate concentration because K_M was highly dependent on pH in the range of 10−11.5.

By observing the kinetic data in Table S2 and comparing the kinetics for the control and the 0.5 M NaCl addition, we found that NaCl had a different effect at pH 8.0 and at pH 10.5. At pH 8.0, the K_M was not affected by NaCl, whereas K_i was increased 4-fold, which would fit the 4-fold increase in k_{cat} due to faster phosphate release (the rate-limiting step).

At pH 10.5 with 0.5 M NaCl, the K_M was 3.5 times higher than the control. The K_i was also increased by 6-fold for 0.5 M NaCl compared to that of the control. However, this increase in K_i induced by NaCl was not reflected in a higher k_{cat}, indicating that the rate-limiting step was no longer the release of phosphate. This suggestion was supported by the fact that sucrose, used to increase the viscosity of the buffers, generally reduced activity. The activity observed at pH 10.5 in 20% (w/v) sucrose was 83% of the control with no sucrose added, whereas no effect on activity was observed in cases in which both 0.5 M NaCl and 20% (w/v) sucrose were added. This suggested that at pH 10.5, the activity in 0.5 M NaCl was not affected by increasing the viscosity. It is also possible that viscosity could affect the rate of a conformational change, especially if the conformational change is entropy-driven and involves the release of bound water molecules.

The following scenarios for VAP activation by ions in the pH range of 8.0−10.0 could be derived.

Salt Affects Kinetics by Allowing Faster Product Release. This has been shown for ECAP[15,30] and is likely also true for VAP. A possible explanation for the pH dependence of salt activation for VAP, disappearing at more alkaline pH, would be that a conformational change occurs in VAP around pH 10.0 and the release of the product is no longer rate-limiting. Then, the hydrolysis of the covalent intermediate would likely become the rate-limiting step (k_3), which would not be affected by the ionic strength of the medium. For ECAP, no comparable conformational change occurs in this pH range, so that the ionic strength activation is not pH-dependent.

Salt Affects Conformational States. Some researchers have proposed two conformational states for ECAP when it is present as a covalently bound phosphate complex (E-P), where one form of the enzyme is suitable for transphosphorylation and the other for hydrolysis.[46] Although suggestions of conformational changes as part of the reaction mechanism of ECAP and other APs have repeatedly been made, they have not been observed experimentally. Often, such theories have been linked with a half-of-sites reaction mechanism,[19−22] in which the binding affinity shifts reciprocally between subunits for substrate binding and product release. The putative conformational change suggested here for VAP could be a reflection of half-of-sites structural dynamics. Changes in tryptophan fluorescence with pH correlated with changes in activity, possibly an indication of such a conformational change. At pH 8.0, one subunit might have a low affinity for the substrate and inorganic phosphate (product), while the other subunit would have a high affinity for the substrate (and product) and be catalytically efficient (Figure 8). In VAP, a conformational change during the reaction cycle might occur after the dephosphorylation reaction, but

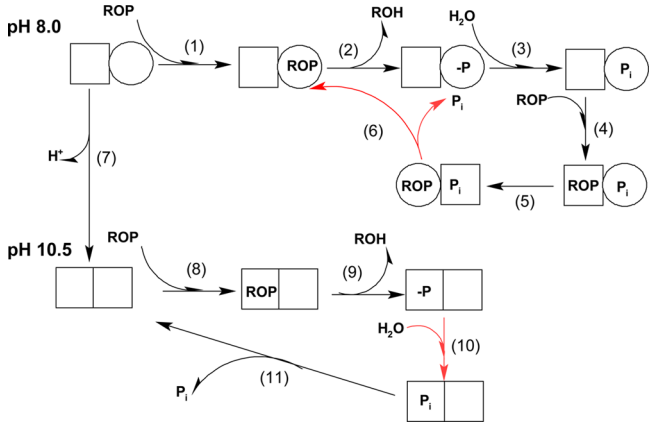

Figure 8. Hypothetical scheme for a half-of-sites reaction mechanism of VAP hydrolysis at pH 8.0 and 10.5 at saturating substrate concentrations. Empty circles denote a subunit with a high affinity for both the substrate and phosphate product, and the open squares denote a subunit with a low affinity for the substrate and phosphate product. At pH 8.0, the release of the phosphate product is the rate-limiting step (step 6 colored red). Before phosphate release, a conformational change occurs where subunits switch between the low-affinity and high-affinity state (step 5). Increasing the pH to 10.5 results in a conformational change triggered by a deprotonation event, so that both subunits adopt the low-affinity state. Subsequently, phosphate release is faster, and the rate-limiting step becomes the dephosphorylation (step 10).

before the release of the phosphate ion, where the subunit switches between the states to release the phosphate. The rate-limiting step at pH 8.0 would be the phosphate product release (or possibly the conformational change) according to this scenario. At pH 10.5, both subunits might adopt the low-affinity state, where K_M and K_i are greatly increased, the consequence being that the release of product is fast, the dephosphorylation rate is slow, and dephosphorylation becomes the rate-limiting step. This kind of mechanism has recently been shown for fluoroacetate dehalogenase from *Rhodopseudomonas palustris* where only one subunit in the asymmetric homodimer underwent a catalytic turnover. The empty subunit played a role in allosteric communication between subunits where an entropy change due to a release of water molecules played a key role.[47] Molecular dynamics simulations of VAP have shown that the subunits are asymmetric and are dynamically promiscuous, having different networks of nanosecond-scale movements.[48]

Anions Bind to a Specific Site in the Active Site of VAP. At a moderate concentration of salt and pH <10.5, VAP activity increased, irrespective of the nature of the anion (Figure 1). Furthermore, the active site heat stability ($T_{50\%}$) increased with NaCl with a pH trend similar to that for activity (Figure 4 and Table 2). A similar pH-dependent anionic activation as shown here for VAP was previously described in a study on an AP from another marine bacterium, *V. alginolyticus*.[16] VAP and *V. alginolyticus* AP have 93% identical sequences and identical active site residues with respect to metal ion coordination. Furthermore, they both have the same large surface loop insert, which was noted as a novel structural characteristic of VAP when its crystallographic structure was reported.[49] For *V. alginolyticus* AP, Cl^- ions were shown to be most effective in enhancing enzyme activity compared to other small anions. However, SO_4^{2-}, a competitive inhibitor, was shown to prevent the effect of Cl^- on activity at pH 7.5. Thus, they concluded that Cl^- bound closely to the substrate in the active site of the *V. alginolyticus* AP. For VAP, the charged residues that are closest to the SO_4^{2-} ion in

DOI: 10.1021/acs.biochem.7b00690
Biochemistry 2017, 56, 5075−5089

the active site, to which the Cl^- might be binding, are Arg129, His277, and His465 (Figure 9). Cl^- could also be coordinated to the Zn ions and be outcompeted by OH^- ions as the pH increases, as discussed above.

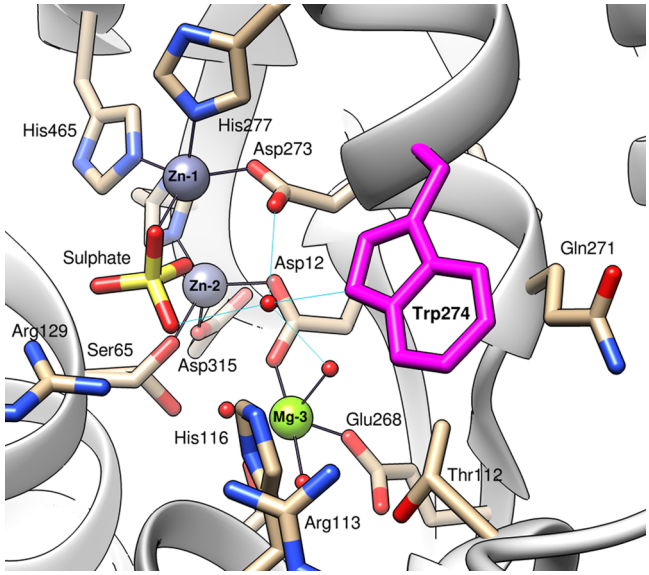

Figure 9. Active site structure of VAP showing residues in the proximity of metal ligands and Trp274 (Protein Data Bank entry 3E2D). Trp274 is colored magenta, and the two Zn^{2+} ions are colored navy-purple. The Mg^{2+} ion is colored bright green and is connected with black lines to its ligands, including two water molecules. Water molecules are represented as red spheres and hydrogen bonds as aquamarine colored lines. A sulfate ion, binding as a competitive inhibitor, is shown in the active site. Note that Ser65 is shown as two crystallographic rotamers.[49]

VAP Inactivation. Wild-type VAP was inactivated quite rapidly under low-salt conditions at room temperature, well below the melting temperature of approximately 50 °C (T_m). Our results indicated that this was not caused by dissociation of dimers to inactive monomers or dissociation of metal ions from the active site. We have previously reported that VAP can be transformed to an inactive dimer by concentrations of urea not sufficiently high to cause full denaturation.[12] This work adds the information that this form of VAP is fully metalated (Figure 5). A deprotonation event was apparently important for maintaining the stability of the active site because $T_{50\%}$ increased from 25.8 to 33.2 °C with an increase in pH from 8.0 to 10.5 in a low-ionic strength buffer. The inactivated form was not easily converted back to the active enzyme, as various experiments of ours with that aim have failed. It may be suggested that some key residue becomes locked in an unfavorable rotameric position by association with a partner of an opposite charge, but further studies of VAP variants are needed to substantiate this idea.

Direct measurements of the dimer−monomer equilibrium are rare for APs. It is not trivial to obtain a signal for the dissociation of the identical monomers using biophysical methods. Sedimentation velocity experiments have been widely used,[50−53] as have size exclusion chromatography (SEC)[12,53,54] and polyacrylamide electrophoresis.[55,56] Some of these methods involve interaction of the protein with a matrix that may perturb the equilibrium.

Here, we measured the dimer dissociation constant for VAP by measuring the specific activity after dilution. The dissociation constant was greatly affected by pH. The K_d was close to 1 nM at pH 10.5 compared to 10−50 nM observed at pH 8.0 under the conditions tested. Inorganic phosphate in the medium (1.0 mM) was shown to increase the K_d of the dimer at pH 8.0, but not at pH 10.5. This was expected, because at pH 10.5 the affinity of the enzyme for phosphate is low. Sodium chloride at 0.5 M increased both the K_d at pH 8.0 and 10.5 with a sigmoidal character at pH 8.0 that was not seen at pH 10.5. This indicated that, at pH 8.0, Cl^- was able to bind to a specific site but not at pH 10.5. The free energy reported here is in the range of 45−55 kJ/mol and is within the limits of 20−70 kJ/mol reported for the dissociation of other homodimers.[57] Denaturing VAP with urea and monitoring the denaturation by Trp fluorescence gave a free energy change for monomer unfolding of 14 kJ/mol.[12] Thus, it is clear that dimer formation contributes greatly toward VAP structural stability. Our laboratory has previously assessed the dimer dissociation for Atlantic cod AP induced by guanidinium chloride (GdmCl)[32] or urea[58] using SEC, Trp fluorescence, and activity. The free energies were 34 and 36 kJ/mol for dimer dissociation with GdmCl and urea, respectively.

Effect of pH on VAP Trp Fluorescence. Because changes in VAP Trp fluorescence at different pH values were in most cases accompanied by changes in activity, it is likely that W274, which is located in the active site, is the residue most openly affected by pH. However, we have previously shown, using a Trp to Phe substitution, that W274 does not contribute greatly to the total Trp emission spectrum of VAP.[12] Interestingly, the emission was increased for the W274F variant compared to that of the wild type, which suggested that W274 is likely a resonance energy transfer (RET) acceptor for other Trp residues. Thus, when W274 was no longer present, more energy was emitted as photons from the remaining Trp residues. There are a few residues close to W274 that could also act as intrinsic quenchers,[59] explaining the sensitivity to subtle structural changes, mainly Q271, H116, D273, and E268 (Figure 9). It is likely that D273 could act as a good quencher by excited-state electron transfer because it is made electron poor by coordination with the Zn^{2+}, and by a key water molecule, which is involved in coordinating the substrate, which also makes a hydrogen bond with the W274 residue.

The residues that might be deprotonated in the neutral-pH range are either histidine or amine groups that are much more efficient quenchers in their charged states. It is, however, well-known that amino acid residues can have exhibit shifts in pK_a values when the residues are located in active sites or hydrophobic environments,[60,61] so further experimentation is needed so firmer conclusions can be reached.

CONCLUSION

We have shown that VAP is highly activated by anions and displays a two-peak pH−activity profile due to a suggested conformational change in the pH range of 9.0−10.5. This presumed conformational change leads to a loss of substrate and product affinity leading to a change in the rate-limiting step from the last step (release of the noncovalently bound product) toward dephosphorylation of the covalent intermediate. These changes correlated with changes in tryptophan fluorescence. The effect of NaCl on the activity is proposed to be 2-fold in nature. First, the salt increased the rate of inorganic phosphate product release by directly binding to a charged group in the active site, most likely a Zn ion. This presumed binding of chloride to Zn would also greatly stabilize the enzyme toward thermal activation in the pH range of 8.0−10.5. Second, NaCl was shown to affect the dimer dissociation constant with a sigmoidal character at pH

DOI: 10.1021/acs.biochem.7b00690
Biochemistry 2017, 56, 5075−5089

8.0, but not at pH 10.5, an indication of specific chloride ion binding at the group(s) involved in connecting the monomers, or shaping the monomers in a productive conformation for dimer formation. Finally, we have shown that the inactivation is not due to dimer dissociation or Zn/Mg ion dissociation but more likely is due to a subtle conformational change in the active site, where key residues in catalysis might be kinetically trapped in an unfavorable position.

■ ASSOCIATED CONTENT

Supporting Information

The Supporting Information is available free of charge on the ACS Publications website at DOI: 10.1021/acs.biochem.7b00690.

Detailed description of the overlap PCR extension used for subcloning of VAP to pET11a vector, VAP production in Lemo21(DE3) cells, effect of pH and additives in buffers on the molar extinction coefficient of *p*-nitrophenol, steady-state enzyme kinetics of VAP at various pH values, and schematic representation of enzyme preparation before Zn^{2+} and Mg^{2+} analyses (PDF)

■ AUTHOR INFORMATION

Corresponding Authors

*E-mail: jgh4@hi.is.
*E-mail: bjarni@hi.is.

ORCID

Jens G. Hjörleifsson: 0000-0002-0471-855X

Funding

Financial support from the Icelandic Research Fund (Project 141619-051) and the Science Institute of the University of Iceland is gratefully acknowledged.

Notes

The authors declare no competing financial interest.

■ ACKNOWLEDGMENTS

We thank Ottar Rolfsson and Arnar Sigurdsson of the Department of System Biology at the University of Iceland for providing us with access to the SpectraMax-M3 fluorescence plate reader and help with its operation.

■ ABBREVIATIONS

VAP, *Vibrio* sp. alkaline phosphatase; ECAP, *E. coli* alkaline phosphatase; CIP, calf intestinal phosphatase; TNAP, tissue nonspecific alkaline phosphatase; PLAP, human placenta alkaline phosphatase; pNPP, *p*-nitrophenyl phosphate; pNP, *p*-nitrophenol; DEA, diethanolamine; CD, circular dichroism; RET, resonance energy transfer; SEC, size exclusion chromatography.

■ REFERENCES

(1) Feller, G., and Gerday, C. (2003) Psychrophilic enzymes: hot topics in cold adaptation. *Nat. Rev. Microbiol. 1*, 200−208.

(2) Pucci, F., and Rooman, M. (2017) Physical and molecular bases of protein thermal stability and cold adaptation. *Curr. Opin. Struct. Biol. 42*, 117−128.

(3) Talley, K., and Alexov, E. (2010) On the pH-optimum of activity and stability of proteins. *Proteins: Struct., Funct., Genet. 78*, 2699−2706.

(4) Thomas, D. N., and Dieckmann, G. S. (2002) Antarctic sea ice: a habitat for extremophiles. *Science 295*, 641−644.

(5) Mock, T., and Thomas, D. N. (2005) Recent advances in sea-ice microbiology. *Environ. Microbiol. 7*, 605−619.

(6) Paterova, J., Rembert, K. B., Heyda, J., Kurra, Y., Okur, H. I., Liu, W. R., Hilty, C., Cremer, P. S., and Jungwirth, P. (2013) Reversal of the Hofmeister series: specific ion effects on peptides. *J. Phys. Chem. B 117*, 8150−8158.

(7) Schwierz, N., Horinek, D., and Netz, R. R. (2015) Specific ion binding to carboxylic surface groups and the pH dependence of the Hofmeister series. *Langmuir 31*, 215−225.

(8) Stec, B., Holtz, K. M., and Kantrowitz, E. R. (2000) A revised mechanism for the alkaline phosphatase reaction involving three metal ions. *J. Mol. Biol. 299*, 1303−1311.

(9) Stock, J. B., Rauch, B., and Roseman, S. (1977) Periplasmic space in *Salmonella typhimurium* and *Escherichia coli*. *J. Biol. Chem. 252*, 7850−7861.

(10) Wilks, J. C., and Slonczewski, J. L. (2007) pH of the cytoplasm and periplasm of *Escherichia coli*: rapid measurement by green fluorescent protein fluorimetry. *J. Bacteriol. 189*, 5601−5607.

(11) Hauksson, J. B., Andresson, O. S., and Asgeirsson, B. (2000) Heat-labile bacterial alkaline phosphatase from a marine *Vibrio sp. Enzyme Microb. Technol. 27*, 66−73.

(12) Hjorleifsson, J. G., and Asgeirsson, B. (2016) Cold-active alkaline phosphatase is irreversibly transformed into an inactive dimer by low urea concentrations. *Biochim. Biophys. Acta, Proteins Proteomics 1864*, 755−765.

(13) Wilson, I. B., Dayan, J., and Cyr, K. (1964) Some properties of alkaline phosphatase from *Escherichia coli* transphosphorylation. *J. Biol. Chem. 239*, 4182−4185.

(14) Bloch, W., and Schlesinger, M. J. (1974) Kinetics of substrate hydrolysis by molecular variants of *Escherichia coli* alkaline phosphatase. *J. Biol. Chem. 249*, 1760−1768.

(15) Fernley, H. N., and Walker, P. C. (1968) Effect of sodium chloride on *Escherichia coli* alkaline phosphatase. *Biochem. J. 110*, 11P−12P.

(16) Hayashi, M., Unemoto, T., and Hayashi, M. (1973) pH- and anion-dependent salt modifications of alkaline phosphatase from a slightly halophilic *Vibrio alginolyticus*. *Biochim. Biophys. Acta 315*, 83−93.

(17) Harkness, D. R. (1968) Studies on human placental alkaline phosphatase. II. Kinetic properties and studies on the apoenzyme. *Arch. Biochem. Biophys. 126*, 513−523.

(18) Hoylaerts, M. F., Ding, L., Narisawa, S., Van Kerckhoven, S., and Millan, J. L. (2006) Mammalian alkaline phosphatase catalysis requires active site structure stabilization via the N-terminal amino acid microenvironment. *Biochemistry 45*, 9756−9766.

(19) Fernley, H. N., and Walker, P. G. (1965) Kinetic behaviour of calf-intestinal alkaline phosphatase with 4-methylumbelliferyl phosphate. *Biochem. J. 97*, 95−103.

(20) Halford, S. E. (1971) *Escherichia coli* alkaline phosphatase. An analysis of transient kinetics. *Biochem. J. 125*, 319−327.

(21) Sun, L., Kantrowitz, E. R., and Galley, W. C. (1997) Room temperature phosphorescence study of phosphate binding in *Escherichia coli* alkaline phosphatase. *Eur. J. Biochem. 245*, 32−39.

(22) Orhanovic, S., and Pavela-Vrancic, M. (2003) Dimer asymmetry and the catalytic cycle of alkaline phosphatase from *Escherichia coli*. *Eur. J. Biochem. 270*, 4356−4364.

(23) Bryksin, A., and Matsumura, I. (2013) Overlap extension PCR cloning. *Methods Mol. Biol. 1073*, 31−42.

(24) Bryksin, A. V., and Matsumura, I. (2010) Overlap extension PCR cloning: a simple and reliable way to create recombinant plasmids. *BioTechniques 48*, 463−465.

(25) Pace, C. N., Vajdos, F., Fee, L., Grimsley, G., and Gray, T. (1995) How to measure and predict the molar absorption coefficient of a protein. *Protein Sci. 4*, 2411−2423.

(26) Hofmeister, F. (1888) Concerning regularities in the protein-precipitating effects of salts and the relationship of these effects to the physiological behaviour of salts. *Naunyn-Schmiedeberg's Arch. Pharmacol. 24*, 247−260.

(27) Hofmeister, F. (1888) On the water withdrawing effect of salts. *Naunyn-Schmiedeberg's Arch. Pharmacol. 25*, 1−30.

(28) Sengupta, R., Pantel, A., Cheng, X., Shkel, I., Peran, I., Stenzoski, N., Raleigh, D. P., and Record, M. T., Jr. (2016) Positioning the

intracellular salt potassium glutamate in the Hofmeister series by chemical unfolding studies of NTL9. *Biochemistry 55*, 2251−2259.
(29) Greaney, G. S., and Somero, G. N. (1979) Effects of anions on the activation thermodynamics and fluorescence emission spectrum of alkaline phosphatase: evidence for enzyme hydration changes during catalysis. *Biochemistry 18*, 5322−5332.
(30) Poe, R. W., Sangadala, V. S., and Brewer, J. M. (1993) Effects of various salts on the steady-state enzymatic activity of *E. coli* alkaline phosphatase. *J. Inorg. Biochem. 50*, 173−180.
(31) Garen, A., and Levinthal, C. (1960) A fine-structure genetic and chemical study of the enzyme alkaline phosphatase of E. coli. I. Purification and characterization of alkaline phosphatase. *Biochim. Biophys. Acta 38*, 470−483.
(32) Asgeirsson, B., Hauksson, J. B., and Gunnarsson, G. H. (2000) Dissociation and unfolding of cold-active alkaline phosphatase from atlantic cod in the presence of guanidinium chloride. *Eur. J. Biochem. 267*, 6403−6412.
(33) Gudjonsdottir, K., and Asgeirsson, B. (2008) Effects of replacing active site residues in a cold-active alkaline phosphatase with those found in its mesophilic counterpart from *Escherichia coli*. *FEBS J. 275*, 117−127.
(34) Beauchamp, D. L., and Khajehpour, M. (2012) Studying salt effects on protein stability using ribonuclease t1 as a model system. *Biophys. Chem. 161*, 29−38.
(35) Zhao, H. (2005) Effect of ions and other compatible solutes on enzyme activity, and its implication for biocatalysis using ionic liquids. *J. Mol. Catal. B: Enzym. 37*, 16−25.
(36) Von Hippel, P. H., and Schleich, T. (1969) Ion effects on the solution structure of biological macromolecules. *Acc. Chem. Res. 2*, 257−265.
(37) Baldwin, R. L. (1996) How Hofmeister ion interactions affect protein stability. *Biophys. J. 71*, 2056−2063.
(38) Zhang, Y. J., and Cremer, P. S. (2009) The inverse and direct Hofmeister series for lysozyme. *Proc. Natl. Acad. Sci. U. S. A. 106*, 15249−15253.
(39) Yang, Z., Liu, X. J., Chen, C., and Halling, P. J. (2010) Hofmeister effects on activity and stability of alkaline phosphatase. *Biochim. Biophys. Acta, Proteins Proteomics 1804*, 821−828.
(40) Norne, J. E., Szajn, H., Csopak, H., Reimarsson, P., and Lindman, B. (1979) The relation between activity and zinc and chloride binding of *Escherichia coli* alkaline phosphatase. *Arch. Biochem. Biophys. 196*, 552−556.
(41) Gettins, P., and Coleman, J. E. (1984) Chloride binding to alkaline phosphatase. ^{113}Cd and ^{35}Cl NMR. *J. Biol. Chem. 259*, 11036−11040.
(42) O'Brien, P. J., and Herschlag, D. (2002) Alkaline phosphatase revisited: hydrolysis of alkyl phosphates. *Biochemistry 41*, 3207−3225.
(43) Lazdunski, C., and Lazdunski, M. (1969) Zn^{2+} and Co^{2+}-Alkaline Phosphatases of *E. coli*. *Eur. J. Biochem. 7*, 294−300.
(44) Krishnaswamy, M., and Kenkare, U. W. (1970) The effect of pH, temperature, and organic solvents on the kinetic parameters of *Escherichia coli* alkaline phosphatase. *J. Biol. Chem. 245*, 3956−3963.
(45) Chaidaroglou, A., and Kantrowitz, E. R. (1989) Alteration of aspartate 101 in the active site of *Escherichia coli* alkaline phosphatase enhances the catalytic activity. *Protein Eng., Des. Sel. 3*, 127−132.
(46) Hinberg, I., and Laidler, K. J. (1972) The kinetics of reactions catalyzed by alkaline phosphatase: the effects of added nucleophiles. *Can. J. Biochem. 50*, 1360−1368.
(47) Kim, T. H., Mehrabi, P., Ren, Z., Sljoka, A., Ing, C., Bezginov, A., Ye, L., Pomes, R., Prosser, R. S., and Pai, E. F. (2017) The role of dimer asymmetry and protomer dynamics in enzyme catalysis. *Science 355*, eaag2355.
(48) Papaleo, E., Renzetti, G., Invernizzi, G., and Asgeirsson, B. (2013) Dynamics fingerprint and inherent asymmetric flexibility of a cold-adapted homodimeric enzyme. A case study of the *Vibrio* alkaline phosphatase. *Biochim. Biophys. Acta, Gen. Subj. 1830*, 2970−2980.
(49) Helland, R., Larsen, R. L., and Asgeirsson, B. (2009) The 1.4 A crystal structure of the large and cold-active *Vibrio sp.* alkaline phosphatase. *Biochim. Biophys. Acta, Proteins Proteomics 1794*, 297−308.
(50) Schlesinger, M. J., and Barrett, K. (1965) The reversible dissociation of the alkaline phosphatase of *Escherichia coli*. I. Formation and reactivation of subunits. *J. Biol. Chem. 240*, 4284−4292.
(51) Applebury, M. L., and Coleman, J. E. (1969) *Escherichia coli* alkaline phosphatase. Metal binding, protein conformation, and quaternary structure. *J. Biol. Chem. 244*, 308−318.
(52) Snyder, S. L., Wilson, I., and Bauer, W. (1972) The subunit composition of *Escherichia coli* alkaline phosphatase in I M tris. *Biochim. Biophys. Acta 258*, 178−187.
(53) Fosset, M., Chappelet-Tordo, D., and Lazdunski, M. (1974) Intestinal alkaline phosphatase. Physical properties and quaternary structure. *Biochemistry 13*, 1783−1788.
(54) Krull, I. S., Stuting, H. H., and Krzysko, S. C. (1988) Conformational studies of bovine alkaline phosphatase in hydrophobic interaction and size-exclusion chromatography with linear diode array and low-angle laser light scattering detection. *J. Chromatogr. 442*, 29−52.
(55) Al-Shawafi, H. A., Komaru, K., and Oda, K. (2017) Molecular defect of tissue-nonspecific alkaline phosphatase bearing a substitution at position 426 associated with hypophosphatasia. *Mol. Cell. Biochem. 427*, 169−176.
(56) Olsen, R. L., Overbo, K., and Myrnes, B. (1991) Alkaline-phosphatase from the hepatopancreas of shrimp (*Pandalus borealis*) - a dimeric enzyme with catalytically active subunits. *Comp Biochem Phys. B 99*, 755−761.
(57) Neet, K. E., and Timm, D. E. (1994) Conformational stability of dimeric proteins: quantitative studies by equilibrium denaturation. *Protein Sci. 3*, 2167−2174.
(58) Asgeirsson, B., and Guojonsdottir, K. (2006) Reversible inactivation of alkaline phosphatase from Atlantic cod (*Gadus morhua*) in urea. *Biochim. Biophys. Acta, Proteins Proteomics 1764*, 190−198.
(59) Chen, Y., and Barkley, M. D. (1998) Toward understanding tryptophan fluorescence in proteins. *Biochemistry 37*, 9976−9982.
(60) Bashford, D., and Karplus, M. (1990) pK_a's of ionizable groups in proteins: atomic detail from a continuum electrostatic model. *Biochemistry 29*, 10219−10225.
(61) Mehler, E. L., Fuxreiter, M., Simon, I., and Garcia-Moreno E, B. (2002) The role of hydrophobic microenvironments in modulating pK_a shifts in proteins. *Proteins: Struct., Funct., Genet. 48*, 283−292.

DOI: 10.1021/acs.biochem.7b00690
Biochemistry 2017, 56, 5075−5089

Supporting information

A pH-dependent binding of chloride to a marine alkaline phosphatase affects catalysis, active site stability and dimer equilibrium

Jens Guðmundur Hjörleifsson[1]* and Bjarni Ásgeirsson[1]*

[1]Department of Biochemistry, Science Institute, University of Iceland, Dunhagi 3, 107 Reykjavik, Iceland.

* Corresponding authors: Bjarni Ásgeirsson, email: bjarni@hi.is and Jens Guðmundur Hjörleifsson, email: jgh4@hi.is

Sub-cloning of VAP to pET11a. A megaprimer PCR reaction was performed using chimeric primers; sense primer: 5‘-CCC CTC TAG AAA TAA TTT TG TTT AAC TTT AAG AAG GAG ATA TAC AT- ATG AAA CCA ATT GTT ACC GCA-3‘ and antisense primer 5‘-CAA GGG GTT ATG CTA GTT ATT GCT CAG CGG-TCA TCA TTT TTC GAA CTG CGG GTG G-3‘, where the underlined sequence denotes the target sequence containing StrepTag2 at the C-terminus of VAP via a two amino acid linker (Ser-Ala) and the forward primer sequence contains the desired plasmid insert sequence (Figure S1). The PCR was done using a Phusion polymerase kit (NEB) as described in Table S1. The megaprimer product from the PCR was gel purified using Monarch® Gel extraction kit (NEB). If the gel purification was omitted, some colonies would contain tautomeric inserts or unspecific incorporated inserts not located at the multiple cloning site (data not shown). The overlap extension PCR was performed as described in Table S1.

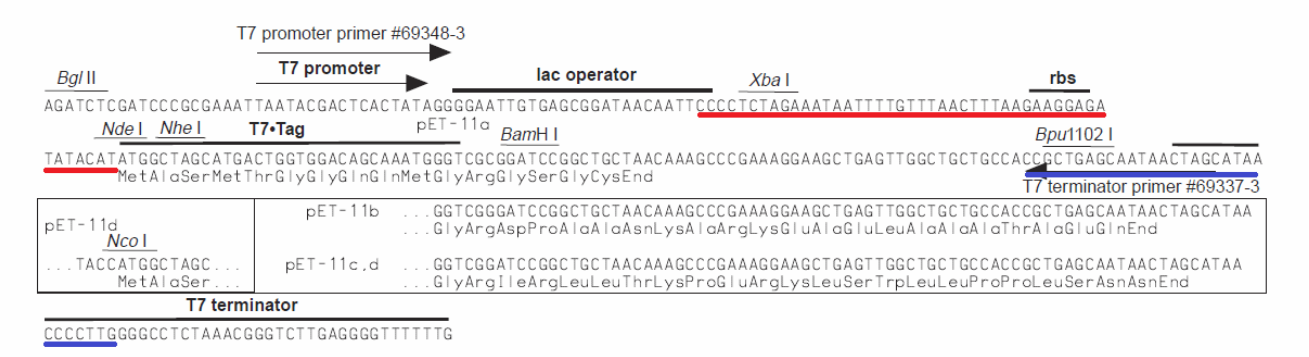

Figure S1: The map of the multiple cloning site of the pET11a plasmid shows the sense primer flanking sequence in red and the antisense flanking sequence in blue. Figure was adapted from NovaGen.

The original methylated template plasmids were digested with *Dpn*I (Thermo Fischer) for 2h before transforming competent TOP10 *E. coli* cells by adding 1 µl of the PCR solution to 50 µl of cells (OD600 0.2-0.4). Clones were then selected from LB agar plates containing 0.1 mg/ml ampicillin and colony PCR performed on 4 clones. Two positive clones from the colony PCR were selected and plasmid purified on GeneJET Plasmid Miniprep Kit (Fermentas, Lithuania) and sequenced (Genewiz, UK) to confirm 100% sequence identity.

Table S1: Settings for overlap extension PCR cloning. All PCR experiments were done in 1× Phusion HF buffer, using 0.2 mM dNTP and 1 unit Phusion polymerase. For the megaprimer PCR, the primer concentration was 0.3 µM per primer. For overlap extension PCR, the megaprimer was used in 200x molar excess over plasmid (here 10 ng plasmid vs 400 ng megaprimer insert).

	Megaprimer PCR		**Overlap extension PCR**	
Initial denaturation	98°C for 30 s		99°C for 2 min	
Denaturation	98°C for 10 s	**30x**	95°C for 50 s	**20x**
Annealing	63°C for 20 s		60°C for 50 s	
Extension	72°C for 33 s		68°C for 12 min	
Final extension	72°C for 10 min		68°C for 12 min	

VAP production in Lemo21(DE3). VAP gene was sub-cloned to pET11a, a T7 promoter plasmid, where in previous studies from our laboratory a tetracycline promoter system was used (pASK-3). A T7 pLysS E. coli modulated system has been previously used for production of another cold-adapted alkaline phosphatase from Antarctic bacterium TAB5 in high yield using autoinduction [1]. Here we used a commercially available strain, E. coli Lemo21 (DE3), which harbours the pLysS plasmid containing the sequence for T7 lysozyme under control of the highly locked and titratable rhamnose promoter.[2, 3] The biggest challenge for the E. coli cell, when overexpressing a periplasmic protein such as VAP, is the saturation of the Sec-export pathway leading to accumulation of unfolded and incorrectly folded intermediates who usually end up in inclusion bodies. By adding rhamnose to the medium in the concentration range of 0.0 - 2.0 mM, T7 lysozyme expression tempers the activity of highly active and overexpressed T7 RNA polymerase, leading to highly titratable modulation of protein expression.

Using the T7 E. coli Lemo21(DE3) system, instead of a tetracycline promoter system from previous studies (pASK-3), VAP was expressed in very high yields. The highest yield was achieved using 0.50 mM L-rhamnose in the medium (Figure S2). LB media gave the highest yield of active protein produced per liter of culture (100 - 200 mg/L) when compared with various enriched media tested (SOB, SOC, 2xYT, TB and SB media). Previously, using the tetracycline promoter system, the typical protein yield was at best 2 - 4 mg/L culture. A crucial factor in maintaining a high yield was proper aeration of the media, keeping the volume of the medium no more than 1/5 of the volume of the culture flask and shake vigorously at 200-300 rpm. The lysate was purified in one step on a StrepTactin resin (binds to the C-terminus StrepTag) as previously when using the tetracycline promoter system.[4, 5] This reusable (up to 20-30x) affinity resin has shown to be very reliable in our lab, achieving 99% purity in one step. An extra wash step with mild detergent (TritonX-100) was needed in some cases using

the T7 expression system and Lemo21(DE3) cells to achieve 99% purity. The purified enzyme had same k_{cat}, K_M, and stability as when using the tetracycline promoter system

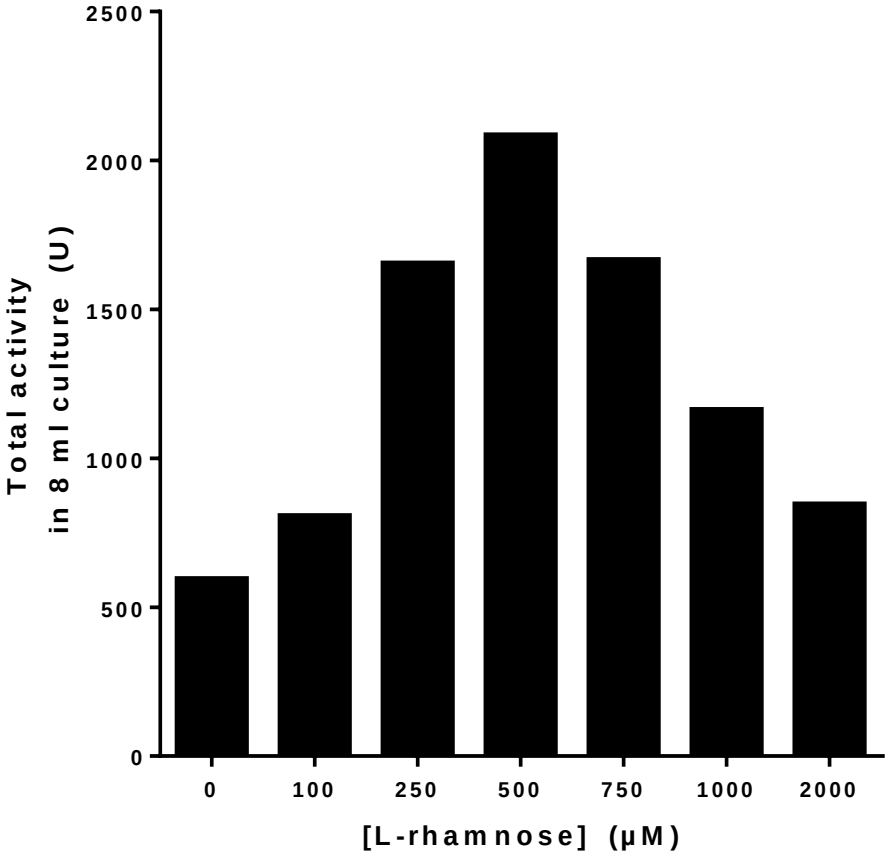

Figure S2. Optimum L-rhamnose concentration evaluation. A starter culture of *E. coli* Lemo21(DE3) was transformed with VAP pET11a plasmid and grown overnight in LB medium containing 100 µg/ml ampicillin, 30 µg/ml chloramphenicol. This was back-diluted 1:100 to the same fresh media containing L-rhamnose ranging from 0-2000 µM and the cells grown at 37°C. When OD600 reached 0.5 - 0.6 the protein production was induced with 0.4 mM IPTG and grown for 16-18 h at 18°C. The cells were then collected and lyzed as described in materials and methods and the activity of the lysate assayed using the standard pNPP activity assay. Activity shown on the y-axis corresponds to total enzyme units in the corresponding 8 ml culture.

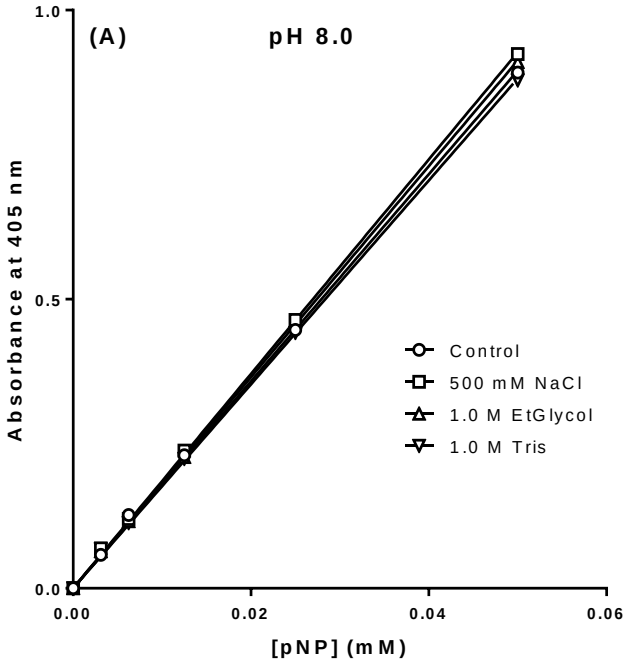

Control	500 mM NaCl	1.0 M EtGlycol	1.0 M Tris
17.90 ± 0.1300	18.54 ± 0.1062	18.25 ± 0.07032	17.63 ± 0.1083

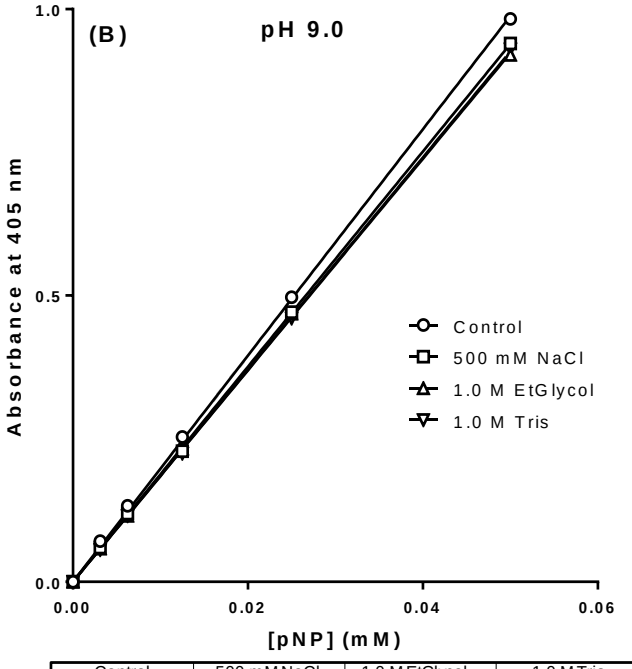

Control	500 mM NaCl	1.0 M EtGlycol	1.0 M Tris
19.76 ± 0.1215	18.79 ± 0.05646	18.47 ± 0.05633	18.53 ± 0.07153

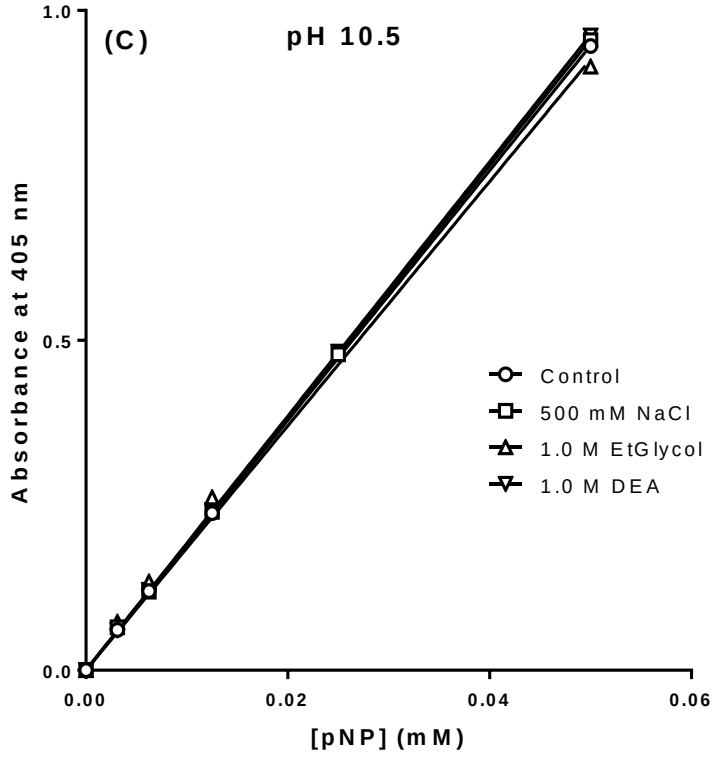

Control	500 mM NaCl	1.0 M EtGlycol	1.0 M DEA
18.93 ± 0.02780	19.12 ± 0.04302	18.52 ± 0.3861	19.27 ± 0.02613

Figure S3: Determination of molar extinction coefficients for p-nitrophenol under various conditions. The effects of ionic strength, pH and nucleophile on the absorption of para-nitrophenol (pNP) was measured. A 5.00 mM aqueous solution of para-nitro phenyl phosphate (pNPP) was allowed to fully hydrolyse in 1 µM VAP overnight. The hydrolysed solution was then diluted to 1.00 mM in buffer (A) 50 mM Tris pH 8.0, (B) 50 mM Tris pH 9.0 and (C) 50 mM CAPS pH 10.5 with either addition of 500 mM NaCl or 1.0 M of a chosen nucleophile (ethylene glycol, Tris or diethanolamine). A standard dilution was performed in the concentration range 0.00 – 0.06 mM pNP and measurement performed at 405 nm. An average molar extinction coefficient of 18.1 $mM^{-1}cm^{-1}$ was used for measurements at pH 8.0, 18.9 $mM^{-1}cm^{-1}$ for pH 9.0 and 19.0 $mM^{-1}cm^{-1}$ for pH 10.5.

Table S2. VAP enzyme steady-state kinetics at various pH.

pH 8.0[a]	**k_{cat} (s^{-1})**	**K_M (µM)**	**K_i (phosphate)**[c] **(µM)**	**k_{cat}/K_M ($M^{-1}s^{-1}$)**	**Fold activity in 20% w/v sucrose**[d]	**P_2/P_1 formation rate**[e]
Control	35.6 ± 3,7	25 ± 4	22 ± 4	$1.4 \cdot 10^6$	0.52 ± 0.02	0.48 ± 0.03
0.5 M NaCl	145 ± 11	26 ± 4	95 ± 13	$5.6 \cdot 10^6$	0.79 ± 0.04	0.49 ± 0.10
1.0 M Tris[b]	351 ± 22	88 ± 5	58 ± 3	$4.0 \cdot 10^6$	0.78 ± 0.02	0.08 ± 0.03
pH 9.0[a]						
Control	102 ± 8	19 ± 2	15 ± 2	$5,5 \cdot 10^6$	0.57 ± 0.05	0.33 ± 0.14
0.5 M NaCl	243 ± 17	61 ± 5	164 ± 12	$4.0 \cdot 10^6$	0.73 ± 0.01	0.64 ± 0.47
1.0 M Tris[b]	760 ± 39	495 ± 32	172 ± 7	$1.5 \cdot 10^6$	0.73 ± 0.02	0.05 ± 0.02
pH 10.5[a]						
Control	80 ± 9	484 ± 38	1460 ± 93	$1.7 \cdot 10^5$	0.82 ± 0.05	0.68 ± 0.21
0.5 M NaCl	99 ± 11	1480 ± 149	8640 ± 2180	$6.7 \cdot 10^4$	0.96 ± 0.07	0.63 ± 0.37
1.0 M DEA[b]	749 ± 41	5210 ± 818	7560 ± 1570	$1.4 \cdot 10^5$	0.71 ± 0.03	0.04 ± 0.03

[a] Activity was measured in 50 mM Tris for pH 8.0 and 9.0 and 50 mM Caps at pH 10.5 at 23°C using pNPP as a substrate in the range 0.0 – 2.0 mM.

[b] For addition of Tris and DEA, the ionic strength was held constant at I = 0.59 M by NaCl addition.

[c] Competitive inhibition of inorganic phosphate was determined at 0.0 mM, 0.50 mM and 1.00 mM inorganic phosphate.

[d] Fold activity is the activity present in 20% w/v sucrose vs. where no sucrose was added.

[e] Fraction of inorganic phosphate product released (P_2) vs. para-nitro phenol released (P_1). P_2 was assayed using the commercial enzymatic phosphate assay, PiPer assay (ThermoFischer)

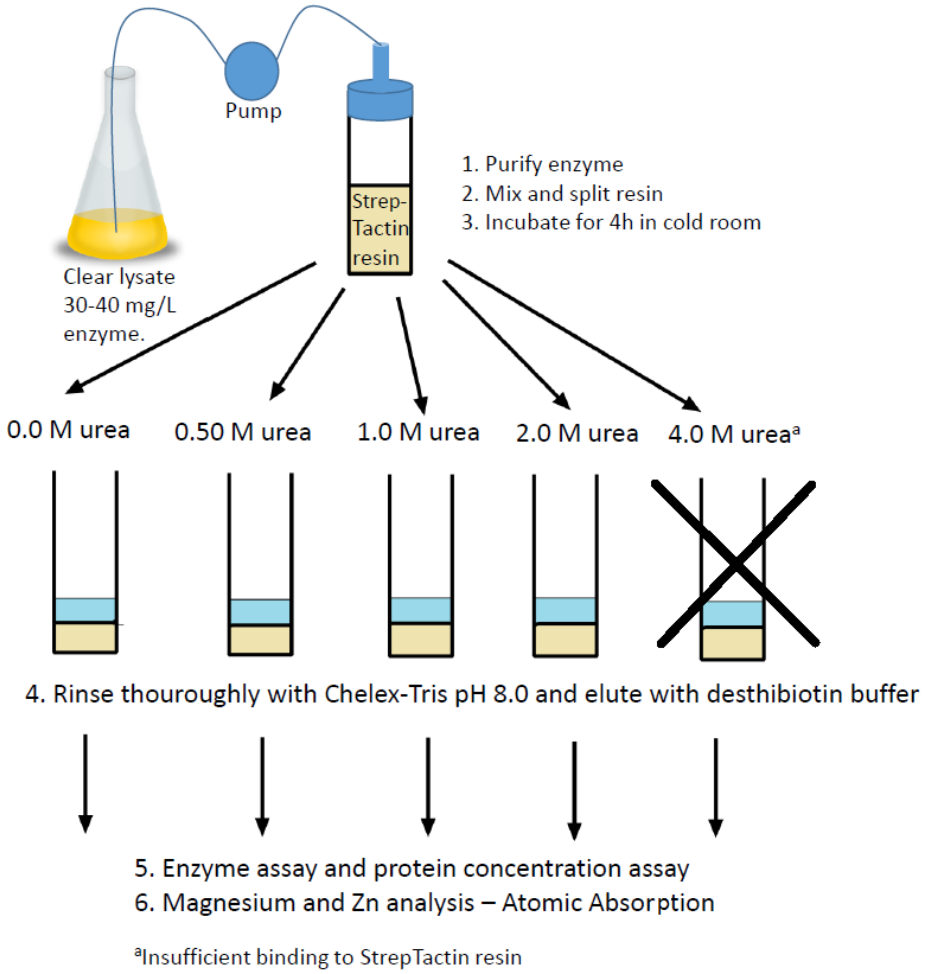

Figure S4: Schematic representation of enzyme purification and preparation before assaying Zn^{2+} and Mg^{2+}.

References

(1) Lu, Z., Chen, W., Liu, R., Hu, X., and Ding, Y. (2010) A novel method for high-level production of psychrophilic TAB5 alkaline phosphatase, *Protein. Expr. Purif. 74*, 217-222.

(2) Schlegel, S., Lofblom, J., Lee, C., Hjelm, A., Klepsch, M., Strous, M., Drew, D., Slotboom, D. J., and de Gier, J. W. (2012) Optimizing membrane protein overexpression in the *Escherichia coli* strain Lemo21(DE3), *J. Mol. Biol. 423*, 648-659.

(3) Wagner, S., Klepsch, M. M., Schlegel, S., Appel, A., Draheim, R., Tarry, M., Hogbom, M., van Wijk, K. J., Slotboom, D. J., Persson, J. O., and de Gier, J. W. (2008) Tuning *Escherichia coli* for membrane protein overexpression, *Proc. Natl. Acad. Sci. U S A 105*, 14371-14376.

(4) Heidarsson, P. O., Sigurdsson, S. T., and Asgeirsson, B. (2009) Structural features and dynamics of a cold-adapted alkaline phosphatase studied by EPR spectroscopy, *FEBS J. 276*, 2725-2735.

(5) Hjorleifsson, J. G., and Asgeirsson, B. (2016) Cold-active alkaline phosphatase is irreversibly transformed into an inactive dimer by low urea concentrations, *Biochim. Biophys. Acta. 1864*, 755-765.

Paper III

Cold-Active Alkaline Phosphatase Undergoes a Subtle Structural Change at the Dimer Interface Upon Inactivation.

Jens. G. Hjörleifsson* and Bjarni Ásgeirsson*

Department of Biochemistry, Science Institute, University of Iceland, Dunhagi 3, 107 Reykjavik, Iceland.

Keywords: Alkaline phosphatase, negative cooperativity, half-of-sites reactivity, dimer, urea denaturation, bimane fluorometry.

Abstract

Most enzyme exist as homodimers or as higher order multimers. The principles that govern the tendency during evolution towards homodimers have been debated. Negative cooperativity is an element that some homodimeric enzymes display, resulting in asymmetric interactions and half-of-sites reactivity. Alkaline phosphatase (AP), a homodimer enzyme, has been shown to negative harbor negative cooperativity, but it is largely unknown how the individual subunits interact and mediate "cross talk" at the dimeric interface. We have previously found that the cold-active AP from *Vibrio splendidus* (VAP) does transition into an inactive dimer which remains structurally similar to the native state and fully metalated. Wanting to understand why this dimer fails to catalyze phosphomonoester hydrolysis brought us to investigate the interfacial contacts between subunits. Here, we chose to monitor the denaturation of the enzyme by incorporating a bimane fluorescence probe at the interface. We found that VAP denatures in a three-state process at pH 8.0 involving an inactive dimer intermediate, but no population of folded monomers. Subtle changes in fluorescence at the interface were detected using the bimane probe, indicating changes in interface interactions. The transition to an inactive dimer in low salt medium was irreversible, but the inactivation event was prevented by 0.5 M NaCl, where chloride presumably binds to Zn ion in the active site. We propose that the half-of-sites reactivity of VAP involves dynamic networks of non-covalent bonds that channel through the interface in each reaction cycle at a site close to the two-fold rotational axis.

Introduction

Quaternary protein structures shape the dynamical ensemble of conformations that accompany the reaction pathway in multimeric proteins and often provide means of regulation. How enzyme subunit interactions affect function is an experimentally challenging task. The benefit of homodimer formation has been attributed to several factors, including increased stability by formation of interface contacts [1, 2], providing extra sites for ligand binding [3], facilitating faster folding to minimize occurrence of misfolded intermediates [4], and a mechanism for allosteric regulation [5]. Many homodimeric enzymes show evidence of cooperativity [6-11], and especially negative cooperativity resulting in half-of-sites reactivity [8, 10]. Thus, the role of having two identical subunits is likely in many cases to increase the conformational space through a dynamical asymmetry, coordinated by interface contacts [12-14]. These contacts often lie close to the twofold rotational axis.

By comparing 100 crystal structures of homodimers, Brown [15] has identified registry slips at interfacial antiparallel β-strands and axial shifts between antiparallel coiled-coils that avoid steric clashes at the symmetry axis. In some cases, homodimers have a pre-existent structural asymmetry resulting in half-of sites reactivity, as found in human caspase 9 [16], *E. coli* aspartate transcarbamoylase [17] and *Rhodopseudomonas palustris* fluoroacetate dehalogenase [18]. Other examples indicate that half-of-sites reactivity is ligand/substrate induced, examples being glyceraldehyde 3-phosphate dehydrogenase [19] and tryptophan-tRNA synthetase [20].

Kinetic and structural analysis of AP from *Escherichia coli* (ECAP) and some mammalian APs suggested negative cooperativity between subunits and a half-of-sites reaction mechanism [21-27]. This type of reaction mechanism has been doubted by others [28-30]. We previously obtained evidence using molecular dynamics calculations for dimer asymmetry in VAP, the cold-adapted AP from *Vibrio splendidus* [14]. Yet, it is still experimentally unconfirmed how changes in dynamics allow for such half-of-sites mechanism.

Several earlier experiments were conducted in order to answer the question of subunit individuality in APs. Bloch and Schlesinger (1974) hybridized an inactive ECAP variant with the wild-type, which showed half the activity of the wild type enzyme [31]. This suggested that only one subunit is needed for catalytic activity. Furthermore, inactive monomers have been frequently observed for ECAP, indicating that monomers are not independent [32-34]. Further example of active dimers come from Levinthal [35] who made an active hybrid AP dimer from individual monomers of *E. coli* and *S. marcescens*, despite only 74% DNA sequence identity. More recently, Hehir et. al (2000) characterized the ECAP heterodimer variants produced earlier by Schlesinger [21] and showed intragenic complementation for these heterodimeric variants. Most of the mutated variants where located at the active site and many where metal ion coordinates [36]. Thus, these results do suggest that an interface is needed to properly form the active sites by some global residue positioning induced through the interface.

ECAP has a unique N-terminal interface domain which is stabilized by knobs to holes inter-subunit coiled-coil antiparallel packing. In fact, out of the 46 published crystal structures of ECAP (wild-type and mutated enzyme variants) the one with the highest resolution (pdb: 3TG0; 1.2 Å) [37], shows interfacial asymmetry at the N-terminal helix by an axial shift which causes L33 of one helix to pack between the helixes on the opposite subunit while the other L33 faces the protein core and causes R34 to adopt different a rotamer position. The other published structures show much less side-chain variation in that area. N-terminal trypsin digestion at the N-terminus of ECAP, which caused cleavage at R11 or R34, decreased the catalytic rate of ECAP and decreased thermal stability [38, 39]. Furthermore, digestion at R34 in one monomer of

ECAP forming a hybrid, resulted in similar catalytic properties as the enzyme cleaved at both subunits [40]. Thus, the unique N-terminus of ECAP might be involved in half-of-sites reactivity as well as being crucial for stability. This N-terminal helical domain is missing in VAP, which instead has a large interface loop which hovers over the active site of the other monomer. No structural asymmetry has been reported at the two-fold rotational axis in the VAP crystal structure in terms of rotamers [41].

We have previously shown that VAP can adopt different conformers by bringing the pH from 7 to 10.5, and that VAP's activity and stability is greatly affected by salt ions [42]. Furthermore, we have discovered that VAP is particularly sensitive to heat (room temperature) and urea, where the inactivated enzyme seems to be fully metallated with two Zn^{2+} and one Mg^{2+} per monomer, and still exists as a dimer [42, 43]. This has brought us to investigate further the nature of the inactivated dimer, which could shed light on how the subunits interact asymmetrically.

Here, we investigated in detail the denaturation of VAP at various conditions, such as pH and different ionic strength. We used the tryptophan and tyrosine induced quenching (TrIQ/TyrIQ) of the fluorescence probe bimane for dimer/monomer equilibrium studies as previously described [44, 45]. Bimane is intrinsically quenched by Trp and Tyr in a defined sphere of 15 Å for Trp [44] and 10 Å for Tyr [45], where optimally, a phenylalanine residue should act as a non-quencher control for the Trp/Tyr quencher positions [45]. Thus, we rationally incorporated bimane at the dimer interface juxtaposing either Tyr or Trp on the other monomer to elucidate the correct model for dimer dissociation and denaturation and to probe for subtle changes at the dimer interface during inactivation. Results indicated that upon inactivation by urea the enzyme is transitioned to an inactive dimer where interface interactions have been altered.

Materials and methods

Materials. Chemicals were obtained from Sigma-Aldrich (Schnelldorf, Germany) or Merck (Darmstadt, Germany) unless stated otherwise. FluroPure™ grade mono-bromo bimane (mBrB) was purchased from Molecular Probes (ThermoFischer). Urea ReagentPlus® 99.5% was obtained from Sigma.

Generation of enzyme variants. VAP tagged with StrepTagII (WSHPQFEK) at the C-terminus via a two-amino acid linker (Ser-Ala) was previously sub-cloned to a pET11a vector [42]. Site-directed mutagenesis was performed using the QuikChange® method (Stratagene) following the manufacturer's protocol. Oligonucleotide primers were synthesized by TAG (Copenhagen, Denmark). Mutated plasmids were transformed into XL10-Gold® competent

cells (Agilent) and the plasmids purified on GeneJet® plasmid silica columns (Fermentas) using the manufacturer's protocol and then sequenced to confirm the mutated sequences (Genewiz, UK).

Enzyme production. Enzyme variants were expressed in Lemo21(DE3) cells (NEB), and purification done in one step on a StrepTactin column by a protocol that has been described elsewhere [42]. The enzyme was eluted in 25 mM Tris, pH 8.0, 10 mM $MgCl_2$, 2.5 mM desthiobiotin, with 15% v/v ethylene glycol added as a storage medium to prevent frost damage. Enzyme purity was judged to be 95-99% pure by SDS PAGE on 4-12% bis-Tris NUPAGE® gels (Life technologies). Enzymes where snap frozen and stored at -20°C and never used in analysis after more than one freeze/thaw cycle.

Fluorescent labeling of enzyme. Enzymes were labelled while protected from light in 20 mM Mops, 2 mM $MgSO_4$, pH 7.5 at 4°C overnight with mBrB at 1 mM, added from a 100 mM stock in acetonitrile. The concentration of enzyme varied from 25-50 µM. The enzyme was applied to an Amicon® Ultra 2 ml spin-filter with a 30 kDa cutoff (Millipore) to remove excess probe. The dilution factor during filtration was at least 10.000-fold and was not deemed sufficient unless the probe absorbance in the flow through at 380 nm was reduced to zero (0.000). mBrB is mostly non-fluorescent, but is broken down to a fluorescent product by photolysis [46]. Thus, to make sure the excess unreacted probe was well below background fluorescence of the enzyme bound probe, the fluorescence of the samples was monitored shortly under constant excitation. If the emission rose with time under excitation, then unreacted probe was still present.

Labeling of the enzyme while still bound on the StrepTactin affinity column at the end of the purification procedure was much less efficient than when done in solution. For in-solution labeling, the labeling efficiency was between 40% and 100% for all variants

Labelling yield was determined by absorbance spectroscopy, using molar extinction coefficients of ε_{380} = 5000 $M^{-1}cm^{-1}$ and ε_{280} = 61310 $M^{-1}cm^{-1}$ for bimane and VAP monomers, respectively. For enzyme variants, where either Trp or Tyr where introduced or substituted, a value of 5500 $M^{-1}cm^{-1}$ or 1490 $M^{-1}cm^{-1}$ was either subtracted or added to the enzyme's molar extinction coefficient (ε_{280}) for Trp and Tyr respectively [47]. The probe's absorbance at 280 nm (almost neglectable) was subtracted in the calculations for enzyme concentration.

Labelled enzyme variants were generally used directly for analysis, but in some cases, they were snap frozen in liquid nitrogen for later analysis. One freezing cycle was not shown to affect the activity of the enzyme or fluorescence of the bimane probe.

Enzyme kinetics. Steady state kinetics were conducted at 10°C in 0.10 M Caps, 0.50 M NaCl, 1 mM $MgCl_2$, pH 9.8. Concentration of para-nitrophenyl phosphate (pNPP) was varied between 0 – 2.0 mM and the initial activity rate measured by the absorbance change at 405 nm over 30 s period using a temperature controlled Evolution 220 spectrophotometer (Thermo Scientific). The exact concentration of pNPP was measured a few hours later after full hydrolysis of the substrate in the cuvettes, by measuring the absorbance at 405 nm using ε_{405} = 18500 $M^{-1}cm^{-1}$. Enzyme concentration was measured at 280 nm using ε_{280} = 61310 $M^{-1}cm^{-1}$ for VAP monomers. K_M and k_{cat} were determined by non-linear fit to the Michealis-Menten equation using GraphPad Prism®.

Urea denaturation. Samples were incubated overnight (14-16 h) at 10°C in 25 mM Mops, 1 mM $MgSO_4$, pH 8.0 or 25 mM Caps, 1 mM $MgSO_4$, pH 10.5 with urea ranging from 0.0 – 6.0 M (added from 8.0 M stock). For bimane-labelled variants, the samples where diluted to A_{380} = 0.001, where the dilution factor from labeled stock was at least 20-fold (stock $A_{380} > 0.020$). When only Trp fluorescence of the wild type was monitored, the enzyme concentration was generally 0.04 mg/ml.

Enzyme activity after urea incubation was measured at 25°C in 1.0 M diethanolamine, 1 mM $MgCl_2$, pH 9.8 using 5 mM pNPP as substrate by monitoring the absorbance change at 405 nm and applying ε_{405} = 18500 $M^{-1}cm^{-1}$.

Fluorescence measurements. All steady state fluorescence measurements were done on a Horiba FluoroMax4-P. For bimane labelled samples, bimane fluorescence was monitored by excitation at 380 nm and the emission measured from 400-600 nm using slit width of 3 nm and 5 nm for excitation and emission respectively. Trp fluorescence was monitored by exciting samples at 295 nm and monitor the fluorescence from 310-400 nm using slit widths of 2 nm and 4 nm for excitation and emission respectively. The bimane probe absorbs slightly at 295 nm and gives a negligible fluorescence background in the Trp fluorescence measurements. The wavelength of maximum fluorescence (λ_{max}) was calculated by fitting the spectra to a 3rd degree polynomial ($y = ax^3 + bx^3 + cx + d$, where y is the fluorescence intensity and x the wavelength) in the range ± 20 nm from the expected value. To acquire λ_{max}, the roots of the first derivative were solved using the quadratic equation for the polynomial.

Time-resolved measurements were performed on a Horiba FluoroMax4-P equipped with a FluoroHub time-correlated single photon counting (TCSPC) system. A NanoLED N370 (370 nm ± 10 nm) from Horiba, which gives a pulse width of <1.2 ns, was used as an excitation

source at 1 Mhz. The emission monochromator was set to 470 nm with slit width of 5 nm, and emission decay rate was measured at 10°C. The instrument prompt was acquired using Ludox colloidal silica at a similar channel stop/start count ratio as for the measured decay, using the same settings except the emission wavelength was set to 370 nm (source excitation maximum). The decay was fitted to a three-exponential model using deconvolution analysis: $I(t) = \alpha_1 \cdot e^{-t/\tau 1} + \alpha_2 \cdot e^{-t/\tau 2} + \alpha_3 \cdot e^{-t/\tau 3}$ where I is the emission count, α_i is the preexponential factor of the i'th component, t is time and τ_i is the lifetime for the i'th component. Then, the relative amplitudes were derived by: $f_i = \alpha_i / \sum \alpha_I$, where f is the relative amplitude and α_I the sum of all the preexponential factors. The average lifetime, $<\tau>$ could then be derived using the equation: $<\tau> = f_1\tau_1 + f_2\tau_2 + f_3\tau_3$. Deconvolution of the prompt was needed to decrease noise in the first channels due to a a 'rebound' occurring at the detector level where photons hit the photon multiplier tube (PMT) then bounce to the detector's glass and then hit again the PMT (this is known by the manufacturer to occur with the N370 LED while using PMT of the R928P type (Personal communication).

Fitting models for VAP denaturation. Generally, fitting strategies described in Walters et al. were used for evaluation of free energy change between enzymatic states [48]. The change in free energy ΔG_i is related to the equilibrium constant K_{eq} for the transition (i) as such:

$$\Delta G_i = -RT \ln(K_{eq}) \tag{1}$$

where R is the gas constant and T the absolute temperature.

The linear extrapolation method was used to estimate $\Delta G_i(H_2O)$ at zero denaturant concentration for each transition (i) [49].

$$\Delta G_i = \Delta G_i(\mathrm{H_2O}) - m[\mathrm{urea}] \tag{2}$$

At pH 8.0, VAP unfolding can be described by a three-state model, where the fraction of native monomers is not populated:

$$\mathrm{N_2} \overset{K_1}{\rightleftharpoons} \mathrm{I_2} \overset{K_u}{\rightleftharpoons} 2\mathrm{U} \tag{3}$$

where N_2 is the native dimer, I_2 a dimer intermediate (inactive) and U the unfolded protein. The equilibrium constant for each transition is described as $K_1 = [\mathrm{I_2}]/[\mathrm{N_2}]$ and $K_u = [\mathrm{U}]^2/[\mathrm{I_2}]$. It can be calculated as:

$$K_I = (1 - f_1) / f_1 \tag{4}$$

$$K_u = 2P_T(1 - f_2)^2 / f_2 \tag{5}$$

where P_T is the total monomer concentration, f_1 is the fraction of protein in the native active state with $f_1 = [I_2]/[N_2]$, and f_2 the fraction in the dimer intermediate state with $f_2 = 2[I_2]/(2[I_2]+[U])$. K_I was determined using activity measurements where f_1 at zero molar urea was set to 1.0 as a relative constant. For K_u the f_2 at each measurement was determined using Trp fluorescence by normalizing the signal with the pre/post slope normalization method [49].

For measurements done at pH 10.5, the denaturation was a two-state process with no populated intermediates:

$$N_2 \overset{K_u}{\rightleftharpoons} 2U \tag{6}$$

Here, K_u was calculated as in Eqn. (5) but f_2 becomes: $f_2 = 2[N_2]/(2[N_2]+[U])$. Either Trp fluorescence or activity measurements as a function of urea could be used to evaluate K_u at pH 10.5.

Refolding/reactivation experiments. For refolding experiments, enzyme between 0.1-0.2 mg/ml was pre-incubated in urea at 4.0 M urea overnight (14-16 h) at 10 °C in 25 mM Mops, 1 mM $MgSO_4$, pH 8.0. Samples were then diluted 10-times in the same buffer with various added salts ($MgSO_4$, $MgCl_2$, Na_2PO_4). The samples where then immediately added to a quartz fluorescence cell (20-30 sec mixing time) and emission recorded at 330-370 nm with 295 nm excitation using slit-widths of 5 nm for both emission and excitation. Emission spectra were then continuously recorded for a 30-min period. This caused slight photobleaching of the sample with time, but did not affect the wavelength of maximum intensity λ_{max}. Before diluting the sample, the emission intensity was recorded using the same settings as above, except the excitation slit-width was set to 2 nm (time zero). The λ_{max} value was calculated as described previously.

The reactivation experiments were conducted identically as the folding experiments at 2.0 M urea (completely inactive) or 0.4 M urea (approximately half activity). Activity was measured as described above. Initial activity was measured in the sample before urea addition.

Results

Fluorescence labeling of VAP with monobromobimane (mBrB). VAP was labelled with mBrB at two regions at the dimer interface for the tryptophan and tyrosine induced quenching (TrIQ/TyrIQ) strategies, where either Trp or Tyr served as intermolecular quenchers for the bimane fluorophore. The dimer of APs has a twofold symmetry (as most homodimers) with an isologous interface. Thus, residues at the interface are not in symmetric positions except close to the twofold rotational axis. Thus, the Cys residues that we introduced in each monomer, in order to attach the bimane probe, did not face each other and form a disulfide. The residues in VAP that can interact symmetrically across the interface are distributed evenly along the twofold rotational axis and are four in total; located at I50-G51, P16-N17, W460-G461 and N433-E434 (lime-green diamonds in Figure 1). Such point symmetries are usually located in antiparallel beta sheets of homodimers (as observed in locations 1 and 3 of Figure 1 in VAP) and less commonly in antiparallel coiled-coil contacts that are packed by ridges to grooves topology (location 2 in VAP in Figure 1). The ECAP N-terminal helix also serves as an example. However, it is fairly uncommon to find these symmetrical interactions at more flexible loop regions (which is the case for location 4 in Figure 1) [15].

The first labeling site that was chosen is located on a short loop juxtaposing F355 (native non-quenching control) at the base of the large interface loop of the other monomer (Figure 1, right inset). This site was chosen due the fact that the enzyme variant F355W has been found to have identical kinetic properties as the wild type [43]. Thus, it is a minimally perturbing mutation despite the fact that this site is also located close to the active site at the base of the large surface interface loop and close to symmetric point 2. Cys was introduced at each position in the loop formed by residues 58-61 (E58C, D59C, A60C, I61C). Their α-carbon distances from F355 at the other monomer are shown in Figure 1. The shortest distance is 6.0 Å for A60-F355 and the longest 10.0 Å for E58-F355. Since A60C would be the most optimally quenched site for the bimane fluorophore in this loop, a Trp residue replacing Phe was introduced at site 355 for that variant (A60C/F355W) to act as intrinsic quencher.

In the second site we studied, Cys was incorporated at K486C, close to symmetric-point 1, which has α-carbon distance of 7.6 Å to Y42 of the other monomer (Figure 1). A Y42F variant was used as a control for the TyrIQ (K486C/Y42F), which also resulted in loss of hydrogen bond between K486 and Y42.

Two labeling control sites, one located at an exposed position in the crown domain (S373) and the other at the large interface loop (S337), were used to evaluate the effect of introducing

bimane at exposed positions. These two sites have previously been labelled in VAP with a methanethiosulfonate spin-label [50].

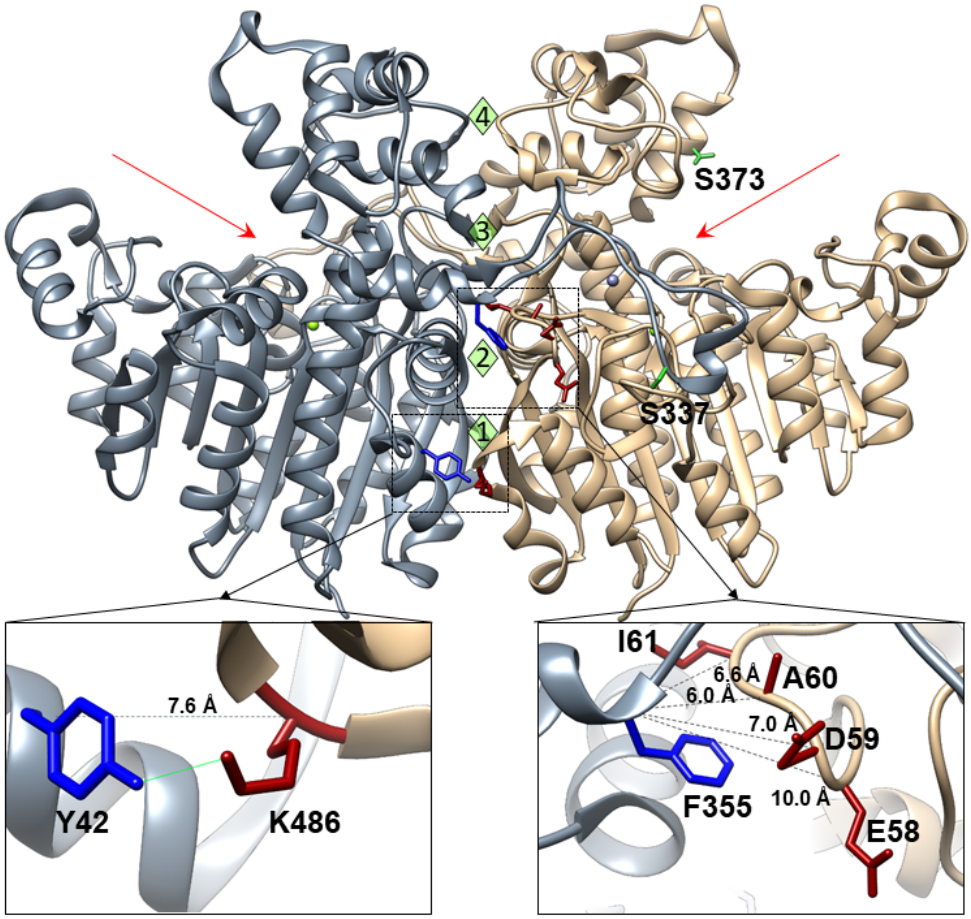

Figure 1. The locations of altered residues in the VAP crystal structure (PDB: 3E2D). Cys was introduced at the interface shown in red in the expanded views (E58C; D59C; A60C; I61C; K486C) and at the surface in positions meant to serve as labeling controls lime-green (S337C and S373C). Red arrows point towards the two independent active sites where the Mg^{2+} ion in the M3 site is shown in green and the two Zn^{2+} ions for each active site are shown in purple. Highlighted in blue are the two residues F355 and Y42 that were meant to act as intermolecular fluorescence quenchers of bimane in the TrIQ/TyrIQ strategy. Their α-α carbon distances from the labelled site are indicated. Lime-green diamonds show the point symmetries at the two-fold rotational axis of the residue pairs I50-G51, P16-N17, W460-G461 and N433-E434, respectively.

VAP has one native Cys residue which was not possible to label in the native state due to low accessibility at that site (Figure S1). This was convenient, since the C67S variant that would have been needed in order to introduce bimane singularly at other sites, has 40% lower k_{cat} than the wild-type [50]. However, with the enzyme unfolded in 4 M urea, the C67 site was near 100% labelled (data not shown). The absorbance maximum was similar for all the variants, ranging from 381-388 nm (free probe in buffer = 396 nm) [46]. The fluorescence emission maximum (λ_{max}) ranged from 464-474 nm, where VAP variants A60C and A60C/F355W had the most blue-shifted emission spectra and were thus likely the most buried. The surface location of the

S337C and S373C controls was reflected in emission maxima at 474 and 472 nm, respectively. Thus, in the other variants the bimane probe was in a slightly buried position, except in K486C which had emission maximum at 473 nm.

Table 1. Kinetics and labeling of VAP variants.

	Labeling efficiency (mol/mol)[a]	λ_{max} **abs (nm)**	λ_{max} **emm (nm)**	k_{cat} **(s^{-1})**[b]	K_M **(μM)**	k_{cat}/K_M **($s^{-1}M^{-1}$)**	k_{cat} **(labeled) (s^{-1})**	K_M **(labeled) (μM)**	k_{cat}/K_M **(labeled) ($s^{-1}M^{-1}$)**
WT[c]	-	-	-	302 ± 20	194 ± 30	1.6×10^6	-	-	-
E58C	0.49	388	471	45 ± 7	390 ± 64	1.2×10^5	24 ± 4	382 ± 52	6.3×10^4
D59C	0.76	386	471	106 ± 16	318 ± 40	3.3×10^5	69 ± 12	252 ± 25	2.7×10^5
A60C	0.63	382	468	105± 7	373 ± 27	2.8×10^5	41 ± 7	213 ± 22	1.9×10^5
I61C	0.64	386	470	49 ± 4	260 ± 31	1.9×10^5	10 ± 3	143 ± 17	7.0×10^4
F355W[c]	-	-	-	255 ± 56	218 ± 20	1.2×10^6	-	-	-
A60C/F355W	1.05	387	464	6 ± 2	314 ± 19	1.9×10^4	2 ±1	185 ± 21	1.1×10^4
K486C	0.43	381	473	195 ± 12	138 ± 36	1.4×10^6	265 ± 27	250 ± 24	9.7×10^5
Y42F	-	-	-	262 ± 33	258 ± 29	1.0×10^6	-	-	-
K486C/Y42F	0.60	383	473	83 ± 10	134 ± 9	6.2×10^5	91 ± 7	167 ± 21	5.4×10^5
S337C	0.42	385	474	92 ± 10	208 ± 22	4.4×10^5	102 ± 18	323 ± 45	3.2×10^5
S373C	0.35	384	472	82 ± 18	220 ± 35	3.7×10^5	70 ± 5	241 ± 39	2.9×10^5

[a] Protein concentration was evaluated using A_{280} and by subtracting the label contribution at 280 nm. Bimane concentration was calculated using $\varepsilon_{380} = 5000\ M^{-1}cm^{-1}$. Absorbance spectra can be found in Figure S2.
[b] Enzyme kinetics were performed in 0.10 M Caps, 1 mM $MgCl_2$, 500 mM NaCl, pH 9.8 °C (10°) using para-nitrophenyl phosphate (pNPP) as substrate.
[c] Data from reference [43].

The emission decay spectra for bimane labelled variants were all fitted with three-variable exponential fits as shown in Table S1. Due to photon rebound seen in the instrument prompt in the first channels (~ 1.0 ns) using the 370 nm LED excitation source, it was hard to accurately determine the shortest lifetime (1-2 ns). Thus, deconvolution analysis for the prompt was used.

In all cases, the bimane probe showed three lifetimes (short, medium and long), which is not uncommon for the bimane probe [44, 45]. For the loop 58-61 variants, the lifetimes were quite similar, except that the amplitude distribution varied. The average lifetime $<\tau>$ was lowest for the E58C labelled site (3.5 ns), which is likely due to proximity to Y77, an intramolecular quencher (α-carbon distance 5.4 Å). Incorporation of a Trp residue to position 355 (F355W) had a small effect on the emission decay, where the average lifetime $<\tau>$ decreased from 6.9 ns to 6.6 ns, indicating that the dynamic quenching component of F355W was small. However, when measuring the decay of the unfolded A60C/F355W variant the average lifetime increased to 10.0 ns, indicating that in the folded state the bimane probe attached to A60C was quenched by other means (main chain or other residues). This average lifetime was similar to the S337C control located at an exposed site. Furthermore, the steady-state emission spectra of A60C compared to A60C/F355W shows that the emission increased slightly when F355W is introduced (Figure 2A). This increase in emission might be caused by the bimane probe being more buried and excluded from the solvent in the A60C/F355W variant, since the λ_{max} decreased from 468 nm to 464 nm.

A similar trend was seen for the K486C bimane-labelled variant. Comparing the steady-state emission of K486C (with Y42 as quencer) and K486C/Y42F (absence of quencer) there was little change in emission (Figure 2C) or in the emission decay (Figure 2D).

Effect of labeling on enzyme kinetics. We have previously observed that incorporation of Cys residues to various sites in VAP decreased the activity of the enzyme substantially [50]. Here, all of the Cys replacements decreased the k_{cat} and most of the substitution increased the K_M (Table 1). For the single Cys incorporations, the k_{cat} was lowest for E58C and I61C, being about 15% of the wild-type. Incorporation of the bimane label decreased k_{cat} further for all the loop 58-61 variants (E58C, D59C, A60C, I61C) while the K_M decreased for D59C, A60C and I61C. For the S337C and S373C variants (labeling controls), there was no change in k_{cat} after labeling, but the K_M increased for S337C after labeling (this residue is located on the large interface loop). The K486C substitution had a lesser impact on k_{cat} compared to the other interface variants, being 65% of the wild-type and K_M was slightly reduced. Furthermore, when the bimane label was introduced at site K486C, the k_{cat} increased with a subsequent increase in K_M , this variant being similar to the wild-type without the biamane attached. In the double variant K486C/Y42F, the k_{cat} decreased further compared to K486C but the K_M was similar. The Y42F mutation by itself did not affect the enzyme kinetics.

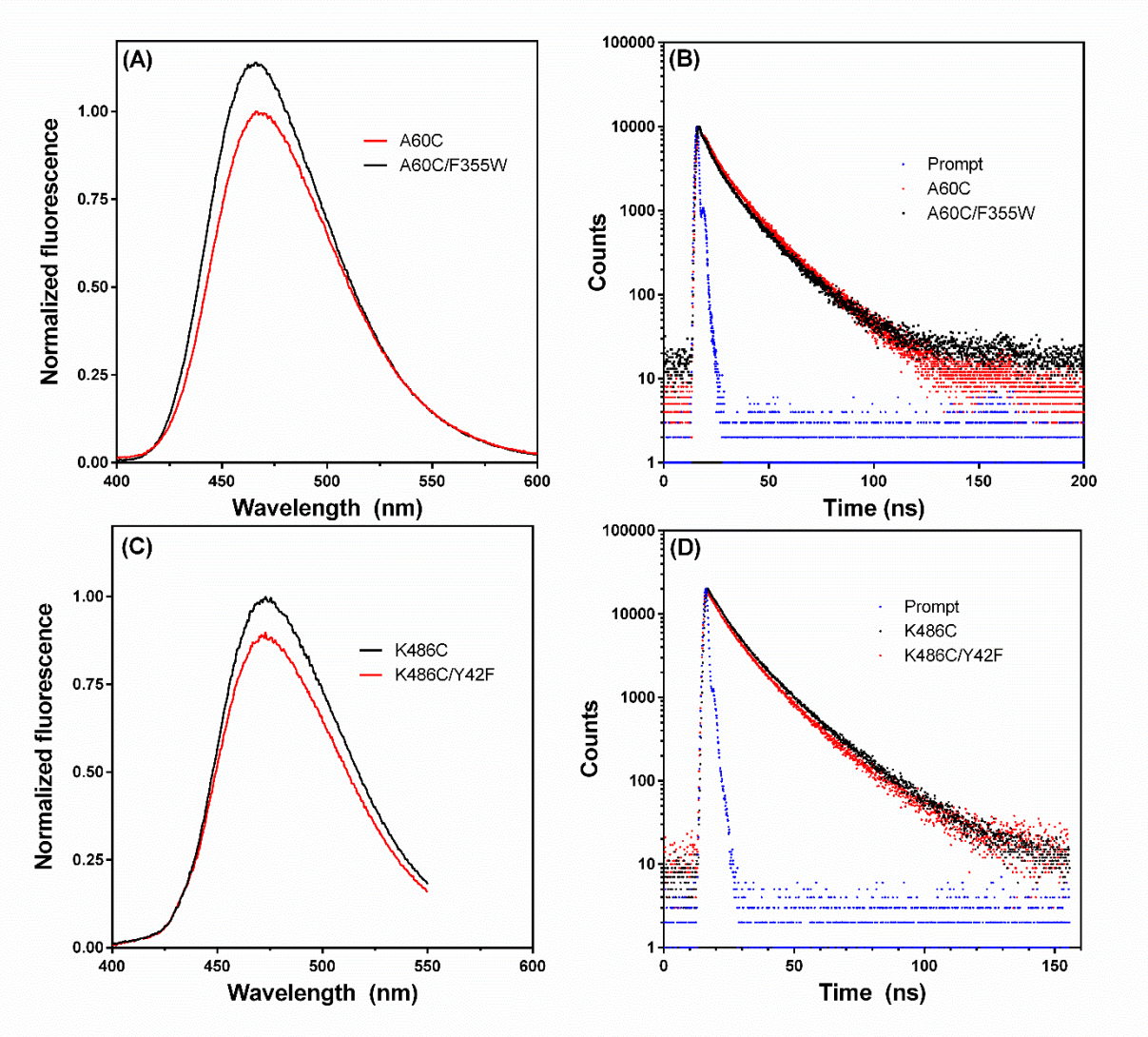

Figure 2. Bimane fluorescence of the interface residues A60C and K486C in VAP. (A, C) Bimane emission spectra of A60C/F355W, K486C and their phenylalanine analogs (controls), A60C and K486C/Y42F. (B, D) Lifetime decays of bimane probes at positions K486C and A60C. The instrument prompt is shown in blue. Enzymes were measured in 25 mM Mops, 1 mM $MgSO_4$, pH 8.0 at 10°C.

The most intriguing kinetic result was seen for the double variant A60C/F355W, where k_{cat} was only 2% of the wild-type and the K_M increased by 60% resulting in a k_{cat}/K_M of less than 1% compaired to the wild-type. Interestingly, the F355W mutation on its own had no effect on the kinetic constants, but lost its neutrality when accompanied by the second mutation in A60C/F355W. This pairing had a dramatic effect on the functional parameters for catalysis. Furthermore, the A60C/F355W variant was difficult to express with only 10% of the culture yield compaired with the other Cys variants (K486C and K486C/Y42F were also problematic).

TrIQ/TyrIQ fluorescence quenching at the interface follows the main denaturation steps of VAP. Previously, we have shown that the urea denaturation mechanism of VAP involves an inactive dimer intermediate [43]. We have wondered if folded, inactive monomers are populated

during the unfolding process $(N_2 \rightleftharpoons I_2 \rightleftharpoons 2I \rightleftharpoons 2U)$, or if they co-unfold as the dimer dissociates $(N_2 \rightleftharpoons I_2 \rightleftharpoons 2U)$. By inducing the dimers to dissociate by dilution and measuring the specific activity of the enzyme, the dimer dissociation constant has been reported to be in the 1-20 nM range, depending on pH and the presence of ions [42]. This gives a free energy change for dimer dissociation of 44-54 kJ/mole. We were curious to see if the inactivation $(N_2 \rightleftharpoons I_2)$ or dimer dissociation could be detected using bimane fluorescence at the selected sites (A60C and K486C) since bimane is both sensitive to changes in polarity and intrinsic quenchers (mainly Tyr and Trp) and would give a local signal at the dimer interface.

For the A60C/F355W variant, the denaturation process was a three-state process using bimane fluorescence as a probe, while the Trp fluorescence curve was two-state (Figure 3A). The first transition in the bimane curve correlated with a drop in activity. However, it should be noted that for the wild-type the fall in activity and the Trp fluorescence transition did not overlap at pH 8.0 as seen here for A60C/F355W (see later in Figure 5) and the transition was much steeper for the wild-type (higher *m*-value) than for the A60C/F355W and A60C variants. Thus, the A60C substitution (and/or labeling) resolved the signals of the two transitional events producing a two-state bimane denaturation curve (Figure 3B). For A60C, the midpoint of the Trp fluorescence curve denaturation was slightly higher than for bimane, which could be due to a destabilization caused by bimane labeling (labelling efficiency ~ 60%). In other words, the Trp fluorescence might have reflected the whole population of molecules, but bimane fluorescence only the labeled enzyme molecules, the latter being less stable.

Similarly, as for A60C/F355W, the structural transition of the K486C labeled variant was three-state as reflected in the bimane fluorescence (Figure 4A). The Trp fluorescence, however, indicated a two-state unfolding process and like the wild-type had almost no overlap with the activity transition. The bimane-labelled K486C/Y42F variant showed a two-state transition for both bimane and Trp fluorescence (Figure 4B). Again, a slight destabilization was caused by the bimane label incorporation. Bimane urea curves for all the other Cys variants in the present study showed a two-state unfolding pathway (Figure S3).

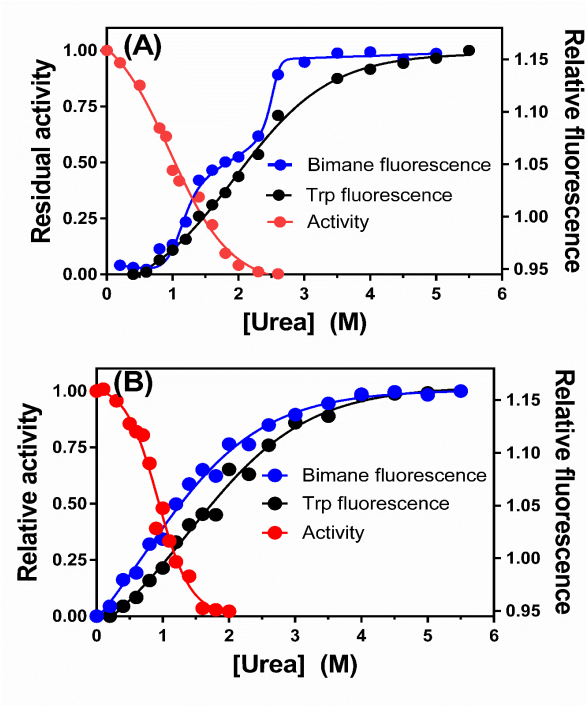

Figure 3. Urea denaturation of the A60C/F355W (A) and A60C (B) VAP variants labelled with the bimane fluorescence probe. After labeling, samples where incubated overnight in 25 mM Mops, 1 mM $MgSO_4$, pH 8.0 with urea ranging from 0-6 M and subsequently assayed for bimane- and tryptophan fluorescence as well as activity. Fluorescence states were monitored by the change in the intensity ratio of 355/340 nm and 468/475 nm for Trp and bimane fluorescence, respectively (right axis).

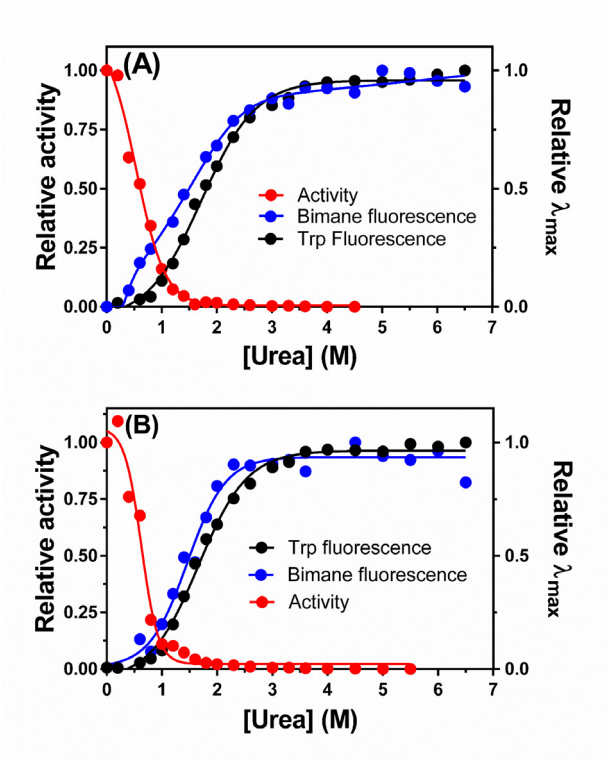

Figure 4. Urea denaturation of K486C (A) and K486C/Y42F (B) VAP variants labelled with the bimane fluorescence probe. After labeling, samples where incubated overnight in 25 mM Mops, 1 mM $MgSO_4$, pH 8.0 in urea ranging from 0-6 M and subsequently assayed for bimane- and tryptophan fluorescence as well as activity. Fluorescence states were monitored by the change in λ_{max} which was normalized.

The free energy for VAP denaturation under different conditions. The results from the TrIQ/TyrIQ denaturation in Figures 3 and 4 indicated a change in the surroundings of the bimane probe upon inactivation regarding polarity of interacting groups. To see if the inactivation was enzyme concentration dependent, urea denaturation was performed under two enzyme concentrations (0.70 and 0.070 μM) at pH 8.0 (Figure 5A). This would indicate if dimer dissociation was a key event. The deactivation transition was not enzyme concentration dependent, whereas the Trp fluorescence denaturation midpoint was shifted towards lower value with lower concentration of enzyme. This indicated that the folded monomers are not populated in the denaturation process and co-unfold as the dimer dissociates ($N_2 \rightleftharpoons I_2 \rightleftharpoons 2U$). Thus, there is likely a link between folding of the enzyme and association of monomers when produced on the ribosomes.

Reactivation of VAP was attempted after incubation in 0.4 M or 2.0 M urea. The former urea concentration was known to reduce the VAP activity by about 50% without influencing signals from structural probes, whereas the latter concentration produced a completely inactive enzyme. The activity was only slightly recovered by dilution in the presence of inhibitor ions (SO_4^{2-} or PO_4^{2-}) used as active site scaffolds in the reactivation buffer (Figure 6A). The assay was performed with a dilution factor that would be sufficient to relieve any inhibition. Magnesium had no effect on reactivation in either case, and without the inhibitor ions the activity decreased with time after dilution ($MgCl_2$ columns in Figure 6A)

The difficulty in reactivating VAP was compared with recovery of folded structure of VAP as gauged by the blue-shift in maximum of the fluorescence signal. This was not completely reversible by a 10-fold dilution after unfolding the enzyme (4.0 M urea) in buffer containing different ions that might support the native structure. The recovery of folded enzyme was much more efficient in the presence of magnesium or the inhibitor ions, phosphate and sulfate ($MgSO_4$ delivers both). The refolding was a quick process, reaching a plateau in approximately 1 minute (Figure 6B). However, the enzyme did not reach full hydrophobic packing, since the λ_{max}, an indication of solvent accessibility of Trp residues, did not recover to the native value.

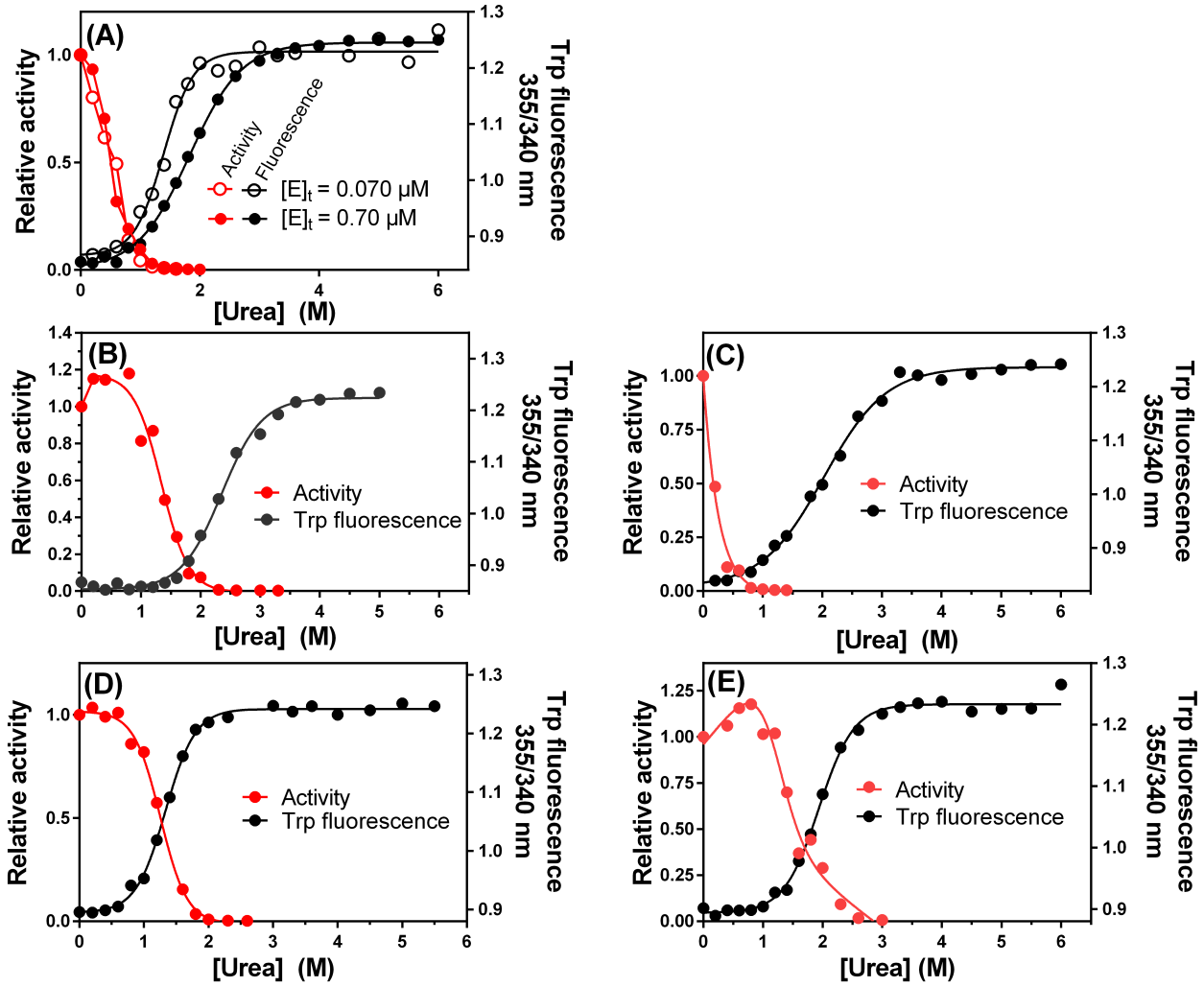

Figure 5. VAP urea denaturation under different conditions. (A) Dependence of enzymatic state transitions induced by urea on enzyme concentration. Samples were incubated overnight in 25 mM Mops, 1 mM $MgSO_4$, pH 8.0 at 10°C with various concentration of urea ranging from 0-6 M. The enzyme was also incubated under the same conditions as in (A) with the addition of 0.5 M NaCl (B) or 10 µM $ZnCl_2$, (C). Furthermore, the enzyme was studied in 25 mM Caps, 1 mM $MgSO_4$, pH 10.5 (D) and 25 mM Caps, 1 mM $MgSO_4$, pH 10.5 + 0.5 M NaCl (E).

Activity was used to reflect the $N_2 \rightleftharpoons I_2$ transition and Trp fluorescence was used to monitor the $I_2 \rightleftharpoons 2U$ transition (Table 2). These could be treated as separate steps since no free folded monomers appeared. At pH 8.0, the ΔG for inactivation was only 2.7 kJ/mol (less than the strength of one hydrogen bond) and 9.8 kJ/mol with 0.5 M NaCl present (Figure 5B and Table 2). Mg^{2+} ions did not affect the inactivation curve but the enzyme's activity was very sensitive to low concentrations of Zn^{2+} which also influenced the way urea at low concentration affected VAP. Thus, at 10 µM Zn^{2+}, the Δ*G* was 1.7 kJ/mol for the structural change that promoted inactivation (Figure 5C) compared with the 2.7 kJ/mol mentioned above. Furthermore, the initial activity in the absence of urea was only 10% with 10 µM Zn^{2+} compared to no addition. At pH 8.0, the Δ*G* for the combined dimer dissociation and monomer unfolding ($I_2 \rightleftharpoons 2U$)

was 48 kJ/mol in buffer and 65 kJ/mol with 0.5 M NaCl present. Zinc (10 µM) had no effect on this transition.

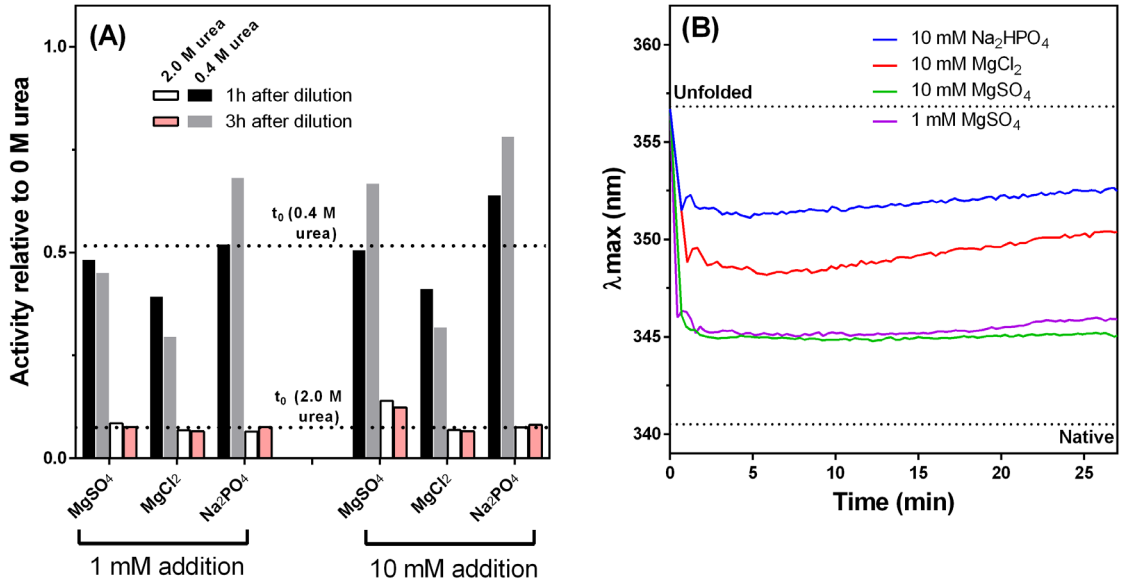

Figure 6. Refolding and reactivation of VAP. (A) Reactivation was tried after incubation in either 0.4 M urea or 2.0 M urea for 4 h by 10-fold dilution in the same buffer without urea (25 mM Mops pH 8.0) but containing $MgCl_2$, $MgSO_4$ or Na_2HPO_4. Activity was measured as described in Materials and Methods after different time points. The activity at time zero (measured before dilution) is shown as dotted lines for 0.4 M urea (the upper dotted line) and 2.0 M urea (lower dotted line). (B) Refolding. Samples were incubated in 4.0 M urea for 4 h and then diluted 10-fold in the same buffer without urea (25 mM Mops pH 8.0) containing $MgCl_2$, $MgSO_4$ or Na_2HPO_4. The Trp emission λ_{max} value was then determined. The dotted lines in the bottom of the graphs denotes the λ_{max} value for the native state without urea addition, for clarity.

Table 2. VAP free energy for denaturation.

	Conditions	**ΔG (kJ/mol)[a]** $N_2 \rightleftharpoons I_2$	**ΔG (kJ/mol)[b]** $I_2 \rightleftharpoons 2U$ (pH 8.0) $N_2 \rightleftharpoons 2U$ (pH 10.5)	**ΔG (kJ/mol)[c]** $N_2 \rightleftharpoons 2U$
pH 8.0	Buffer[d]	2.7 ± 0.3	48 ± 2	-
	Buffer + 0.5 M NaCl	9.8 ± 1.6	65 ± 4	-
	Buffer + 10 µM Zn	1.7 ± 0.2	43 ± 2	-
pH 10.5	Buffer[d]	-	57 ± 1	58 ± 5
	Buffer + 0.5 M NaCl	-	62 ± 2	51 ± 6

[a]Activity vs. urea was used to probe the formation of the inactive dimer intermediate at pH 8.0.
[b]Trp fluorescence vs. urea was used to monitor the dissociation/unfolding of the dimer.
[c]At pH 10.5, activity overlapped with Trp fluorescence urea transitions and could thus also monitor the dissociation/unfolding of the dimer.
[d]At pH 8.0 the buffer composition was 25 mM Mops, 1 mM $MgSO_4$ and at pH 10.5 it was 25 mM Caps, 1 mM $MgSO_4$.

At pH 10.5, the active site stability of VAP was greatly enhanced due to a possible conformational change [42], the enzyme being inactivated at similar concentration of urea as needed to unfold the enzyme (Figure 5D). Thus, the model for inactivation became different from that at pH 8.0 being $N_2 \rightleftharpoons 2U$, where the deactivation and Trp fluorescence transition overlapped completely and either activity or Trp fluorescence reflected the total ΔG. The ΔG at pH 10.5 was estimated at 57 kJ/mol as monitored by Trp fluorescence and 58 kJ/mol using activity. With the addition of 0.5 M NaCl at pH 10.5, there was no significant change in this ΔG value (Figure 5E). However, there was a gradual increase in activity at urea concentration in the range 0-1 M with 0.5 M NaCl present which peaked at 120% of the initial activity. This was seen both at pH 8.0 and pH 10.5 (Figure 5B, E). Similar activation has been reported for other APs induced by low GdmCl concentrations [51, 52].

Discussion

Specific considerations relating to the TrIQ/TyrIQ method. The distance dependent quenching of bimane fluorescence probe by tryptophan or tyrosine (TrIQ/TyrIQ), the method that we employed in this paper, was successfully used earlier to monitor hinge-bending in lysozyme [45] and lid movements in *Thermomyces lanuginosus* lipase [53]. It was well established by labeling lysozyme at different sites, that Trp and Tyr residues in proteins quench bimane fluorescence in a well-defined spherical quenching radius [44, 45]. However, for VAP, when bimane was introduced at sites juxtaposing a Trp or Tyr present on the other subunit, no quenching was observed in the native state (Figure 2). The VAP crystal structure was used to measure the α-carbon distances between the bimane and quencher in the various variants and this was deemed to be inside the sphere of quenching, at least for dynamic quenching (collisional). Furthermore, for the A60C/F355W variant, the distance was only 6.0 Å, where according to theory, bimane should be highly quenched.

What could cause these deviations from expectation based on prior results of others? One explanation could be that VAP is a cold-active enzyme and is more flexible and mobile than the mesophilic lysozyme model resulting in less pronounced static quenching component due to rapid motility. A more likely reason is that the loop under study (residues 58-61) adopts another conformer on average in solution than in the packed crystal lattice, or is very mobile in solution. The third reason might be that the defined sphere of TrIQ/TyrIQ quenching is more valid for intramolecular quenching than intermolecular quenching. Having said that, we cannot rule out that the mutations themselves might have promoted distortion of the interface,

especially in the A60C/F355W variant which was close to inactive and showed a blue shift in λ_{max} emission. Nonetheless, it was clear that the lifetime of the bimane probe and its emission increased upon denaturation. Also, the solvent exposure (λ_{max}) changed when the enzyme was deactivated by urea. This effect was only seen when Trp (F355W) or Tyr (Y42) quencher was present at the interface positions opposite of the bimane probe.

VAP denaturation. Using the TrIQ/TyrIQ method, we rationally incorporated the fluorescent probe bimane to the dimer interface, and could derive the most probable denaturation mechanism. Thus, at pH 8.0, the denaturation pathway induced by urea involves an inactive dimer intermediate where the intermediate co-unfolds as the dimer dissociates $(N_2 \rightleftharpoons I_2 \rightleftharpoons 2U)$. Bimane labels at sites A60C or K486C gave local signal as the enzyme was inactivated $(N_2 \rightleftharpoons I_2)$, but only when positioned inside the sphere of quenching of Trp or Tyr at the other monomer (Figure 3 and 4). The deactivation transitions were not enzyme concentration dependent, while the Trp denaturation midpoint (unfolding transition) was shifted towards lower values with lower enzyme concentration (Figure 5A). This can only be explained by unfolding and dissociation taking place simultaneously. Furthermore, we have previously measured the dissociation constant of the VAP dimers by dilution [42], and it was in agreement to the ΔG values measured here. If a model with a populated ensemble of folded monomers $(2I \rightleftharpoons 2U)$ would have been applied to the Trp fluorescence denaturation curve, then the total ΔG would only have been ~10-15 kJ/mol.

The effect of pH and NaCl was evaluated using the presently derived denaturation model. Sodium chloride was shown to increase the stability of the native dimer towards inactivation by increasing ΔG ~ 4-fold at 0.5 M. There was also a stability increase for the $I_2 \rightleftharpoons 2U$ transition in the presence of 0.5 M NaCl which was due to stabilization of the tertiary structure of the monomers [42]. Bringing the pH to 10.5 (above the pK_a transition mentioned above), the denaturation model simplifies to $N_2 \rightleftharpoons 2U$, i.e. with no dimer intermediate populated where the inactivation curve and Trp denaturation curve overlapped (Figure 5D). Interestingly, the ΔG at pH 10.5 was similar to the value obtained at pH 8.0 with 0.5 M NaCl present. At pH 10.5, NaCl had no effect on the estimated free energy change.

We have previously proposed that at pH 8.0, chloride from the addition of NaCl binds to a Zn ion in the active site maintaining active site integrity [42]. Chloride binding to Zn is further supported by Gettins and Coleman (1984) who observed Cl^- coordinated to Zn ion at the M1 site for ECAP using ^{35}Cl and ^{113}Cd nuclear magnetic resonance (NMR) [54]. Moreover, chloride

ion was observed bound to the Zn ion at site M1 in the crystal structure of AP from an extreme halophile *Halomonas sp. 593*. This is the same site where phosphate is coordinated (or sulphate ion) and has a very similar tertiary structure to VAP [55]. Unlike for VAP, no SO_4^{2-} was used in the crystallization conditions (commonly used in high concentration in AP crystallization) of the halophilic AP. Thus, SO_4^{2-} might have displaced a Cl^- during crystallization of VAP. A closely related AP from *Vibrio alginolyticus* was similarly activated by NaCl as VAP, and SO_4^{2-} was shown to prevent the activation effect of Cl^-. This indicated that Cl^- competes with SO_4^{2-} at the same site (here Zn at the M1 site) [56]. Taken together, the effect of NaCl on VAP is likely reflected in Cl^- binding to Zn in site M1. The mechanism of rate enhancement would be encapsulated in the faster displacement of the inorganic phosphate ion at the end of the reaction cycle. However, it could be insightful to see if this kind of reaction mechanism involving chloride, is general for all APs or only applies to some.

We have recently been interested in the inhibitory effect of Zn^{2+}, since VAP is very intolerant to Zn^{2+} (90% of activity is lost at 10 μM). The inhibition most likely results in a competition between Mg^{2+} and Zn^{2+} in the M3 site where Mg^{2+} is either needed to activate the nucleophilic Ser [57] or stabilize interaction beyond the primary coordination sphere, or both [58, 59]. The coordination sphere becomes tetrahedral instead of being octahedral with Mg^{2+}. Thus, VAP is similarly sensitive to Zn^{2+} as the mammalian phosphatases [60, 61]. Only ECAP is generally known to be tolerant to millimolar Zn^{2+}. However, an ECAP variant resembling mammalian APs (D153H/K328H) showed similar properties as the mammalian APs towards Zn^{2+} inactivation [62-64]. In the D153H ECAP variant, a tetrahedrally coordinated Zn^{2+} was bound in the M3 site in contrast to octahedral geometry when magnesium is bound there [63]. In VAP, His occupies the equivalent position to D153 in ECAP (H116) and Trp in the position of K328 in ECAP (W274).

The inactivation process of VAP by total unfolding is irreversible [42, 43, 65], irrespective of the concentration of Mg^{2+} in buffers, or the method used for inactivation (heat or salts). Here, we showed that activity can be recovered slowly and only partially in the presence of competitive inhibitor ions (SO_4^{2+} and PO_4^{2+}). The ions, which bind and cross-link the interior of the active-site, might help recover correct positions and/or rotameric states of the substrate binding groups, such as Zn^{2+} or Arg166 (Figure 6A). Although the refolding of the tertiary structure of the enzyme was quick (less than 1 min), the initial fluorescence signal was only partially recovered in the presence of either magnesium or competitive inhibitor ions (Figure 6B).

Interface "cross-talk" and half-of-sites reactivity. The half-of-sites reactivity of APs, where one active site ejects the product when the other binds a new substrate through a reciprocal structural change, has been difficult to measure directly. A plausible explanation for the difficulty is that the half-of-sites nature must involve a subtle conformational change that is difficult to detect in a mixed state. During purification, APs usually have a phosphate occupied in each active site, which needs to be removed, by denaturation and dialysis [24-26], which is not always possible do to the inactivation process being irreversible. Furthermore, the presumed asymmetry that must be present at some point in the catalytic cycle might only be reflected in one subunit. In other words, only one subunit might be active in catalysis while the other subunit has undergone a conformational change in order to release the product from the active subunit. Possibly, such conformational changes in the inactive subunits may be driven by a positive change in entropy through bound water networks that spur on the catalytic events in the active subunit [18]. Some have also suggested that Mg^{2+} assists in binding of substrate and the release of product in each cycle, and may come and go repeatedly [26]. Furthermore, by studying the inactivation rates of Apo-ECAP, magnesium binding to one Zn-AP monomer was shown provide stability and indicated long distance interaction between active sites for metal ion binding [66].

Upon denaturation, the TrIQ/TyrIQ data indicated that when the enzyme adopts the inactive dimer form, the bimane probe at positions A60 adopts another conformer relative to F355W. The change was also detected at site K486 opposite Y42 at the other monomer, but was subtler. These changes (three-state denaturation in Figure 3A and 4A) are not seen unless Trp or Tyr is incorporated at the opposite subunit, strengthening the argument for an intersubunit interaction.

If VAP (and APs in general) utilize a reaction mechanism of half-of-sites nature, then the enzyme's activity should be particularly intolerant to changes in these interface regions due to a network(s) of interactions, providing a link between the two active sites through the interface. This effect might involve the crystal water molecules observed both in the active site and at the monomer interface in the crystal structure of VAP (3E2D) [41] and other APs.

Figure 7 shows the average effect of interface mutations on k_{cat} (Figure 7A) and K_M (Figure 7B). Mutations in the large interface loop (Q334L, R336L and Y346F) only moderately decreased k_{cat} but did not affect K_M (region 1). All the other single variants involving Ser → Cys substitutions (region II, III and IV) had a negative effect on k_{cat}. Alterations in region II produced an increase in K_M, while changes in regions III and IV lowered K_M. Thus, the interface around region II and III might be important in forming catalytically important interface

networks. Furthermore, for region II (loop 58-61) the catalytic efficiency dropped when bimane was introduced in all cases.

Point symmetry locations differ between APs, mostly due to gene inserts or deletions, usually located at the crown domain or the interface (e.g. the N-terminal helix for ECAP and the VAP large surface loop insert). Asymmetric collective motions in dimers are mediated through these axes where the subunits can rotate relative to each other or by axial shifts that cause break of symmetry leading to different rotameric states of interface side-chains [18, 67]. By comparing the crystal structures of VAP (3E2D), ECAP (1ED9) and PLAP (1ZEF) there is only one common point of symmetry located at the small antiparallel beta sheet where W460 (for VAP) is located (Figure S4). Thus, if the half-of-sites reactivity is present in all APs then this "conserved" symmetry point might be crucial. In fact, we have shown that W460F has only 10% catalytic efficiency of the wild-type and W460I is close to inactive [43]. This residue is conserved in all APs as an aromatic amino acid (usually Tyr or Trp). Also, *Shewanella sp.* AP has a fourth metal ion binding site with Mg^{2+} bound close to the interfacial symmetry axis (where W460 resides in VAP) [68]. It remains to be tested if the W460I variant in VAP was monomeric as mutations in PLAP at N417 (corresponding to N395 in TNAP and T462 in VAP) cause hypophosphatasia in humans due to the formation of an inactive monomer [69]. However, for PLAP the enzyme was correctly exported to the cell membrane and had similar N-glycosylation as the wild-type. Possibly an inactive dimer was formed, which did not survive the semi-native SDS-PAGE treatment as well as the wild-type due to a less stable dimer.

How would asymmetry be transmitted through this site? For caspase 9, a Phe residue is reoriented at the symmetric axis to avoid steric class resulting in a long range activation at the active site giving rise to half-of-sites reactivity [16]. Possibly, W460 might show similar flip-flop rotation in the catalytic cycle (so called "g+" or "g-" rotameric conformations). For this to happen, the main chain at the anti-parallel strand (residues 458-462) needs to have some rotational freedom. In fact, the strand is bent at the symmetrical axis between W460 and G461, which makes it drawn either as a loop or a β-strand, depending on graphical software (Figure 4S).

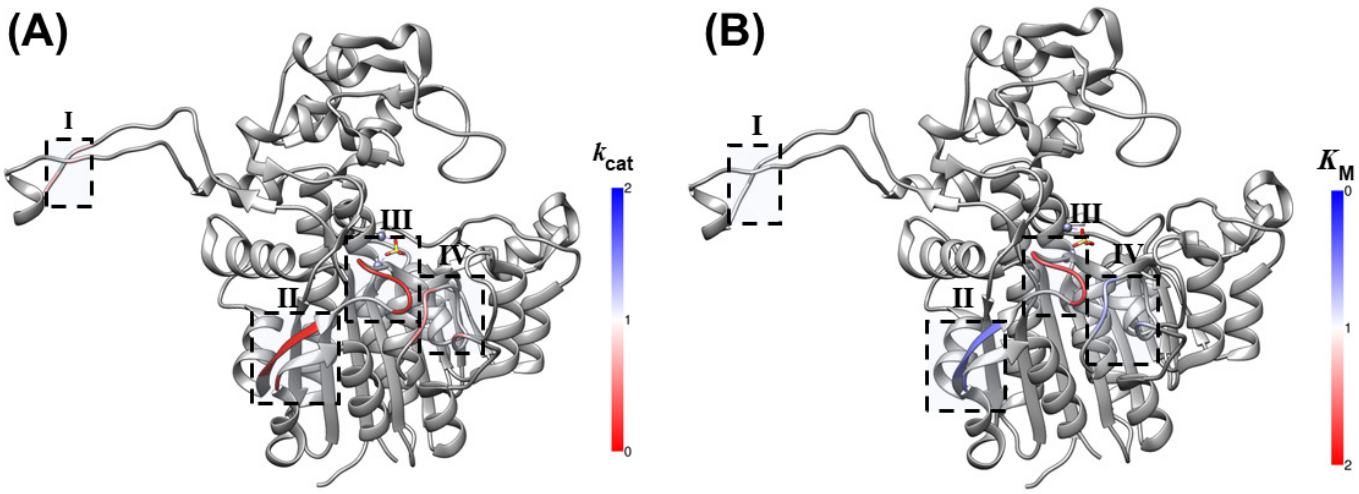

Figure 7. The four interface regions where the effect of residue replacements in VAP affected steady-state kinetics. Four interface regions where compared using the average k_{cat} (A) and K_M values (B) calculated for each region relative to the wild-type values. Region I is on the long insertion-loop characteristic of VAP. The comparison there consisted of variants Q334L, R336L and Y346F (unpublished). Region II consisted of variants K486C, I50C, G51C, S52C and S53C [70]. Region III consisted of variants E58C, D59C, A60C and I61C, and Region IV consisted of variants S78C, S79C, S80C and S87C [50, 70]. Blue color intensity denotes a positive effect (lower K_M or higher k_{cat}) and red color a negative effect (higher K_M or lower k_{cat}). An average value for all variants was calculated for each region to simplify the interpretation. Note that region IV forms interfacial contacts with the large interface loop mentioned above as region I.

Conclusion.

At pH 8.0, VAP denatures in a three-state process. First, an inactive dimer is formed and secondly, the subunits co-unfold as they dissociate. NaCl stabilized the enzyme towards inactivation and provided stabilization toward the denaturation of monomers resulting in a ΔG of 75 kJ/mol for the whole $N_2 \rightleftharpoons I_2 \rightleftharpoons 2U$ transition. Bringing the pH up to 10.5 stabilized the dimer towards inactivation and the denaturation pathway became a two-state process ($N_2 \rightleftharpoons 2U$) not affected by NaCl. TrIQ and TyrIQ quenching of the fluorescence probe bimane at the interface showed that upon inactivation of the dimer the subunits lose communications which indicate half-of-sites reactivity. Furthermore, we propose that interface network dynamics pass through a common point located by group symmetry on a short antiparallel beta sheet at the interface beneath the crown domain, close to the active site.

AUTHOR INFORMATION

Corresponding Author

* Corresponding authors: Bjarni Ásgeirsson, email: bjarni@hi.is and Jens Guðmundur Hjörleifsson, email: jgh4@hi.is

Associated content

Supporting information. Table with time resolved fluorescence data. The location of Cys67 in the VAP crystal structure. Absorbance spectra of labeled enzyme variants. Denaturation curves of bimane variants with urea. VAPs residues 458-462 at the symmetric axis aligned to ECAP and PLAP.

Author Contributions

The manuscript was written through contributions of both authors. Both authors have given approval to the final version of the manuscript.

Funding Sources

Financial support from the Icelandic Research Fund (project 141619-051) and the Science Institute of the University of Iceland is gratefully acknowledged.

Abbreviations

AP, alkaline phosphatase; VAP, *Vibrio* alkaline phosphatase; ECAP, *E. coli* alkaline phosphatase; TrIQ/TyrIQ, tryptophan and tyrosine induced quenching; mBrB, mono-bromo bimane; pNPP, para-nitrophenyl phosphate; PMT, photon multiplier tube; LED, light emitting diode; GdmCl, guanidium chloride; PLAP, placental alkaline phosphatase;

References

(1) Marianayagam, N. J., Sunde, M., and Matthews, J. M. (2004) The power of two: protein dimerization in biology, *Trends Biochem Sci 29*, 618-625.

(2) Marsh, J. A., and Teichmann, S. A. (2015) Structure, dynamics, assembly, and evolution of protein complexes, *Annu Rev Biochem 84*, 551-575.

(3) Monod, J., Wyman, J., and Changeux, J. P. (1965) On the nature of allosteric transitions: A plausible model, *J Mol Biol 12*, 88-118.

(4) Mei, G., Di Venere, A., Rosato, N., and Finazzi-Agro, A. (2005) The importance of being dimeric, *FEBS J 272*, 16-27.

(5) Traut, T. W. (1994) Dissociation of enzyme oligomers: a mechanism for allosteric regulation, *Crit Rev Biochem Mol Biol 29*, 125-163.

(6) Danyal, K., Shaw, S., Page, T. R., Duval, S., Horitani, M., Marts, A. R., Lukoyanov, D., Dean, D. R., Raugei, S., Hoffman, B. M., Seefeldt, L. C., and Antony, E. (2016) Negative cooperativity in the nitrogenase Fe protein electron delivery cycle, *Proc Natl Acad Sci U S A 113*, E5783-E5791.

(7) Freiburger, L. A., Baettig, O. M., Sprules, T., Berghuis, A. M., Auclair, K., and Mittermaier, A. K. (2011) Competing allosteric mechanisms modulate substrate binding in a dimeric enzyme, *Nat Struct Mol Biol 18*, 288-294.

(8) Joseph, E., Le, C. Q., Nguyen, T., Oyugi, M., Hossain, M. S., Foss, F. W., Jr., and Johnson-Winters, K. (2016) Evidence of negative cooperativity and half-site reactivity within an F420-dependent enzyme: Kinetic analysis of F420H2:NADP(+) oxidoreductase, *Biochemistry 55*, 1082-1090.

(9) Lanfranco, M. F., Garate, F., Engdahl, A. J., and Maillard, R. A. (2017) Asymmetric configurations in a reengineered homodimer reveal multiple subunit communication pathways in protein allostery, *J Biol Chem 292*, 6086-6093.

(10) Liu, Q., Chai, J., Moche, M., Guy, J., Lindqvist, Y., and Shanklin, J. (2015) Half-of-the-sites reactivity of the castor delta9-18:0-acyl carrier protein desaturase, *Plant Physiol 169*, 432-441.

(11) Simpson, R. T., and Valee, B. L. (1970) Negative homotropic interactions in binding of substrate to alkaline phosphatase of *Escherichia coli*, *Biochemistry 9*, 953-958.

(12) Gunasekaran, K., Ma, B., and Nussinov, R. (2004) Is allostery an intrinsic property of all dynamic proteins?, *Proteins 57*, 433-443.

(13) Popovych, N., Sun, S., Ebright, R. H., and Kalodimos, C. G. (2006) Dynamically driven protein allostery, *Nat Struct Mol Biol 13*, 831-838.

(14) Papaleo, E., Renzetti, G., Invernizzi, G., and Asgeirsson, B. (2013) Dynamics fingerprint and inherent asymmetric flexibility of a cold-adapted homodimeric enzyme. A case study of the *Vibrio* alkaline phosphatase, *Biochim Biophys Acta 1830*, 2970-2980.

(15) Brown, J. H. (2006) Breaking symmetry in protein dimers: designs and functions, *Protein Sci 15*, 1-13.

(16) Renatus, M., Stennicke, H. R., Scott, F. L., Liddington, R. C., and Salvesen, G. S. (2001) Dimer formation drives the activation of the cell death protease caspase 9, *Proc Natl Acad Sci U S A 98*, 14250-14255.

(17) Jin, L., Stec, B., Lipscomb, W. N., and Kantrowitz, E. R. (1999) Insights into the mechanisms of catalysis and heterotropic regulation of *Escherichia coli* aspartate transcarbamoylase based upon a structure of the enzyme complexed with the bisubstrate analogue N-phosphonacetyl-L-aspartate at 2.1 Å, *Proteins 37*, 729-742.

(18) Kim, T. H., Mehrabi, P., Ren, Z., Sljoka, A., Ing, C., Bezginov, A., Ye, L., Pomes, R., Prosser, R. S., and Pai, E. F. (2017) The role of dimer asymmetry and protomer dynamics in enzyme catalysis, *Science 355*, eaag2355.

(19) Song, S. Y., Xu, Y. B., Lin, Z. J., and Tsou, C. L. (1999) Structure of active site carboxymethylated D-glyceraldehyde-3-phosphate dehydrogenase from *Palinurus versicolor*, *J Mol Biol 287*, 719-725.
(20) Ilyin, V. A., Temple, B., Hu, M., Li, G., Yin, Y., Vachette, P., and Carter, C. W., Jr. (2000) 2.9 A crystal structure of ligand-free tryptophanyl-tRNA synthetase: domain movements fragment the adenine nucleotide binding site, *Protein Sci 9*, 218-231.
(21) Bloch, W., and Schlesinger, M. J. (1974) Kinetics of substrate hydrolysis by molecular variants of *Escherichia coli* alkaline phosphatase, *J Biol Chem 249*, 1760-1768.
(22) Bale, J. R., Chock, P. B., and Huang, C. Y. (1980) The nature of negative cooperativity in alkaline phosphatase. Kinetic patterns contrary to the flip-flop model, *J Biol Chem 255*, 8424-8430.
(23) Del Arco, A., Burguillo, F. J., Roig, M. G., Usero, J. L., Izquierdo, C., and Herraez, M. A. (1982) Negative cooperativity in alkaline phosphatase from *E. coli*: new kinetic evidence from a steady-state study, *Int J Biochem 14*, 127-140.
(24) Cioni, P., Piras, L., and Strambini, G. B. (1989) Tryptophan phosphorescence as a monitor of the structural role of metal ions in alkaline phosphatase, *Eur J Biochem 185*, 573-579.
(25) Sun, L., Kantrowitz, E. R., and Galley, W. C. (1997) Room temperature phosphorescence study of phosphate binding in *Escherichia coli* alkaline phosphatase, *Eur J Biochem 245*, 32-39.
(26) Orhanovic, S., and Pavela-Vrancic, M. (2003) Dimer asymmetry and the catalytic cycle of alkaline phosphatase from *Escherichia coli*, *Eur J Biochem 270*, 4356-4364.
(27) Hoylaerts, M. F., Manes, T., and Millan, J. L. (1997) Mammalian alkaline phosphatases are allosteric enzymes, *J Biol Chem 272*, 22781-22787.
(28) O'Brien, P. J., and Herschlag, D. (2002) Alkaline phosphatase revisited: hydrolysis of alkyl phosphates, *Biochemistry 41*, 3207-3225.
(29) Coleman, J. E. (1992) Structure and mechanism of alkaline phosphatase, *Annu Rev Biophys Biomol Struct 21*, 441-483.
(30) Meighen, E., and Yue, R. (1975) Hybrids of chemical derivatives of *Escherichia coli* alkaline phosphatase, *Biochim Biophys Acta 412*, 262-272.
(31) Schlesinger, M. J. (1967) Formation of a defective alkaline phosphatase subunit by a mutant of *Escherichia coli*, *J Biol Chem 242*, 1604-1611.
(32) Applebury, M. L., and Coleman, J. E. (1969) *Escherichia coli* alkaline phosphatase. Metal binding, protein conformation, and quaternary structure, *J Biol Chem 244*, 308-318.
(33) Reynolds, J. A., and Schlesinger, M. J. (1968) Hydrogen ion equilibria of conformational states of *Escherichia* coli alkaline phosphatase, *Biochemistry 7*, 2080-2085.
(34) Boulanger, R. R., Jr., and Kantrowitz, E. R. (2003) Characterization of a monomeric *Escherichia coli* alkaline phosphatase formed upon a single amino acid substitution, *J Biol Chem 278*, 23497-23501.
(35) Levinthal, C., Signer, E. R., and Fetherolf, K. (1962) Reactivation and hybridization of reduced alkaline phosphatase, *Proc Natl Acad Sci U S A 48*, 1230-1237.
(36) Hehir, M. J., Murphy, J. E., and Kantrowitz, E. R. (2000) Characterization of heterodimeric alkaline phosphatases from *Escherichia coli*: An investigation of intragenic complementation, *J Mol Biol 304*, 645-656.
(37) Bobyr, E., Lassila, J. K., Wiersma-Koch, H. I., Fenn, T. D., Lee, J. J., Nikolic-Hughes, I., Hodgson, K. O., Rees, D. C., Hedman, B., and Herschlag, D. (2012) High-resolution analysis of Zn^{2+} coordination in the alkaline phosphatase superfamily by EXAFS and X-ray crystallography, *J Mol Biol 415*, 102-117.
(38) Roberts, C. H., and Chlebowski, J. F. (1984) Trypsin modification of *Escherichia coli* alkaline phosphatase, *J Biol Chem 259*, 729-733.

(39) Tyler-Cross, R., Roberts, C. H., and Chlebowski, J. F. (1989) Proteolytic modification of *Escherichia coli* alkaline phosphatase, *J Biol Chem 264*, 4523-4528.
(40) Olafsdottir, S., and Chlebowski, J. F. (1989) A hybrid *Escherichia coli* alkaline phosphatase formed on proteolysis, *J Biol Chem 264*, 4529-4535.
(41) Helland, R., Larsen, R. L., and Asgeirsson, B. (2009) The 1.4 Å crystal structure of the large and cold-active *Vibrio sp*. alkaline phosphatase, *Biochim Biophys Acta 1794*, 297-308.
(42) Hjorleifsson, J. G., and Asgeirsson, B. (2017) pH-dependent binding of chloride to a marine alkaline phosphatase affects the catalysis, active site stability, and dimer equilibrium, *Biochemistry 56*, 5075-5089.
(43) Hjorleifsson, J. G., and Asgeirsson, B. (2016) Cold-active alkaline phosphatase is irreversibly transformed into an inactive dimer by low urea concentrations, *Biochim Biophys Acta 1864*, 755-765.
(44) Mansoor, S. E., Dewitt, M. A., and Farrens, D. L. (2010) Distance mapping in proteins using fluorescence spectroscopy: the tryptophan-induced quenching (TrIQ) method, *Biochemistry 49*, 9722-9731.
(45) Jones Brunette, A. M., and Farrens, D. L. (2014) Distance mapping in proteins using fluorescence spectroscopy: tyrosine, like tryptophan, quenches bimane fluorescence in a distance-dependent manner, *Biochemistry 53*, 6290-6301.
(46) Kosower, E. M., and Kosower, N. S. (1995) Bromobimane probes for thiols, *Methods Enzymol 251*, 133-148.
(47) Pace, C. N., Vajdos, F., Fee, L., Grimsley, G., and Gray, T. (1995) How to measure and predict the molar absorption-coefficient of a protein, *Protein Sci 4*, 2411-2423.
(48) Walters, J., Milam, S. L., and Clark, A. C. (2009) Practical approaches to protein folding and assembly: spectroscopic strategies in thermodynamics and kinetics, *Methods Enzymol 455*, 1-39.
(49) Pace, C. N. (1986) Determination and analysis of urea and guanidine hydrochloride denaturation curves, *Methods Enzymol 131*, 266-280.
(50) Heidarsson, P. O., Sigurdsson, S. T., and Asgeirsson, B. (2009) Structural features and dynamics of a cold-adapted alkaline phosphatase studied by EPR spectroscopy, *FEBS J 276*, 2725-2735.
(51) Miggiano, G. A., Mordente, A., Pischiutta, M. G., Martorana, G. E., and Castelli, A. (1987) Early conformational changes and activity modulation induced by guanidinium chloride on intestinal alkaline phosphatase, *Biochem J 248*, 551-556.
(52) Chen, Q. X., Zhang, W., Zheng, W. Z., Zhang, Z., Yan, S. X., Zhang, T., and Zhou, H. M. (1996) Comparison of inactivation and unfolding of green crab (*Scylla serrata*) alkaline phosphatase during denaturation by guanidinium chloride, *J Protein Chem 15*, 359-365.
(53) Skjold-Jorgensen, J., Bhatia, V. K., Vind, J., Svendsen, A., Bjerrum, M. J., and Farrens, D. (2015) The enzymatic activity of lipases correlates with polarity-induced conformational changes: A Trp-induced quenching fluorescence study, *Biochemistry 54*, 4186-4196.
(54) Gettins, P., and Coleman, J. E. (1984) Chloride binding to alkaline phosphatase. ^{113}Cd and ^{35}Cl NMR, *J Biol Chem 259*, 11036-11040.
(55) Arai, S., Yonezawa, Y., Ishibashi, M., Matsumoto, F., Adachi, M., Tamada, T., Tokunaga, H., Blaber, M., Tokunaga, M., and Kuroki, R. (2014) Structural characteristics of alkaline phosphatase from the moderately halophilic bacterium *Halomonas sp.* 593, *Acta Crystallogr D Biol Crystallogr 70*, 811-820.
(56) Hayashi, M., Unemoto, T., and Hayashi, M. (1973) pH- and anion-dependent salt modifications of alkaline phosphatase from a slightly halophilic *Vibrio alginolyticus*, *Biochim Biophys Acta 315*, 83-93.

(57) Stec, B., Holtz, K. M., and Kantrowitz, E. R. (2000) A revised mechanism for the alkaline phosphatase reaction involving three metal ions, *J Mol Biol 299*, 1303-1311.
(58) Wang, E., Koutsioulis, D., Leiros, H. K., Andersen, O. A., Bouriotis, V., Hough, E., and Heikinheimo, P. (2007) Crystal structure of alkaline phosphatase from the Antarctic bacterium TAB5, *J Mol Biol 366*, 1318-1331.
(59) Koutsioulis, D., Lyskowski, A., Maki, S., Guthrie, E., Feller, G., Bouriotis, V., and Heikinheimo, P. (2010) Coordination sphere of the third metal site is essential to the activity and metal selectivity of alkaline phosphatases, *Protein Sci 19*, 75-84.
(60) Hung, H. C., and Chang, G. G. (2001) Differentiation of the slow-binding mechanism for magnesium ion activation and zinc ion inhibition of human placental alkaline phosphatase, *Protein Sci 10*, 34-45.
(61) Cathala, G., and Brunel, C. (1975) Bovine kidney alkaline phosphatase. Catalytic properties, subunit interactions in the catalytic process, and mechanism of Mg^{2+} stimulation, *J Biol Chem 250*, 6046-6053.
(62) Murphy, J. E., Tibbitts, T. T., and Kantrowitz, E. R. (1995) Mutations at positions 153 and 328 in *Escherichia coli* alkaline phosphatase provide insight towards the structure and function of mammalian and yeast alkaline phosphatases, *J Mol Biol 253*, 604-617.
(63) Murphy, J. E., Xu, X., and Kantrowitz, E. R. (1993) Conversion of a magnesium binding site into a zinc binding site by a single amino acid substitution in *Escherichia coli* alkaline phosphatase, *J Biol Chem 268*, 21497-21500.
(64) Janeway, C. M., Xu, X., Murphy, J. E., Chaidaroglou, A., and Kantrowitz, E. R. (1993) Magnesium in the active site of *Escherichia coli* alkaline phosphatase is important for both structural stabilization and catalysis, *Biochemistry 32*, 1601-1609.
(65) Gudjonsdottir, K., and Asgeirsson, B. (2008) Effects of replacing active site residues in a cold-active alkaline phosphatase with those found in its mesophilic counterpart from *Escherichia coli*, *FEBS J 275*, 117-127.
(66) Dirnbach, E., Steel, D. G., and Gafni, A. (2001) Mg^{2+} binding to alkaline phosphatase correlates with slow changes in protein lability, *Biochemistry 40*, 11219-11226.
(67) Strater, N., Hakansson, K., Schnappauf, G., Braus, G., and Lipscomb, W. N. (1996) Crystal structure of the T state of allosteric yeast chorismate mutase and comparison with the R state, *Proc Natl Acad Sci U S A 93*, 3330-3334.
(68) Tsuruta, H., Mikami, B., Higashi, T., and Aizono, Y. (2010) Crystal structure of cold-active alkaline phosphatase from the psychrophile *shewanella sp*, *Biosci Biotech Bioch 74*, 69-74.
(69) Sultana, S., Al-Shawafi, H. A., Makita, S., Sohda, M., Amizuka, N., Takagi, R., and Oda, K. (2013) An asparagine at position 417 of tissue-nonspecific alkaline phosphatase is essential for its structure and function as revealed by analysis of the N417S mutation associated with severe hypophosphatasia, *Mol Genet Metab 109*, 282-288.
(70) Asgeirsson, B., Adalbjornsson, B. V., and Gylfason, G. A. (2007) Engineered disulfide bonds increase active-site local stability and reduce catalytic activity of a cold-adapted alkaline phosphatase, *Biochim Biophys Acta 1774*, 679-687.

Supplemental information

Cold-Active Alkaline Phosphatase Undergoes a Subtle Structural Change at the Dimer Interface Upon Inactivation

Jens Guðmundur Hjörleifsson[1]* and Bjarni Ásgeirsson[1]*

[1]Department of Biochemistry, Science Institute, University of Iceland, Dunhagi 3, 107 Reykjavik, Iceland.

* Corresponding authors: Bjarni Ásgeirsson, email: bjarni@hi.is and Jens Guðmundur Hjörleifsson, email: jgh4@hi.is

Table S1.

Enzyme variant	τ_1 (ns)[a]	τ_2 (ns)	τ_3 (ns)[d]	f_1[b]	f_2	f_3	<τ> (ns)	χ^2
S373C	1,4 ± 0.2	7.2 ± 0,8	17.6 ± 0.2	0.43	0.36	0.21	6.8	1.1
S337C	1.8 ± 0.6	9.7 ± 0.4	18.9 ± 0.4	0.18	0.63	0.19	10.0	1.6
E58C	1,2 ± 0.1	6.5 ± 0.1	17.4 ± 0.2	0.58	0.28	0.13	3.5	1.3
D59C	1.4 ± 0.4	8.8 ± 0.5	17.8 ± 0.3	0.29	0.47	0.24	8.8	1.3
A60C	1.4 ± 0.1	8.0 ± 0.4	19.0 ± 0.2	0.45	0.38	0.17	6.9	1.3
A60C/F355W	1.8 ± 0.1	8.1 ± 0.9	19.1± 0.3	0.49	0.36	0.15	6.6	1.2
Unfolded[c] A60C/F355W	4.0 ± 1.7	9.7 ± 3.0	13.4 ± 0.6	0.18	0.48	0.35	10.0	1.2
K486C	0.8 ± 0.1	6.7 ± 0.4	17.0 ± 0.2	0.46	0.38	0.17	5.8	1.2
K486C/Y42F	0.9 ± 0.1	7.2 ± 0.3	16.9 ± 0.2	0.51	0.35	0.13	5.2	1.2

[a] Fluorescence decay was measured using NanoLED N370 source on a Horiba Fluormax 4-P equipped with a FluorHub TCSPC system and emission monochromator set at 470 nm using 5 nm slit width. Measurements were done in 20 mM Mops, 1 mM $MgSO_4$, pH 8.0 at 10 °C. The decay was fitted to a three-exponential decay model using deconvolution analysis: $I(t) = \alpha_1 \cdot e^{-t/\tau 1} + \alpha_2 \cdot e^{-t/\tau 2} + \alpha_3 \cdot e^{-t/\tau 3}$.
[b] $f_i = \alpha_i / \sum \alpha_I$, [c] $\langle\tau\rangle = f_1\tau_1 + f_2\tau_2 + f_3\tau_3$. χ^2 is the chi-squared value of the fit.
[c] Enzyme incubated in 4.5 M urea under same conditions before measurement
[d] Note that longer lifetimes for bimane are reported, likely due to the emission being recorded at 10°C, compared to 25°C, where viscosity of water is higher (increased solvent relaxation).

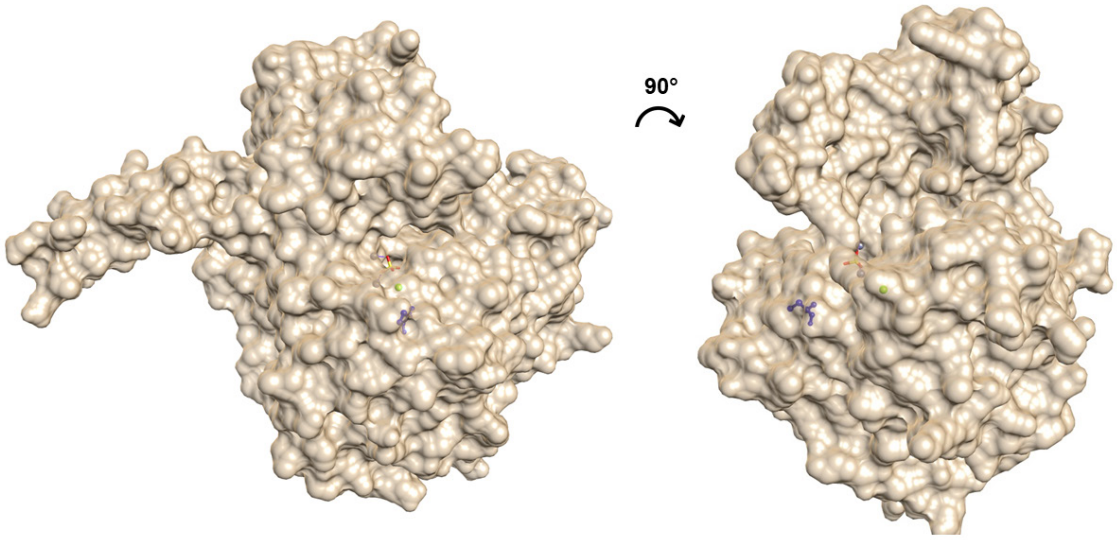

Figure S1. Cys67 is buried away from the solvent and not accessible for labeling. The surface plot is 50% transparent showing C67 in blue, sulphate ion in the active site in yellow, Zn^{2+} ons in purple and Mg^{2+} in lime green (PDB: 3E2D).

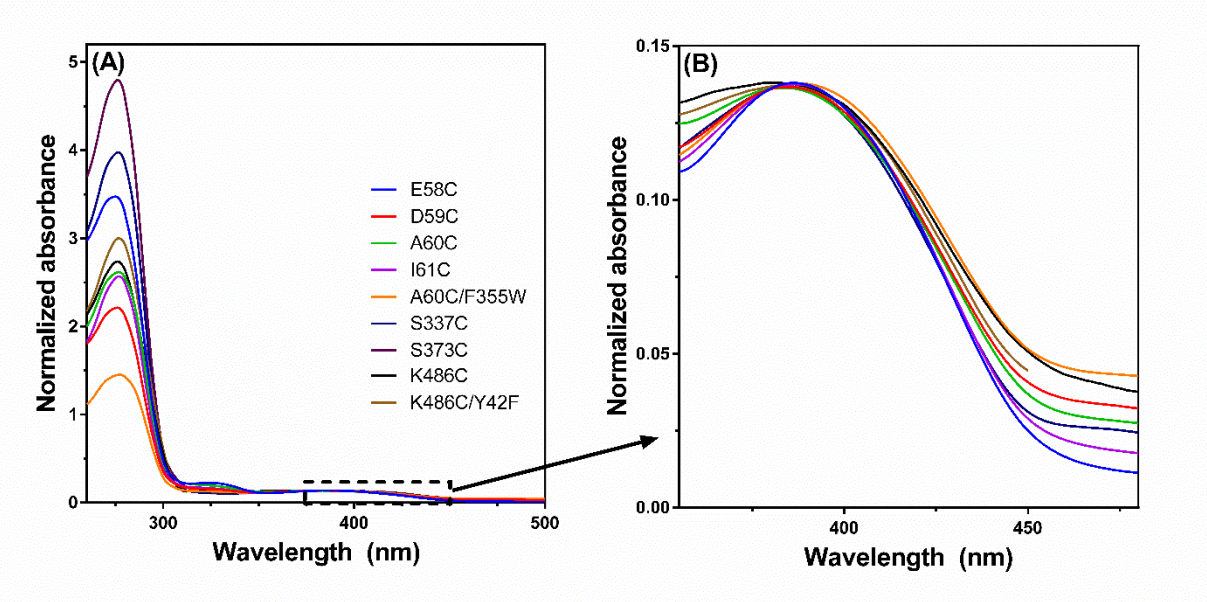

Figure S2. Labeling of VAP Cys variants with monobromo bimane (mBrB). Absorbance spectra of labeled samples were normalized at 380 nm. Labeling was done using 1 mM mBrB, 20 mM Mops, 2 mM $MgSO_4$, pH 7.5 at 4°C overnight. Free probe was filtered away on Amicon Ultra-30 columns. The dilution was at least 10.000 fold and no absorbance at 380 nm was present in the flow-through.

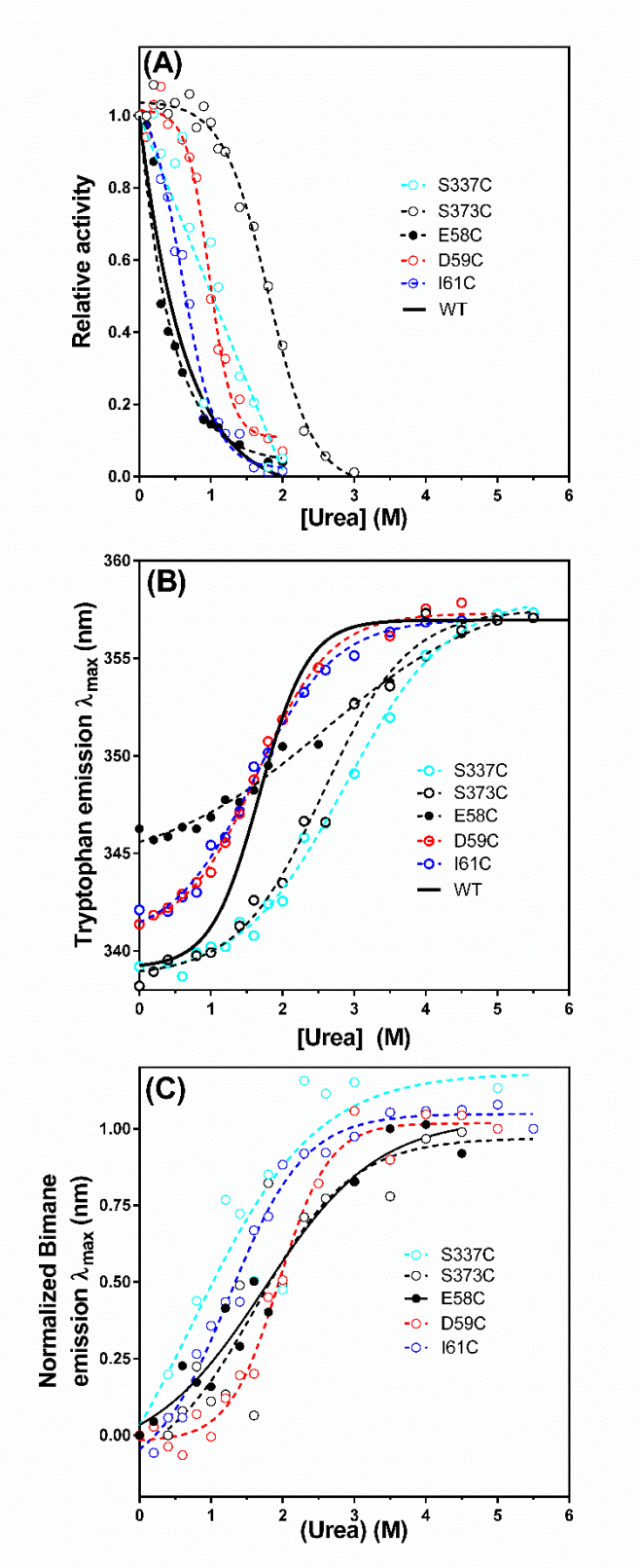

Figure S3. Denaturation of bimane variants. (A) Activity as a function of urea, (B) Trp maximum emission wavelength (λ_{max}) and (C) bimane maximum emission wavelength (λ_{max}) where the lowest value was normalized and set to zero and the highest value to 1.0.

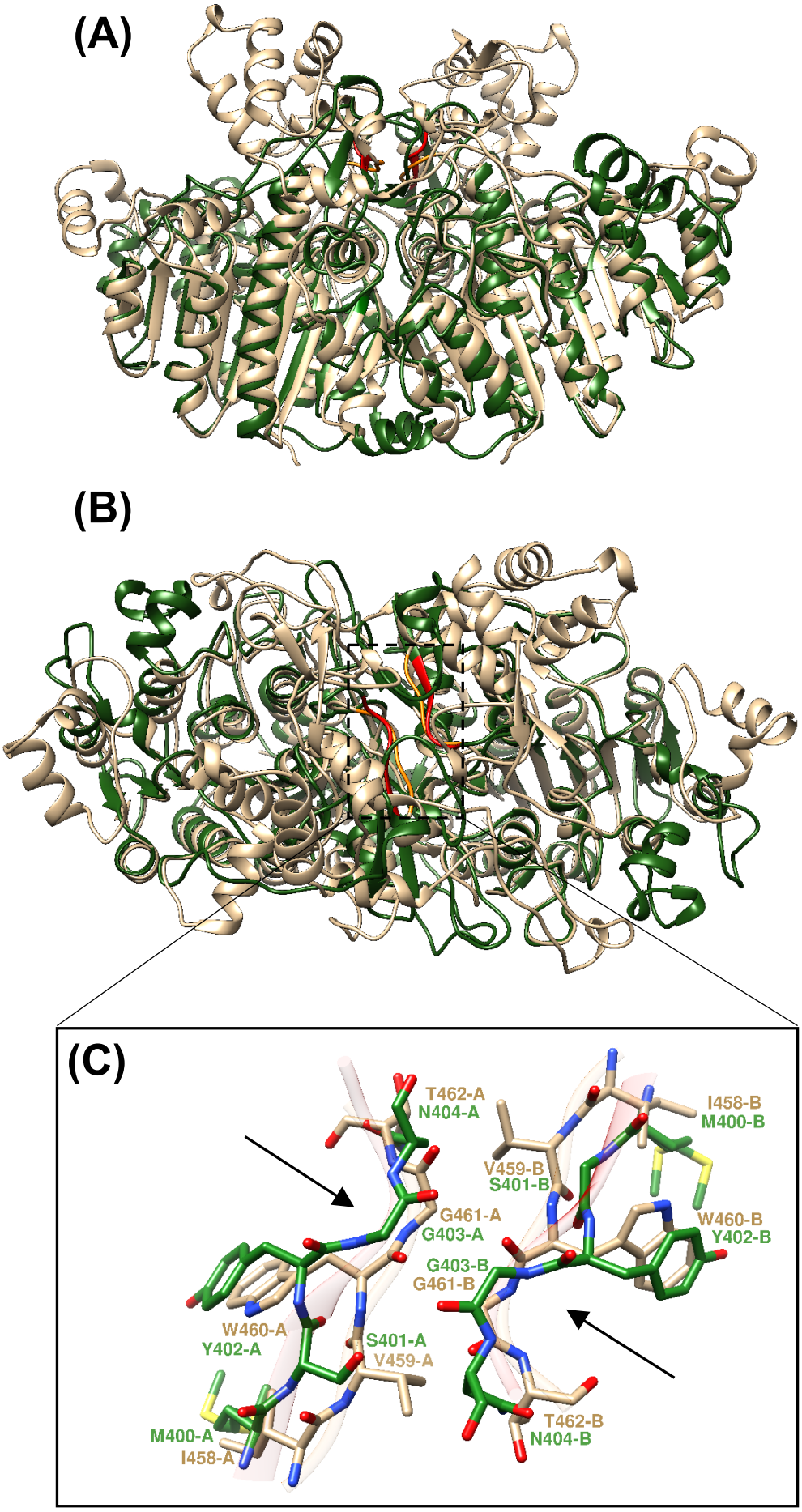
(A)
(B)
(C)
T462-A
N404-A
I458-B
M400-B
V459-B
S401-B
G461-A
G403-A
W460-B
Y402-B
G403-B
G461-B
W460-A
Y402-A
S401-A
V459-A
M400-A
I458-A
T462-B
N404-B

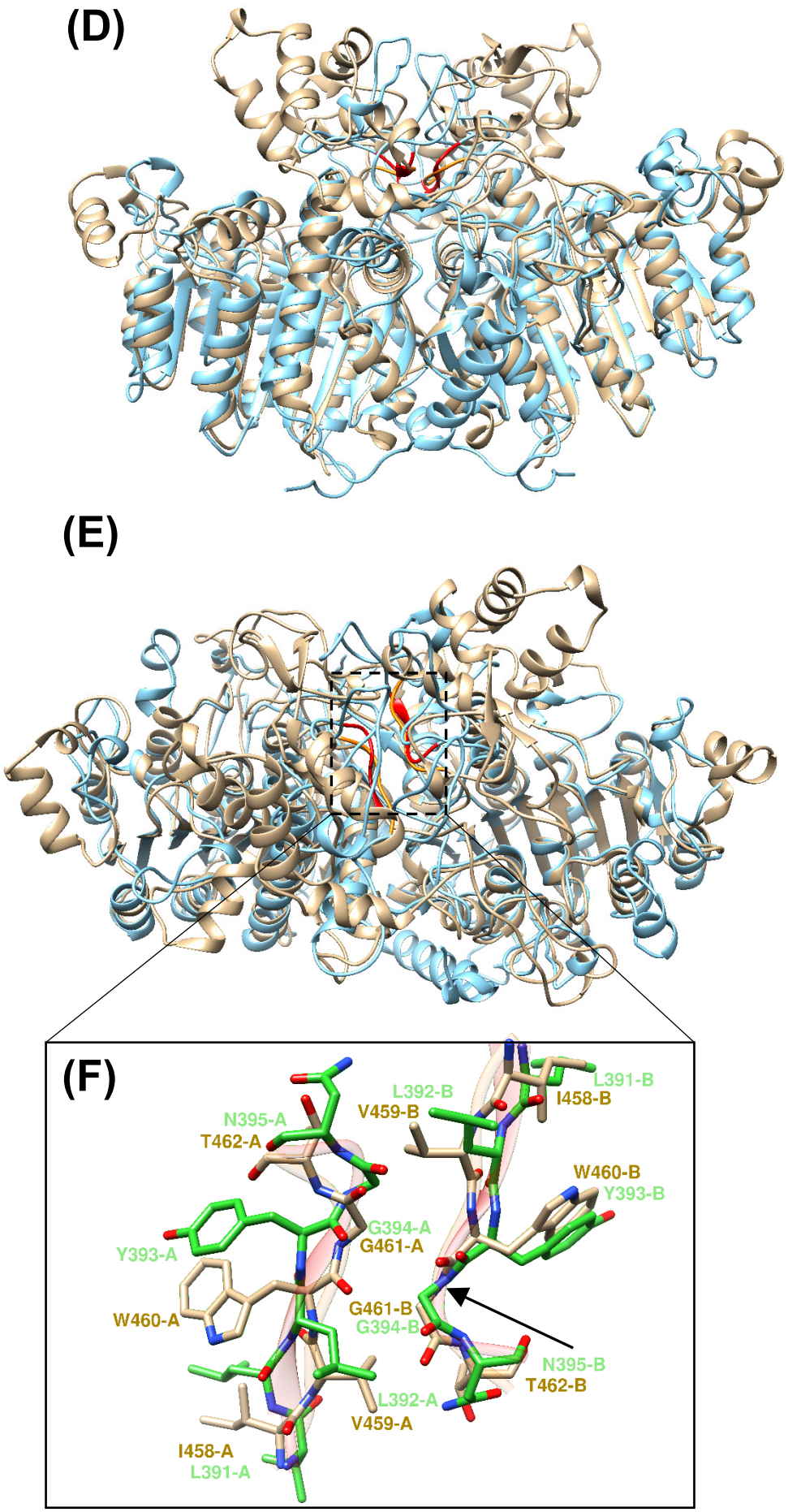
(D)
(E)
(F)
L392-B
V459-B
L391-B
I458-B
N395-A
T462-A
W460-B
Y393-B
G394-A
G461-A
Y393-A
G461-B
G394-B
W460-A
N395-B
T462-B
L392-A
V459-A
I458-A
L391-A

Figure S4. Residues 458-462 of VAP at the symmetric axis aligned to corresponding area in ECAP (A, B, C) and PLAP (D, E, F). Residues 458-462 are colored orange for VAP and in red for the corresponding residues for ECAP and PLAP. (C, F) Expanded view, showing the main-chain and residues in lime-green for ECAP (C) and PLAP (F) and in tan for VAP. Arrows denote a kink in the main chain at the two-fold symmetrical axis, between residues W460 and G461. Note that in VAP (3E2D) and ECAP (3TG0) the crystallographic units containst the dimer while for PLAP (1ZEF) the crystallographic unit only shows one of the monomers. Thus, the biological unit is generated from the same chain. Structural alignment was performed in USCF Chimera, using Needleman-Wunch alignment algorithm and BLOSUM-62 matrix where iteration was performed until atom pair pruning exceeded 2.0 Å.

Paper IV

Modulation of activity and stability of a dimeric cold-adapted enzyme acting on a disordered region at the monomer-monomer interface

Elena Papaleo[1†], Manuela Magnúsdóttir [2†], Jens Guðmundur Hjörleifsson[2], Gaetano Invernizzi[1], Bjarni Ásgeirsson[2]*

[1]Department of Biotechnology and Biosciences, University of Milano-Bicocca, Piazza Della Scienza 2, 20126, Milan, Italy
[2] Department of Biochemistry, Science Institute, University of Iceland, Dunhagi 3, 107 Reykjavik, Iceland

Running Title: *Major loop affects the stability and activity of VAP*

†The authors equally contributed to this work
* Corresponding authors: Elena Papaleo, email: elena.papaleo@bio.ku.dk , elena.papaleo.78@gmail.com and Bjarni Ásgeirsson, email: bjarni@hi.is

Keywords: disordered loop, molecular dynamics, catalytic activity, psychrophile, thermal stability, mutations, long range

Background: Extremophilic enzymes use diverse and elusive mechanisms to modulate activity/stability at the atom-level.
Results: Mutations designed to conserve/alter communication from interface to the catalytic site differently affect thermodynamics and kinetics.
Conclusions: We can modulate activity and stability acting on single residues in a disordered interface.
Significance: The role of remote sites on enzyme function has broad interest for fundamental and applicative biochemistry.

Cold-adapted enzymes have attracted research interest due to their high catalytic efficiency at low temperatures compared with enzymes from mesophilic or thermophilic organisms. The role played by remote residues away from the catalytic site of cold-adapted enzymes is still not well understood. Here, we focused on the disordered 'major loop' at the interface between the two monomers of a dimeric alkaline phosphatase by molecular simulations, experimental mutagenesis, kinetic analyses and thermal stability assays. We designed three different mutant variants that our calculations predicted to either affect or conserve intermolecular interactions of the enzyme. Noteworthy, a R336L variant, which alters the hydrogen-bond network from the major loop of one subunit to the catalytic site of the second subunit, showed an increased k_{cat}. By disrupting the hydrogen bonds mediated by Arg336, we showed conclusively the importance of the structural communication mediated by this residue and its capability to modulate over a long range the conformational states of the residues in the catalytic site. A single mutation (F355Y) predicted to maintain the steric effects mediated by the side chain resulted, instead, in conserved dynamics and catalytic efficiency and increased dimer stability. Our results imply a functional role for the unstructured major loop of this cold-adapted enzyme and show how we can modify the catalytic activity and stability by acting on the networks of interactions within the protein. Indeed, we have been able to even improve the k_{cat} by just a critical mutation in the major loop, guided here by simulations.

Thermal stability of enzymes and the effects of temperature on their function is of central importance for the basic understanding of how enzymes can function over such a wide range of temperatures (1, 2). The knowledge of the physical chemistry involved also benefits industrial and biotechnological applications of extremophilic enzymes (3–7). Protein plasticity is a key element for enzyme catalysis and the motions related to catalysis are an intrinsic property of most enzymes (8–10) even if it is not possible to generalize it. Indeed, the exact relationship between dynamics and catalysis in enzymes is still debated (11–14).
The main determinants of stability and function seems often to depend on the specific proteins under investigation (15–17), thus requiring further studies before we can achieve a full and accurate picture. Enhanced flexibility in certain protein regions or in proximity of the active site has been suggested as an important factor in enzyme catalysis (18). Several studies carried out with a large array of different techniques have collected evidence for diverse local flexibility patterns in

enzymes adapted at different temperatures including amide hydrogen-deuterium exchange studies using Fourier-transform infrared spectroscopy (19) or mass spectrometry (20, 21), quenching of tryptophan fluorescence (21–24) neutron scattering and EPR (25–27), NMR (28–30) and molecular dynamics (MD) simulations (31–38).

The differences in dynamics linked to temperature adaptation are not always so obvious. Indeed, the flexibility of enzymes from psychrophilic and thermophilic organisms does not always obey the 'corresponding states hypothesis' (39), i.e. they do not always show similar dynamics at their respective temperatures (2, 16, 40, 41). Moreover, specific and well-localized areas including loops that regulate the active site, substrate or cofactor binding sites may often exhibit greater flexibility in the cold-adapted variants (18, 23, 29, 31, 32, 34, 35, 42–44). It must also be kept in mind that functionally critical motions are localized not only near the active site, but they can be also linked to a remote dynamic network of non-covalent interactions (45–48). The term 'local' may indeed intuitively be connected to the proximity of the active site only, but as mentioned above those 'spots' may also lie elsewhere in the structure, i.e. important hinge regions or surface loops (18, 32, 48–54). Thus, even remote region of the enzyme, far away from the catalytic residues, can have a contribution and impact on catalysis, as attested by the effects induced upon mutations at those distal sites (35, 47, 48, 55–58). The idea that flexible local areas of functional importance can, in some cases, be decoupled from the global stability of the enzyme seems to hold promise in explaining catalytic efficiency in cold-adapted enzymes (43, 59–62).

Here, we turned our attention to a long and unstructured region (major loop) of an alkaline phosphatase (AP) previously isolated and characterized from a *Vibrio* bacterium (63). This long surface loop is not generally found in other APs. It traverses the gap between monomers, linking the monomers in the dimer together by swapping loops (**Figure 1**)(64). Another cold-active AP from an Antarctic bacterium does not conserve the disordered insertion at the monomer-monomer interface and it has overall a much smaller structure (65), making the role of the major loop even more enigmatic. More recently, another AP variant from *Cobetia marina* was described with a long insertion loop (66).

We know that disordered loops can play a crucial role in positioning the catalytic residues of enzymes, in modulating accessibility of the active site and even exerting their effects long range (52, 67–70). It remains, however, a difficult task to predict their structural and functional role in proteins.

In the present study, we integrated mutagenesis of residues in VAP major loop with all-atom microsecond explicit solvent MD simulations (71), a state of the art force field (72), and network analysis of protein dynamics (73). We showed that a disordered monomer-monomer interface of VAP influences long-range the active site acting through a network of hydrogen bonds. We succeeded in designing either mutations, which alter the intermolecular interactions from the disordered interface to the active site and as a consequence impair stability and increase catalytic efficiency, and mutations with neutral effects that overall maintain the wild type characteristics.

EXPERIMENTAL PROCEDURES

Materials. Chemicals were generally obtained from Sigma-Aldrich (Schnelldorf, Germany) or Merck (Darmstadt, Germany). Strep-Tactin Sepharose, (2-(4'-hydroxy-benzene-azo) benzoic acid (HABA), desthiobiotin and anhydrotetracyclin (AHTC) were from IBA GmbH (Germany). Bacto Yeast extract was obtained from Becton, Dickinson and Company (France). Primers were obtained from TAG (Copenhagen). Pfu polymerase, DnpI nuclease and markers were from Fermentas (St. Leon-Rot, Germany).

Generation of VAP variants. Mutagenesis was performed on the VAP gene in the pASK3-plus StrepTactin vector (pBAS40) where additional nine residues are linked with the StrepTag due to the insertion place in the multiple cloning site at *PstI* and *EcoRI* (27). The protein derived from this plasmid is referred to as VAP-St9 and has in total 16 additional residues at its C-terminal end. Plasmids were initially transformed into DH5α cells and plated on LB-agar with ampicillin (100 μL/mg). Selected colonies were isolated and plasmid DNA purified for DNA sequencing using NucleoSpin® Plasmid QuickPure kit (Macherey-Nagel) following the manufacturer's instructions. DNA sequencing was performed commercially (Beckman Coulter Genomics, Takeley, U.K.).

Protein production. For production of proteins, competent LMG-194 cells (Invitrogen) were transformed with 50-100 ng plasmid. A single colony was picked from an LB-agar disc and grown in 15 ml LB-broth with 100 μg/μl ampicilin at 37°C. This was divided into 4L LB-broth, containing 100 μg/μl amp LB-broth and

grown at 18°C until the cell density measured at 600 nm was 0.4-0.6 (18 hrs). Expression was then induced by adding anhydrotetracycline (final concentration 0.2 μg/L) to each flask. The cells were collected by centrifugation at 10.000 xg for 10 min (4°C). The cell mass was resuspended in 20 mM Tris-HCl, 10 mM $MgCl_2$, pH 8.0 with 0.1% (w/v) Triton X-100 and 0.5 mg/ml lysozyme (Sigma-Aldrich) and incubated at 4°C for 4-5 hrs before freezing at -20°C.

DNAase I (Sigma-Aldrich) was added at 0.05 μg/ml to the thawed cell suspension. After 30 min, a clear supernatant was obtained by centrifugation at 10.000 xg for 30 min at 4°C. The sample (100 ml) was applied at a flow rate of <1ml/min to a StrepTacin Sepharose® column after equilibration with buffer (20 mM Tris-HCl, 10 mM $MgCl_2$, pH 8.0). The column was then washed with the same buffer having additionally 150 mM NaCl prior to elution of VAP using 2.5 mM desthiobiotin in buffer without NaCl but with 15% (v/v) ethylene glycol. Active fractions were frozen in liquid nitrogen and stored at -20 °C. Purity was checked using SDS-PAGE. Protein concentration was determined by adsorption measurements at 280 nm using calculated extinctions coefficients, ε_{280} (M^{-1} cm^{-1}) = (#Trp) (5,500) + (#Tyr) (1,490) + (#cystines)(125) (74) .

VAP enzyme activity assay. Standard assays during purification were performed with 5.0 mM *p*-nitrophenyl phosphate (*p*-NPP) in 1.0 M diethanolamine with 1.0 mM $MgCl_2$ at pH 9.8 and 25 °C. Absorbance was measured at 405 nm over a 30 sec period in a temperature regulated Heλios spectrophotometer. An extinction coefficient of 18.5 $M^{-1}cm^{-1}$ was used at pH 9.8.

Kinetics. Steady-state kinetics were performed under transphosphorylating condition using 0.1 M Caps, 1.0 mM $MgCl_2$, 15% (v/v) ethylene glycol at pH 9.8 and 10°C. The pH was corrected by the relationship for temperature variation. The substrate was diluted in the range 0.001 mM to 0.30 mM. Rate constants were obtained by direct fit to the Michaelis-Menten equation using the software Kaleidagraph®.

Thermal stability measurements. Determination of $T_{50\%}$, defined here as the temperature needed to reduce initial activity by 50% over 30 min, was performed by incubating an aliquot of enzyme in a glass tube containing pre-heated buffer in the range of 10-27°C. Experiments were initiated by adding enzyme (10-15 μl) to the medium (300-500 μl). The rate constant at each temperature was determined by regularly withdrawing aliquots and following the drop in activity using the standard assay at 25°C. From an Arrhenius plot (ln*k* vs. 1/T), the activation energy (E_a) was obtained. $T_{50\%}$ was calculated from the Arrhenius equation, where the *k* (s^{-1}) for 50% loss of activity after 30 min was used in each case (*k*=ln 2/30 min x 60 s/min^{-1}) to give $T_{50\%}=(E_a \times 1000)/R(\ln A - \ln k)$.

Samples for T_m determination were dialyzed overnight in 25 mM Mops, 1 mM $MgSO_4$ at pH 8.0 and absorbance at 280 nm measured to determine protein concentration. A JASCO J-810 circular dichroism (CD) spectropolarimeter was used to determine melting-curves at 222 nm over the temperature range 15-90°C in a 2 mm cuvette with a rise in temperature of 1 °C/min. For monomer unfolding, a two-state pathway was assumed (N ⇆ U, where N is native and U is unfolded). The original traces were normalized. T_m was determined at F_U=0.5 by a direct fit to a sigmoid curve using the software Kaleidagraph®.

Urea denaturation experiments.

For monomer unfolding, tryptophan fluorescence of VAP variants was measured with a Spex FluorMax® or a FluoroMax4® instrument in 25 mM Mops, 1 mM $MgSO_4$, 0.02 mg/mL enzyme, pH 8.0 (at 10°C) containing different concentrations of urea in the 0-8 M range. The samples were incubated at 10°C for 4 h before measuring the fluorescence. For each urea concentration, a blank solution without added enzyme was also measured and subtracted from the sample. Emission data was collected in the range 310-400 nm with slit-width of 5.0 nm for both emission and excitation at 295 nm using 0.5 nm increments and recording three averaged scans. Spectras were smoothed by fitting the spectras to a 5th degree polynomial function, $y = ax^5 + bx^4 + cx^3 + dx^2 + ex + f$, in MS Excel using the LINEST function, where y is emission counts per second and x is wavelength.

The wavelength of maximum emission intensity (λ_{max}) was determined by finding the x-intercept of the first derivative of the polynomial function (by solving the roots of a quartic equation). By plotting λ_{max} vs. [urea] the curves where fitted with sigmoidal Hill equation where a two-state equilibrium was assumed. The unfolding equilibrium constant $K_f = f_N/f_U$ was obtained at different urea concentrations where fraction unfolded (f_U) was calculated for the transition area between the linear pre- and post-transition parts of the normalized curves and fraction folded obtained by subtraction ($f_N=1-f_U$). Three independent measurements were performed on each enzyme variant. The free energy of folding at 10°C (ΔG_f) was calculated using the linear extrapolation method as described by Pace (75).

Dimer dissociation was assumed to be directly linked to loss of activity, since APs generally have inactive monomers. Dimer association is then described by $2M \leftrightarrows D$, where D is dimer and M is monomer and the dimer association equilibrium constant is $K_D = f_D / {}_M^2$, where f_M is the fraction of monomers and f_D is the fraction of dimers. For determining K_D, samples were incubated for 4h at 10°C with urea concentrations ranging from 0-2 M urea. Activity was measured at 10°C and three independent experiments performed for each variant. The fraction of dissociated dimer was calculated by assuming that at 0.0 M urea f_D is 1.0. As before, the linear extrapolation method was used to calculate the free energy of dimer association at 10 °C (ΔG_D).

Molecular dynamics (MD) simulations. All MD simulations were performed with *Gromacs 4.6* package compatible with graphics processing units (GPUs) using the CHARMM22* force field (72) for wild-type (VAP_{wt}), R336L (VAP_{R336L}), F355Y (VAP_{F355Y}) and Y346F (VAP_{Y346F}) VAP variants. We used the wild type VAP X-ray structure (PDB entry 3E2D (64)) and *in silico* mutated structures as starting structures for our simulations. The starting structures were soaked in a dodecahedral box of 45 000 TIP3P water molecules (76) (total size of the system = 150 544 atoms) and simulations performed in periodic boundary conditions.

Each system was prepared for the productive MD runs as previously described (62). Productive 1-μs MD simulations were carried out in the NVT ensemble using the velocity-rescale thermostat (77) with a coupling constant of 0.2 ps at 303 K. The LINCS algorithm (78) was used to constraint the heavy atom bond lengths, allowing the use of a 2 fs time step. Long-range electrostatic interactions were calculated using the Particle-Mesh Ewald (PME) summation scheme. Both Van der Waals and Coulomb interactions were truncated at 10 Å.

To assess the conformational stability of the protein during the MD simulations, the time-dependent root mean square deviation of the mainchain atoms and the protein radius of gyration with respect to the initial structure were calculated and the first 20 ns of simulations were then discarded to avoid artifacts due to the equilibration phase. We also carried out C-alpha (Cα) Principal Component Analysis (PCA) of MD trajectories (79). We then evaluate the cosine content along the first 20 PCs to ensure that our simulations did not encounter the risk to sample random diffusive motions, a behavior highlighted to high cosine content (~ 1) in MD simulations (80). We indeed observed a low cosine content (lower than 0.28) in all the simulations.

Analysis of MD simulations. The hydrogen bonds were calculated by *PyInteraph* suite of tools, as previously described (73). The hydrogen bonds and their networks were then mapped on the three-dimensional (3D) structure using the *Interaction Plotter Pymol* plugin released with *PyInteraph* (73). Hydrophobic interactions were also calculated by *PyInteraph* using, as a cutoff, a distance of 5.5 Å between the centers of mass of each side chain.

FoldX calculations. The *FoldX* 3.0 (81) energy function was used to estimate the free-energy changes upon mutations on the protein monomeric and dimeric structure using the 3E2D PDB entry. The *RepairPDB* function of *FoldX* was first used on the wild type structure. The mutant structures were then generated using the *BuildModel* function averaging over five independent runs. The *Analyze Complex* and *Stability* functions were used to calculate the ΔΔG values for dimer interface dissociation and monomer unfolding, respectively. The changes in native stability upon mutation were estimated as the difference between the energy of the mutant and wild type variants ($\Delta\Delta G = \Delta G_{mut} - \Delta G_{wt}$). ΔΔG values above 6.7 kJ/mol should significantly affect stability because they correspond to twice the standard deviation of *FoldX* (82).

RESULTS

Design of four VAP variants with deletion or mutations in the residues of the major loop to alter or conserve the network of intermolecular hydrogen bonds

Figure 1 shows the overall VAP structure and the position of the major loops (Insert II, residues 323-355) of each subunit, along with the location of the residues selected for mutagenesis (Arg336, Tyr346, Phe355) at the monomer-monomer interface. The residues of the major loop are at a distal site with respect to the catalytic residues (i.e. more than 10 Å distance from it).

To select the mutation sites for our study, we carried out 1-μs MD of the wild type enzyme (VAP_{wt}) and we estimated the population of the intermolecular and intramolecular interactions, with particular attention to hydrogen bonds. In fairly agreement with what observed in the crystallographic structure, the residues in the major loop feature relatively few intramolecular hydrogen bonds and eleven intermolecular hydrogen bonds (64).

In particular, Arg336 is placed in a central position within the major loop and it is involved

in hydrogen bonds with side chains of Ser79 (less than 16%), Asp59 (~36%) and Glu81 (~77%) (**Table 1 and Figure 2,** orange cylinders). Asp59 and Arg336 in the X-ray structure were at a distance of 6.5 Å, thus not compatible with hydrogen-bond formation. Nevertheless the loop where Asp59 is located is flexible in our simulations in agreement with the high associated B-factor values in the X-ray structure. Fluctuations of this loop allow for the two residues to come closer to each other in our MD simulations. Our previous MD study with a different force field and shorter simulations also pointed out structural communication of Arg336 to the catalytic cleft through to the Asp59 side chain (83). The Arg336 side chain is also involved in intra-loop hydrogen bonds (**Table 1**). We, thus, designed a R336L mutation to test the effects mediated by Arg336 hydrogen bonds on protein stability and activity. The Arg to Leu mutation was indeed selected to prevent any sidechain-mediated polar interactions and at the simultaneously only causing a slight decrease of the side-chain steric hindrance. Indeed, 1-μs MD simulations of VAP_{R336L} show that the R336L mutation overall preserves the intramolecular interactions mediated by the main-chain atoms of the 336 residue and the hydrophobic interactions mediated by the aliphatic atoms of Arg336 side chain (**Table 1**).

We then selected two mutation sites, i.e. Tyr346 and Phe355, in which we designed mutations that are expected to have minor effects on the hydrogen-bond network to evaluate how sensitive protein stability and activity of VAP are to minor changes in low-populated intermolecular interactions.

In the wild type MD ensemble, Tyr346 side chain formed only transient hydrogen bonds (population of less than 16%) with the main chain of Ser80 and side chain of Glu81 (**Table 1 and Figure 2**, green cylinders), thus connecting the major loop and the loop that connects helices α3 (where the nucleophilic residue Ser65 is located) and α4. Thus, the Y346F variant was designed to evaluate if those transient hydrogen bonds might exert any effects on VAP activity and stability, without impairing hydrophobic/aromatic interactions mediated by the tyrosine side chain. Indeed, 1-μs MD simulation of VAP_{Y346F} shows that the Y346F mutation causes the loss of the transient side-chain mediated interaction with Ser80 and Glu81 but does not prevent the formation of main chain hydrogen bonds. Tyr and Phe are both aromatic residues and they conserve the intramolecular hydrophobic/aromatic interactions with the surroundings (such as with 336Arg, 341Phe and 348Pro with population higher than 30%) (**Table 1**).

Phe355 is the residue at the C-terminal end of the major loop, by a small extension of the previous definition that ended at residue 351 (64). We investigated the mutation F355Y with view of providing additional hydrogen bonds, whereas the mutations mentioned above were all designed to assess the effects of reducing polar interactions at the interface between the two subunits. The analysis of hydrogen bonds in the VAP_{F355Y} MD ensemble pointed out the capability of the OH-group of Tyr355 to mediate intermolecular hydrogen bond mainly with Glu58 and Gln28 (**Table 1**), the latter with a very low population. The mutation also maintains the hydrophobic interactions mediated by Phe355 side chain at the interface with Ile61 of the other subunit and with Pro30 and Ala29 of the same subunit (**Table 1** and **Figure 2,** black cylinders).

Overall, our MD simulations of VAP_{wt} suggest that the intermolecular interface between the major loop of one subunit and the opposite subunit is very loosening in solution, as expected for a cold-adapted enzyme, with only few and often transient hydrogen bonds that contribute to it. Arg336 is at the heart of the intermolecular interactions carried out by the major loop and it can exert its effect long-range from the major loop of one subunit to the catalytic site of the opposite subunit (83). It is thus the only mutation site expected to affect both stability and activity. The other mutations are expected to play only a minor role on the kinetic and stability patterns of the enzyme.

Effects on local and global heat stability.

The effects induced by the single mutations R336L, Y346F and F355Y on the monomer and interface stability were quantitatively estimated by *FoldX* (81), which permits the calculation of free energies (ΔΔG) upon mutations. The results are reported in **Table 2**. None of the mutations were expected to greatly affect monomer stability, and R336L was the only one predicted to alter the stability of the dimeric assembly by more than 20 kJ/mol.

We then experimentally characterized the stability of VAP variants both by measuring the activity and spectroscopic differences in response to heat or urea. Due to the low sustainability of activity for some of the variants in aqueous buffer, the enzyme kinetics experiments were performed with the addition of 15% (v/v) ethylene glycol. This generated slightly higher k_{cat} and K_m values than

previously published for the wild type enzyme (27, 84). Global stability, however, was measured without the addition of ethylene glycol by following the integrity of the secondary structures at 222 nm by circular dichroism (CD). **Table 2** shows how the removal of hydrogen bonds had the effect of reducing global stability (T_m) of all the variants where hydrogen bonds between the major loop and the opposite monomer were removed, being approximately 5°C lower for VAP_{R336L} compared with VAP_{wt}. As the unfolding of monomers has the dissociation of the dimer as a prelude, a reduction in subunit cross-interactions could be reflected in T_m; T_m otherwise assumed to be dominated by the monomer unfolding event. This was also suggested by *FoldX* calculations for R336L, where this mutation is predicted to affect the dimer stability but not the monomeric assembly. The addition of hydrogen bonds at the base of the major loop (VAP_{F455Y}) did not increase global stability significantly (T_m).

We also determined how long the VAP variants were able to sustain their functional form when challenged by heat (**Table 2**). Results are given in degrees, where the factor $T_{50\%}$ is defined as the temperature that will reduce the activity by half in 30 min. All the variants gave a statistically significant decrease in $T_{50\%}$. VAP_{R336L} resulted in an 8°C lowering in the temperature, which is the largest effect observed in this study. These findings indicate altogether that the terminal part of the major loop, where the arginine is located, is important to hold residues that form or support the structure of the active site area in their optimal positions and it exerts this effect long-range.

The effects of urea on the stability of VAP_{wt} and three VAP variants. To gain more insight into the inactivation and unfolding events in VAP, the enzyme was incubated with increasing concentration of urea and allowed to equilibrate for 4hr at 10°C. Since VAP has practically inactive monomers as most APs, the equilibrium constant for dimer dissociation could be measured for urea concentrations in the range of 0-2 M. Consequently, the free energy of dimer association (ΔG_D) was calculated using the linear extrapolation method (**Table 2).**

For VAP_{wt}, the activity declined at very low urea concentrations indicating very early dissociation of dimers (**Figure 3A).** Activity was close to zero before the monomers started to unfold, which shows that monomers are indeed inactive.

Fluorescence red-shift of tryptophan emission spectra was used to monitor unfolding of monomers in 0-8 M urea (**Figure 3B)**. Small fluctuations in fluorescence were observed in the lowest range of urea (0-1.5 M) that may indicate that tryptophan accessibility was changing when the monomers separated. This was especially prominent for F355Y. In fact, one of the five Trp residues of VAP (Trp460) is buried between two helices by ridges to grooves packing where one of the helices faces the other monomer in proximity to the dimer interface. Size exclusion gel filtration experiments (*data not shown*) confirmed that the dimeric structure falls apart over this range of urea.

Urea unfolding curves were similar for R336L and F355Y with $D_{1/2}$ at 2.2 and 2.1 M respectively. For VAP_{wt} the $D_{1/2}$ was 2.7 M, which is significantly lower. However the steepness of the VAP_{wt} curve (Hill slope) is also much lower (correlates with m-values in linear extrapolation).

The ΔG_D and ΔG_M values for VAP_{wt} were -8.5 ± 1.4 kJ/mol and -13.9 ± 3.2 kJ/mol, respectively (**Table 2**). For R336L, ΔG_D was drastically increased to -2.2 kJ/mol which correlates well with the low $T_{50\%}$ value of 12.8 °C. However, monomer stability was not significantly changed. On the other hand, the F355Y variant had improved dimer stability with ΔG_D of -14.0 kJ/mol, but monomer stability was unaffected.

For the variant with the lowest dimer stability, R336L, >50% of its activity was lost at 0.1 M urea. In contrast, the activity of the F355Y variant increased somewhat initially at 0-0.2 M urea and fell after that as expected. An increase in AP activity at low urea concentration has previously been reported for intestinal AP with guanidium chloride (85).

Kinetic properties of the VAP variants. To further characterize the effects induced by mutations of the major loop, we determined the kinetic constants of the VAP variants. **Table 3** summarizes these results. The k_{cat} value of VAP_{Y346F} (35 s^{-1}) was lower than for the wild type enzyme (97 s^{-1}). On the other hand, VAP_{R336L} showed a moderate increase in k_{cat} (120 s^{-1}) while the F355Y variant had the same k_{cat} as the wild type (97 s^{-1}). The K_m values remained unchanged for VAP_{R336L} and VAP_{F355Y}, whereas lowered K_m values were observed for VAP_{Y356F}. None of the residues that are directly involved in substrate binding were altered here. Thus, the higher substrate affinity of VAP_{Y356F} was not reflected in higher k_{cat} values, indicating that the rate-limiting step of the reaction is late in line with the reaction mechanism where the release of the product is the slowest step and dictates the overall reaction rate at alkaline pHs (86). R336L was the only mutation able to increase the catalytic efficiency

of the cold-adapted enzyme and this is related to an effect on k_{cat}.

R336L mutation modulates the conformational landscape of the catalytic residues Ser65 and Arg129

The VAP_{R336L} variant was the only variant predicted to have a higher impact on hydrogen bonds at the interface between the two subunits compared with VAP_{wt} (**Table 1**). In particular long-range communication with the catalytic Ser65 through the intermediate interaction with Asp59 and Glu81 was evident. The other variants displayed effects only on either low-populated hydrogen bonds or hydrogen bonds mediated by the main-chain atoms. Overall, both the Y346F and F355Y variants retained the hydrophobic and aromatic interactions of the wild type side chain (**Table 1**).

We showed experimentally that VAP_{R336L} not only featured a lower thermal stability (Table 2), but it also featured higher k_{cat} with respect to the wild type (**Table 3**). Therefore, we investigated if the R336L replacement is able to alter the conformational dynamics of the nucleophilic Ser65 of VAP. We thus estimated the population of the rotameric states of the χ_1 side chain dihedral of Ser65 in VAP_{wt} (**Figure 4A**, blue curves) and VAP_{R336L} (**Figure 4A**, orange curves) by MD simulations. Ser65 side chain is observed in two states with occupancy of 0.5 each in the X-ray structure of VAP_{wt}, suggesting an inherent conformational freedom of this residue. These two states of the Ser65 side chain can be classified as trans (t) or minus (m) rotamers of the χ_1 dihedral angle. The plus (p) rotamer was neither observed in the crystallographic structure nor in our 1-μs MD simulation of VAP_{wt}. With the R336L replacement VAP is able to exert a long-range effect to this site, allowing Ser65 to sample the p rotamer (**Figure 5A**). Moreover, Arg129, which takes part with Ser65 in the interaction with the phosphate group of the substrate (87–90), is also stabilized by the R336L replacement (**Figure 5B**) in a plus state along its χ_1, bond. This is the rotomer observed when the phosphate is bound in the catalytic cleft (**Figure 5C**). A superimposition of VAP structures from our simulations and the structure of another cold-active AP (PDB entry 1SHN) in complex with the phosphate shows that the plus states of both Arg129 and Ser65 are the states competent for coordination of the phosphate group (**Figure 5C**). This suggests that the R336L variant is able to alter the conformational landscape of VAP's active residues, allowing them to sample efficiently states that are important for catalysis. This correlates well with an increased catalytic efficiency of the VAP_{R336L} variant.

DISCUSSION

Several recent studies have addressed the influence of surface loops on catalytic function and stability of enzymes (52, 53, 69, 70, 91, 92) illustrating the central role they play in the function of many enzymes. They often serve the function of modulating accessibility of the active site or closing off the active site once the substrate is bound, in addition to promoting catalysis by orienting and bringing groups together without the involvement of the solvent

It has previously been shown, that the isozyme-specific properties of mammalian alkaline phosphatases can be modulated by modifications in a flexible surface loop (93) or acting on a local network of interactions close to the catalytic site (94).

VAP has also a prominent disordered region in a location that suggests intimate interactions with the opposite subunit in the dimer and the potential for mediating conformational changes relevant for function and communication to the active site (95). Indeed, our previous MD study pointed out a long-range communication from the major loop (Arg336) to the catalytic cleft through the Asp59 side chain using Protein Structure Network approaches (83), which is confirmed here by a more accurate force field and longer simulations in the microsecond timescale. Moreover, we here show that the Arg is involved in intermolecular hydrogen bond networks that link the major loop to the catalytic site. Disrupting the hydrogen-bond cluster mediated by the arginine with the R336L mutation, we showed conclusively the importance of the long-range communication mediated by Arg336. This is indeed supported by the experimental results showing consistent decrease in both global stability (T_m) and local heat-stability of the catalytically competent structure. Our calculations also suggest that the Leu mutation at this site is likely to compromise the dimeric assembly more than monomer stability.

The VAP_{R336L} variant showed unchanged substrate affinity (K_m) and a more rapid turnover rate (higher k_{cat}) that would fit a looser and more dynamic structure and have its roots in changing the conformational propensity of the residues of the catalytic site Ser65 and Arg129 toward states competent for catalysis. Thus, the R336L VAP variant provides an example of a tight link between activity, stability and dynamics in cold-adapted enzymes.

Hydrogen bonds mediated by the wild type Tyr346, or the Tyr residue replaced at position 355 in VAP_{F355Y}, contributed only partially to protein stability. And in the case of F355Y, activity was unchanged. Our MD simulations show that these two variants can maintain the hydrophobic interactions at the interface, and that both the Y355 in the VAP_{F355Y} variant and Y346 in the wild-type VAP are contributing only to very low-populated hydrogen bonds.

Tracking in detail how residue substitutions lead to functional effects is very complicated due to the constraints set by available experimental techniques. We here show that by integrating microsecond atomistic simulations and network description of protein dynamics, we could design variants of VAP with different activity and stability profiles.

In particular, our study demonstrates that interactions between the two monomers of the dimeric VAP, mediated by residues in the large disordered loop, are determinants of its stability and activity properties. The removal of hydrogen bonds that MD simulations showed are important for long-range communication to the active site produced variants with even higher k_{cat} than the cold-adapted wild type enzyme. This was complemented with compromised structural stability as the general theory of cold-active enzymes predicts. In the R336L variant in particular, the k_{cat}/K_m was increased by over 40% by just a single residue replacement.

In a broader context, we managed to show that loosening interface contacts between the two VAP subunits by replacement of crucial residues provides a way to orchestrate structural dynamics in a productive way. It is possible to improve on the native enzyme in terms of k_{cat} by a critical residue replacement, guided here by MD. However, this had the effect of making the enzyme very unstable to heat. It would seem, therefore, that VAP has reached close to an evolutionary end-point in loosening monomer associations and that the large loop is absolutely necessary in providing dimer cohesion.

Acknowledgment

This research was supported by an ISCRA-CINECA HPC Grant 2014 on Eurora to E.P. We would like to thank professor Hannes Jónsson for providing access to the Sol computer cluster at the Science Institute of the University of Iceland, where part of the simulations were carried out. G.I. is recipient of a Marie Curie Intra European Fellowship. Gratitude is extended to the Icelandic Research Fund (grant number 100213021) and the University of Iceland Research Fund for supporting this project financially. We also thank Giulia Renzetti and Jóhanna Vilhjálmsdóttir for excellent technical assistance in the early stages of the project.

Author contributions

EP and BA conceived, designed and coordinate the study. EP, BA and JG wrote the manuscript. EP, MM, JG and GI performed the experiments and analyzed the data. All the authors reviewed and approved the final version of the manuscript.

References

1. Somero, G. N. (1995) Proteins and temperature. *Annu. Rev. Physiol.* **57**, 43–68

2. Feller, G., and Gerday, C. (2003) Psychrophilic enzymes: hot topics in cold adaptation. *Nat. Rev. Microbiol.* **1**, 200–8

3. Gerday, C., Aittaleb, M., Bentahir, M., Chessa, J. P., Claverie, P., Collins, T., D'Amico, S., Dumont, J., Garsoux, G., Georlette, D., Hoyoux, A., Lonhienne, T., Meuwis, M. A., and Feller, G. (2000) Cold-adapted enzymes: from fundamentals to biotechnology. *Trends Biotechnol.* **18**, 103–7

4. Cavicchioli, R., Siddiqui, K. S., Andrews, D., and Sowers, K. R. (2002) Low-temperature extremophiles and their applications. *Curr. Opin. Biotechnol.* **13**, 253–61

5. Van den Burg, B. (2003) Extremophiles as a source for novel enzymes. *Curr. Opin. Microbiol.* **6**, 213–8

6. Podar, M., and Reysenbach, A.-L. (2006) New opportunities revealed by biotechnological explorations of extremophiles. *Curr. Opin. Biotechnol.* **17**, 250–5

7. Hanoian, P., Liu, C. T., Hammes-Schiffer, S., and Benkovic, S. (2015) Perspectives on electrostatics and conformational motions in enzyme catalysis. *Acc. Chem. Res.* **48**, 482–9

8. Henzler-Wildman, K. A., Lei, M., Thai, V., Kerns, S. J., Karplus, M., and Kern, D. (2007) A hierarchy of timescales in protein dynamics is linked to enzyme catalysis. *Nature* **450**, 913–6

9. Ma, B., and Nussinov, R. (2010) Enzyme dynamics point to stepwise conformational selection in catalysis. *Curr. Opin. Chem. Biol.* **14**, 652–9

10. Hammes, G. G., Benkovic, S. J., and Hammes-Schiffer, S. (2011) Flexibility, diversity, and cooperativity: pillars of enzyme catalysis. *Biochemistry* **50**, 10422–30

11. Doshi, U., and Hamelberg, D. (2014) The dilemma of conformational dynamics in enzyme catalysis: perspectives from theory and experiment. *Adv. Exp. Med. Biol.* **805**, 221–43

12. Kamerlin, S. C. L., and Warshel, A. (2010) At the dawn of the 21st century: Is dynamics the missing link for understanding enzyme catalysis? *Proteins* **78**, 1339–75

13. Roca, M., Messer, B., Hilvert, D., and Warshel, A. (2008) On the relationship between folding and chemical landscapes in enzyme catalysis. *Proc. Natl. Acad. Sci. U. S. A.* **105**, 13877–82

14. Tawfik, D. S. (2014) Accuracy-rate tradeoffs: how do enzymes meet demands of selectivity and catalytic efficiency? *Curr. Opin. Chem. Biol.* **21**, 73–80

15. Struvay, C., and Feller, G. (2012) Optimization to low temperature activity in psychrophilic enzymes. *Int. J. Mol. Sci.* **13**, 11643–65

16. Papaleo, E., Tiberti, M., Invernizzi, G., Pasi, M., and Ranzani, V. (2011) Molecular determinants of enzyme cold adaptation: comparative structural and computational studies of cold- and warm-adapted enzymes. *Curr. Protein Pept. Sci.* **12**, 657–83

17. Luk, L. Y. P., Loveridge, E. J., and Allemann, R. K. (2014) Different dynamical effects in mesophilic and hyperthermophilic dihydrofolate reductases. *J. Am. Chem. Soc.* **136**, 6862–5

18. Fields, P. A., and Somero, G. N. (1998) Hot spots in cold adaptation: localized increases in conformational flexibility in lactate dehydrogenase A4 orthologs of Antarctic notothenioid fishes. *Proc. Natl. Acad. Sci. U. S. A.* **95**, 11476–81

19. Aurilia, V., Rioux-Dubé, J.-F., Marabotti, A., Pézolet, M., and D'Auria, S. (2009) Structure and dynamics of cold-adapted enzymes as investigated by FT-IR spectroscopy and MD. The case of an esterase from Pseudoalteromonas haloplanktis. *J. Phys. Chem. B* **113**, 7753–61

20. Oyeyemi, O. A., Sours, K. M., Lee, T., Kohen, A., Resing, K. A., Ahn, N. G., and Klinman, J. P. (2011) Comparative hydrogen-deuterium exchange for a mesophilic vs thermophilic dihydrofolate reductase at 25 °C: identification of a single active site region with enhanced flexibility in the mesophilic protein. *Biochemistry* **50**, 8251–60

21. Secundo, F., Russo, C., Giordano, A., Carrea, G., Rossi, M., and Raia, C. A. (2005) Temperature-induced conformational change at the catalytic site of Sulfolobus solfataricus alcohol dehydrogenase highlighted by Asn249Tyr substitution. A hydrogen/deuterium exchange, kinetic, and fluorescence quenching study. *Biochemistry* **44**, 11040–8

22. Sigtryggsdóttir, A. R., Papaleo, E., Thorbjarnardóttir, S. H., and Kristjánsson, M. M. (2014) Flexibility of cold- and heat-adapted subtilisin-like serine proteinases evaluated with fluorescence quenching and molecular dynamics. *Biochim. Biophys. Acta* **1844**, 705–12

23. Chiuri, R., Maiorano, G., Rizzello, A., del Mercato, L. L., Cingolani, R., Rinaldi, R., Maffia, M., and Pompa, P. P. (2009) Exploring local flexibility/rigidity in psychrophilic and mesophilic carbonic anhydrases. *Biophys. J.* **96**, 1586–96

24. Aghajari, N., Van Petegem, F., Villeret, V., Chessa, J.-P., Gerday, C., Haser, R., and Van Beeumen, J. (2003) Crystal structures of a psychrophilic metalloprotease reveal new insights into catalysis by cold-adapted proteases. *Proteins* **50**, 636–47

25. Tehei, M., Madern, D., Franzetti, B., and Zaccai, G. (2005) Neutron scattering reveals the dynamic basis of protein adaptation to extreme temperature. *J. Biol. Chem.* **280**, 40974–9

26. Madrona, Y., Hollingsworth, S. A., Khan, B., and Poulos, T. L. (2013) P450cin active site water: implications for substrate binding and solvent accessibility. *Biochemistry* **52**, 5039–50

27. Heidarsson, P. O., Sigurdsson, S. T., and Asgeirsson, B. (2009) Structural features and dynamics of a cold-adapted alkaline phosphatase studied by EPR spectroscopy. *FEBS J.* **276**, 2725–35

28. Henzler-Wildman, K., and Kern, D. (2007) Dynamic personalities of proteins. *Nature* **450**, 964–72

29. Jaremko, Ł., Jaremko, M., Elfaki, I., Mueller, J. W., Ejchart, A., Bayer, P., and Zhukov, I. (2011) Structure and dynamics of the first archaeal parvulin reveal a new functionally important loop in parvulin-type prolyl isomerases. *J. Biol. Chem.* **286**, 6554–65

30. Loveridge, E. J., Tey, L.-H., Behiry, E. M., Dawson, W. M., Evans, R. M., Whittaker, S. B.-M., Günther, U. L., Williams, C., Crump, M. P., and Allemann, R. K. (2011) The role of large-scale motions in catalysis by dihydrofolate reductase. *J. Am. Chem. Soc.* **133**, 20561–70

31. Mereghetti, P., Riccardi, L., Brandsdal, B. O., Fantucci, P., De Gioia, L., and Papaleo, E. (2010) Near native-state conformational landscape of psychrophilic and mesophilic enzymes: probing the folding funnel model. *J. Phys. Chem. B* **114**, 7609–19

32. Papaleo, E., Pasi, M., Riccardi, L., Sambi, I., Fantucci, P., and De Gioia, L. (2008) Protein flexibility in psychrophilic and mesophilic trypsins. Evidence of evolutionary conservation of protein dynamics in trypsin-like serine-proteases. *FEBS Lett.* **582**, 1008–18

33. Daily, M. D., Phillips, G. N., and Cui, Q. (2011) Interconversion of functional motions between mesophilic and thermophilic adenylate kinases. *PLoS Comput. Biol.* **7**, e1002103

34. Martinez, R., Schwaneberg, U., and Roccatano, D. (2011) Temperature effects on structure and dynamics of the psychrophilic protease subtilisin S41 and its thermostable mutants in solution. *Protein Eng. Des. Sel.* **24**, 533–44

35. Papaleo, E., Pasi, M., Tiberti, M., and De Gioia, L. (2011) Molecular dynamics of mesophilic-like mutants of a cold-adapted enzyme: insights into distal effects induced by the mutations. *PLoS One* **6**, e24214

36. Pezeshgi Modarres, H., Dorokhov, B. D., Popov, V. O., Ravin, N. V, Skryabin, K. G., and Dal Peraro, M. (2015) Understanding and Engineering Thermostability in DNA Ligase from Thermococcus sp. 1519. *Biochemistry*, *in press*.

37. Papaleo, E., Riccardi, L., Villa, C., Fantucci, P., and De Gioia, L. (2006) Flexibility and enzymatic cold-adaptation: a comparative molecular dynamics investigation of the elastase family. *Biochim. Biophys. Acta* **1764**, 1397–406

38. Pasi, M., Riccardi, L., Fantucci, P., De Gioia, L., and Papaleo, E. (2009) Dynamic properties of a psychrophilic alpha-amylase in comparison with a mesophilic homologue. *J. Phys. Chem. B* **113**, 13585–95

39. Somero, G. (1978) Temperature Adaptation of Enzymes: Biological Optimization Through Structure-Function Compromises. *Annu Rev Ecol Syst.* **9**, 1–29

40. Siddiqui, K. S., and Cavicchioli, R. (2006) Cold-adapted enzymes. *Annu. Rev. Biochem.* **75**, 403–33

41. Elias, M., Wieczorek, G., Rosenne, S., and Tawfik, D. S. (2014) The universality of enzymatic rate-temperature dependency. *Trends Biochem. Sci.* **39**, 1–7

42. Daily, M. D., Phillips, G. N., and Cui, Q. (2010) Many local motions cooperate to produce the adenylate kinase conformational transition. *J. Mol. Biol.* **400**, 618–31

43. Leiros, H.-K. S., Pey, A. L., Innselset, M., Moe, E., Leiros, I., Steen, I. H., and Martinez, A. (2007) Structure of phenylalanine hydroxylase from Colwellia psychrerythraea 34H, a monomeric cold active enzyme with local flexibility around the active site and high overall stability. *J. Biol. Chem.* **282**, 21973–86

44. Kosugi, T., and Hayashi, S. (2012) Crucial role of protein flexibility in formation of a stable reaction transition state in an α-amylase catalysis. *J. Am. Chem. Soc.* **134**, 7045–55

45. Eisenmesser, E. Z., Millet, O., Labeikovsky, W., Korzhnev, D. M., Wolf-Watz, M., Bosco, D. A., Skalicky, J. J., Kay, L. E., and Kern, D. (2005) Intrinsic dynamics of an enzyme underlies catalysis. *Nature* **438**, 117–21

46. Fraser, J. S., Clarkson, M. W., Degnan, S. C., Erion, R., Kern, D., and Alber, T. (2009) Hidden alternative structures of proline isomerase essential for catalysis. *Nature* **462**, 669–73

47. Papaleo, E., Renzetti, G., and Tiberti, M. (2012) Mechanisms of intramolecular communication in a hyperthermophilic acylaminoacyl peptidase: a molecular dynamics investigation. *PLoS One* **7**, e35686

48. Boehr, D. D., Schnell, J. R., McElheny, D., Bae, S.-H., Duggan, B. M., Benkovic, S. J., Dyson, H. J., and Wright, P. E. (2013) A distal mutation perturbs dynamic amino acid networks in dihydrofolate reductase. *Biochemistry*, **52,** 4605-4619

49. Liang, Z.-X., Tsigos, I., Bouriotis, V., and Klinman, J. P. (2004) Impact of protein flexibility on hydride-transfer parameters in thermophilic and psychrophilic alcohol dehydrogenases. *J. Am. Chem. Soc.* **126**, 9500–1

50. Nagel, Z. D., Cun, S., and Klinman, J. P. (2013) Identification of a Long-Range Protein Network that Modulates Active Site Dynamics in Extremophilic Alcohol Dehydrogenases. *J. Biol. Chem.* **288,** 14087-97

51. Isaksen, G. V., Åqvist, J., and Brandsdal, B. O. (2014) Protein Surface Softness Is the Origin of Enzyme Cold-Adaptation of Trypsin. *PLoS Comput. Biol.* **10**, e1003813

52. Gunasekaran, K., Ma, B., and Nussinov, R. (2003) Triggering loops and enzyme function: identification of loops that trigger and modulate movements. *J. Mol. Biol.* **332**, 143–59

53. Ma, B., Tsai, C.-J., Haliloğlu, T., and Nussinov, R. (2011) Dynamic allostery: linkers are not merely flexible. *Structure* **19**, 907–17

54. Uversky, V. N. (2015) Functional roles of transiently and intrinsically disordered regions within proteins. *FEBS J.* **282**, 1182-1189

55. D'Amico, S., Gerday, C., and Feller, G. (2003) Temperature adaptation of proteins: engineering mesophilic-like activity and stability in a cold-adapted alpha-amylase. *J. Mol. Biol.* **332**, 981–8

56. Lee, J., and Goodey, N. M. (2011) Catalytic contributions from remote regions of enzyme structure. *Chem. Rev.* **111**, 7595–624

57. Jiménez-Osés, G., Osuna, S., Gao, X., Sawaya, M. R., Gilson, L., Collier, S. J., Huisman, G. W., Yeates, T. O., Tang, Y., and Houk, K. N. (2014) The role of distant mutations and allosteric regulation on LovD active site dynamics. *Nat. Chem. Biol.* **10,** 431-436

58. Osuna, S., Jiménez-Osés, G., Noey, E. L., and Houk, K. N. (2015) Molecular Dynamics Explorations of Active Site

Structure in Designed and Evolved Enzymes. *Acc. Chem. Res.* **48**, 1080-1090

59. Fedøy, A.-E., Yang, N., Martinez, A., Leiros, H.-K. S., and Steen, I. H. (2007) Structural and functional properties of isocitrate dehydrogenase from the psychrophilic bacterium Desulfotalea psychrophila reveal a cold-active enzyme with an unusual high thermal stability. *J. Mol. Biol.* **372**, 130–49

60. Wintrode, P. L., and Arnold, F. H. (2000) Temperature adaptation of enzymes: lessons from laboratory evolution. *Adv. Protein Chem.* **55**, 161–225

61. Arnold, F. H., Wintrode, P. L., Miyazaki, K., and Gershenson, A. (2001) How enzymes adapt: lessons from directed evolution. *Trends Biochem. Sci.* **26**, 100–6

62. Jónsdóttir, L. B., Ellertsson, B. Ö., Invernizzi, G., Magnúsdóttir, M., Thorbjarnardóttir, S. H., Papaleo, E., and Kristjánsson, M. M. (2014) The Role of Salt Bridges on the Temperature Adaptation of Aqualysin I, a Thermostable Subtilisin-like Proteinase. *Biochim. Biophys. Acta*. **1844**, 2174-2181

63. Hauksson, J., Andrésson, O., and Ásgeirsson, B. (2000) Heat-labile bacterial alkaline phosphatase from a marine Vibrio sp. *Enzyme Microb. Technol.* **27**, 66–73

64. Helland, R., Larsen, R. L., and Asgeirsson, B. (2009) The 1.4 A crystal structure of the large and cold-active Vibrio sp. alkaline phosphatase. *Biochim. Biophys. Acta* **1794**, 297–308

65. Rina, M., Pozidis, C., Mavromatis, K., Tzanodaskalaki, M., Kokkinidis, M., and Bouriotis, V. (2000) Alkaline phosphatase from the Antarctic strain TAB5. Properties and psychrophilic adaptations. *Eur. J. Biochem.* **267**, 1230–8

66. Golotin, V., Balabanova, L., Likhatskaya, G., and Rasskazov, V. (2015) Recombinant production and characterization of a highly active alkaline phosphatase from marine bacterium Cobetia marina. *Mar. Biotechnol. (NY).* **17**, 130–43

67. Tokuriki, N., and Tawfik, D. S. (2009) Protein dynamism and evolvability. *Science* **324**, 203–7

68. Kurkcuoglu, Z., Bakan, A., Kocaman, D., Bahar, I., and Doruker, P. (2012) Coupling between catalytic loop motions and enzyme global dynamics. *PLoS Comput. Biol.* **8**, e1002705

69. Nestl, B., and Hauer, B. (2014) Flexibe Loops in Proteins. *ACS Catal.*, **4,** 3201-3211

70. Papaleo, E., Ranzani, V., Tripodi, F., Vitriolo, A., Cirulli, C., Fantucci, P., Alberghina, L., Vanoni, M., De Gioia, L., and Coccetti, P. (2011) An acidic loop and cognate phosphorylation sites define a molecular switch that modulates ubiquitin charging activity in Cdc34-like enzymes. *PLoS Comput. Biol.* **7**, e1002056

71. Dror, R. O., Dirks, R. M., Grossman, J. P., Xu, H., and Shaw, D. E. (2012) Biomolecular simulation: a computational microscope for molecular biology. *Annu. Rev. Biophys.* **41**, 429–52

72. Piana, S., Lindorff-Larsen, K., and Shaw, D. E. (2011) How robust are protein folding simulations with respect to force field parameterization? *Biophys. J.* **100**, L47–9

73. Tiberti, M., Invernizzi, G., Lambrughi, M., Inbar, Y., Schreiber, G., and Papaleo, E. (2014) PyInteraph: A Framework for the Analysis of Interaction Networks in Structural Ensembles of Proteins. *J. Chem. Inf. Model.* **54**, 1537–51

74. Pace, C. N., Vajdos, F., Fee, L., Grimsley, G., and Gray, T. (1995) How to measure and predict the molar absorption coefficient of a protein. *Protein Sci.* **4**, 2411–23

75. Pace, C. N. (1986) Determination and analysis of urea and guanidine hydrochloride denaturation curves. *Methods Enzymol.* **131**, 266–80

76. Jorgensen, W. L., Chandrasekhar, J., Madura, J. D., Impey, R. W., and Klein, M. L. (1983) Comparison of simple potential functions for simulating liquid water. *J. Chem. Phys.* **79**

77. Bussi, G., Donadio, D., and Parrinello, M. (2007) Canonical sampling through velocity rescaling. *J. Chem. Phys.* **126**, 014101

78. Hess, B., Bekker, H., Berendsen, H., and Fraaije, J. LINCS: A linear constraint solver for molecular simulations.

79. Amadei, A., Linssen, A. B., and Berendsen, H. J. (1993) Essential dynamics of proteins. *Proteins* **17**, 412–25

80. Hess, B. (2000) Similarities between principal components of protein dynamics and random diffusion. *Phys. Rev. E. Stat. Phys. Plasmas. Fluids. Relat. Interdiscip. Topics* **62**, 8438–48

81. Schymkowitz, J., Borg, J., Stricher, F., Nys, R., Rousseau, F., and Serrano, L. (2005) The FoldX web server: an online force field. *Nucleic Acids Res.* **33**, W382–8 December 12, 2012).

82. Guerois, R., Nielsen, J. E., and Serrano, L. (2002) Predicting changes in the stability of proteins and protein complexes: a study of more than 1000 mutations. *J. Mol. Biol.* **320**, 369–87

83. Papaleo, E., Renzetti, G., Invernizzi, G., and Asgeirsson, B. (2013) Dynamics fingerprint and inherent asymmetric flexibility of a cold-adapted homodimeric enzyme. A case study of the Vibrio alkaline phosphatase. *Biochim. Biophys. Acta* **1830**, 2970–80

84. Gudjónsdóttir, K., and Asgeirsson, B. (2008) Effects of replacing active site residues in a cold-active alkaline phosphatase with those found in its mesophilic counterpart from Escherichia coli. *FEBS J.* **275**, 117–27

85. Miggiano, G. A., Mordente, A., Pischiutta, M. G., Martorana, G. E., and Castelli, A. (1987) Early conformational changes and activity modulation induced by guanidinium chloride on intestinal alkaline phosphatase. *Biochem. J.* **248**, 551–6

86. Hull, W. E., Halford, S. E., Gutfreund, H., and Sykes, B. D. (1976) 31P nuclear magnetic resonance study of alkaline phosphatase: the role of inorganic phosphate in limiting the enzyme turnover rate at alkaline pH. *Biochemistry* **15**, 1547–61

87. Borosky, G. L., and Lin, S. (2011) Computational modeling of the catalytic mechanism of human placental alkaline phosphatase (PLAP). *J. Chem. Inf. Model.* **51**, 2538–48

88. López-Canut, V., Roca, M., Bertrán, J., Moliner, V., and Tuñón, I. (2011) Promiscuity in alkaline phosphatase superfamily. Unraveling evolution through molecular simulations. *J. Am. Chem. Soc.* **133**, 12050–62

89. Stec, B., Holtz, K. M., and Kantrowitz, E. R. (2000) A revised mechanism for the alkaline phosphatase reaction involving three metal ions. *J. Mol. Biol.* **299**, 1303–11

90. De Backer, M. M. E., McSweeney, S., Lindley, P. F., and Hough, E. (2004) Ligand-binding and metal-exchange crystallographic studies on shrimp alkaline phosphatase. *Acta Crystallogr. D. Biol. Crystallogr.* **60**, 1555–61

91. Malabanan, M. M., Amyes, T. L., and Richard, J. P. (2010) A role for flexible loops in enzyme catalysis. *Curr. Opin. Struct. Biol.* **20**, 702–10

92. Ring, C. S., Kneller, D. G., Langridge, R., and Cohen, F. E. (1992) Taxonomy and conformational analysis of loops in proteins. *J. Mol. Biol.* **224**, 685–99

93. Bossi, M., Hoylaerts, M. F., and Millán, J. L. (1993) Modifications in a flexible surface loop modulate the isozyme-specific properties of mammalian alkaline phosphatases. *J. Biol. Chem.* **268**, 25409–16

94. Sunden, F., Peck, A., Salzman, J., Ressl, S., and Herschlag, D. (2015) Extensive site-directed mutagenesis reveals interconnected functional units in the Alkaline Phosphatase active site. *Elife* **4**

95. Papaleo, E., Renzetti, G., Invernizzi, G., and Asgeirsson, B. (2013) Dynamics fingerprint and inherent asymmetric flexibility of a cold-adapted homodimeric enzyme. A case study of the Vibrio alkaline phosphatase. *Biochim. Biophys. Acta,* **1830,** 2970-2980

Tables

Table 1. Hydrogen bonds and hydrophobic interactions relevant to the mutation sites in VAP_{wt}, VAP_{R336L}, VAP_{Y346F} and VAP_{F355Y} variants. These results are for the mutation sites in the major loop of subunit A only, for sake of clarity. One should note that the results for the other subunit are very similar with changes in populations generally lower than 4-7% for corresponding pairs of residues. The populations for each interaction are given in parenthesis. '$_A$' and '$_B$' indicate residues belonging to subunit A and B according to the X-ray VAP structure, respectively.

	VAPwt	**Mutant variants**
Arg/Leu336	H-bonds sc-sc 336Arg$_A$-59Asp$_B$ (36.89%) 336Arg$_A$-79Ser$_B$ (16.78%) 336Arg$_A$-81Glu$_B$ (77.16%) 336Arg$_A$-334Gln$_A$ (11.47%) Hbonds sc-mc 336Arg$_A$-343Asp$_A$ (52.26%) Hbonds mc-sc 336Arg$_A$-344Arg$_A$ (13.55%) Hbonds mc-mc 336Arg$_A$-344Arg$_A$ (68.95%) 336Arg$_A$-339Glu$_A$ (28.09%) Hydrophobic/Aromatic int. 336Arg$_A$-341Phe$_A$ (79.6%) 336Arg$_A$-346Tyr$_A$ (68.1%)	**VAP_{R336L}** Hbonds mc-sc 336Leu$_A$-344Arg$_A$ (38.44%) Hbonds mc-mc 336Leu$_A$-344Arg$_A$ (78.19%) 336Leu$_A$-343Asp$_A$ (10.73%) Hydrophobic/Aromatic int. 336Leu$_A$-341Phe$_A$ (35.1%) 336Leu$_A$-346Tyr$_A$ (30.2%)
Tyr/Phe346	H-bonds sc-sc 346Tyr$_A$-81Glu$_B$ (13.18%) Hbonds sc-mc 346Tyr$_A$-80Ser$_B$ (16.31%) Hbonds mc-mc 346Tyr$_A$-334Gln$_A$ (88.53%) 346Tyr$_A$-343Asp$_A$ (20.58%) Hydrophobic/Aromatic int. 346Tyr$_A$-336Arg$_A$ (68.1%) 346Tyr$_A$-348Pro$_A$ (78.4%)	**VAP_{Y346F}** Hbonds mc-mc 346Phe$_A$-334Gln$_A$ (90.00%) Hydrophobic/Aromatic int. 346Phe$_A$-336Arg$_A$ (32.3%) 346Phe$_A$-348Pro$_A$ (38.8%) 346Phe$_A$-341Phe$_A$ (28.6%)
Phe/Tyr355	 Hbonds mc-mc 355Phe$_A$-359Asp$_A$ (96.18%) 355Phe$_A$-358Leu$_A$ (87.60%) Hydrophobic/Aromatic int. 355Phe$_A$-29Ala$_A$ (30.8%) 355Phe$_A$-30Pro$_A$ (22.3%) 355Phe$_A$-61Ile$_B$ (19.7%)	**VAP_{F355Y}** Hbonds sc-sc 355Tyr$_A$-28Gln$_B$ (18.57%) 355Tyr$_A$-58Glu$_B$ (47.01%) Hbonds mc-mc 355Tyr$_A$-359Asp$_A$ (54.12%) 355Tyr$_A$-358Leu$_A$ (93.04%) Hydrophobic/Aromatic int. 355Tyr$_A$-29Ala$_A$ (70.1%) 355Tyr$_A$-30Pro$_A$ (29.2%) 355Tyr$_A$-61Ile$_B$ (45.2%)

Table 2. *In silico* prediction of ΔΔG upon mutations and experimental stability of VAP variants. The ΔΔG values calculated as ΔG_{mut}-ΔG_{wt} by *FoldX* are reported both for the monomer and the effects induced at the monomer-monomer interface in the dimeric structure. A positive ΔΔG value indicates destabilizing mutations, i.e. mutations that cause an increase in the fraction of unfolded proteins. We considered as significant differences (¥) only the ones that are higher than 6.7 kJ/mol, which corresponds to twice the standard deviation associated to *FoldX*. The melting temperature (T_m) was experimentally determined by CD at 222 nm. The buffer was 25 mM MOPS, 1 mM $MgSO_4$ at pH 8.0 (25 °C). Heat-stability of the active enzyme was determined in 20 mM Tris, and 10 mM $MgCl_2$, pH 8.0 (corrected for temperature) as the temperature needed to reduce the initial activity by half in 30 min ($T_{50\%}$). The free energy of dimer association (ΔG_D) was determined in 25 mM MOPS, 1 mM $MgSO_4$, pH 8.0 at 10°C by urea denaturation using the VAP enzyme activity assay (see materials and methods). Free energy of two state monomer unfolding (ΔG_M) was measured under same conditions by following intrinsic fluorescence redshift of tryptophan induced by urea. For thermal stability measurements, results came from several independent measurements (n=3-6) and free energy measurements came from three independent measurements (n=3)

Variant	***FoldX* ΔΔG (kJ/mol) Monomer**	***FoldX* ΔΔG (kJ/mol) monomer-monomer**	**T_m (°C)**	**$T_{50\%}$ (°C)**	**ΔG_D (kJ/mol) 2M ⇆ D**	**ΔG_M (kJ/mol)** U ⇆ M
VAP_{wt}	//	//	50.8 ± 0.6	25.8 ± 1.4	-8,5 ± 1.4	-13.9 ± 3.2
VAP_{R336L}	-1.46 ± 0.42	22.0 ± 2.51 ¥	45.0±5.1*	12.8 ± 1.2*	-2.2 ± 0.8	-14.3 ± 2.4
VAP_{Y346F}	-0.84 ± 0.02	-2.63 ± 0.06	48.8 ± 1.0 *	21.4 ± 1.4*	N/A	N/A
VAP_{F355Y}	-0.63 ± 0.08	-1.71 ± 0.08	50.2 ± 1.3	20.3 ± 1.1*	-14.0 ± 1.3	-14.8 ± 2.1

N/A: not attempted.

* Significant difference at 5% or lower by Student's T-test compared with VAP_{wt}

Table 3. Kinetic constants for the different VAP variants. The values of k_{cat} and K_m were determined using p-nitrophenyl phosphate in 0.1 M CAPS, 1.0 mM $MgCl_2$ and 15% (v/v) ethylene glycol at pH 9.8 and 10 °C. The kinetic results represent means with standard deviations from the different number of experiments as shown. VAP-St9 (VAP_{wt}) is the wild type enzyme with a StrepTag added to the C-terminal with a nine-residues linker sequence.

Variant	**k_{cat} (s^{-1})**	**K_m (μM)**	**k_{cat}/K_m ($mM^{-1}s^{-1}$)**
VAP_{wt} (n=10)	97 ± 14	56 ± 7	1732 ± 330
VAP_{R336L} (n=9)	120 ± 22 *	48 ± 12	2500 ± 775*
VAP_{Y346F} (n=8)	35 ± 5 *	22 ± 3*	1592 ± 314
VAP_{F355Y} (n=11)	97 ± 18	53 ± 4	1830 ± 366

* Differences from VAP_{wt} that are statistically significant at the 5% confidence level or better (P value better than 0.05).

Figure Legends

Figure 1. The major loop in *Vibrio* alkaline phosphatase (VAP). A) The two monomers of VAP are shown as light-blue and white cartoons, respectively. Magnesium and zinc ions are depicted as black and blue spheres, respectively. The mutation sites are highlighted as marine and grey sticks in the two subunits. The insert in the figure shows the major loop from monomer A at the interface with the monomer B. The distances between Tyr346 and Phe355 with respect to the metal-binding site are highlighted as a reference.
B) The radius of gyration (Rg) of each simulation over the simulation time is also reported as a reference of stability of the MD trajectories. The values are very close to the Rg calculated from the crystallographic structure of VAP (31 Å).

Figure 2. Interactions of the mutation sites in the different VAP variants, as derived from the analysis of our MD simulations. The two panels show two different views of the interactions at the interface between major loop from monomer A and the monomer B of VAP. The hydrogen bonds (or hydrophobic interactions in the case of Phe355) mediated by Arg336, Phe355, Tyr346 *and the residues 337-341* are shown as orange, black, green and magenta cylinders, respectively. The cylinder thickness is proportional to the population of the interaction in the MD ensemble. The additional residue shown as stick and dot is the nucleophile Ser65. The two monomers of VAP are shown as light-blue and white cartoons, respectively. Magnesium and Zinc ions are depicted as black and blue spheres, respectively. Only interactions mediated by the side-chain groups of Arg336, Phe355 and Tyr346 are shown in this figure. For a full list of the interactions mediated by each mutation site in wild type and mutant VAP variants see **Table 1**.

Figure 3. Inactivation and unfolding by urea. (A) Inactivation of VAP by urea. Samples containing 0.02 mg/ml of enzyme, 25 mM MOPS, 1 mM $MgSO_4$ pH 8.0 and urea ranging from 0-2 M were incubated for 4 h at 10° C before activity was measured using the VAP enzyme activity assay (see materials and methods). Activity was measured in duplicates for three independent experiments (n=3) and the average of relative activity was plotted against the concentration of urea. (**B)** Unfolding monitored using tryptophan emission redshift induced by urea. Samples were treated as in A and emission spectra from 310 to 410 nm were recorded with tryptophan excitation at 295 nm (see materials and methods). Denaturation curves were fitted with a sigmoidal equation where $D_{1/2}$ was 2.7, 2.2 and 2.1 M urea for VAP_{wt}, R336L and F355Y, respectively. Unfolding data consisted of three independent measurements.

Figure 4. Rotameric states of Ser65 and Arg129 in VAP_{wt} and VAP_{R336L}. A) The populations of the χ_1 dihedral angles of the nucleophile Ser65 are shown for VAP_{wt} (blue curve) and VAP_{R336L} (orange curve) simulations. A snapshot for each rotameric state (trans, minus or plus) is shown as a reference including also the location of the metal ions, i.e. Mg^{2+} and Zn^{2+} as black and blue spheres, respectively. B) The populations of the χ_1 dihedral angles of Arg129 are shown for VAP_{wt} (blue curve) and VAP_{R336L} (orange curve) simulations. C) The different rotameric states of Ser65 (t,m and p that indicate trans, minus and plus χ_1 rotamers, respectively), A129 in the plus state and the metal binding site of VAP (Mg^{2+} and Zn^{2+} in black and blue, respectively) are shown, together with the position that a phosphate group is expected to occupy in the AP catalytic site, according to the structure solved for another cold-adapted AP enzyme (PDB entry 1SHN).

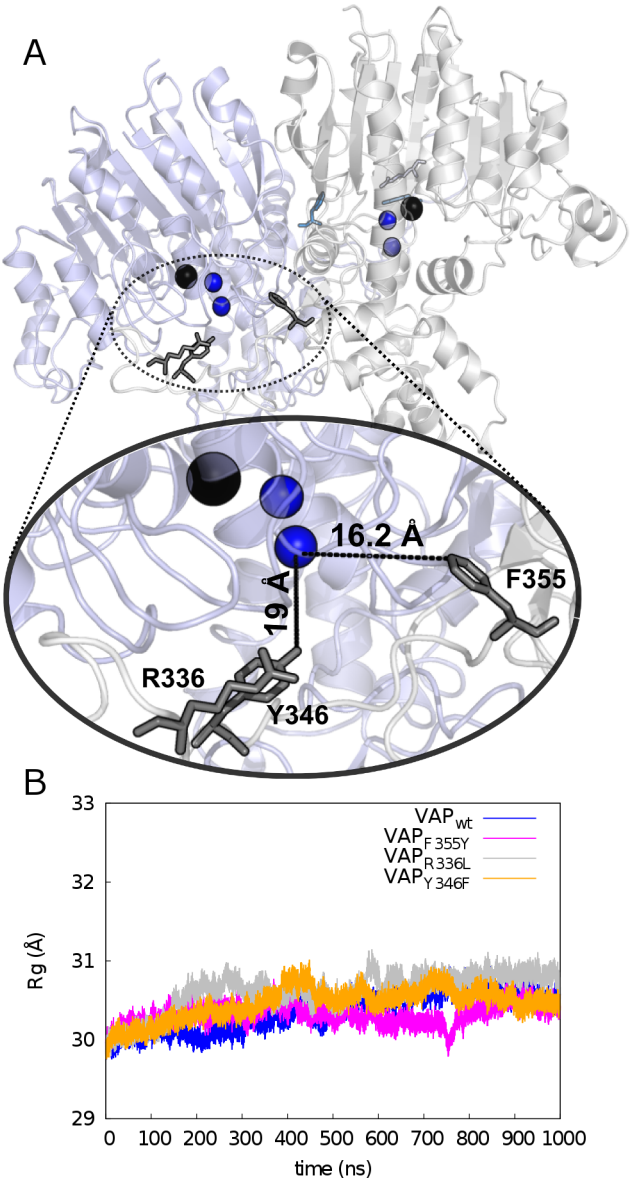
A
16.2 Å
19 Å
F355
R336
Y346
B
VAP wt
VAP F 355Y
VAP R 336L
VAP Y 346F
Rg (Å)
33
32
31
30
29
0
100
200
300
400
500
600
700
800
900
1000
time (ns)

Figure 1

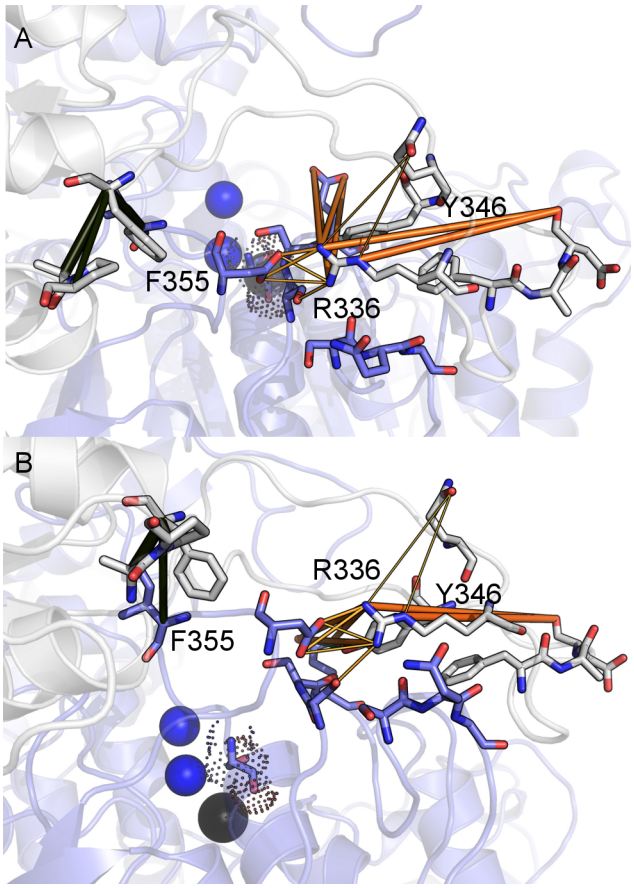

Figure 2

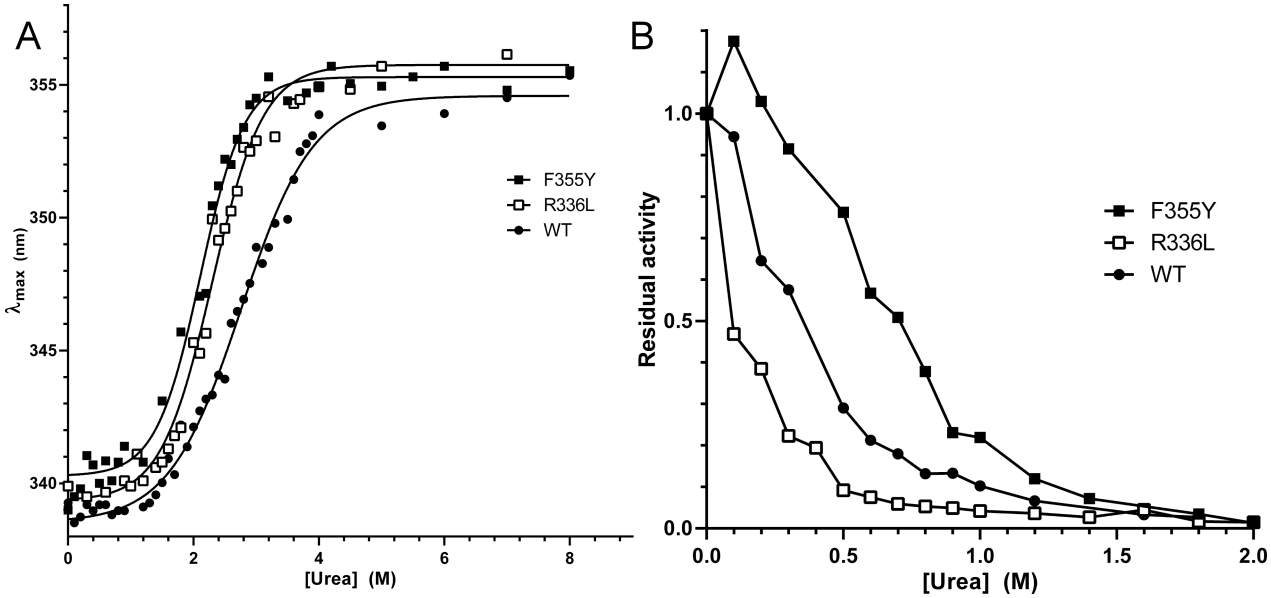
A
355
350
345
340
λ_{max} (nm)
0
2
4
6
8
[Urea] (M)
F355Y
R336L
WT
B
1.0
0.5
0.0
Residual activity
0.0
0.5
1.0
1.5
2.0
[Urea] (M)
F355Y
R336L
WT

Figure 3

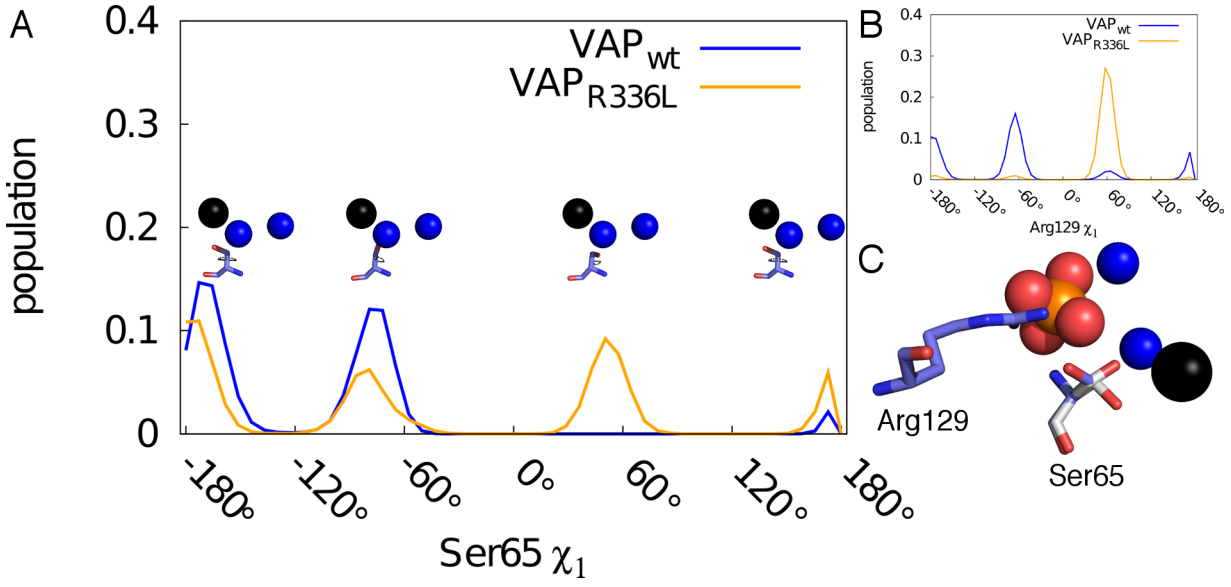
A
population
0.4
0.3
0.2
0.1
0
VAP wt
VAP R336L
-180°
-120°
-60°
0°
60°
120°
180°
Ser65 χ1
B
population
0.4
0.3
0.2
0.1
0
VAP wt
VAP R336L
-180°
-120°
-60°
0°
60°
120°
180°
Arg129 χ1
C
Arg129
Ser65

Figure 4

Conferences and talks

(12) Hjörleifsson J.G, Ásgeirsson, B. (2017) A rare two peak pH profile of *Vibrio splendidus alkaline* phosphatase and how anions increase its activity and stability. Presented in the 31st Annual Symposium of the Protein Society in Montreal CA.

(11) Hjörleifsson, J.G. (2017). A Thursday seminar at the Medical School scheduled on the 4th February.

(10) Hjörleifsson, J.G. (2016). PhD. committee meeting, results presentation and future perspectives, University of Iceland, 14th of December, VR-II building conference room.

(9) Hjörleifsson, J.G (2016). *Dimer dynamics and ionic influences on activity and stability*. Second year PhD Seminar at weekly departmental chemistry seminar series, University of Iceland, 17th of October, VR-II building.

(8) Ásgeirsson, B., Hjörleifsson, J.G., Pálmadóttir, T. & Chakraborty, S. (2016) *Promiscuous hydrolysis of p-nitrophenyl sulphate ester by Vibrio alkaline phosphatase coincides with loss of active site magnesium ions and loss of phosphatase activity.* Presented in the 30th Annual Symposium of the Protein Society in Baltimore USA.

(7) Hjörleifsson, J.G. and Ásgeirsson, B. (2016). *Subunit interaction and asymmetry of cold-active alkaline phosphatase studied using bimane label at dimer interface.* Presented in the 30th Annual Symposium of the Protein Society in Baltimore USA.

(6) Hjörleifsson, J.G. & Ásgeirsson, B (2015) *A highly buried and conserved tryptophan residues close to the dimer interface in a cold-adapted phosphatase is phosphorescent and important for activity*. Icelandic Chemical Society Conference: Chemistry and Life. Ráðstefna Efnís: Efnafræði & Lífið. Reykjavík, 9th of October, Hotel Radison (same as for Protein Society Symposium 2015).

(5) Hjörleifsson, J.G. and Ásgeirsson, B. (2015) *A highly buried and conserved tryptophan residue close to the dimer interface in a cold-adapted phosphatase is phosphorescent and important for activity.* The Icelandic Centre for Research (RANNIS) Annual Convention (same as for Protein Society Symposium 2015).

(4) Hjörleifsson, J.G. and Ásgeirsson, B. (2015) *Dimer dynamics and promiscuity in a cold-active enzyme: The case of alkaline phosphatase.* The Icelandic Center for

Research Conference (RANNIS), 12. mars 2015. Radison Hotel, Reykjavik. (Same title as previous but a different presentation).

(3) Ásgeirsson, B., Manuela Magnúsdóttir, Hjörleifsson, J.G. (2015). *Dimer dynamics and promiscuity in a cold-active enzyme: The case of alkaline phosphatase.* Presented at the 29th Annual Symposium of the Protein Society in Barcelona.

(2) Hjörleifsson, J.G. and Ásgeirsson, B. (2015) *A highly buried and conserved tryptophan residue close to the dimer interface in a cold-adapted phosphatase is phosphorescent and important for activity.* Presented at the 29th Annual Symposium of the Protein Society in Barcelona.

(1) Hjörleifsson, J.G. (2014) *Hairpin deoxyribozymes. Optimization and design of a stable all DNA containing gene knockdown agent.* Presentation of master thesis at weekly departmental chemistry seminar series, University of Iceland, 25th September, VR-II building, School of Engineering and Natural Sciences.